Marine nutrient dynamics of the KwaZulu–Natal Bight: Assessing bacterial numbers, biomass and productivity

by

Travis Hank Kunnen

Submitted in fulfilment of the academic requirements for the degree of Master of Science in the School of Life Science, Biological and Conservation Sciences, University of KwaZulu–Natal, Durban.

Supervised by Dr. David Muir and Dr. Ursula Scharler

February 2013

ABSTRACT

The KwaZulu–Natal Bight is formed from a narrow indentation in the SE coast of South Africa with the waters within considered to be oligotrophic. These waters therefore depend on both allochthonous sources of nutrients such as intermittent upwelling of deeper water and nutrients supplied by riverine inputs, as well as the autochthonous nutrients supplied by phytoplankton production, microbial fixation and recycling of nutrients by the microbial loop. Two African Coelacanth Ecosystem Programme cruises were undertaken during 2010, during the wet summer, and dry winter months. During each cruise, the waters of the KZN–B were sampled rapidly to provide spatial scales (synoptic) of bacterial abundance and biomass, as well as at four predetermined locations to determine temporal scales (focus) of bacterial abundance, biomass and productivity. During the synoptic section, samples were taken in surface waters, close to F–max (the depth at which phytoplankton were at their most dense as determined by *in situ* fluorometry), below the F–max (where depths exceeded 50 m), and near the bottom. These samples were fixed with formaldehyde, stained with DAPI and cells were visualised by epifluorescent microscopy. During the focus section, samples were taken in surface waters, close to F–max and below F–max and incubated with ^{3}H–Thymidine to determine bacterial productivity. Bacterioplankton dynamics (numbers, biomass and productivity) for both cruises, synoptic section, were higher within the photic zone and near riverine influenced waters, with summer showing higher dynamics than winter. Irrespective of season, bacterioplankton dynamics decreased with increasing distance from the coast as well as with increasing depth, potentially via bottom–up control mechanisms. Results obtained from the focus section of both cruises showed a significant difference between seasons for the Thukela Mouth and Richards Bay North, while no difference at the Durban Eddy. These results from the focus section suggest that bacterioplankton temporal dynamics were more top–down controlled, rather than environmentally influenced, resulting in fluctuating dynamics over time. Overall, it is proposed that the degree of inorganic nutrient supply to the phytoplankton, resulted in the formation of DOM for use by the heterotrophic bacteria, resulting in a bottom–up control mechanism, where Chl–*a* concentrations within the euphotic zone induces either top–down or bottom–up control mechanisms on the heterotrophic bacteria directly affecting their numbers, biomass and productivity.

PREFACE

The experimental work described in this dissertation was carried out in the School of Life Sciences, University of KwaZulu–Natal, Durban, from January 2010 to June 2012, under the supervision of Dr. Dave Muir and Dr. Ursula Scharler.

These studies represent original work by the author and have not otherwise been submitted in any form for any degree or diploma to any tertiary institution. Where use has been made of the work of others it is duly acknowledged in the text.

DECLARATION 1 - PLAGIARISM

I, _____ declare that

1. The research reported in this thesis, except where otherwise indicated, is my original research.

2. This thesis has not been submitted for any degree or examination at any other university.

3. This thesis does not contain other persons' data, pictures, graphs or other information, unless specifically acknowledged as being sourced from other persons.

4. This thesis does not contain other persons' writing, unless specifically acknowledged as being sourced from other researchers. Where other written sources have been quoted, then:
   a. Their words have been re-written but the general information attributed to them has been referenced
   b. Where their exact words have been used, then their writing has been placed in italics and inside quotation marks, and referenced.

5. This thesis does not contain text, graphics or tables copied and pasted from the Internet, unless specifically acknowledged, and the source being detailed in the thesis and in the References sections.

Signed: _____

DECLARATION 2 - PUBLICATIONS

DETAILS OF CONTRIBUTION TO PUBLICATIONS that form part and / or include research presented in this thesis (include publications in preparation, submitted, *in press* and published and give details of the contributions of each author to the experimental work and writing of each publication).

Publication 1: Bacterial population dynamics on the KwaZulu-Natal Bight: A seasonal comparison.

Publication 2: Methods in Appendix

Signed: _____

ACKNOWLEDGEMENTS

Firstly, this project as part of the greater African Coelacanth Ecosystem Programme would not have been possible without the funding provided by the National Research Foundation. To the Captain and crew of the F.R.S. Algoa, many thanks for your professionalism and dedication while aboard your vessel, and for your tireless efforts, day in and day out, in obtaining my samples. Thanks go to Ander de Lecea for running my bacterial productivity experiments during the first cruise. To Dr. Johan van der Molen, Ander de Lecea, Aadila Omarjee and Lisa de Charmoy thank you for your help, support and companionship while aboard the F.R.S Algoa during those long weeks.

As microbes go, this project required a lot of microscopy work, and for that I thank Dr. James Wesely–Smith, Sharon Eggers and Priscilla Maartens from the Electron Microscope Unit within the University of KwaZulu–Natal (Westville campus). Thank you for your help and for putting up with me over the years.

To Clive Jackson, thank you for your initial help in assessing the problems with the liquid scintillation counter and to Marilyn Bodasing for hunting down the required person to come and fix the machine. Thanks also go out to Riaan Roussow for his assistance in understanding the applications of Image Pro Plus macros.

Lastly, but certainly not least, to my supervisors, Dr. Dave Muir and Dr. Ursula Scharler, thank you for your tireless efforts in directing me on the right path.

“The world belongs to the very small

– and it has done for a very long time.”

~ Bill Bryson

This work is dedicated to Brenda Hazel Kunnen.

Who fought the good battle,

But lost the war.

TABLE OF CONTENTS

LIST OF FIGURES

LIST OF TABLES

ABBREVIATIONS AND NOTATIONS USED

ACEP	African Coelacanth Ecosystem Programme
BE	Bottom Ecozone
Chl–*a*	Chlorophyll *a*
CTD	Conductivity Temperature and Depth
DAPI	2.4 diamidino–6–phenylindole acid
DCD	Deepest Common Depth
DIVA	Data–Interpolating Variational Analysis
DOM	Dissolved Organic Matter
DPM_C	Disintegrations of the control per minute
DPM_S	Disintegrations of the sample per minute
DWAF	Department of Water Affairs and Forestry
FE	Fluorescence maximum Ecozone
F–max	Fluorescence maximum
HOT	Hawaii Ocean Time–series
IE	Intermediate Ecozone
IPP	Image Pro–Plus
KZN–B	KwaZulu–Natal Bight
MS	Microsoft
N	Nitrogen
NDF	Neutral Density Filter
P	Phosphorus

POM	Particulate Organic Matter
PP	Primary productivity
SE	Surface Ecozone
SNR	Signal to Noise Ratio
T1	Transect 1
T2	Transect 2
T3	Transect 3
T4	Transect 4
TTI	^{3}H–Thymidine incorporation rates
TCA	Trichloracetic acid
VBA	Visual Basic for Applications

CHAPTER 1: INTRODUCTION

The KwaZulu–Natal Bight (KZN–B) is an indented region of the coastline situated along the eastern coast of South Africa (Meyer et al., 2002) (Fig. 1.1). The continental shelf along which the KZN–B lies is for the most part very narrow, being only about 15 km wide to the north and south of the KZN–B (Lutjeharms, 2006). Within the KZN–B itself, the shelf widens considerably to an average of 50 km from the coast line towards the 200 m isobath (Lutjeharms, 2006). This widening begins near Cape St. Lucia and then levels out from Richards Bay towards the Thukela River, and then decreases down towards Durban (Fig. 1.1). The waters of the KZN–B can be classified as subtropical, oligotrophic water that originate from the Mozambique Channel. The KZN–B derives nutrients from allochthonous sources such as riverine, estuarine and oceanic, and from autochthonous sources, specifically phytoplankton primary productivity (PP) and organic and inorganic nutrients from coastal upwelling of nutrient rich deeper water from the Agulhas Current (Lutjeharms et al., 2000a; Lutjeharms and Machu, 2000).

Upwelling along the KwaZulu–Natal coast is caused by the impact of the southward flowing, deep Agulhas Current striking the extended continental shelf (Fig. 1.2). The first main source of upwelling is found at the northern end of the KZN–B near Cape St. Lucia and Richards Bay (Fig. 1.2–A). Upwelling within this area is kinematically driven (that is, by the physical force of the water) and it is the main source of upwelled water onto the shelf bank for the KZN–B, appearing to be present for much of the year (Lutjeharms et al., 2000a; Lutjeharms and Machu, 2000; Lutjeharms, 2006). Bottom water is also episodically upwelled to a lesser degree along the continental shelf edge (Meyer et al., 2002; Lutjeharms, 2006) (Fig. 1.2–B). This shelf edge upwelling occurs due to the edge shearing (friction) of the water passing along the outer shelf edge.

Another source of nutrient input into the KZN–B is due to the formation of an intermittent oceanic eddy near Durban (Meyer et al., 2002; Lutjeharms, 2006) (Fig. 1.2–D). This eddy is most likely caused by the physical structure of the continental shelf within this area, combined with the Agulhas Current overshooting the shelf edge, forming a trapped lee eddy (Meyer et al., 2002; Lutjeharms, 2006) (Fig. 1.2–C). The trapped lee eddy frequently creates a cyclonic eddy, which has the capacity to supply the southern areas of the KZN–B with eddy derived upwelled nutrients (Meyer et al., 2002). The nutrient rich bottom water that is drawn onto the whole KZN–B from the Agulhas Current comprises South Indian Subtropical Surface Waters and Indian Tropical Surface Waters (Lutjeharms et al., 2000b; Meyer et al., 2002; Lutjeharms, 2006).

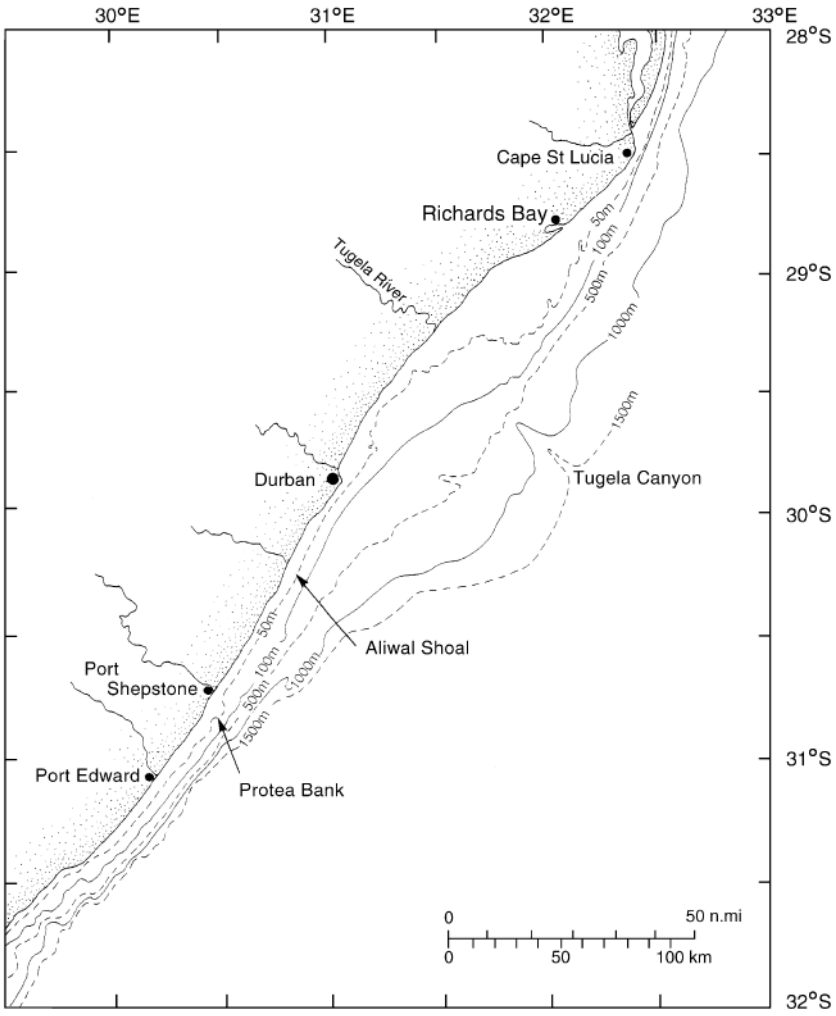

Figure 1.1: The KwaZulu–Natal Bight, an indented region of the east coast of South Africa, with corresponding continental shelf and underlying physical structure shown as bottom topography. Figure from Meyer et al. (2002).

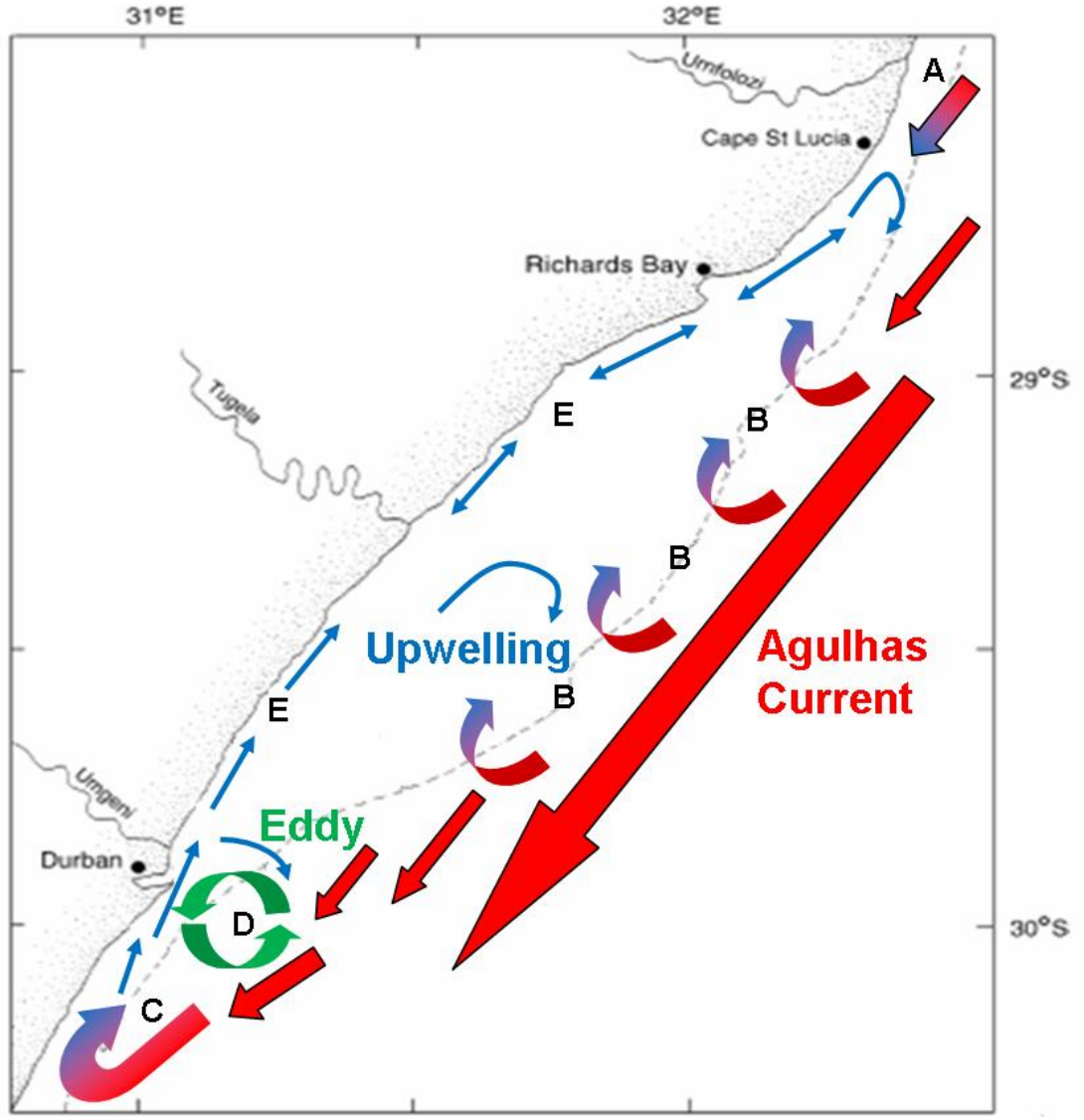

Figure 1.2: Authors impression of Agulhas Current kinematically driven upwelling (A), edge shear upwelling (B), eddy formation (C and D) and water movement (E) across the KZN–B. The dotted line indicates the 200 m isobath. Upwelling and currents based on Lutjeharms (2006). Original background figure modified from Meyer et al. (2002).

Surface waters of the KZN–B, under non–upwelling conditions, generally show the following characteristics during mid year: temperature ca. 24°C; salinity ca. 17.5; NO_3 ca. 1 µmol·L^{-1} and chlorophyll *a* (Chl–*a*) ca. 0.5 mg·m^{-3} (Lutjeharms et al., 2000a; Lutjeharms et al., 2000b; Meyer et al.,

2002)*. In comparison to non–upwelling conditions, during times of upwelling, surface waters of the KZN–B have shown the following characteristics: lower temperatures of ca. 11°C; higher salinities of ca. 35.6; higher nutrient levels with NO_3 concentrations of ca. 4 µmol·L^{-1} and higher Chl–*a* values of ca. 1.5 mg·m^{-3} (Lutjeharms et al., 2000a; Lutjeharms et al., 2000b; Meyer et al., 2002). The appearance of deeper water advected up from the Agulhas Current into the surface waters of the KZN–B is indicated by lower temperatures, higher salinities and higher nutrient concentrations as described above. Such attributes are a clear sign of freshly upwelled water into the surface waters of the KZN–B.

In the absence of surface upwelling within the KZN–B, Meyer et al. (2002) reported surface NO_3 concentrations of ca. 1 µmol·L^{-1} and Chl–*a* concentrations of ca. 0.5 mg·m^{-3}. These values are close to those reported in other oligotrophic systems. Goosen et al. (1997) reported NO_3 concentrations around 1.47 µmol·L^{-1} in Kenyan coastal waters and Pérez et al. (2005) reported NO_3 concentrations < 1 µmol·L^{-1}, with Chl–*a* concentrations of < 0.2 mg·m^{-3} in the upper nutrient depleted waters of the equatorial Atlantic Ocean. Sherr et al. (2002) however, reported Chl–*a* concentrations up to 5.2 ± SD 2.0 mg·m^{-3} in the near shore waters of Cape Hatteras in March 1996, with temperature and nitrate concentrations showing 4.6 ± SD 0.4°C and 0.32 ± SD 0.50 µmol·L^{-1}, respectively. In the absence of upwelling, the KZN–B is oligotrophic, and therefore, the KZN–B is dependent on external nutrient sources for its productivity.

Despite fresh nutrients being brought into the KZN–B by either upwelling, eddies or from terrestrial origin, these nutrients are not equally distributed within and across the KZN–B. Nutrient concentrations differ by depth at a specific location, as well as horizontally at a known depth. This can be attributed to the kinetic force of the bottom water being advected; the degree of mixing of freshly upwelled water with Agulhas surface water; wind induced mixing at the surface and the presence of biological activity slowly reducing the quantity of available nutrients (Meyer et al., 2002). Variations in nutrient distribution across the KZN–B are shown by Lutjeharms et al. (2000b) and Meyer et al. (2002) who clearly indicate that the most intense area of upwelling is situated in the north, near Cape St. Lucia and Richards Bay.

Within this northern area of the KZN–B at 10 m depth, Meyer et al. (2002) reported a maximum concentration of nitrate, up to 15 µmol·L^{-1}, phosphate, up to 1.2 µmol·L^{-1} and silicate, up to 0.9 µmol·L^{-1} compared to the rest of the KZN–B at the same depth (< 1 µmol·L^{-1}, < 0.7 µmol·L^{-1}, < 0.1 µmol·L^{-1}, respectively). Within the same northern area, Lutjeharms et al. (2000b) reported decreased

* All data from Lutjeharms et al. (2000b) and Meyer et al. (2002) come from the time of their study, the *Natal Bight Cruise*, 16 to 22 July 1989.

temperatures (ca. 19°C) and increased salinity (ca. 35.25) at the same depth. Both Lutjeharms et al. (2000b) and Meyer et al. (2002) also reported that Chl–*a* levels near Richards Bay (up to 1.2 $mg \cdot m^{-3}$) were higher than in the rest of the KZN–B (< 0.5 $mg \cdot m^{-3}$), with Chl–*a* levels slowly decreasing southward over the shelf. Variations in nutrient concentrations in surface waters are also present near Durban, although nutrient levels were not as high as those reported for the Richards Bay upwelling area (Lutjeharms et al., 2000b; Meyer et al., 2002).

Variations in nutrient concentrations are also present vertically within the water column. Meyer et al. (2002) reported an increase in nitrate from 1 to 17 $\mu mol \cdot L^{-1}$, phosphate from 0.5 to 1.3 $\mu mol \cdot L^{-1}$ and silicate from 4 to 12 $\mu mol \cdot L^{-1}$ in waters below 75 m throughout the KZN–B, indicating a possible nutri–cline. The evidence of such abrupt nutri–clines is more evident in the northern areas of the KZN–B, where the influx of nutrients is higher in both quantity and quality. During upwelling near Richards Bay, surface waters within the upper 30 m showed nutrient ranges for nitrate (2 to 15 $\mu mol \cdot L^{-1}$), phosphate (0.5 to 1.2 $\mu mol \cdot L^{-1}$) and silicate (0.4 to 12 $\mu mol \cdot L^{-1}$) (Meyer et al., 2002). Here, this photic zone nutrient signature has been correlated with Chl–*a* concentrations, a proxy for primary producer biomass.

Chl–*a* concentrations to the north of Richards Bay have been previously reported by Meyer et al. (2002) to be between 1.2 to 1.5 $mg \cdot m^{-3}$. This level dropped rapidly from the widening of the shelf, with distance heading south along the coast, so that within about 50 km over the shelf, the Chl–*a* concentration was 0.5 to 1 $mg \cdot m^{-3}$ to the south of Richards Bay (Meyer et al., 2002). The southward decrease in nutrient concentrations as well as Chl–*a* concentrations, from Richards Bay with distance, shows a clear autotrophic biological utilization of inorganic nutrients, primarily by phytoplankton (Meyer et al., 2002). Further to the south, with decreasing inorganic nutrient levels, Chl–*a* concentrations decreased even further to < 0.1 $mg \cdot m^{-3}$ (Lutjeharms et al., 2000b; Meyer et al., 2002). Microcosm experiments conducted by Zohary et al. (2005) showed that the addition of both nitrate and phosphate resulted in a 4 to 80 fold increase in chlorophyll, numbers of ciliates, bacterial activity and other pigments. This may be the case within the KZN–B, with kinematically driven, nutrient rich water being upwelled into the surface (photic zone) waters of the KZN–B, providing additional nutrients to fuel growth.

Upwelling of nutrients along the shelf edge, although not as substantial as the upwelling found near Richards Bay, is not as isolated and does show a wider geographical distribution (Lutjeharms et al., 2000b; Meyer et al., 2002). The intense upwelling near Richards Bay is topographically isolated, while the upwelling along the KZN–B shelf edge is not. Nutrient levels along the shelf edge are still higher than the more central, coastal, section of the KZN–B on the shelf (Meyer et al., 2002). For waters above 30 m within the KZN–B, nutrient levels reported by Meyer et al. (2002) were nitrate: 1

to 2 µmol·L^{-1}, phosphate: 0.48 to 0.72 µmol·L^{-1} and silicate: 0.4 to 4 µmol·L^{-1}. Below 75 m, nutrient levels were much higher, as would be expected with deep waters, showing nutrient concentrations of nitrate: 2 to 18 µmol·L^{-1}, phosphate: 0.7 to 1.5 µmol·L^{-1} and silicate: 6 to 15 µmol·L^{-1} (Meyer et al., 2002).

Durban Eddy upwelling is caused by the Agulhas Current overshooting the shelf edge, forming a trapped lee eddy. This usually creates an ephemeral cyclonic eddy that draws up nutrient rich water from the Agulhas Current and introduces deeper waters into the surface waters of the KZN–B. Nutrient levels for this area reported by Meyer et al. (2002) during the time of their study indicate that the Durban Eddy was present. For waters above 30 m, nutrient levels were nitrate, 0.15 to 2 µmol·L^{-1}; phosphate, 0.35 to 0.65 µmol·L^{-1} and silicate, 2.66 to 4.05 µmol·L^{-1} (Meyer et al., 2002). Below 75 m nutrient levels were higher, as would be expected in water that is upwelled by a cyclonic eddy, showing nutrient concentrations of 0.18 to 18.33 µmol·L^{-1}, 0.46 to 5.43 µmol·L^{-1} and 3.03 to 13.60 µmol·L^{-1}, respectively (Meyer et al., 2002).

The input of terrestrially derived nutrients into the coastal waters of the KZN–B cannot be overlooked as a possible source of nutrients, and includes nitrates and phosphates from agricultural runoff. To date, there is little available information about terrestrial based nutrient input into coastal KZN–B waters. Available data sources include Meyer et al. (2002), indicating phosphate levels around 0.1 to 0.8 µmol·L^{-1} within the plume of the Thukela River at 30 m. DWAF (1995) in Source–to–Sea (2004), reported average estimated nitrogen concentrations of 50 µg·L^{-1} (= 3.57 µmol·L^{-1}) and average estimated phosphorus concentrations of 19 µg·L^{-1} (= 0.61 µmol·L^{-1}) near the Thukela River. van Ballegooyen et al. (2007) reported nutrient input into the KZN–B region from groundwater sources for nitrogen to be < 2 mg·L^{-1} (= < 0.14 µmol·L^{-1}).

Nutrient input into the KZN–B may be seasonally affected by rainy summer months and dry winter months. During the rainy summer months, riverine outflow is usually at its peak, bringing terrestrial based organic and inorganic matter into the KZN–B. The inorganic matter is utilised by phytoplankton during the long summer days, and may result in an excess of phytoplankton derived, dissolved organic matter, which in turn can be utilized by heterotrophic bacteria. As a result, heterotrophic bacteria may show higher numbers and biomass near river mouth plumes and coastal areas as well as around upwelling regions. Conversely, shading by suspended matter could result in less dissolved organic matter being released by phytoplankton and thus decrease bacterial numbers and bacterial biomass. In contrast, during the dry winter months riverine outflow usually decreases, and the KZN–B may become mainly dependent for fresh nutrients on the nutrient rich upwelled bottom water (to sustain this system), as well as the internal nutrient recycling by heterotrophic bacteria. During both the wet summer and dry winter months, phytoplankton communities would be

localized around areas of inorganic nutrient input. As the inorganic nutrients are mixed, shifted, reduced or diluted, the phytoplankton communities being dependent on the inorganic nutrients, through drifting, would become patchy within the photic zone. The heterotrophic bacteria, being mainly dependent on the exuded dissolved organic matter from the phytoplankton would also become patchy in close proximity to the phytoplankton. The phytoplankton in turn, would rely on the recycled nutrients gained from the bacteria.

Overall, the biological signal in relation to nutrient dynamics is most strongly seen as the rapid spatial rise in measurable Chl–*a* levels within the greater Richards Bay area (Meyer et al., 2002). This signal decreases from Richards Bay to just north of the Thukela River mouth along with all the other indicators of diluted shelf edge induced upwelling (lower temperatures, higher salinities and increased nutrients) (Lutjeharms et al., 2000a; Lutjeharms et al., 2000b; Meyer et al., 2002). Near the Thukela River mouth it would appear that primary productivity (PP) generally increases, possibly due to the input of nutrients derived from the Thukela River mouth. Most notably, this increase in Chl–*a* was probably due to the input of phosphate from the Thukela River previously measured at 30 m (Meyer et al., 2002).

It has been shown by Zohary et al. (2005) that phytoplankton can be nitrogen and phosphorus co–limited, and that the addition of phosphorus to waters already containing nitrogen results in an increase in chlorophyll levels. Since the KZN–B is nutrient depleted, it cannot sustain high PP without a constant supply of inorganic nutrients, especially nitrates and phosphates. Heterotrophic bacteria therefore have an essential role to play as re–cyclers of these nutrients, in the microbial loop.

The microbial loop (Azam et al., 1983; Fenchel, 2008) conceptualizes the pathways of nutrients and energy flow between the microscopic organisms within aquatic ecosystems (Fig. 1.3). It includes the autotrophic phytoplankton, heterotrophic flagellates, microzooplankton and heterotrophic bacteria (Azam et al., 1983; Fenchel, 2008). The interactions between these groups of organisms revolve around the recycling of organic nutrients into inorganic form (Azam et al., 1983) including limiting (micro or macro nutrients that control the active growth of a population) and non–limiting nutrients.

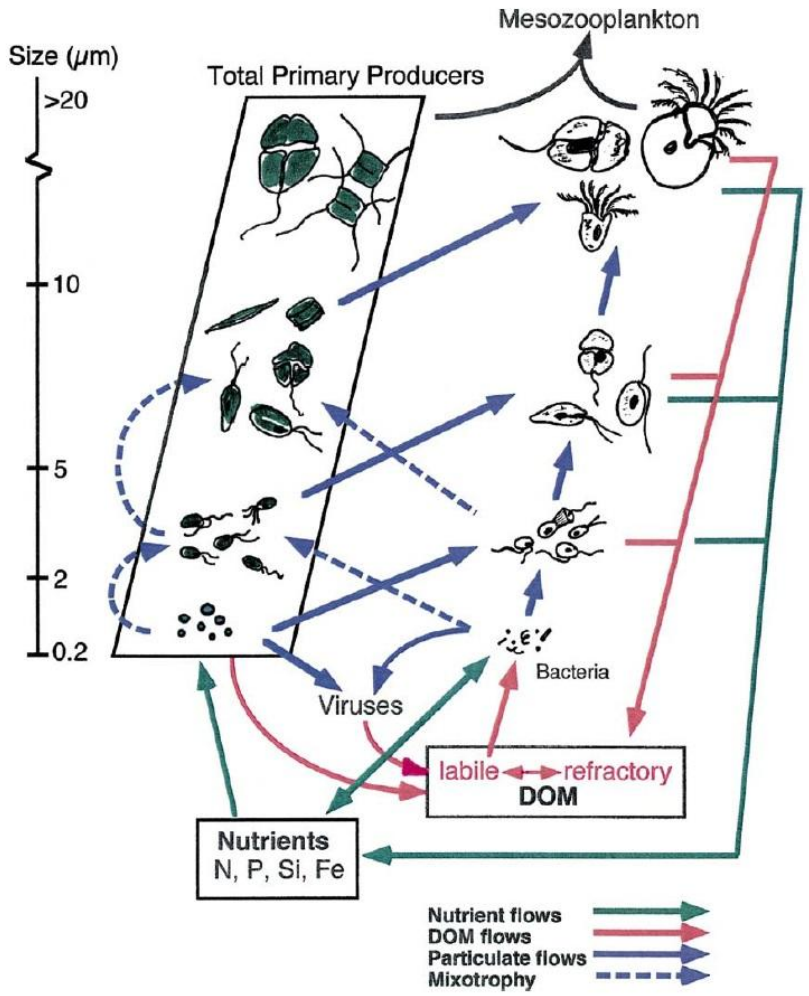

Figure 1.3: The microbial loop as conceptualized by Landry and Kirchman (2002).

Since phytoplankton are autotrophic (organisms that require the presence of photosynthetically available sunlight for anabolism), they utilize the available inorganic nutrients present within the photic zone to produce cellular material. This material is eventually released into the water column in several ways, including cell lysis (usually viral mediated (Fuhrman, 1999; Wommack and Colwell, 2000; Menge and Weitz, 2009)), sloppy feeding (incompletely consumed organisms resulting in cellular material leakage), cellular exudates and cellular death (Rheinheimer, 1985; Lovejoy et al., 2000). Most of these result in the release of dissolved organic matter (DOM) consisting of carbon, free amino acids, bound amino acids, fatty acids, free carbohydrates, bound carbohydrates, protein, lipids and hydrocarbons (Rheinheimer, 1985). Phytoplankton particulate organic matter is also derived, directly or indirectly, from the release of DOM. When phytoplankton cells are lysed, some structural forms of the phytoplankton still exist, parts of the cell wall for example, forming particulate organic

matter (POM), along with DOM released. This is the same for sloppy feeding, as probably much of the cell still remains, and cellular death, where the whole cell remains and must be degraded.

The consumers within this loop, the nanoflagellates, flagellates and microzooplankton (ciliates) are heterotrophic organisms that require the assimilation of organic material for anabolism, and consume organisms or detritus for their energy needs (Wood, 1965; Rheinheimer, 1985). These protists maintain the capacity to also utilize DOM as an organic energy source. It has been shown by Umorin (1992) that bacteria and DOM are fed on simultaneously by flagellates. Tranvik et al. (1993) have also shown a positive correlation between bacterial sized prey rates of clearance and macromolecular uptake capacity indicating that protists can consume colloids (explained here as DOM evenly dispersed throughout the water column) of varying sizes encompassing the size ranges of bacteria. Protists however, are unable to compete with heterotrophic bacteria in the utilization of low molecular weight dissolved compounds when found at low concentrations [(Haas and Webb, 1979; Fenchel, 1987) as cited in Tranvik et al. (1993)]. The introduction of organic nutrients by the consumers into the water column also occurs in many ways, mainly being the release of faecal pellets, sloppy feeding and cellular death. Here, the majority of the organics released are in the form of POM, consisting of such material as recalcitrant carbon compounds, faecal pellets and marine snow. Marine snow is particulate matter, both organic and inorganic that flocculates while descending to form visible aggregates over time (Fenchel, 2008).

There is a close link between heterotrophic bacteria and the organic matter produced by phytoplankton (Fuhrman and Azam, 1980; Azam et al., 1983; Lovejoy et al., 2000; Andrade et al., 2003; Richardson and Jackson, 2007) as it has been shown that bacterial growth is limited primarily by the availability of labile organic substrates (Church et al., 2000). Heterotrophic bacteria are able to utilize DOM as an easy source of organic energy for their own growth and reproduction by converting DOM into POM anabolically. This invariably results in an increase in bacterial numbers, biomass and productivity in areas of elevated phytoplankton production. Heterotrophic bacteria are also able to use POM, and are the principal mechanism whereby POM is reconverted into DOM (Lovejoy et al., 2000). The scavenging ability of heterotrophic bacteria takes organic waste products and reintroduces recycled nutrients back into the system. By incorporating the nutrients found within organic waste (from DOM, POM and detritus) into their cellular makeup, they make these nutrients available to the consumers which prey on them (Azam et al., 1983; Fenchel, 2008). In this way, the beginning of a larger system of trophic exchange begins, as larger organisms will feed off the larger size fractions within the microbial loop.

The microbial loop is thus the interaction between phytoplankton and DOM, microscopic consumers and POM, and the bacterial ability to utilize organic material reintroducing these nutrients back into the water column.

Heterotrophic bacteria within our oceans are essential for the basic functioning of the flow of matter between trophic levels, where limiting nutrients are rapidly recycled by heterotrophic bacteria, and reused by primary producers (Fig. 1.4).

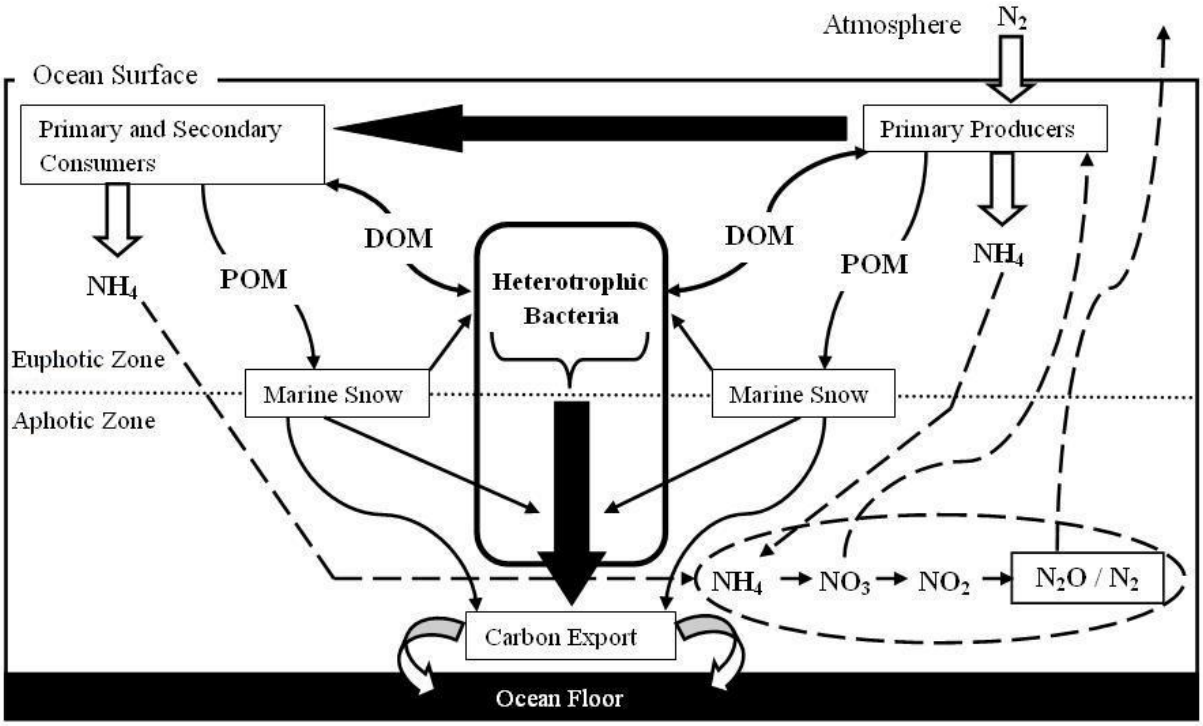

Figure 1.4: Basic organic and inorganic matter flow through the heterotrophic bacterial pathway. Carbon (DOM and POM) flows are represented by solid lines, while nitrogen flow is represented by dashed lines. Figure recreated based on Munn (2004) figures 9.1 and 9.2.

Interactions between bacteriophages (bacterial specific viruses) and bacteria are also very important within the microbial loop (Fenchel, 2008). Here, the interaction of host specific viral mediated lysis controls the cycling of biomass and carbon within the bacterial pool (Landry and Kirchman, 2002). In this way, host specific viruses are able to control bacterial population numbers, so that a single bacterial population or species does not overpopulate a single ecosystem. In any predator – prey interaction, the increase in one species' abundance will result in the increase of that organism's predator.

The result of bacterial viral lysis is the release of bacterial exudates, those remaining after viral replication, into the dissolved organic pool. Although bacteria are small in size, and therefore do not contain much carbon, their large numbers ensure that viral based host specific lysis may release considerable quantities of nutrients into the water column. These nutrients from the dissolved organic pool can be used by other bacterial species of other populations within the surrounding area, to increase their numbers and biomass, thus resulting in not only a simple species predator – prey interaction, but a more complex population predator – prey interaction (Azam et al., 1983; Fenchel, 2008).

Not all bacteria within marine systems are able to use the nutrients that are available. Bacterial dormancy, first proposed by Stevenson (1978), occurs in all aquatic habitats. Here Stevenson's (1978) hypothesis was based on exogenous dormancy forming smaller cells within the population when under certain stressors, such as starvation, that could decrease bacterial cell size and activity. Such an effect was shown by Gasol et al. (1995) where the size of inactive bacteria averaged 0.055 μm^3 while active bacteria averaged 0.12 μm^3. Sherr et al. (2002) showed a similar result where particle associated bacteria were more active compared to the total population based on 5 cyano–2, 3 ditoyl tetrazolium chloride reduction. Results obtained by Bernard et al. (2000) using flow cytometry also support the above.

A study by DuFour and Torréton (1996) within the euphotic zone in the tropical North Eastern Atlantic Ocean covering three trophic sites, showed that the oligotrophic site had the lowest cell volume (0.022 ± SD 0.004 μm^3) and the highest percentage of active cells (6.1 ± SD 2.4) compared to the mesotrophic (0.027 ± SD 0.005 μm^3 and 4.0 ± SD 1.6) and eutrophic (0.042 ± SD 0.005 μm^3 and 5.5 ± SD 0.6) sites. These values are similar to those presented by Luna et al. (2002) within coastal sediments, where only about 4 to 6% of the live stock showed active metabolism.

The standing stock of bacteria in the water column accounts for a large proportion of the available biomass within aquatic systems (Fergusen and Rublee, 1976). The metabolically active bacteria are preferentially preyed upon for their higher nutritional value (Bernard et al., 2000; Sherr et al., 2002), as it is generally known that with an increase in nutrient availability, there is generally an increase in bacterial size (Roszak and Colwell, 1987; Berman et al., 1994). This has been shown previously by the linear relationship between bacterial size and activity (Gasol et al., 1995) as well as the metabolically active selective feeding capacity of bacterivores as shown by Bernard et al. (2000) and Sherr et al. (2002).

This suggests that only a small percentage of total bacteria at any given time are being preyed upon. In this way, there is always a standing stock of inactive or dormant bacteria that are able to

replace those active bacteria, that are consumed or lost (Andrade et al., 2003). Molecular studies conducted by Bernard et al. (2000) showed that there is a small proportion of active bacteria and a very large proportion of inactive bacteria within the water column, and that a few cells of each species of the population from this inactive group are metabolically active within the smaller, more active, metabolic group. So if the loss of any one highly active bacterial species, due to overpopulation (through heavy grazing), host specific viral mediated lysis or any other form of reduction, could result in the opening of a niche to be filled in by those active bacterial cells present in lower numbers.

The efficacy of bacterial nutrient utilization as stated by Goosen et al. (1997), that even with a 50% bacterial growth efficiency, the organic nutrients supplied by phytoplankton are not sufficient to maintain bacterial growth. The bacteria must then be acquiring organic nutrients from other sources, possibly from within the bacteria – predation – viral lysis mini loop, DOM and POM from sloppy feeding by metazoans, or from the existing pool of refractory DOM and POM (Lønborg et al., 2009b).

There is evidence for limitation and co–limitation of bacteria and phytoplankton depending on the availability of phosphorus (P) and nitrogen (N) in the Eastern Mediterranean (Zohary et al., 2005). Zohary et al. (2005) determined that with the presence of P only, bacteria showed very high activity, measured by Leucine incorporation, with no increase in numbers for bacteria or phytoplankton. This was possibly due to positive cascade effects on higher trophic levels, resulting in the grazing of phytoplankton and bacterial cells, or alternatively that in the presence of excess P, bacterial cells became N limited (Zohary et al., 2005). Phosphorus limitation is also reported within the ultra–oligotrophic Levantine Basin within the eastern Mediterranean. Here, Tanaka et al. (2007) reported very low bacterial counts within surface waters, but deeper into the euphotic layer, there existed a strong coupling between bacteria and their grazers. This strong coupling existed because nutrient levels were so low, that the rapid recycling of limiting nutrients was essential to sustain the food web. Tanaka et al. (2007) also determined that this layer within the euphotic zone corresponded to a higher phosphate regeneration depth, compared to the rest of the water column.

Oligotrophic systems are typified by lower mean inorganic nutrient levels [$P–PO_4$: 0.02 µmol $P \cdot L^{-1}$; $N–NO_3$ + $N–NO_2$: 0.21 µmol $N \cdot L^{-1}$; $N–NH_4$: 0.36 µmol $N \cdot L^{-1}$ (Karydis, 2009)] and therefore lower phytoplankton / algal biomass (Karydis, 2009) possibly resulting in lower bacterial numbers, biomass and productivity. Where there are insufficient inorganic nutrients to fully support PP, the amount of DOM (and resulting POM) released into the water column is invariably insufficient to sustain high bacterial production. Bacterial cells however, have a high surface:volume ratio and are rapidly, and efficiently, able to utilize the available nutrients present within their surroundings, so that relative high numbers can be maintained with low productivity.

Contrasting systems such as mesotrophic systems with medium mean levels of inorganic nutrients [$P–PO_4$: 0.09 µmol $P·L^{-1}$; $N–NO_3$ + $N–NO_2$: 0.33 µmol $N·L^{-1}$; $N–NH_4$: 0.84 µmol $N·L^{-1}$ (Karydis, 2009)] and eutrophic systems with high mean levels of inorganic nutrients [$P–PO_4$: 0.34 µmol $P·L^{-1}$; $N–NO_3$ + $N–NO_2$: 0.53 µmol $N·L^{-1}$; $N–NH_4$: 1.15 µmol $N·L^{-1}$ (Karydis, 2009)] potentially have a sufficient supply of inorganic nutrients to continuously support PP. DOM and POM concentrations within mesotrophic and eutrophic systems should therefore increase, leading to a rise in bacterial dynamics (numbers, biomass and productivity). With more consumers, and increased amounts of organic nutrients available within the water column to sustain bacterial productivity and bacterial populations, the level of bacterial productivity and thus bacterivory should increase. Thus with a fully linked food web, creating negative feedbacks into bacterial productivity, bacterial populations remain very active with bacterial abundance kept in check [(Smetacek et al., 1990) as cited in Wiebinga et al. (1997)]. A system with sufficient nutrient supply would therefore be able to maintain a higher degree of ecological complexity, because of the stability the heterotrophic bacteria provide with regards to nutrient recycling and regeneration.

In some cases, the organic matter supplied by phytoplankton alone is not enough to sustain high bacterial productivity, therefore phytoplankton cannot be the sole source for bacterial organic matter (Goosen et al., 1997). Goosen et al. (1997) performed studies in Kenyan coastal waters that showed that the net percentage use by bacteria of phytoplankton based organic matter ranged from as little as 7% (at 20 m) to as much as 2588% (at 105 m) between the two cruises undertaken. The extremely high usage of 2588% was explained by Goosen et al. (1997) to be caused by the South East monsoon during the time of study. During the monsoon season, high rain fall increases terrestrial based riverine outflow of nutrients into coastal marine systems. These outflows would have high concentrations of organic (POM, detritus and tripton [collections of detritus and fine particles of minerals (Wood, 1965)]) and inorganic nutrients. The increased inorganic nutrients available to phytoplankton could result in increased DOM within the water column (in the absence of shading), while the organic nutrients would be directly assimilated by heterotrophic bacteria. The organic nutrients supplied by terrestrial input could possibly exceed the DOM supplied and produced by the phytoplankton. Using the study performed by Goosen et al. (1997) as an example, during the monsoon season, sunlight was diminished and the amount of suspended matter in the water column was very high. Turbulence would increase from increased wind velocities leading to shading which would also hamper PP. The particulate material introduced into such coastal areas would supply heterotrophic bacterial cells a suitable substrate to metabolize on, being higher in nutritional value compared to the surrounding waters (Stevenson, 1978). It has been shown that heterotrophic bacterial activity does invariably increase with increasing concentrations of particulate matter, from sources such as POM, marine snow, suspended sediment and tripton (Wood, 1965; Rheinheimer, 1985; Sherr et al., 2002). Such

particulate matter introduced into a system would therefore provide a large substrate surface for bacterial settling and activity, as well possible shelter from predators, leading to increased rates of heterotrophic bacterial productivity. This would invariably increase both bacterial numbers and biomass within the surrounding area, as well as on the substrate, and provide a food source for grazers where phytoplankton numbers have been diminished by shading, loss of sunlight and turbulence.

It would then appear that the level of interaction between phytoplankton and heterotrophic bacteria is dependent on the level of available inorganic nutrients. The more inorganic nutrients that are available to phytoplankton, the more DOM released, and POM produced resulting in higher bacterial numbers and biomass. In systems dominated by picophytoplankton, usually showing low nutrient levels, the interactions between the microbial loop and the food web would potentially result in the rapid recycling of limiting nutrients (such as P). This usually occurs within a well defined, but low trophic level interaction microbial loop that has the ability to sustain the food web with regard to productivity, in the requirements for limiting nutrients (Pérez et al., 2005).

This was shown by Lønborg et al. (2009b) in Loch Creran, where heterotrophic bacteria initially took up P then N, followed by carbon. The majority of P (a limiting nutrient) was recycled within the fjord to maintain ecological stability, while a large percentage of the non–recycled N and carbon from the main fjord system, was degraded or utilized along the remainder of the fjord system (Lønborg et al., 2009b). It is possible to assume, that heterotrophic bacterial populations might prefer such organic matter that has been freshly produced under high nutrient conditions, as such organic exudates will most likely contain higher amounts of P (Lønborg et al., 2009a; Lønborg et al., 2009b). At times of nutrient stress, phytoplankton continue to metabolize inorganic nutrients but tend to release compounds with a higher carbon content (Lønborg et al., 2009b). Under conditions of low nutrient availability, cellular exudates from phytoplankton will have higher carbon content (more refractory). These refractory exudates may not be efficiently assimilated by heterotrophic bacteria within the euphotic zone, as it has been shown that bacterial populations preferentially assimilate labile carbon compounds from phytoplankton (Rivkin et al., 1996; Church et al., 2000; Lønborg et al., 2009a; Lønborg et al., 2009b). The remaining refractory organic material, although still metabolized by bacteria on its decent towards the ocean floor, are a carbon sink, as carbon is exported into the ocean depths (Fig. 1.4).

Although phytoplankton are the main producers of carbon based organic matter within aquatic ecosystems, the utilization and conversion of this organic matter and nutrients therein by heterotrophic bacteria, is what makes ecological food webs function by ensuring a relatively steady supply of growth limiting nutrients to the organisms within the ecosystem (Landry and Kirchman, 2002). By incorporating the microbial loop, inner cycling within the loop and consumers from larger ecological

food webs, heterotrophic bacteria are the pathway of converting organic waste products (POM and DOM containing limiting nutrients) into a usable nutrient source that becomes available to higher trophic levels as biomass (Fuhrman and Azam, 1980) instead of losing such organic matter to the ocean floor. Heterotrophic bacteria provide a fluctuating (including e.g. grazing) but stable (due to the standing stock) supply of recycled organic matter, to sustain larger, more complex food webs that can in turn supply even larger ecosystems.

To date, little or no work on heterotrophic bacteria has been done in the KZN–B. Early studies performed by Schleyer (1980) on a sub–tidal reef, near Durban, were performed to assay heterotrophic bacterial potential from labelled algal extract. During the experiment, Schleyer (1980) determined an initial increase in bacterial proliferation which gradually declined with pleomorphic changes in the population, from an increase in the size of the dominant small cocci towards an increase in the abundance of rods and comma's. It has been shown previously by Fergusen and Rublee (1976), that while cocci are more abundant in coastal waters (80%), they are not as active as rod shaped bacterial cells. It can therefore be said, that in coastal areas, where the possibility of particulate matter and substrate material is high, as well as in areas of high organic nutrient input, that such pleomorphic changes within bacterial communities are possible, which can lead to increased bacterial numbers, biomass and productivity within the system.

The first phase of the African Coelacanth Ecosystem Programme (ACEP) was undertaken to understand the processes that support marine life. This was done by implementing numerous projects for biodiversity, genetics, environmental education and conservation planning including a KZN–B wide survey for gathering biological, chemical and geological data. As part of the second phase of ACEP (ACEP II), the KZN–B was surveyed in depth to determine and understand the dynamics (physical, geological and biological) of the ecosystem functioning within the study area. This project was undertaken to determine bacterial numbers, bacterial biomass and bacterial productivity within the KZN–B, and discuss the importance of heterotrophic bacteria within this oligotrophic system with regard to nutrient re–cycling, nutrient regeneration and resource availability. For this current work, I hypothesized that; 1. Bacterial populations vary seasonally; 2. Bacterial populations vary by depth; 3. Bacterial populations are distributed in close relation to their organic nutrient sources: and 4. Phytoplankton are distributed in close relation to their inorganic nutrient sources.

CHAPTER 2: MATERIALS AND METHODS

2.1: Sample Collection

Sea water samples were collected during two research cruises within the KZN–B aboard the F.R.S Algoa, one in the summer period of 22 January to 20 February 2010, and the next during the winter period of 21 July to 25 August 2010. Each cruise consisted of 2 parts, an initial synoptic cruise, and a focus cruise. The synoptic cruise entailed sampling the entire KZN–B within a short time, about 8 to 10 days, starting at the southernmost coastal station (Fig. 2.1.1, line 1 station 1), and sampling seaward along transect line 1, then turning north until the next transect line and sampling coastward. The focus cruise entailed sampling predetermined locations, each over a period of 2 days, 5 days apart over a 2 week period, starting at the most southward station and moving north.

During the summer cruise, representative stations within the KZN–B were sampled during the synoptic section (Fig. 2.1.1), with the focus sites being the Durban Eddy (Lat 31.155° E; longitude 29.925° S), Thukela mouth (Lat 31.608° E; Lon 29.231° S) and Richards Bay North (Lat 32.311° E; Lon 28.677° S). These sites were preselected for the prominent oceanographic features within their surrounding area. An additional site, named Mid shelf (Lat 31.671° E; Lon 29.458° S), was sampled en route, serendipitously chosen due to the green coloured surface water. During the summer cruise, 16 lines and 66 stations (including the focus) were sampled in total.

During the winter cruise (Fig. 2.1.2), representative stations for all major upwelling areas within the KZN–B were sampled during the synoptic section, with the focus sites being the Durban Eddy (Lat 31.155° E; Lon 29.924° S), Thukela mouth (Lat 31.608° E; Lon 29.230° S), Richards Bay South (Lat 32.025° E; Lon 29.184° S) and Richards Bay North (Lat 32.312° E; Lon 28.676° S). As for the summer cruise, these focus sites were preselected for the prominent oceanographic features within their surrounding area. For the focus site Richards Bay South, only one day of sampling was possible, due to harsh weather conditions. During the winter cruise, 8 lines and 28 stations (including the focus) were sampled in total.

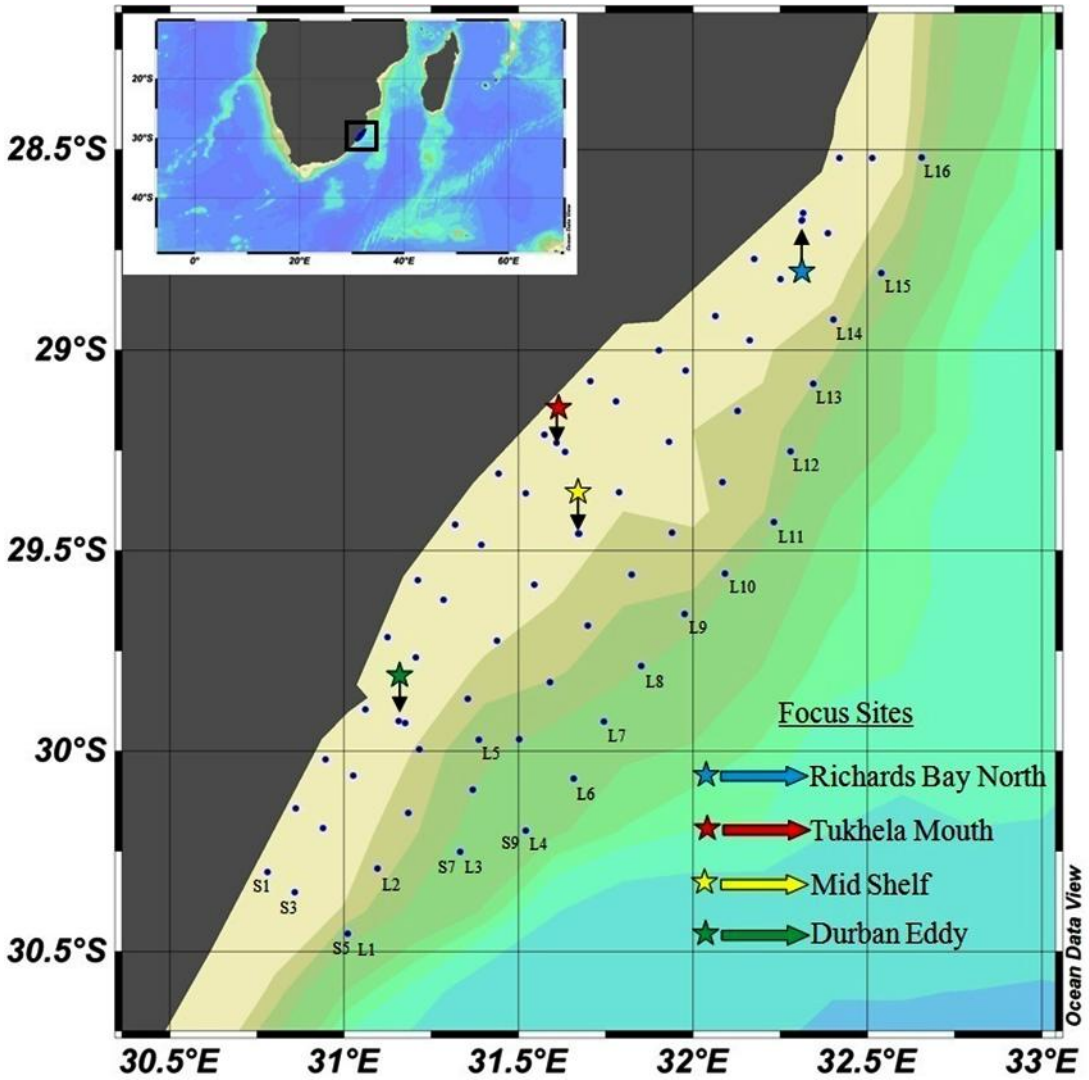

Figure 2.1.1: Synoptic (blue dots) and focus (colored stars) sampling locations within the KZN–B during the summer cruise. S1, S3, S5, S7 and S9 denote stations 1, 3, 5, 7 and 9 respectively throughout the KZN–B. L1, L2, L3, etc. denote transect lines 1, 2, 3, etc., respectively throughout the KZN–B.

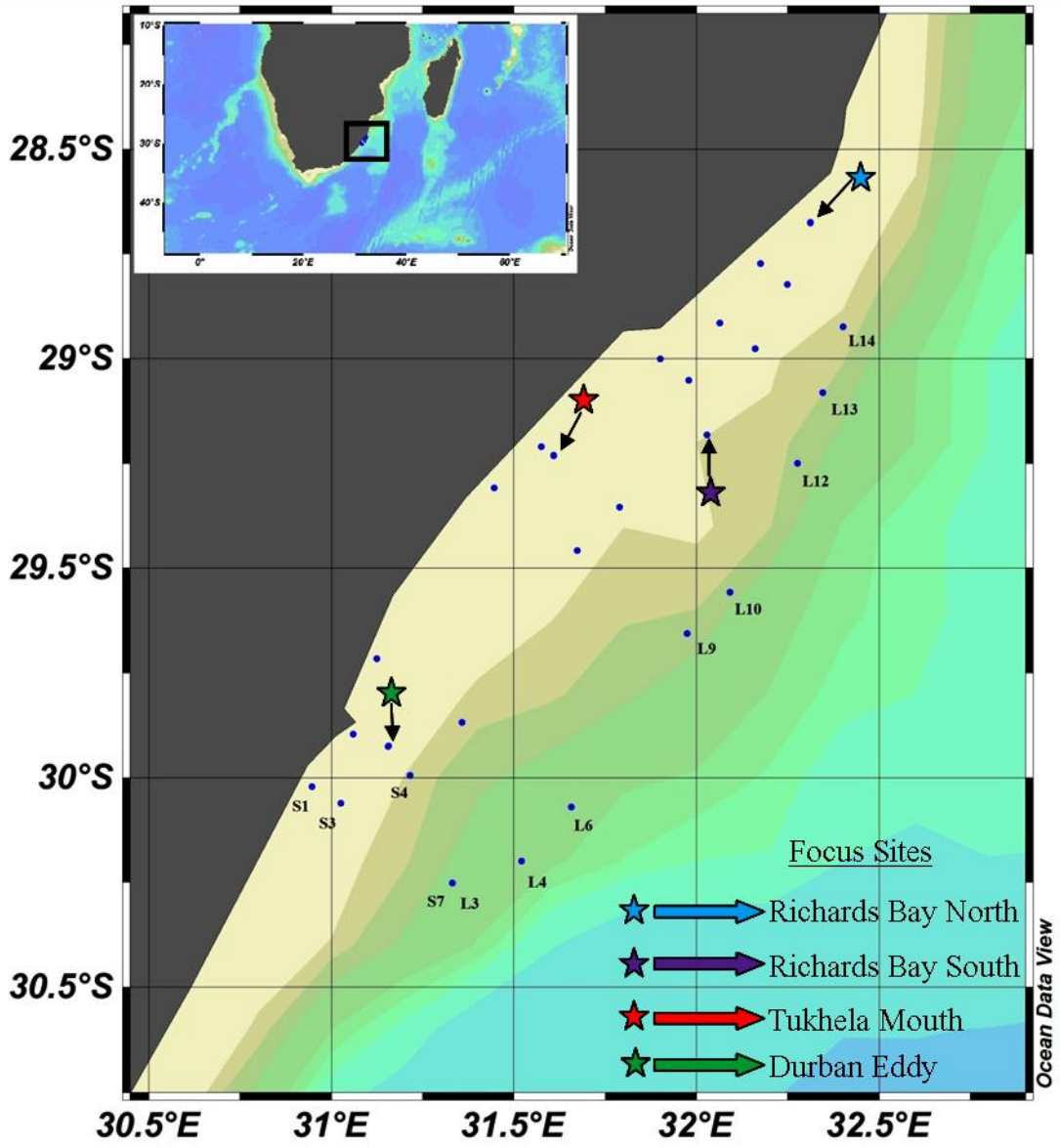

Figure 2.1.2: Synoptic (blue dots) and focus (colored stars) sampling locations within the KZN–B during the winter cruise. S1, S3, S4 and S7 denote stations 1, 3, 4 and 7 respectively throughout the KZN–B. L3, L4, L6, etc. denote transect lines 3, 4, 6, etc., respectively throughout the KZN–B.

For both cruises, CTD (conductivity temperature and depth) profile data was captured by means of a SBE 9plus CTD underwater unit (serial number: 9P32142–0746), with sea water samples collected using an attached 12 sample niskin bottle (5 L) rosette sampler. In waters shallower than 50 m, samples were taken at the surface, chlorophyll maximum (the depth at which phytoplankton were at their most dense as determined by *in situ* fluorometry, hereafter referred to as F–max) and near the bottom of the water column (hereafter referred to as bottom). In areas where waters were greater than

50 m in depth, four samples were taken including an intermediate sample between F–max and bottom. For the synoptic cruise, one 20 ml sub sample from each sampled depth was placed into a 20 ml scintillation vial (Sigma Aldrich, Z 190527 – 15AK, glass vial with foamed PE liner). Samples were fixed (4% f.c.) with borax–buffered formalin (made to saturation with commercially available Buffalo Borax and distilled autoclaved water) and stored in a cool area until back on land (within 9 days of the first sample being taken), where they were refrigerated (~ 5°C).

2.2: Bacterial Numbers and Biomass determination

Bacterial numbers and biomass were determined according to methods modified from Porter and Feig (1980), Hobbie et al. (1977) and Daley and Hobbie (1975). A 50% solution of DAPI (2.4 diamidino–6–phenylindole acid) was prepared by adding 1 mg DAPI DILACTATE (SIGMA – D9564–10MG) $\cdot ml^{-1}$ distilled autoclaved water which was kept frozen until use. A working solution of DAPI was made by adding 50 µl thawed stock DAPI to 1 ml distilled autoclaved filtered water in a foil wrapped bijou bottle. Working DAPI was used within 2 days.

From each seawater sample, after a thorough vortex to ensure homogeneity, between 2 and 5 ml was analysed. Working DAPI was added to the sample to make a final concentration of 0.25%. This was incubated in the dark for 5 min (Porter and Feig, 1980; Suzuki et al., 1993; Hymel and Plante, 1998). A supporting dampened Whatman® glass microfibre filter (Schleicher and Schuell, CAT No. 1822 – 025) was placed above the scintered glass of the filter apparatus, onto which a 0.22 µm black isopore filter (Sigma–Aldrich Z365130–100EA), or a 0.22 µm black polycarbonate filter (GE Water and Process Technologies, CAT No. K02BP04700) was placed. A brief vacuum at 0.43 $kp \cdot cm^{-2}$ was applied to flatten the nucleopore filter. The sample was briefly vortexed and pipetted into the filtering tower. This was followed by adding 10 ml of pre–filtered (0.2 µm) autoclaved seawater passed through a 0.22 µm disposable syringe filter (MILLEX® – GS, REF – SLGS033SS). Vacuum was applied at a constant suction of 0.43 $kp \cdot cm^{-2}$ until almost all fluids had passed through the filter. The sides of the filter tower were then rinsed with 5 ml of the above mentioned sterile seawater. After all liquids were drawn through, the vacuum was turned off, the filter removed, and placed in a foil lined petri dish. This procedure was performed for all samples to be evaluated by epifluorescent microscopy viewing.

Following the methods of Francisco et al. (1973) and Watson et al. (1977), the black isopore or polycarbonate filter was placed onto spread immersion oil (Agar Scientific) on a clean glass slide. This was followed by another drop of immersion oil and a cover slip (Francisco et al., 1973). All prepared samples were then viewed under UV illumination with a Nikon Eclipse 80i epifluorescent microscope

within 2.5 hours. The filter set comprised a UV – 2A filter with an excitation wavelength of 330 – 380 nm, dichromic mirror of 400 nm and barrier filter of 420 nm. The neutral density filter (NDF) was set at 4 for the summer samples and at 8 for the winter samples.* The software program NIS Elements F (NIKON) was used for image capture, using a Nikon Digital Sight DS–F1i digital camera for each sample. Ten random fields of view were digitally captured within the working filtered area, each field being 15115.11 μm^2 at 1000× magnification using an oil immersion lens.

2.3: Image Analysis

Image Pro–Plus (IPP) is an extremely powerful multifunctional image analysis program, used for processing images from any digital source. Using Image Pro–Plus v.6.2, macros (a list of preset computer program instructions set to be carried out on demand) were written to automatically stack unfocused images (see Appendix [stacking macro] and Fig. 2.3.1) and to count and size all objects (see Appendix [counting macro's]) within an adjustable segmentation (partitioning of a digital image) range (Fig. 2.3.2). Within the entire captured field of view, every cell, including possible cells with no definitive structure but enough emission to distinguish a pseudo edge (bright halos), other artefacts, as well as cells bright enough to be included within the set limits, were counted and measured (Fig. 2.3.3). All data were automatically captured and exported to a Microsoft (MS) Excel file for analysis.

* This change was by no means due to the difference between the two sample groups. It was found that during image capture with the NDF set at 4, and later analysis of the summer samples, that the high background light emissions impeded automated image analysis (see section 2.3). This I believe occurred by the formation of "pixelated" artificial halos or structures from image stacking (Fig. 2.3.2, white square), which were later counted as bacterial cells or artefacts (Fig. 2.3.3, white square), sometimes into the hundreds and thousands on one image. The decision to change to a higher NDF setting was therefore done purely to decrease the background light emission intensity from the filter during image capture, to reduce this effect of pixilation.

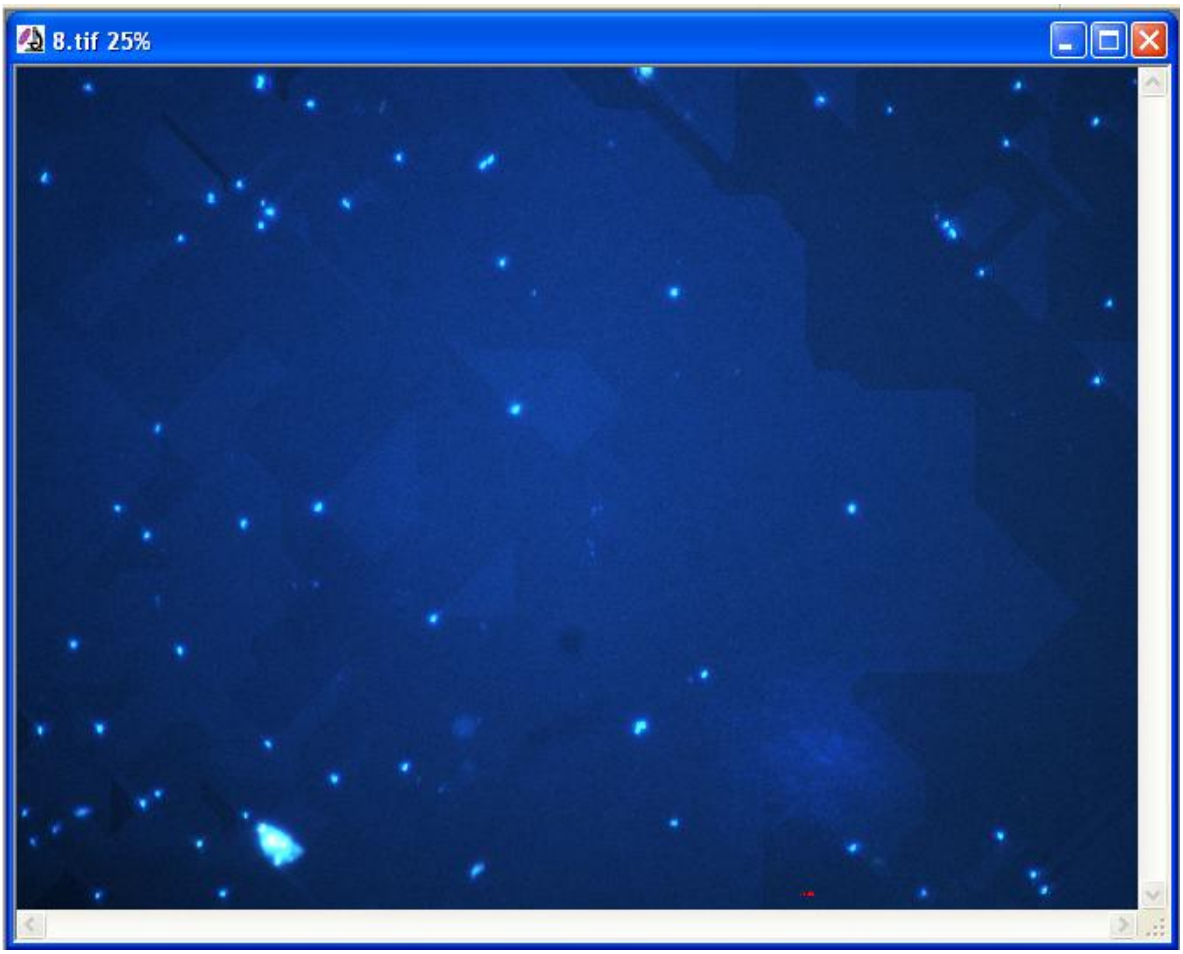

Figure 2.3.1: A stacked image made from numerous unfocused images to be used for automated counting and sizing.

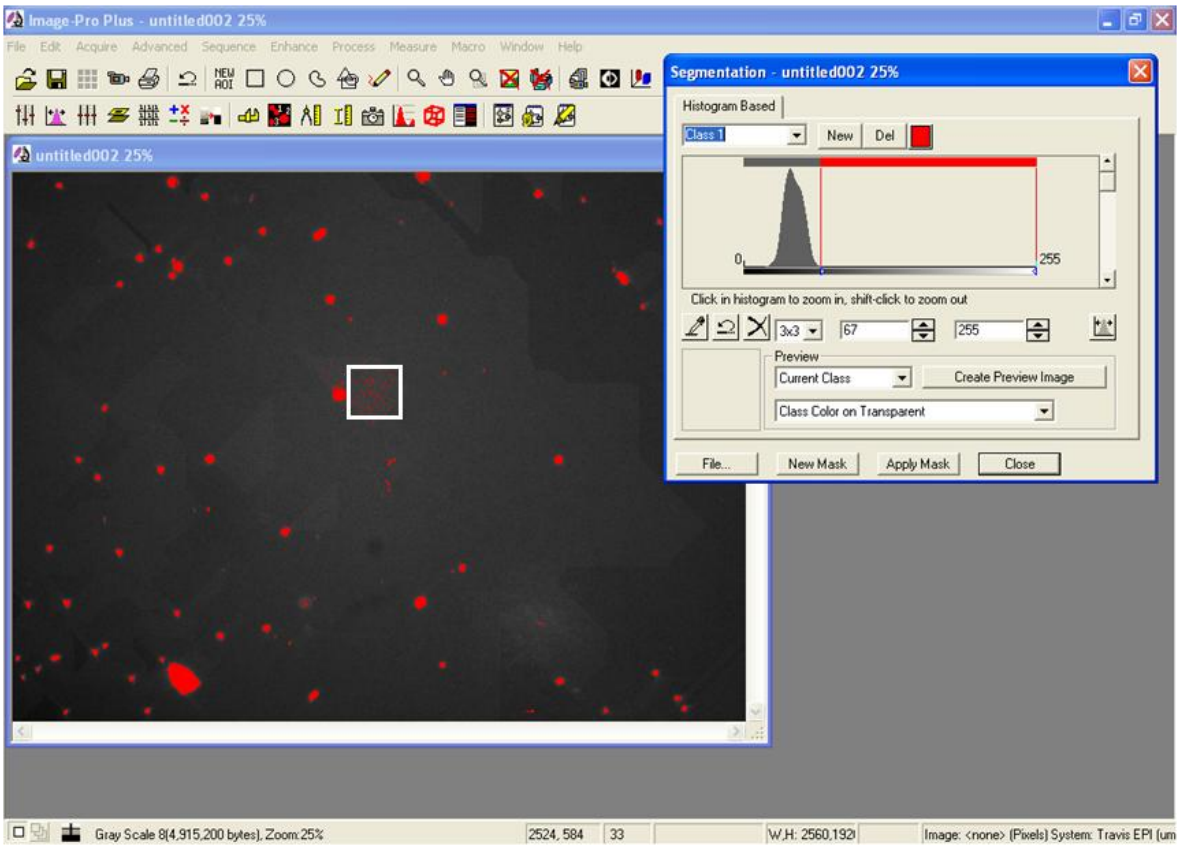

Figure 2.3.2: The adjustable segmentation range window found within Image–Pro Plus v.6.2. The histogram in the upper right is used when manually adjusting ranges for automatically counting and sizing cells. Shown here is the segmentation range of 67 to 255. The range here refers to the amount of segmentation (partitioning) that is required in order to eliminate unwanted pixels while keeping bacterial cells. Everything coloured red in the main window will be counted and sized based on this range. The white square encloses an area where the formation of pixelated halos or structures has occurred, seen as small red dots. Note that this figure is based on Fig. 2.3.1 from above.

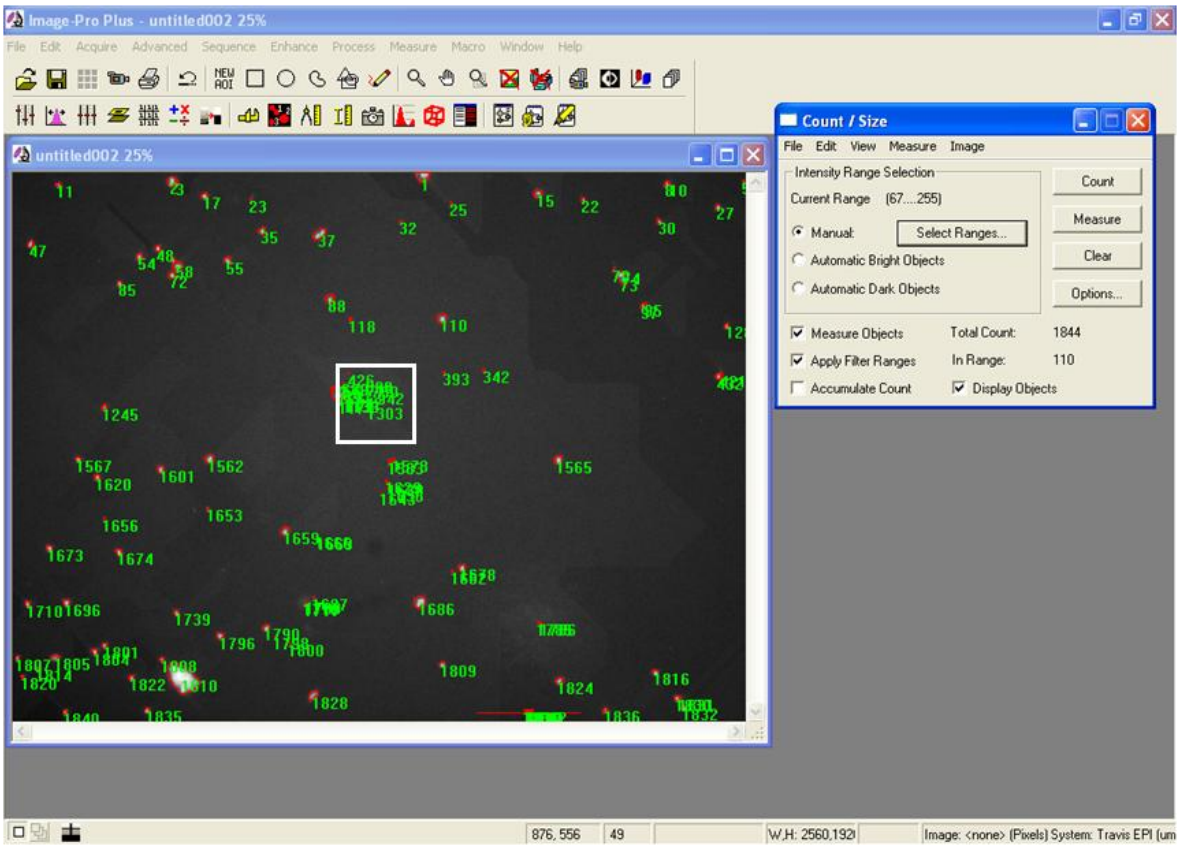

Figure 2.3.3: Automated counting window after segmentation selection and counting. Cells or artefacts that have been counted and sized are shown to have a red border, with a corresponding number in green. The white square encloses an area of counted pixilation. Note that this figure is based on Fig. 2.3.2 from above.

2.4: Data Analysis

Macros (see Appendix) were written using MS Excel VBA (Visual Basic for Applications) to automatically analyze and calculate the data within the Excel file captured from IPP. Basic codes for some of the more complex script were accessed from www1. (2010), www2. (2010), www3. (2010) and www4. (2010) and later rewritten or modified to comply with the macro format written here. The Excel macro was primarily written to delete data where object length was either < 0.2 µm or > 2.4 µm, and to delete data where object width was < 0.2 µm. The size ranges set within the present work were determined from previous work performed on surface seawater samples taken within the KZN–B in 2009, using scanning electron microscope images.

As part of my BSc Honours project in 2009 I performed an initial assessment to determine which microscopy method (using epifluorescent microscopy and scanning electron microscopy) was

best suited to counting and sizing bacterial cells. As part of this project, after running experiments on pure lab based bacterial cultures obtained and isolated from surface waters within the KZN–B (Durban), I determined that the use of the scanning electron microscope (SEM) gave an increased optical resolution without the presence of a halo in determining bacterial cell sizes. Also as part of this experiment, I used a live environmental sample taken in the same waters and at the same depth. What I found was the size ranges for this environmental sample, based on SEM images, ranged from 0.1 to 2.4 µm. I decided to increase the lower range to 0.2 µm as the SEM picked up 7.28% of the cell population (n = 302) falling within the 0.2 µm limit compared to 0.33% of the population with a size < 0.2 µm. By doing this, this would also help lessen pixilation when viewing cells under epifluorescent microscopy. The higher range of 2.4 µm was kept because 1. this was the maximum length of a cell found within the environmental sample within surface waters, and 2. during experiments on fed *Escherichia coli* cells, cells > 2.4 µm only accounted for 0.28% of the population (n = 721). The caveat of my BSc Honours study was that I only had access to surface water samples, and since reduced organic nutrients limit bacterial growth with increasing depth, it is entirely possible that the lower limit of 0.2 µm was insufficient in counting all cells, however, the filter pore size used for this MSc thesis was 0.22 µm and the chances of bacterial cells ≤ 0.2 µm passing through the filter pores is high. Given even that some micrococci cells did adhere to some filters during my BSc Honours work, these cells clumped together and would be individually indistinguishable if viewed under an epifluorescence microscope.

Based on my BSc honours work, the size ranges of < 0.2 µm or > 2.4 µm were set as I assumed that anything outside these limits was unlikely to be a bacterial cell (for this current work), and artefacts can be eliminated based on their large size (Schönholzer et al., 2002). In a study by Fergusen and Rublee (1976) on subsurface waters using the direct count method with Acridine Orange as their nucleic stain, 80% of their bacterial sample population were cocci, being ≤ 0.5 µm in diameter, while rod shaped cells accounted for 19.5%, with 94% of these rod shaped cells being 1 to 2 µm long.. I am therefore confident that the ranges set are sufficient to include all bacterial cells, and exclude any large detritus or artefact data captured.

Auto–calculation of bacterial numbers was done by including the following equation into the MS Excel macro to obtain total bacterial numbers·ml^{-1}:

$$N = (S_1 \times 10^6 \times n)/(S_2 \times V) \quad \text{.....(1)}$$

where N is the final bacterial population count from the sample (cells·ml^{-1}), S_1 is the working surface area of the filter used (1.77×10^2 mm^2), n is the total number of cells counted, S_2 is the total (10) area of field of view (151151.1111 µm^2) where n was acquired, and V is the volume (ml) of sample removed for analysis.

Auto–calculation of bacterial bio–volume data (in μm^3) from the captured length and width data from IPP was done by incorporating the following equation obtained from Bratbak (1985) into the MS Excel macro:

$$\mu m^3 = (\pi / 4) \times Width^2 \times [Length - (Width / 3)] \quad \text{.....(2)}$$

where width is the maximum linear width (µm) of the cell, and length is the maximum linear length (µm) of the cell.

Auto–calculation of bacterial biomass ($gC \cdot \mu m^{-3}$) from the above bio–volume equation was performed by including the following conversion factor from Bratbak (1985) into the MS Excel macro: 5.6×10^{-13} g of $C \cdot \mu m^{-3}$

2.5: Depth Integration and P / B ratio

Data from selected sites within selected lines making up four transects within the KZN–B (see Results) for Chl–*a*, bacterial numbers and bacterial biomass were integrated over depth. Integrated depth was calculated for each ecozone (see Results Fig. 3.1), representing the water column both above and below the sample depth, with the exception of the bottom ecozone where the water column above only was calculated. This was done by using the following equations:

$$S_{DI} = S_D \times 2 \quad \text{.....(3)}$$

$$F_{DI} = (F_D - S_{DI}) \times 2 \quad \text{.....(4)}$$

$$I_{DI} = (I_D - [F_{DI} + S_{DI}]) \times 2 \quad \text{.....(5)}$$

$$B_{DI} = (B_D - [I_{DI} + F_{DI} + S_{DI}] \quad \text{.....(6)}$$

$$DI = (S_{DI} \times S_V) + (F_{DI} \times F_V) + (I_{DI} \times I_V) + (B_{DI} \times B_V) \quad \text{.....(7)}$$

where S_{DI}, F_{DI}, I_{DI} and B_{DI} are the calculated depths (m) for the integration of the Surface, F–max, Intermediate and Bottom depths respectively. S_D, F_D, I_D and B_D are the depths (m) where the Surface, F–max, Intermediate and Bottom samples were respectively taken. DI is the final depth integration ($\cdot m^{-2}$) where the calculated depths of integration (S_{DI}, F_{DI}, I_{DI} and B_{DI}) are multiplied by the data value, S_V (Surface), F_V (F–max), I_V (Intermediate) and B_V (Bottom) for either Chl–*a* or bacterial numbers or bacterial biomass for that specific depth.

In some cases where the F–max and the Intermediate depths were close enough to give negative integrated values (usually in shallower waters), the following calculations were substituted:

$$F_{DIS} = (FD - S_{DI}) + ([I_D - F_D]/2) \quad \text{.....(8)}$$

$$I_{DIS} = (ID - F_{DIS}) + ([I_D - F_D]/2) \quad \text{.....(9)}$$

where F_{DIS} and I_{DIS} are the substituted calculations and values used instead of F_{DI} and I_{DI} respectively.

To compare the summer and winter cruise data, data were reintegrated to the deepest common depth (DCD). This was done by using the following calculation:

$$DI_{DCD} = (DI/DI_{TD}) \times DCD \quad \text{.....(10)}$$

where DI_{DCD} is the depth integrated data to the deepest common depth, DI is the calculated depth integration for a station (equation 7), DI_{TD} is the maximum depth of the water column (m) and DCD is the deepest common depth (m), taken as a whole number, for a particular line or station throughout the sampling area.

The P / B (productivity to biomass) ratio was calculated only for bacterial carbon. This was done by taking the bacterial biomass productivity (determined with ^{3}H–Thymidine) and dividing it by the paired sampled bacterial biomass (determined by epifluorescent microscopy) both from focus cruises.

2.6: Bacterial Productivity

Bacterial productivity was determined by a method adapted from Smith and Azam (1992). For the summer cruise, 1.3 ml and for the winter cruise, 1.8 ml of collected seawater was placed into three 2.0 ml eppendorf tubes preloaded with ^{3}H–Thymidine (20 nM f.c., 87 Ci·mmol^{-1}, American Radiolabeled Chemicals ART 0178A) on board the ship. A tube preloaded with ^{3}H–Thymidine and 100 µl trichloracetic acid (TCA) was used as a control. TCA was prepared beforehand to saturation (Sigma). All tubes were then mixed by inversion, wrapped in foil and incubated at sea surface temperature for 5 hours in a running seawater bath on board. After the incubation period, 100 µl of cold TCA was added to all tubes to stop the incubation. Tubes were then mixed by inversion and stored at −20°C in an onboard portable freezer. Tubes were later placed into a normal standing freezer when back on land. A 20 ml accompanying sample for population determination, to be assessed by epifluorescent microscopy, was also taken for each sample within the focus cruise. This sample was fixed and stored as above. All samples were analysed within one year of collection.

Still following the method adapted from Smith and Azam (1992), when back on land, samples were removed from the freezer, thawed at room temperature and pipetted into a 2 ml eppendorf tube. After a 30 second vortex, samples were centrifuged for 15 minutes at 10,000 × g. The supernatant was decanted. One ml of ice cold 5% TCA (prepared with autoclaved distilled water) was added. This was vortexed for 10 seconds, and centrifuged for 15 minutes at 10,000 × g. The supernatant was discarded as above, and 1 ml of scintillation cocktail (ReadySolv^{TM} HP – Beckman Coulter – P / N 510815–AC) was pipetted into the eppendorf tube. The pellet and cocktail were then vortexed for 30 seconds and the eppendorf cap removed. The eppendorf tube was then placed into a clean scintillation vial (Sigma Aldrich, Z 190527 – 15AK, glass vial with foamed PE liner) to be radio–assayed. Control vials for the scintillation count were prepared by adding 1 ml of scintillation cocktail to an eppendorf tube, without TCA or sample.

Samples were analysed with a Packard TRI–CARB 1900 TR Liquid Scintillation Analyzer in triplicate using protocol plug 10,* with external and internal calibration, and internal quench correction (Andrade et al., 2003). Unquenched standards (Packard – Unquenched Pico–Standards [5 ml] – serial # 6008400) and internal normalization and calibration were run before each batch sample run.

^{3}H–Thymidine incorporation rates (TTI, expressed as $pM \cdot L^{-1} \cdot h^{-1}$) by heterotrophic bacteria were calculated from the equation obtained from Wiebinga et al. (1997):

$$TTI = (DPM_S - DPM_C) \times (SV \times T \times SA \times 2.22)^{-1} \quad \text{.....(11)}$$

where DPM_S is the disintegrations of the sample per minute, DPM_C is the disintegrations of the control per minute, SV is the sample volume measured (L), T is incubation time (h) and SA is the specific activity of the radio–nucleotide ($Ci \cdot mol^{-1}$).

Conversion of TTI into bacterial numbers was performed by using the following mean conversion factor (2×10^{18}) obtained from DuFour and Torréton (1996):

$$Cells \cdot L^{-1} \cdot h^{-1} = (TTI / 10^{-12}) \times (2 \times 10^{18}) \quad \text{.....(12)}$$

* Protocol plug 10 consisted on the following machine settings. It was set to count ^{3}H by DPM (disintegrations per minute), with 1 cycle and a count time of 4.00 minutes for each sample. There was no 2 Sigma Coincidence set. It was also set for: counts per vial to 1; vials per sample to 1; vials per standard to 1; with the 1st vial being the background standard. The QIP was set to tSIE/AEC with no percentage of reference. The data mode was set to DPM with the ES Terminator set to count.

Calculation of bacterial carbon productivity was done by incorporating 34 fgC·cell^{-1} measured, obtained from Wiebinga et al. (1997):

$$gC \cdot L^{-1} \cdot h^{-1} = (Cells \cdot L^{-1} \cdot h^{-1}) \times (34 \times 10^{-15}) \quad \text{.....(13)}$$

2.7: Ocean Data View Plots

All oceanographic data plots were created using Ocean Data View 4.0 (Schlitzer, 2010) using DIVA (Data–Interpolating Variational Analysis) gridding.* Default settings for the X (20) and Y (20) scale length and the quality limit (2.5) were not changed. Colour mapping was kept linear for each graph which ensured maximum comparability differentiation of the colour scale (Z axis). The SNR (Signal to Noise Ratio) for the DIVA remained at the default of 50.00.

2.8: Common Data

Other data reported within this thesis but not described above were common data from the ACEP II cruise. Such data include temperature, salinity, silicate, phosphate, nitrate, nitrite, corrected fluorescence and Chl–*a* concentrations. All nutrient samples were analysed in the Marine Research Institute at the University of Cape Town using standard Astoria-Pacific techniques on a Technicon Autoanalyzer II which was adapted to an Astoria Nutrient Analyser (Astoria–Pacific Int., Clackamas, U.S.A.), while Chl–*a* biomass was determined using a WET Labs ECO–fluorometer (Philomath, U.S.A.) which was part of the CTD.

* DIVA is a gridding software that analyses and interpolates data within an algorithm to estimate data. DIVA plots can, and usually are, presented as color plots, and uses available input data sources to estimate data between actual data points. For this reason, when insufficient data is available to estimate, DIVA does not plot the estimated data (based on default settings). When this happens, areas of background white appear within the color data. Note that the appearance of a white background colour between the coloured data means the absence of data, and not a zero value.

2.9: Statistical Analysis

All statistical analysis was performed with IBM SPSS 21 for Windows. Two–way and three–way ANOVA's were performed on all bacterial, physico–chemical and Chl–*a* data with season, location (or a derivative thereof) and depth (ecozone) as main factors. When either assumption of normality and heterogeneity of the ANOVA was violated, data were transformed [log (x+1)]. If the assumptions were still violated after transformation, data were ranked in SPSS before performing the ANOVA.

CHAPTER 3: RESULTS

The results for the summer and winter, synoptic and focus cruises are presented below. Transect lines showing depth profiles within the KZN–B sampling area are shown. Transect 1 (T1) situated south of the KZN–B, is almost perpendicular to Durban, and crosses the area where the Durban Eddy is intermittently present. Within this "southern KZN–B", eddy derived nutrients are intermittent, and surface water is doubtfully affected by kinematically driven upwelling and edge shearing. Transects 2 (T2) and 3 (T3), situated within the KZN–B were selected because they run parallel to a major river mouth, the Thukela River. Within this "central KZN–B", the shelf is wide and water is possibly influenced by edge shear upwelling, upwelling from Richards Bay, the Thukela River and water movement. Transect 4 (T4) situated north of the KZN–B, running almost perpendicular to Richards Bay, was chosen because this is an area of proposed intense upwelling. Upwelling within this "northern KZN–B" is thought to be fresh due to the widening of the shelf within this area, forcing kinematically driven upwelling.

Within the results, reference is made to ecozones. I describe ecozones here as grouped sample depths representing a spatial depth where samples were taken. For example, throughout sampling, the F–max was never found at one depth, but over a range of depths. This created difficulties representing the data graphically. To counter this, I assigned the ecozone F–max or FE (see Fig. 3.1), for all samples taken at F–max, irrespective of depth. This means that throughout the F–max ecozone, values were all from the same grouped sample depth (ecozone), but varied by actual sample depth (m), even though data are plotted on an isosurface two dimension plot. The same was done for Surface or SE (surface ecozone), Intermediate or IE (intermediate ecozone) and for Bottom or BE (bottom ecozone).

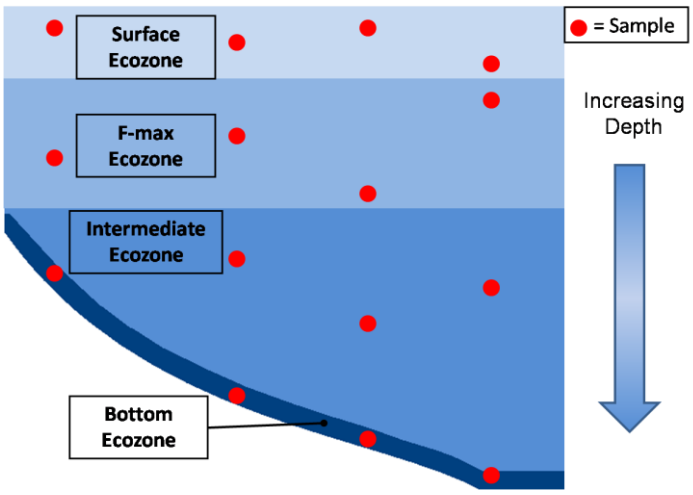

Figure 3.1: Graphical representation of grouped sample depths referred to as ecozones.

I have separated the KZN–B into three sections based on geographic features, such as the outcroppings of coastline that border the KZN–B to the North and South. For this thesis, I describe the southern KZN–B as consisting of survey lines 1 to 5, the central KZN–B as consisting of survey lines 6 to 12, and the northern KZN–B as consisting of survey lines 13 to 16.

3.1: Summer Cruise – Synoptic sampling sites

Results for the first cruise undertaken during the summer months of 2010, during the synoptic sampling of the KZN–B, are shown below. The majority of the data are presented as depth profiles along transect lines. Most of the figures have a corresponding inset for each transect showing the geographic location. For some figures, the space was too small to accommodate the inset, and only the label is present. For these cases, refer to a previous figure for geographic location.

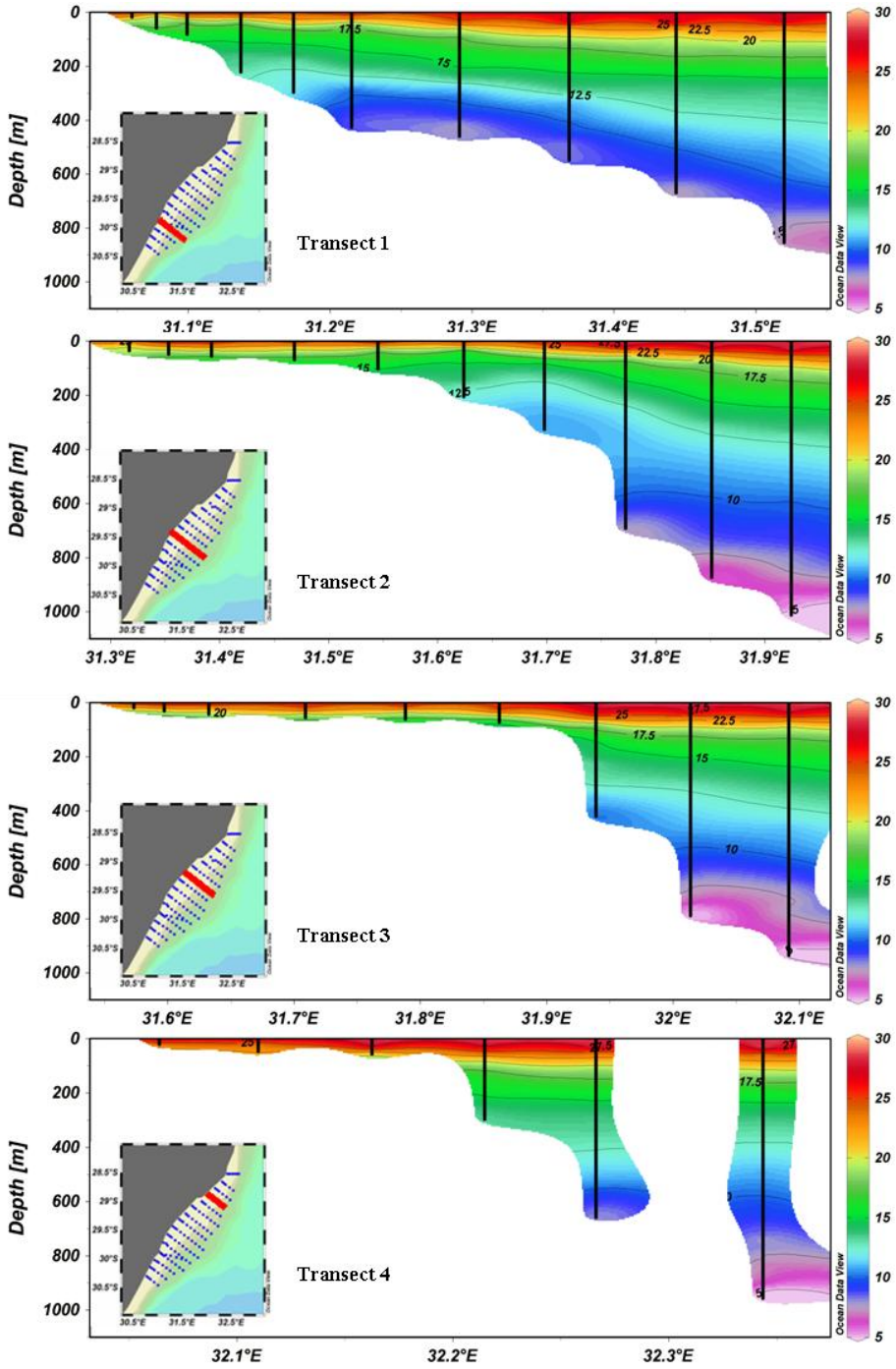

Figure 3.1.1: Temperature (°C) profile at selected survey lines through the KZN–B for the summer synoptic cruise using full CTD hydrographic data. Black vertical lines represent individual stations while contour lines represent isotherms. The inset within each image shows the location of the transect line in red.* All subsequent profiles are the same format.

* Note that the white background colour between the coloured data means the absence of data, and not a zero value. This applies to all figures presented.

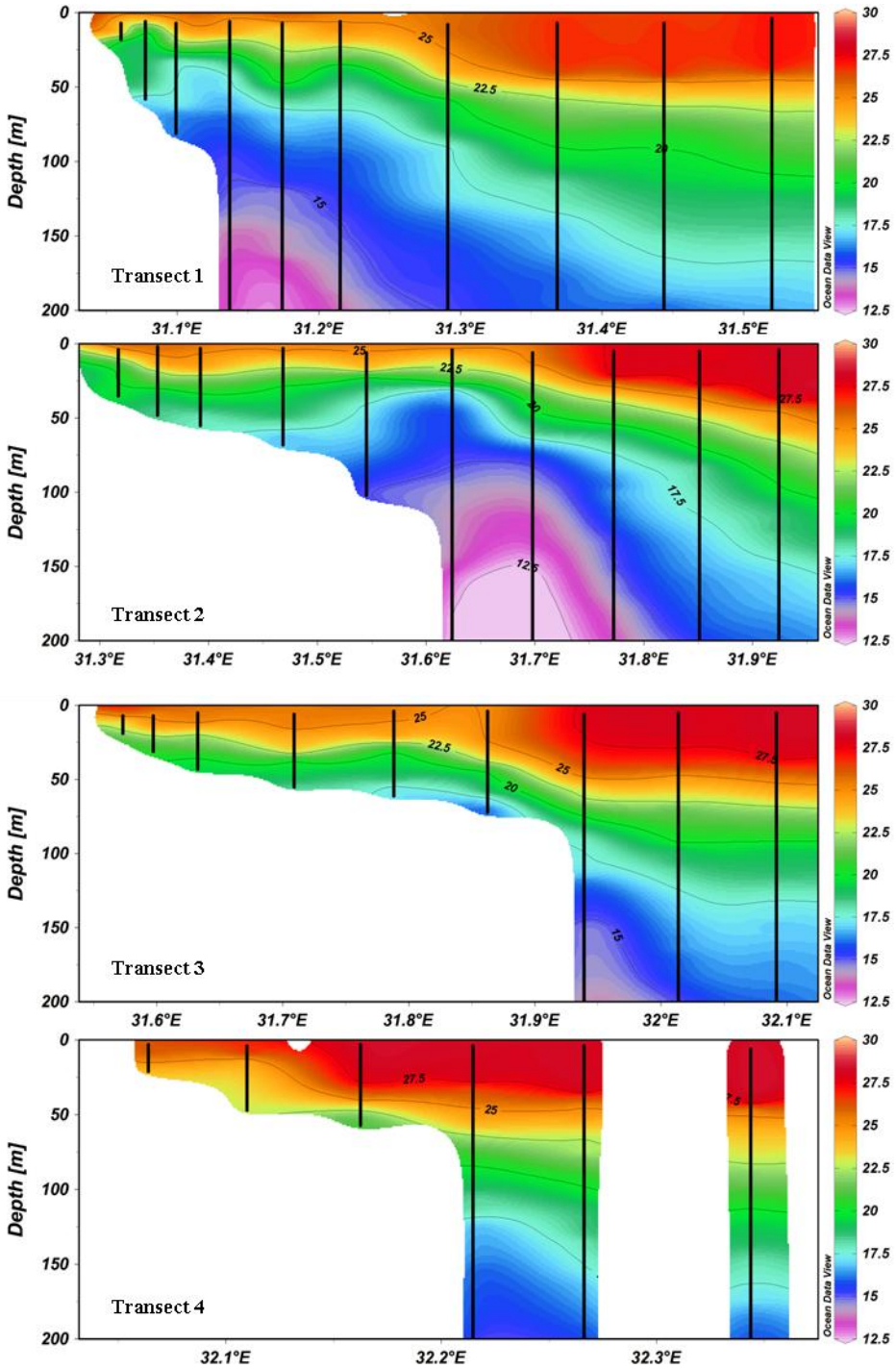

Figure 3.1.2: Temperature (°C) profile for the first 200 m at selected survey lines through the KZN–B for the summer synoptic cruise using full CTD hydrographic data.

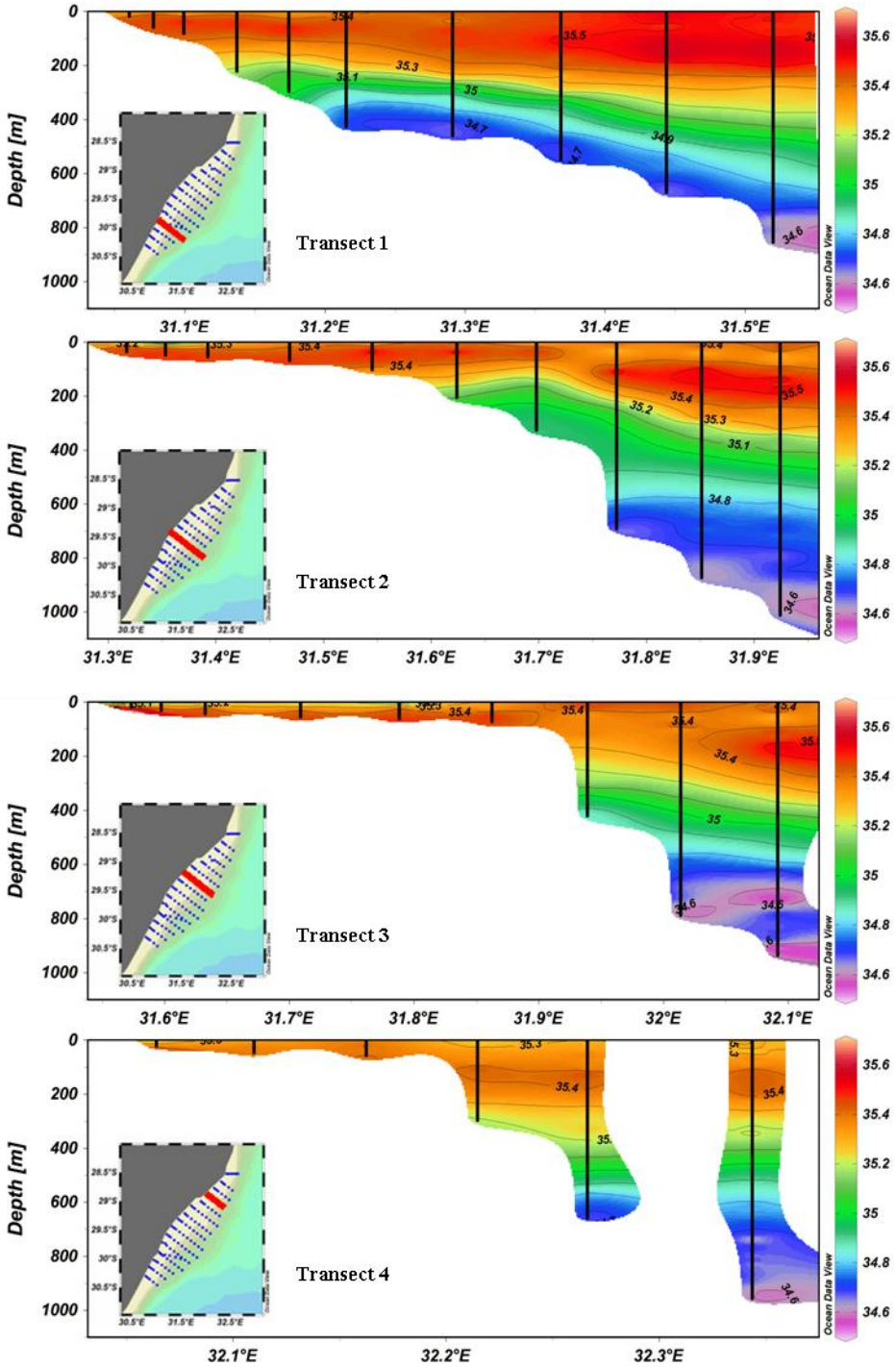

Figure 3.1.3: Salinity profile at selected survey lines through the KZN–B for the summer synoptic cruise using full CTD hydrographic data.

Temperature profiles show a layer of very warm (25 to 30°C), stratified water lying at the surface across the whole KZN–B (Figs. 3.1.1 and 3.1.2) with the northern KZN–B being the warmest ($F = 5.238$, df = 2, $p = 0.006$, post–hoc $p < 0.001$, Tbl. 3.5.7, pg 87), while overall temperatures ranged from 3.3 to 28.7°C. Below this very warm surface water, the thermocline (15 to 17.5°C) varies with depth throughout the KZN–B, appearing to be much shallower along T2 and T3 over the shelf. Elevated salinity levels appear to coincide with high temperatures within KZN–B surface waters (Figs. 3.1.1 to 3.1.3). Highest salinities were found above the thermocline as well as above the halocline with salinities ranging from 33.32 to 35.57, with the northern KZN–B showing the lowest salinity levels ($F = 7.315$, df = 2, $p = 0.001$, post–hoc $p < 0.05$, Tbl. 3.5.7, pg 87). The halocline was determined to be within the range of 35 to 35.1. Salinity levels were much higher over deeper waters off the shelf compared to more coastal and shelf associated waters showing a significant difference between ecozones ($F = 6.137$, df = 3, $p < 0.001$ Tbl. 3.5.7, pg 87). Below the thermocline, waters colder than 15°C were found, reaching about 5°C between 900 to 1100 m with a significant temperature difference found between ecozones ($F = 66.027$, df = 3, $p < 0.001$, Tbl. 3.5.7, pg 87). Salinity levels also decreased with depth below the halocline to a minimum of 34.6 between 900 to 1100 m. Along T1, water colder than 10°C and between 34.7 and 34.9 extended well onto the shelf up to about 300 m. This extension of cold, less saline water is not present along the other transects, with this water type lying well below the shelf between 600 to 800 m. Along T2, a cold and less saline “protuberance” (distension) rises to within about 100 m of the surface between 31.6°E and 31.75°E (Figs. 3.1.1 and 3.1.3), coinciding with a steep drop or rise in bottom topography between 31.75°E and 31.8°E. This appears to raise the thermocline and halocline at this location, while only constricting the thermocline.

Figs. 3.1.4 to 3.1.7 below present data for nutrients that was accessible to all members of the ACEP II team as common data. These include silicate, phosphate, nitrate and nitrite. Minimum and maximum values recorded from the whole KZN–B sampling area, for the summer cruise, for each nutrient are as follows; silicate: below the detection limit (0.01) to 37.52 µmol $Si \cdot L^{-1}$; phosphate: below the detection limit (0.01) to 2.09 µmol $P \cdot L^{-1}$; nitrate: below the detection limit (0.01) to 29.5 µmol $N \cdot L^{-1}$ and nitrite: below the detection limit (0.01) to 1.41 µmol $N \cdot L^{-1}$, respectively.

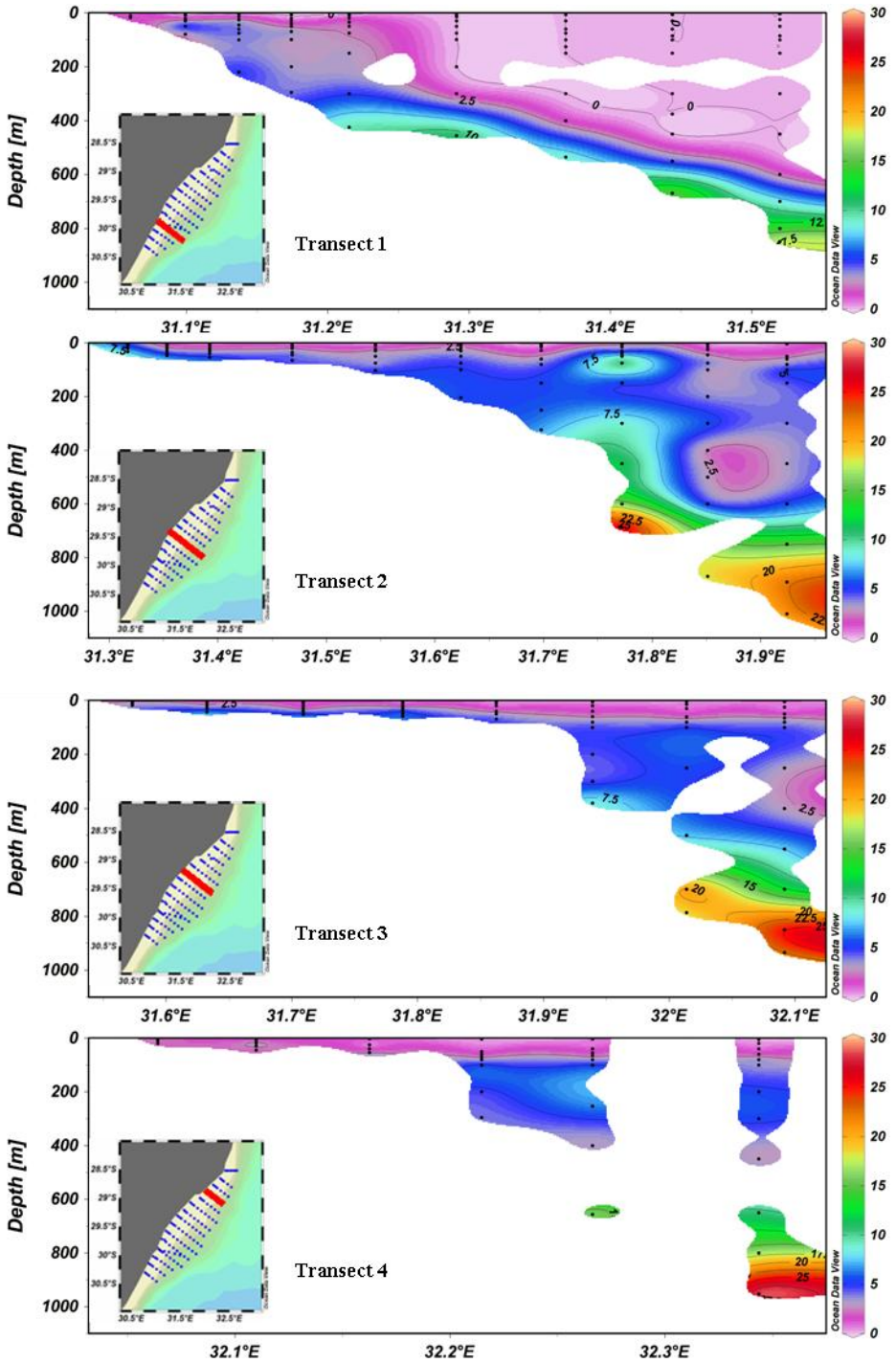

Figure 3.1.4: Silicate (µmol Si·L^{-1}) profile at selected survey lines through the KZN–B for the summer synoptic cruise using full bottle collection data.

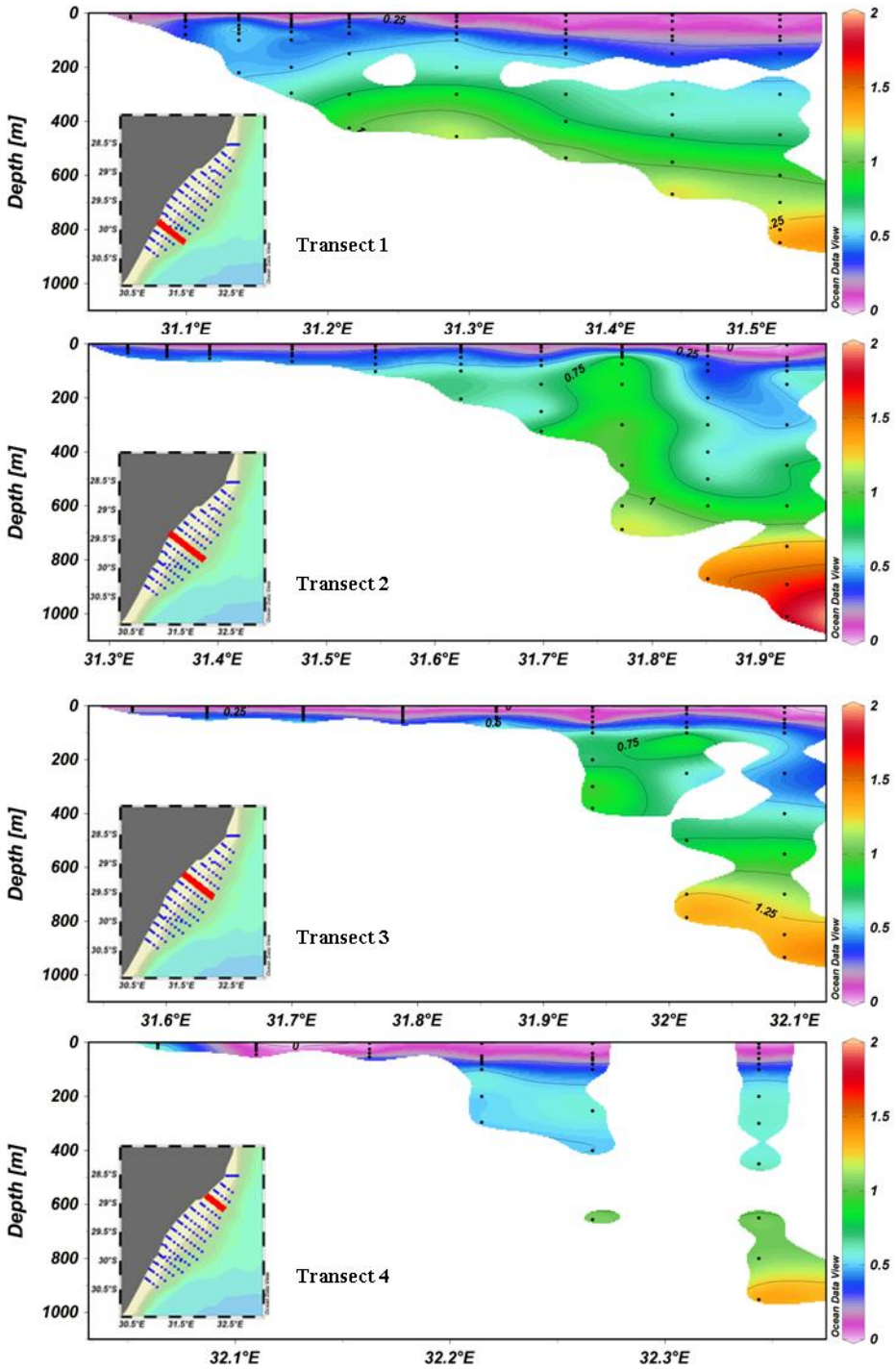

Figure 3.1.5: Phosphate (µmol P·L^{-1}) profile at selected survey lines through the KZN–B for the summer synoptic cruise using full bottle collection data.

Silicate concentrations within the surface waters of the KZN–B were very low during the time of study (Fig. 3.1.4) with the BE showing the highest concentrations ($F = 29.943$, $df = 3$, $p < 0.001$, post–hoc $p < 0.001$, Tbl. 3.5.7, pg 87), with the whole KZN–B ranging from below the detection limit (0.01) to 37.52 μmol $Si \cdot L^{-1}$. Silicate concentrations found along T1 for most of the water column, up to about 300 m, were below the detection limit with a significant difference found between the southern KZN–B, having the lowest concentrations, and the other sections ($F = 22.018$, $df = 2$, $p < 0.001$, post–hoc $p < 0.001$, Tbl. 3.5.7, pg 87). For T2 to T4, silicate concentrations increased with depth as well as with distance from the coast within the water column. T1 on the other hand showed increased silicate concentrations, but only along or very close to the bottom. Within the four transects, the highest silicate concentration was found below 800 m with a maximum of 28.41 μmol $Si \cdot L^{-1}$. Along T1, as for temperature (Fig. 3.1.1) and salinity (Fig. 3.1.3) where colder less saline water extended onto the shelf, water with higher silicate concentrations up to 10 μmol $Si \cdot L^{-1}$ extended up onto the shelf. This extension, as for temperature and salinity was not present within the other transects representing the KZN–B. The "protuberance" (distension) as reported for temperature and salinity above was also present along T2 within the same geographic location.

Phosphate concentrations within the surface waters of the KZN–B were low during the time of study (Fig. 3.1.5) with the BE and IE showing significantly higher concentrations ($F = 42.599$, $df = 3$, $p < 0.001$, post–hoc $p < 0.001$, Tbl. 3.5.7, pg 87), with the whole KZN–B ranging from below the detection limit (0.01) to 2.09 μmol $P \cdot L^{-1}$. The extension of water onto the shelf seen along T1 carried with it higher phosphate concentrations up to 0.75 μmol $P \cdot L^{-1}$. T2 and T3 within the central KZN–B showed phosphate concentrations to be higher below the surface waters compared to T1 and T4 over deeper waters, although no statistical difference was found between sections ($F = 0.104$, $df = 2$, $p = 0.901$, Tbl. 3.5.7, pg 87). The "protuberance" as previously reported along T2 appears to have increased phosphate concentrations closer to the surface waters along this transect. T4 within the northern KZN–B showed much lower phosphate concentrations between 100 and 400 m, about 0.55 μmol $P \cdot L^{-1}$, compared to the other transects with about 0.75 μmol $P \cdot L^{-1}$. As seen with silicate (Fig. 3.1.4), phosphate concentrations increased with distance from the coast as well as with depth.

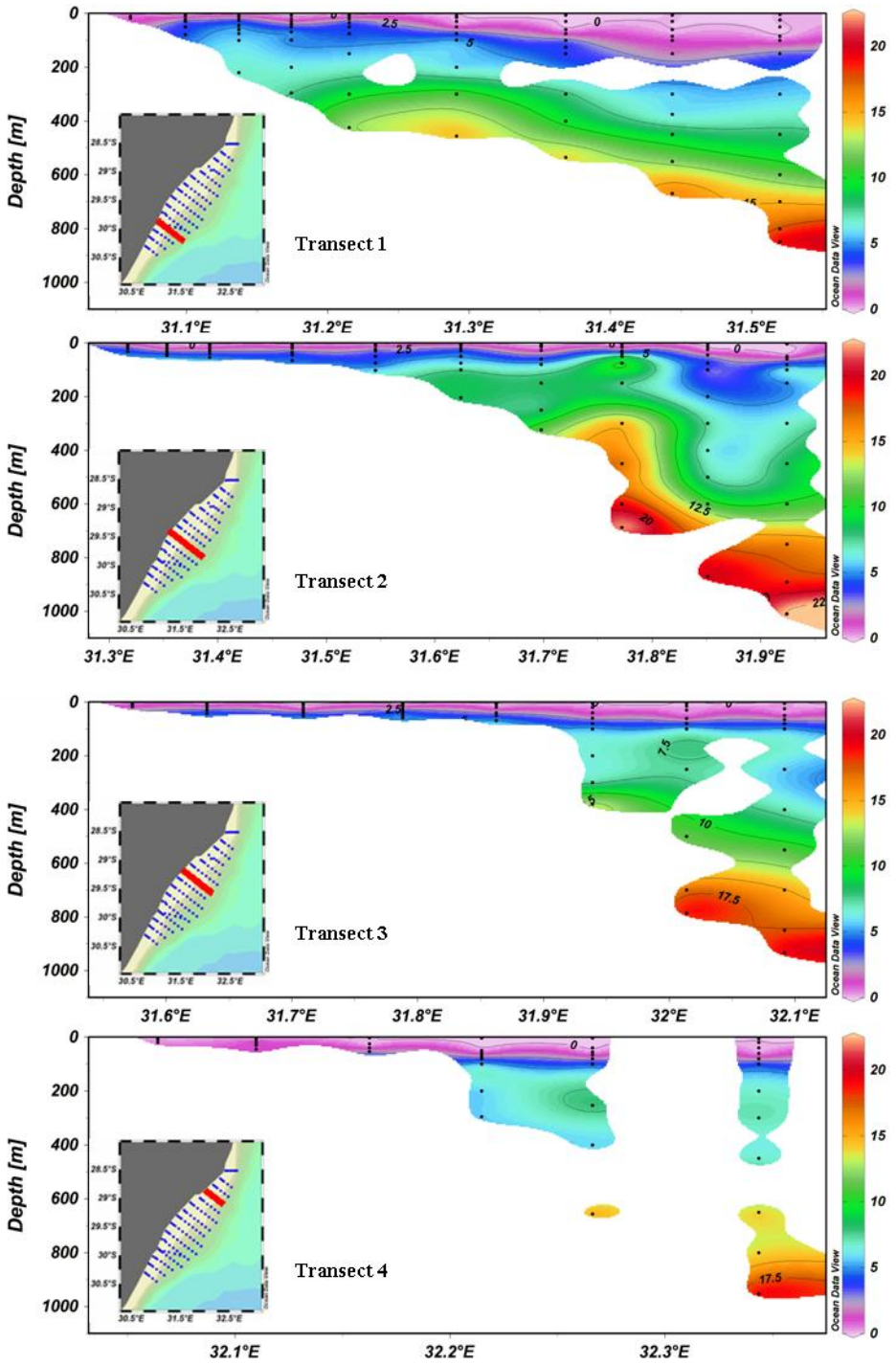

Figure 3.1.6: Nitrate (µmol N·L^{-1}) profile at selected survey lines through the KZN–B for the summer synoptic cruise using full bottle collection data.

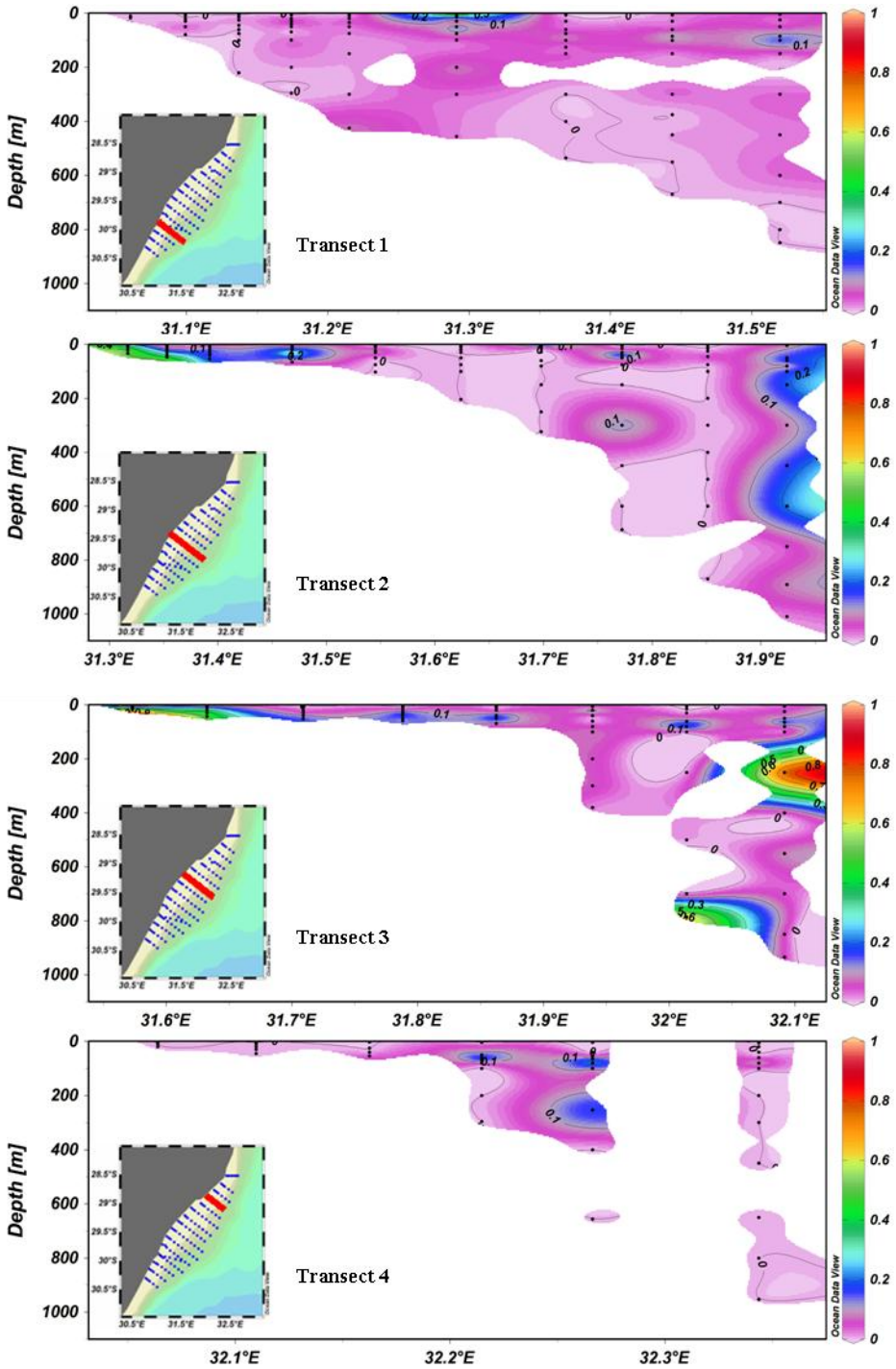

Figure 3.1.7: Nitrite (µmol N·L^{-1}) profile at selected survey lines through the KZN–B for the summer synoptic cruise using full bottle collection data.

Nitrate concentrations within the KZN–B (Fig. 3.1.6) were very similar to the spatial concentrations of phosphate (Fig. 3.1.5), with nitrate concentrations ranging from below the detection limit (0.01) to 29.5 μmol $N{\cdot}L^{-1}$. Surface waters showed low nitrate concentrations during the time of sampling with concentrations increasing with depth ($F = 65.396$, df = 3, $p < 0.001$, post–hoc $p < 0.001$, Tbl. 3.5.7, pg 87) as well as with distance from the coast. The water extension on the shelf along T1 carried with it water with nitrate concentrations of about 10 μmol $N{\cdot}L^{-1}$ up to about 300 m. T2 and T3 within the central KZN–B showed the most variability in nitrate concentrations with depth over deeper waters. Nitrate concentrations within the "protuberance" along T2 were higher near surface waters with about 7.5 μmol $N{\cdot}L^{-1}$ near 100 m. The highest concentration of nitrate within the four transects was found along T2 below 900 m with about 22 μmol $N{\cdot}L^{-1}$. Nitrate concentrations along T4 within the northern KZN–B, as for phosphate, were lower between 100 and 400 m compared to the other transects, however the data were not significantly different between sections ($F = 0.080$, df = 2, $p = 0.923$, Tbl. 3.5.7, pg 87). Nitrate patterns within the deeper waters, below 800 m for all transects, showed higher concentrations of at least 17.5 μmol $N{\cdot}L^{-1}$, with overall significantly higher nitrate concentrations at the IE and BE ($F = 65.396$, df = 3, $p < 0.001$, post–hoc $p < 0.001$, Tbl. 3.5.7, pg 87), where phosphate concentrations (Fig. 3.1.5) at the same depths were variable.

Nitrite concentrations for the majority of the water column of the KZN–B as represented by the four transects was below the detection limit during the time of sampling (Fig. 3.1.7) and ranged from below the detection limit (0.01) to 1.41 μmol $N{\cdot}L^{-1}$. Nitrite concentrations within the surface waters as well as with depth and distance from the coast were extremely variable. Nitrite concentrations within the FE were statistically higher than those of the other ecozones ($F = 5.140$, df = 3, $p = 0.002$, post–hoc $p < 0.05$, Tbl. 3.5.7, pg 87). Highest surface nitrite concentrations were found along T2 and T3 near the coast within the upper 50 m of the water column, as well as at the end of the transect sampling lines near open water. The highest nitrite concentration was found along T2 at the end of the sample line near 200 m with around 0.8 μmol $N{\cdot}L^{-1}$. For previous nutrient data (silicate, phosphate and nitrate) where the highest respective concentrations were found with depth below 800 m, for nitrite, with the exception of T3, highest concentrations were present within the water column above 800 m.

Figs. 3.1.8 to 3.1.10 below present corrected fluorescence and Chl–*a* data that were accessible to all members of the ACEP II team as common data. Minimum and maximum values recorded from the whole KZN–B sampling area, for the summer cruise, for corrected fluorescence were 0 and 4.243 $mg{\cdot}m^{-3}$, while for Chl–*a* was 0.003 and 2.492 $mg{\cdot}m^{-3}$, respectively.

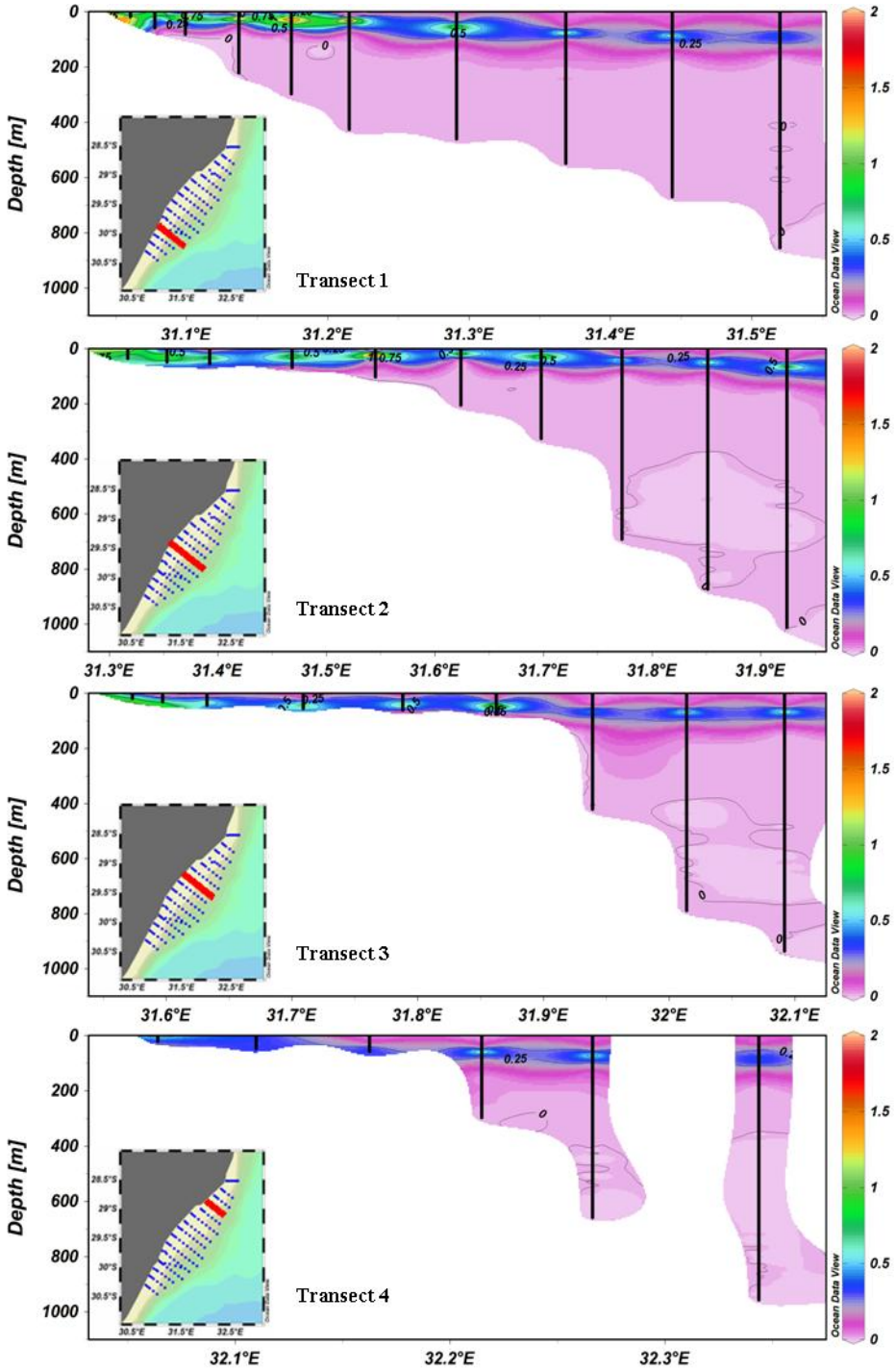

Figure 3.1.8: Corrected fluorescence ($mg \cdot m^{-3}$) profile at selected survey lines through the KZN–B for the summer synoptic cruise using full CTD hydrographic data.

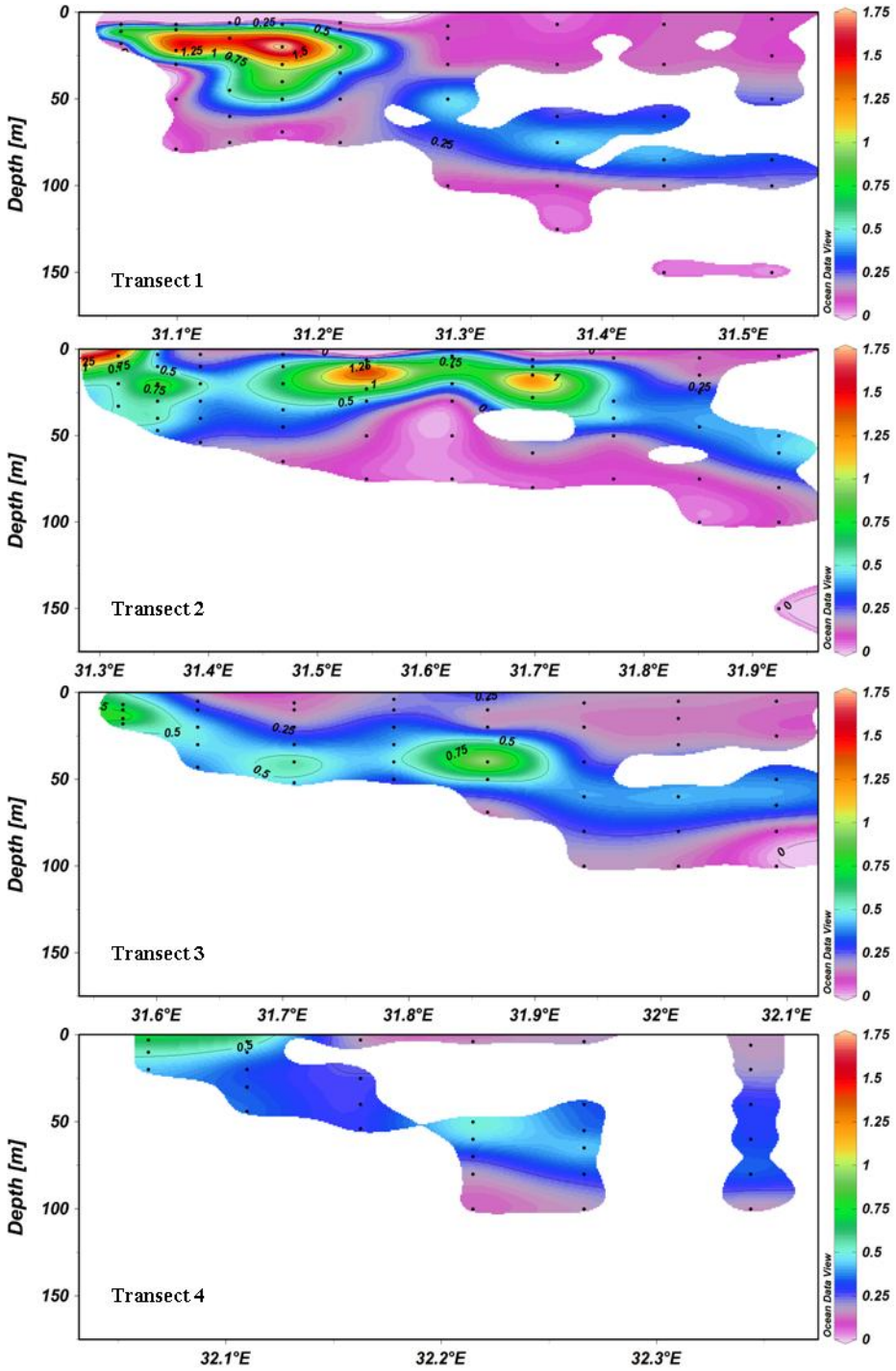

Figure 3.1.9: Chlorophyll–*a* (mg·m^{-3}) profile at selected lines through the KZN–B for the summer synoptic cruise using full bottle collection data.

Corrected fluorescence values for the KZN–B (Fig. 3.1.8), a proxy for Chl–*a*, indicate that all of the data collected during this first cruise was within the upper 150 m and ranged from 0 to 4.243 mg·m^{-3}. Below 150 m, corrected fluorescence values for all transects throughout the water column were below the detection limit. Sample waters for Chl–*a* as collected by bottle data (Fig. 3.1.9)

indicate that the majority of the Chl–*a* was present within the upper 50 m of the water column and ranged from 0.003 to 2.492 mg·m^{-3}, with the FE showing the highest Chl–*a* concentrations (F = 43.269, df = 3, $p < 0.001$, post–hoc $p < 0.001$, Tbl. 3.5.7, pg 87) followed by the SE. Higher Chl–*a* values were found within T1 to T3, up to 1.5 mg·m^{-3}, with T4 showing low Chl–*a* detection, about 0.6 mg·m^{-3}, however no statistical difference was found between sections (F = 1.109, df = 2, $p = 0.332$, Tbl. 3.5.7, pg 87). Chl–*a* measurements were higher nearer to the coast as well as around river mouths (the Thukela and Mvoti), but were overall variable and patchy (Fig. 3.1.10). Chl–*a* data integrated by depth are presented further on (Tbl. 3.1.1).

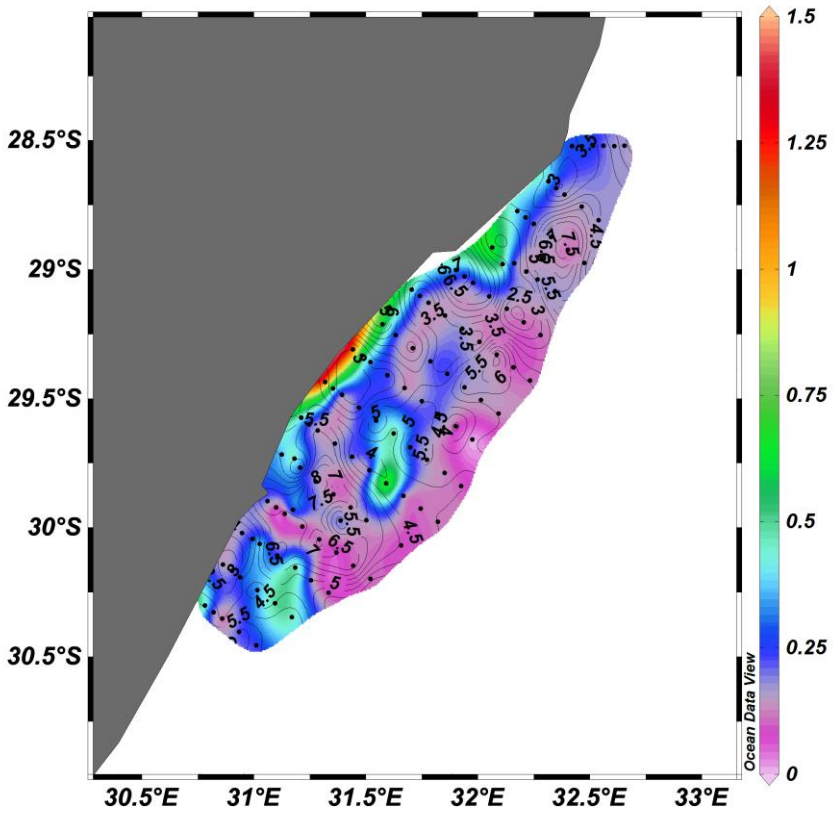

Figure 3.1.10: Chlorophyll–*a* (mg·m^{-3}) isosurface plot for the summer cruise, surface ecozone, using all available data. Contour lines show approximate depth (m) of sampling. Sampling stations in the background are shown as black dots. All subsequent profiles are the same format.

Figs. 3.1.11 and 3.1.12 below present ecozone (see Fig. 3.1) bacterial data (numbers and biomass) that were the focal point of this study. Minimum and maximum values recorded from the whole KZN–B sampling area, for the summer cruise, for bacterial numbers were 3.75×10^{3} and 6.20×10^{5} cells·ml^{-1}, and for bacterial biomass was 2.97×10^{-10} and 1.83×10^{-7} gC·ml^{-1}, respectively.

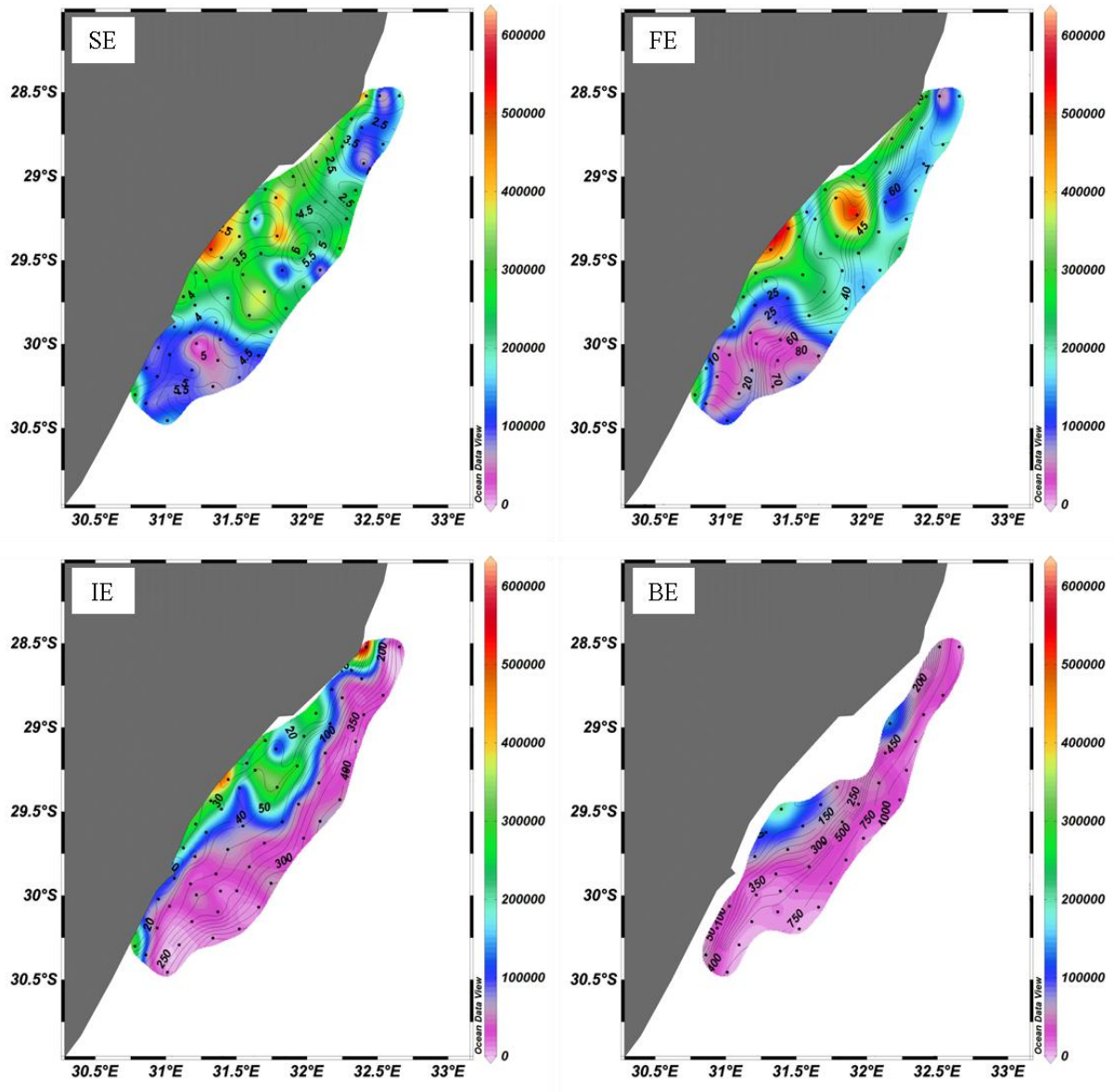

Figure 3.1.11: Bacterial numbers (cells·ml^{-1}) isosurface plots for the summer cruise, sample depths. The ecozones that are plotted are: SE (Surface Ecozone); FE (F–max Ecozone); IE (Intermediate Ecozone) and BE (Bottom Ecozone).

Bacterial numbers within the surface waters of the KZN–B (SE and FE) were higher within the central KZN–B (lines 6 to 12) between Durban and Richards Bay (Fig. 3.1.11) compared to the remainder of the KZN–B. Statistical evaluation showed statistically higher numbers in the SE and FE compared to the IE and BE ($F = 16.748$, $df = 3$, $p < 0.001$, post–hoc, $p < 0.001$, Tbl. 3.5.3, pg 85), but there was no significant difference between sections ($F = 1.372$, $df = 2$, $p = 0.255$, Tbl. 3.5.3, pg 85). Bacterial numbers for the whole KZN–B ranged from 3.75×10^{3} to 6.20×10^{5} cells·ml^{-1}. Bacterial numbers were higher closer to the coast line, extending north along the coast past Richards Bay, as well as around river mouths (the Thukela and Mvoti) within the central KZN–B. Within the sampling

area to the north of Richards Bay, bacterial numbers were higher along the coast line (SE, line 14 station 1) with 3.42×10^5 cells·ml^{-1}, compared to bacterial numbers closer to the open ocean (SE, line 14 station 5) with 6.21×10^4 cells·ml^{-1}. Bacterial numbers to the south of Durban, still within the surface waters extending out towards the open ocean (SE, line 3 station 7, 8.67×10^3 cells·ml^{-1}), were much lower than bacterial numbers found within the central (SE, line 8 station 9, 2.45×10^5 cells·ml^{-1}) and northern (SE, line 15 station 5, 1.51×10^5 cells·ml^{-1}) sections of the KZN–B within the same ecozone. However there was no significant difference between sections ($F = 1.372$, $df = 2$, $p = 0.255$, Tbl. 3.5.3, pg 85). Within the IE, bacterial numbers found above 100 m were higher than bacterial numbers found below 100 m within the IE and the BE, with bacterial numbers dropping below 100 000 cells·ml^{-1} below 150 m. The highest concentration of bacterial cells was found within the IE, line 16 station 1, at 35m with 6.20×10^5 cells·ml^{-1}.

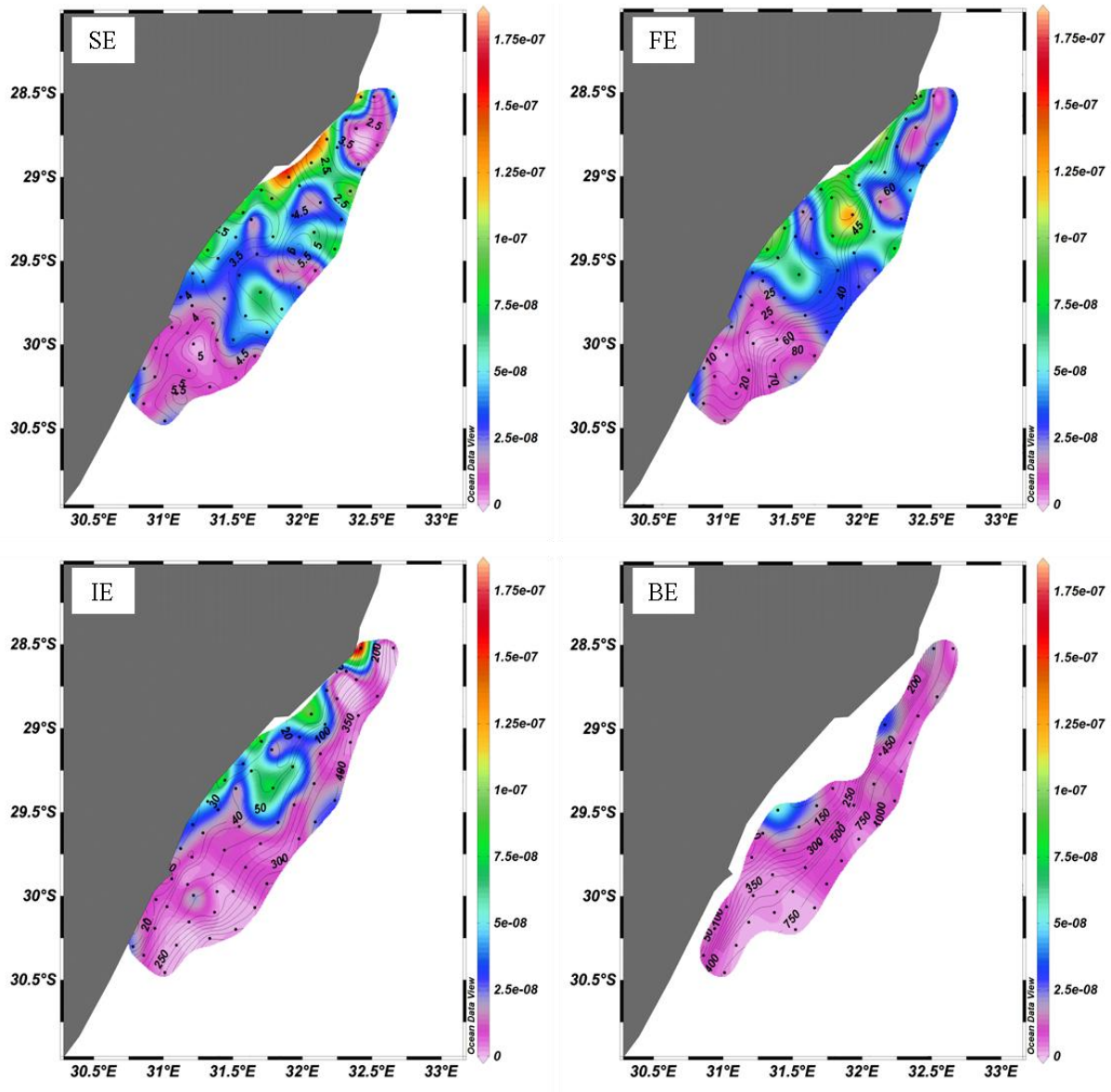

Figure 3.1.12: Bacterial biomass ($gC \cdot ml^{-1}$) isosurface plots for the summer cruise, sample depths. The ecozones that are plotted are: SE (Surface Ecozone); FE (F–max Ecozone); IE (Intermediate Ecozone) and BE (Bottom Ecozone).

Bacterial biomass (Fig. 3.1.12) follows the same patterns as bacterial numbers (Fig. 3.1.11) with bacterial biomass ranging from 2.97×10^{-10} to 1.83×10^{-7} $gC \cdot ml^{-1}$. Higher concentrations of bacterial biomass within the surface waters (SE and FE) of the KZN–B, although patchy, appear also to be limited to within the central section of the KZN–B between Durban and Richards Bay. Post–hoc tests performed within the ANOVA as described above, confirm the statistical difference for bacterial biomass between the SE and FE compared to the IE and BE ($F = 6.931$, $df = 3$, $p < 0.001$, post–hoc $p < 0.05$, Tbl. 3.5.4, pg 85). But no statistical difference was found between sections ($F = 1.593$, $df = 2$, $p = 0.205$, Tbl. 3.5.4, pg 85). Higher bacterial biomass also appears to be limited to the coast line as well as near Richards Bay and around river mouths (the Thukela and Mvoti) within the central KZN–

B. Higher bacterial biomass within the IE appears to be limited to areas around the Thukela and Mvoti rivers and near Richards Bay. Bacterial biomass below 150 m within the IE and the BE was lower than 2.6×10^{-8} gC·ml^{-1}, while the highest for all ecozones was found within the IE at line 16 station 1, at 35m with 1.83×10^{-7} gC·ml^{-1} matching the location for highest bacterial numbers.

Table 3.1.1: Chlorophyll–*a* (Chl–*a*) and bacterial numbers and biomass data integrated by maximum (max) depth for the summer cruise. Lines 4, 8, 10 and 13 correspond to transect 1, 2, 3 and 4 respectively. The three stations within each line correspond to a coastal station (1st station), shelf station (2nd station) and an ocean station (3rd station). Note that bacterial biomass here is presented as mgC·m^{-2} to match the units of Chl–*a*.

			Depth Integration (·m^{-2} sea surface)		
Line	**Station**	**Max depth (m)**	**Chl–*a* (mg)**	**Numbers (cells)**	**Biomass (mgC)**
	1	17.88	8.27	2.36×10^{6}	2.68×10^{-4}
4	4	424.98	20.70	1.35×10^{7}	4.96×10^{-3}
	8	849.58	47.16	2.22×10^{7}	4.37×10^{-3}
	1	33.68	22.53	1.28×10^{7}	2.16×10^{-3}
8	5	101.59	27.92	1.48×10^{7}	3.20×10^{-3}
	9	865.78	27.21	3.23×10^{7}	7.50×10^{-3}
	1	17.49	11.56	4.19×10^{6}	8.39×10^{-4}
10	5	58.88	19.98	1.62×10^{7}	3.92×10^{-3}
	9	935.10	41.45	5.96×10^{7}	1.81×10^{-2}
	1	20.73	10.61	5.75×10^{6}	1.89×10^{-3}
13	3	54.65	13.93	8.45×10^{6}	2.78×10^{-3}
	6	952.23	50.02	3.70×10^{7}	9.27×10^{-3}

When integrated over depth (Tbl. 3.1.1), all variables show a significant increase with increasing distance from the coast, being highest the furthest away from the coast ($F = 14.597$, $F = 11.648$, $F = 6.363$, respectively for the dependent variables with, $df = 2$, $p < 0.05$ and post–hoc $p < 0.05$ for all, Tbl. 3.1.2). This increase is more evident for bacterial numbers, reaching cell abundances well into the millions per m^2 of sea surface, and for many stations into the tens of millions per m^2 of sea surface. The majority of the Chl–*a* data show that volumes were highest over deeper waters (remembering that corrected fluorescence values did not exceed 150 m, Fig. 3.1.8), with significantly lower volumes near the coast ($F = 14.597$, $df = 2$, $p = 0.001$, post–hoc $p < 0.05$, Tbl. 3.1.2). Bacterial biomass appears to vary by line as well as by station. Highest bacterial biomass appears in close relation to highest Chl–*a* values, except along line 8 and 13 where bacterial biomass appears to decrease with increasing Chl–*a* values.

Table 3.1.2: Results from a parametric multi–way ANOVA performed on depth integrated data (Tbl. 3.1.1) for the summer synoptic cruise. The main factor is Position (Coastal, Shelf and Oceanic).

Factor	Dependent Variable	F	df	*p*
	Chl a	14.597	2	0.001
Position	Bacterial Numbers	11.648	2	0.003
	Bacterial Biomass	6.363	2	0.019

Assumptions of Normality [(Z = 0.564, p = 0.908), (Z = 0.697, p = 0.717), (Z = 0.911, p = 0.378), respectively] and Heterogeneity (F = 0.000, p = 1.000) were both satisfied.
Post–Hoc Test (Tukey) showed the following differences:
1) Chl a: (Coastal, Shelf) < Oceanic with $p < 0.05$
2) Numbers: (Coastal, Shelf) < Oceanic with $p < 0.05$
3) Biomass: (Coastal, Shelf) < (Central, Oceanic) with $p < 0.05$

Statistical analysis on the depth integrated data (Tbl. 3.1.2) shows a significant difference for position for all variables tested. For each variable, integrated data were highest for the oceanic position compared to the shelf and coastal positions (Tbl. 3.1.2).

3.2: Summer Cruise – Focus sampling sites

Results for the first cruise undertaken during the summer months of 2010 for the four focus sampling sites within the KZN–B are shown below. Temperature, salinity and corrected fluorescence were chosen to represent vertical profiles to show the structure of the water column during the time of sampling. Bacterial data are presented as bar graphs due to the distance between sample sites.

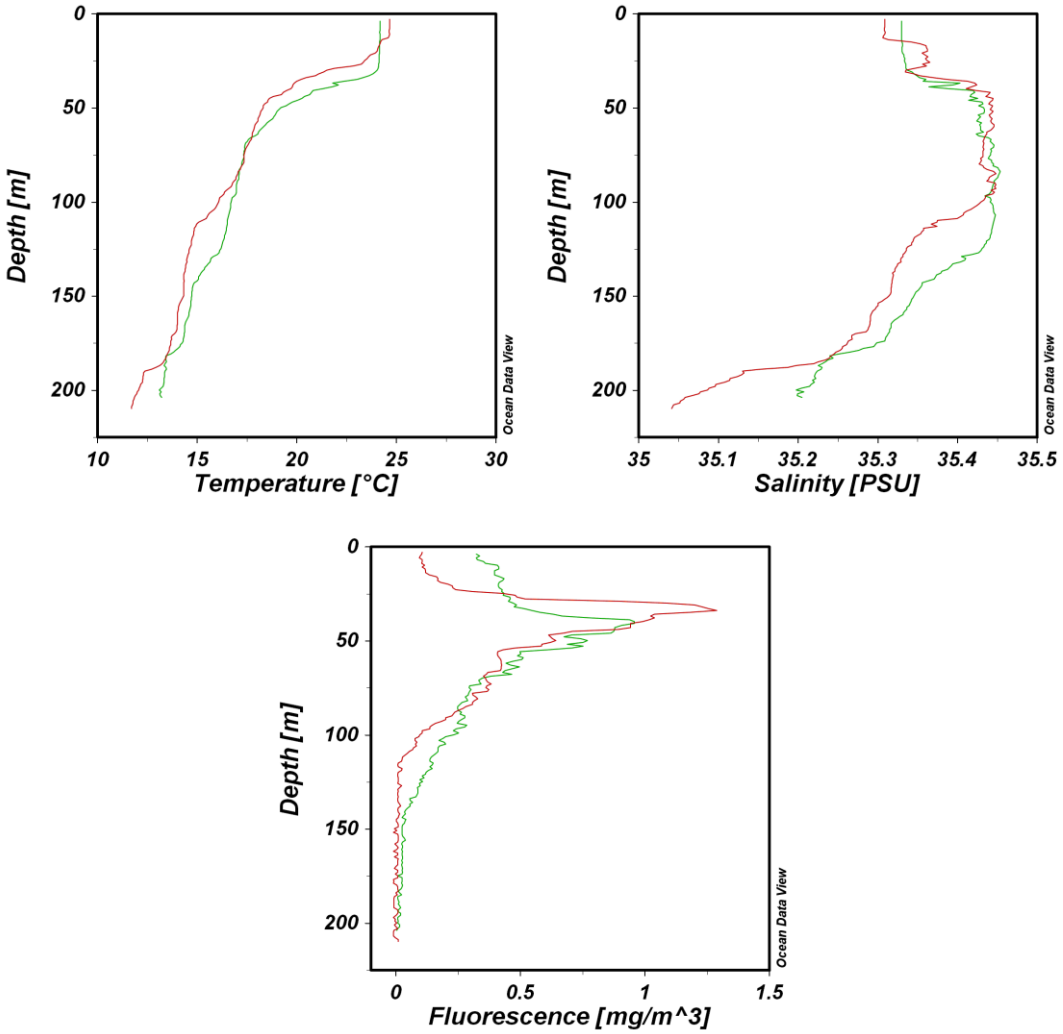

Figure 3.2.1: Vertical profiles through the water column at the Durban Eddy focus site for the summer cruise showing temperature, salinity and corrected fluorescence with depth. The red line indicates the first day of sampling while the green line the second.

The water structure for the Durban Eddy for the two sample days was very similar (Fig. 3.2.1). The temperature profile clearly shows surface water temperature to have been around 24.5°C with a distinct thermocline between 20 to 50 m for both days sampled. Below this, water temperature drops to about 12°C near 225 m with statistical differences present between ecozones ($F = 37.378$, $df = 2$, p

< 0.001, Tbl. 3.5.8, pg 89). Salinity levels for both days within the upper 100 m were very similar, about 35.32 within the first 75 m, but ecozones were nevertheless significantly different from one another (F = 5.393, df = 2, *p* = 0.013, Tbl. 3.5.8, pg 89). The presence and depth of the thermocline and halocline were measured on both sampling days at the focus site.

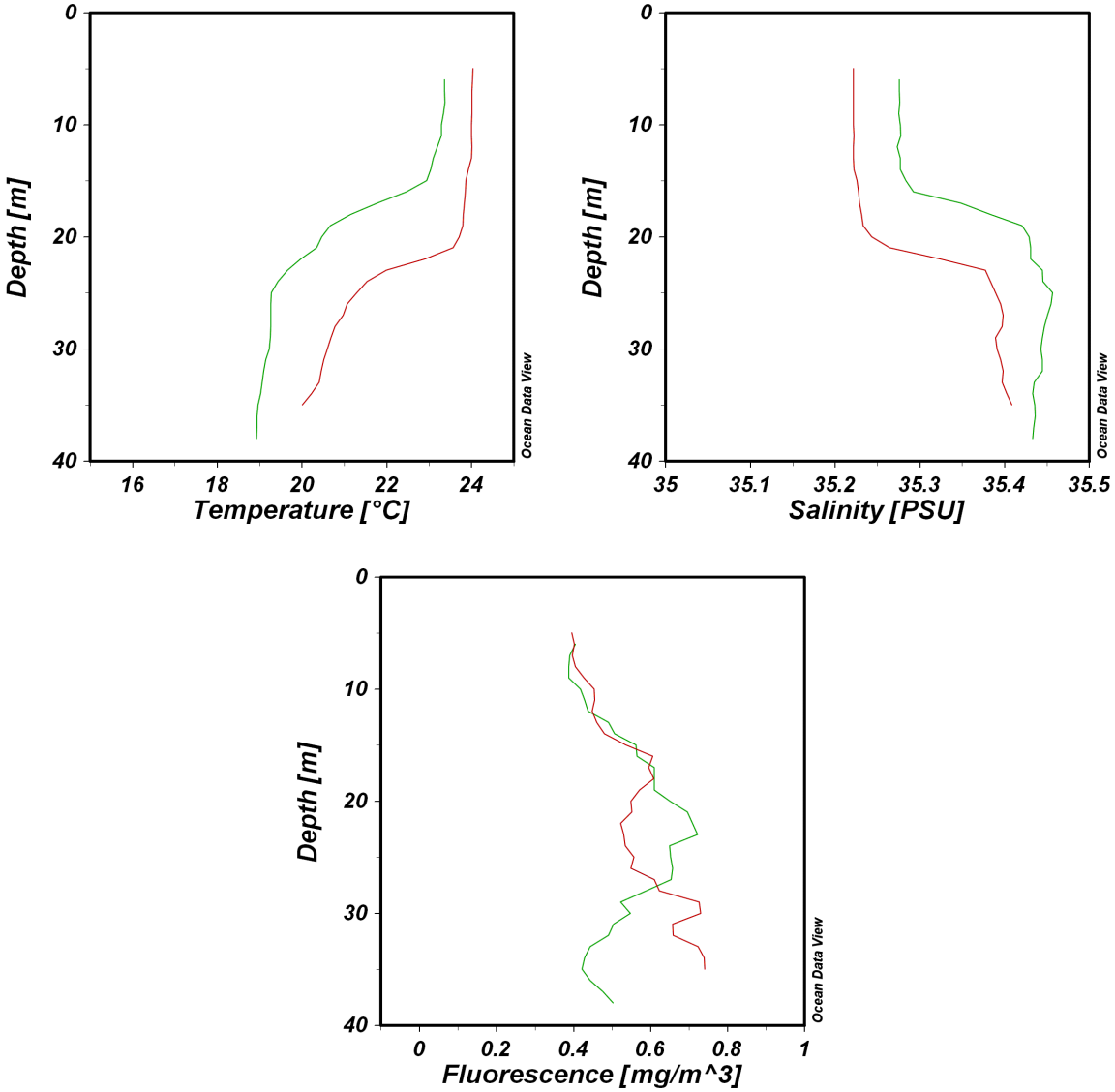

Figure 3.2.2: Vertical profiles through the water column at the Thukela Mouth focus site for the summer cruise showing temperature, salinity and corrected fluorescence with depth. The red line indicates the first day of sampling while the green line the second.

Again, as for the Durban Eddy, the Thukela Mouth focus site (Fig. 3.2.2) vertical profile is very similar. Only the thermocline and halocline, present between 15 to 22.5 m is worth reporting.

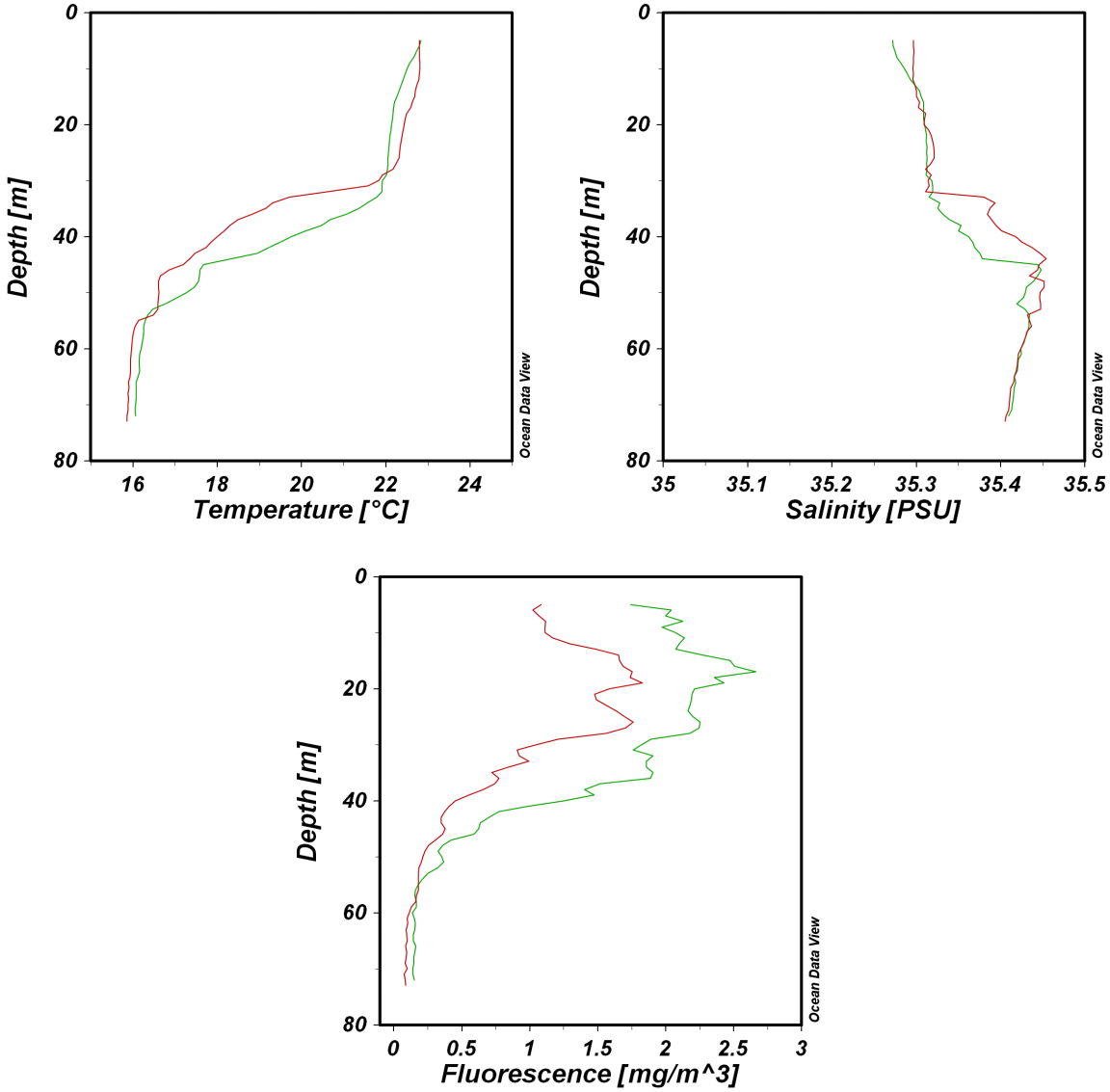

Figure 3.2.3: Vertical profiles through the water column at the Mid Shelf focus site for the summer cruise showing temperature, salinity and corrected fluorescence with depth. The red line indicates the first day of sampling while the green line the second.

The thermocline and halocline for the Mid Shelf focus site (Fig. 3.2.3) were present between 32 and 47 m. Maximum corrected fluorescence values were recorded above the thermocline and halocline with 2.7 $mg \cdot m^{-3}$ during day two.

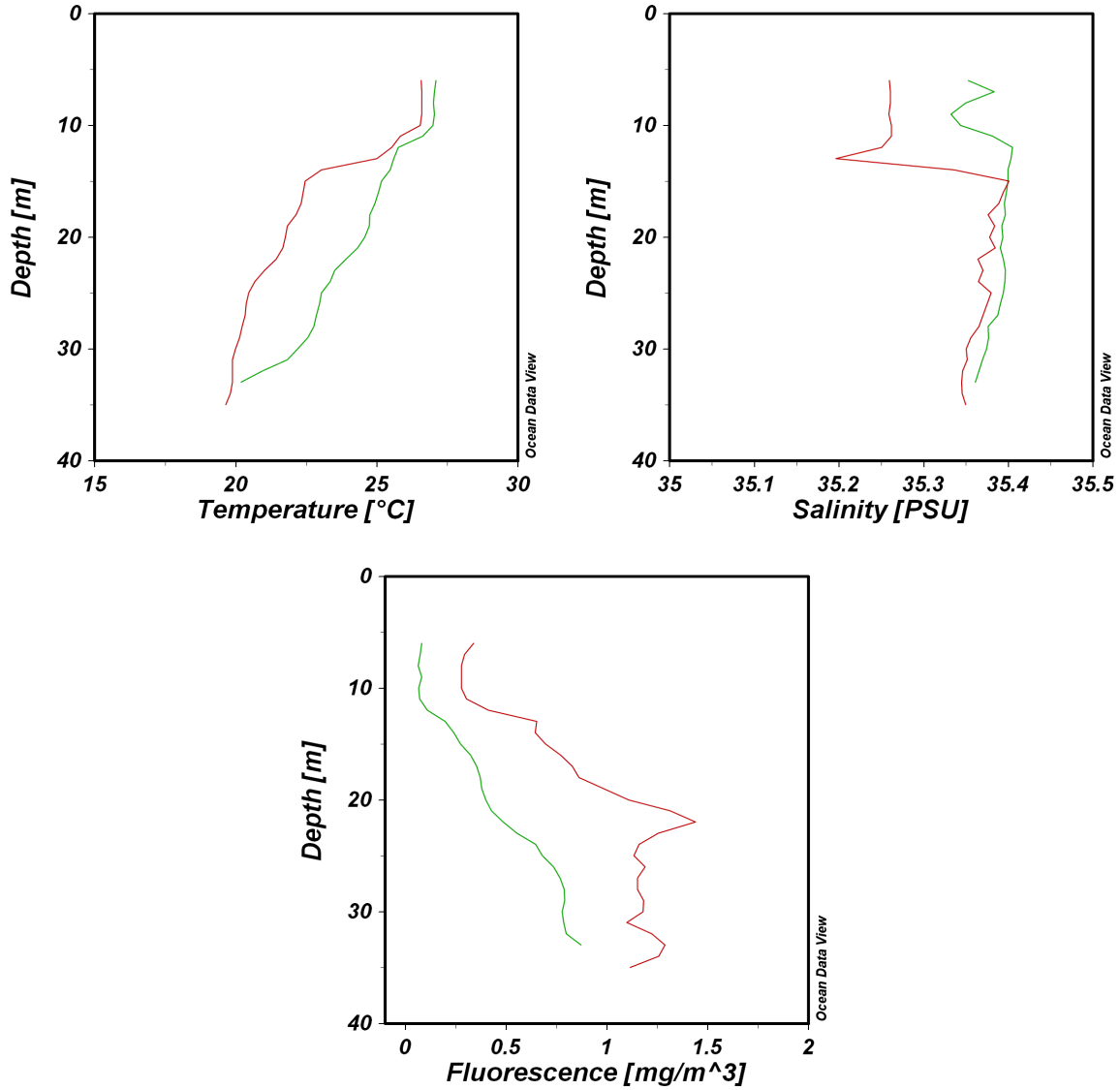

Figure 3.2.4: Vertical profiles through the water column at the Richards Bay North focus site for the summer cruise showing temperature, salinity and corrected fluorescence with depth. The red line indicates the first day of sampling while the green line the second.

The water structure for the Richards Bay North focus site possibly shows signs of two different water masses between the two sample days (Fig. 3.2.4). Temperature and salinity profiles on day one show the upper 10 m of the water column to be very well mixed. Below this the thermocline and a very abrupt halocline were present between 10 and 14 m. Corrected fluorescence levels during day one were the highest at this focus site, about 1.5 mg·m^{-3} between 20 and 25 m. The second possible water mass detected during the second day of sampling showed similar surface water temperatures with a less pronounced thermocline (Fig. 3.2.4). An increase in surface salinity from 35.25 on day one to about 35.36 on day two was observed with the halocline being shallower on the second day by about 5 m. Corrected fluorescence values on day two were lower than those recorded during day one.

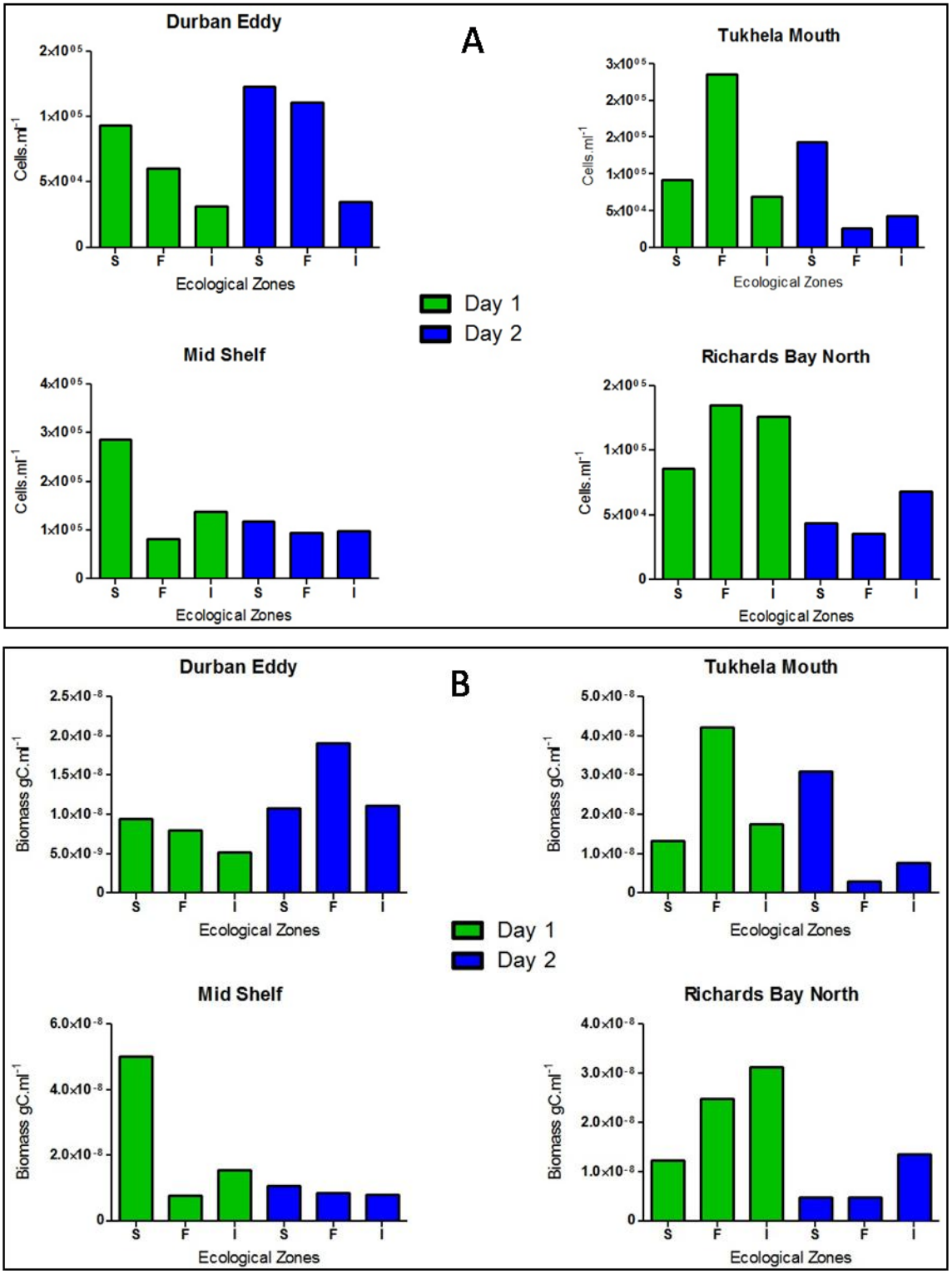

Figure 3.2.5: Bacterial numbers (cells·ml^{-1}) [A] and bacterial biomass (gC·ml^{-1}) [B] for the four focus sites during the summer cruise. The ecological zones (ecozones) that are plotted here are: S (Surface Ecozone); F (F–max Ecozone) and I (Intermediate Ecozone).

Bacterial dynamics for the Durban Eddy, during day one, showed that both bacterial numbers (Fig. 3.2.5 A) and bacterial biomass (Fig. 3.2.5 B) were highest within the SE, which then decreased with increasing ecozone depth. During day two, bacterial numbers were higher at the SE and the FE, while remained the same at the IE. Bacterial biomass for the Durban Eddy changed on day two with the FE showing the highest bacterial biomass, while the SE and the IE were similar.

Bacterial dynamics at the Thukela Mouth focus site, over both days of sampling, showed very similar patterns between bacterial numbers (Fig. 3.2.5 A) and bacterial biomass (Fig. 3.2.5 B) for all ecozones. Both bacterial numbers and bacterial biomass were highest during day one at the FE. At the Mid Shelf focus site, bacterial numbers and biomass also showed similar patterns over both days of sampling for all ecozones. The SE at the Mid Shelf focus site on day one showed the highest bacterial numbers and biomass for all the focus sites, with 2.86×10^{5} cells·ml^{-1} and 5×10^{-8} gC·ml^{-1}, respectively.

The Richards Bay North focus site during day one did not show any major patterns between ecozones in bacterial numbers and bacterial biomass. During day one, bacterial numbers were highest at the FE while bacterial biomass was highest at the IE. Bacterial dynamics during day two were similar with highest bacterial numbers and biomass appearing within the IE.

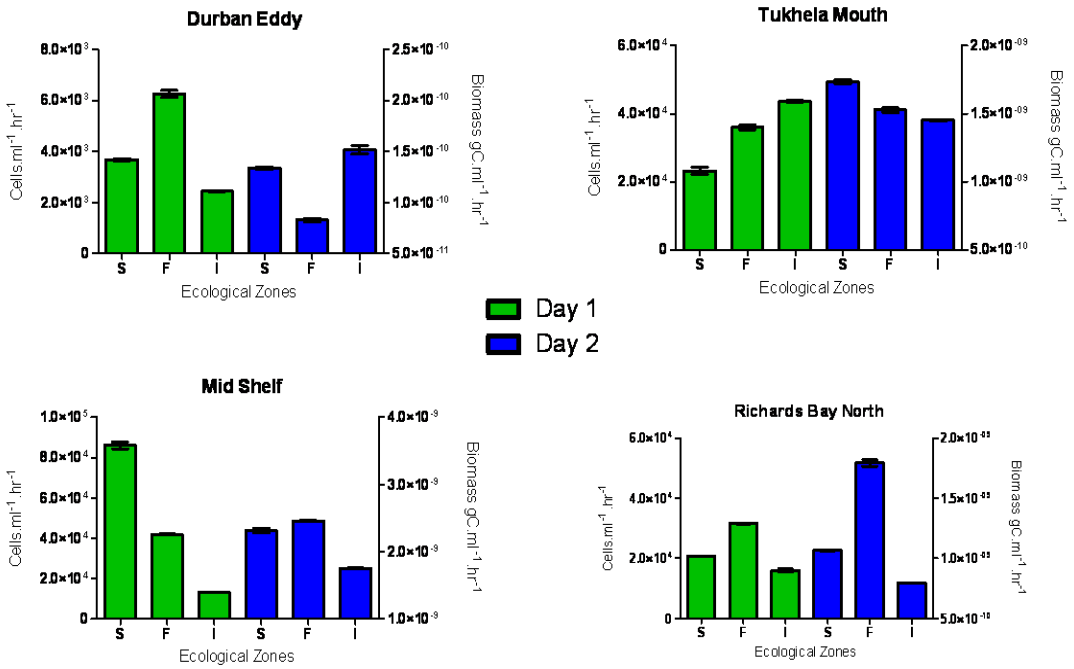

Figure 3.2.6: Bacterial productivity as determined by numbers (cells·ml^{-1}·hr^{-1}) and biomass (gC·ml^{-1}·hr^{-1}) for the four focus sites during the summer cruise. The ecological zones (ecozones) that are plotted here are: S (Surface Ecozone); F (F–max Ecozone) and I (Intermediate Ecozone). Error bars are included, but in some cases are very small.

For the summer focus cruise, bacterial productivity ranged from 1.31×10^{3} to 8.62×10^{4} cells·ml^{-1}·hr^{-1} and 4.46×10^{-11} to 2.93×10^{-9} gC·ml^{-1}·hr^{-1}. Of the four focus sites, the Durban Eddy showed the lowest overall productivity on day one [6.26×10^{3} cells·ml^{-1}·hr^{-1} and 2.13×10^{-10} gC·ml^{-1}·hr^{-1} at the FE (Fig. 3.2.6)]. Bacterial productivity for the Thukela Mouth, from the SE to the IE, increased on day one while decreased on day two. Bacterial productivity for the Mid Shelf was the highest for all focus sites with maximum productivity at the SE on day one with 8.62×10^{4} cells·ml^{-1}·hr^{-1} and 2.93×10^{-9} gC·ml^{-1}·hr^{-1}, with all other ecozones at this site being at least half or less than this. The lowest bacterial productivity for the Mid Shelf was measured on day one at the IE, with 1.32×10^{4} cells·ml^{-1}·hr^{-1} and 4.50×10^{-10} gC·ml^{-1}·hr^{-1}. Highest bacterial productivity for Richards Bay North was at the FE on day two with 5.17×10^{4} cells·ml^{-1}·hr^{-1} and 1.76×10^{-9} gC·ml^{-1}·hr^{-1}, with little variation in the other ecozones. There was no statistical difference between ecozones for bacterial productivity regarding numbers or biomass of the Durban Eddy, Thukela Mouth and Richards Bay North focus sites ($F = 0.034$, df = 2, $p = 0.966$ and $F = 0.188$, df = 2, $p = 0.830$, respectively, Tbls. 3.5.5 and 3.5.6, pg 86). There was however, a significant difference between these three focus sites for bacterial productivity regarding numbers and biomass ($F = 12.084$, df = 2, $p = 0.001$ and $F = 5.029$, df = 2, $p = 0.019$, respectively, Tbls. 3.5.5 and 3.5.6, pg 86), with the Durban Eddy showing the lowest productivity in numbers and biomass (post–hoc $p < 0.05$ for all, Tbls. 3.5.5 and 3.5.6 pg 86).

Table 3.2.1: Daily productivity biomass (P / B) ratios for the summer cruise focus sites, for two days of sampling, at the Surface Ecozone (SE), F–max Ecozone (FE) and the Intermediate Ecozone (IE) or the Bottom Ecozone (BE).

		Focus Sample Site			
Day	**Ecozone**	**Durban Eddy**	**Thukela Mouth**	**Mid Shelf**	**Richards Bay North**
1	SE	0.0132	0.0593	0.0585	0.0569
	FE	0.0266	0.0290	0.1874	0.0433
	IE / BE	0.0160	0.0846	0.0291	0.0174
2	SE	0.0105	0.0542	0.1399	0.1642
	FE	0.0023	0.4694	0.1947	0.3730
	IE / BE	0.0125	0.1694	0.1059	0.0297

P / B ratios for the Durban Eddy were very low when compared to the other focus sites (Tbl. 3.2.1), but not significantly different to the other focus sites ($F = 1.433$, df = 3, $p = 0.282$, Tbl. 3.2.2). The highest P / B ratio was found for the Thukela Mouth focus site during day two within the FE (0.4694), but P / B ratios were low throughout the other ecozones at this site. Although as shown in Fig. 3.2.5 above, where the Mid Shelf focus site showed the highest bacterial productivity on day one at the SE, the P / B ratio was only 0.0585, not that much higher from values reported from the Durban

Eddy. P / B ratios determined for Richards Bay North were higher than those found for the Durban Eddy, but showed some variation between the Thukela Mouth and Mid Shelf focus sites.

Table 3.2.2: Results from a parametric two–way ANOVA performed on P / B data (Tbl. 3.2.1) for the summer focus cruise. The main factors are Focus Site [Durban Eddy (DE), Thukela Mouth (TM), Mid Shelf (MS) and Richards Bay North (RN)] and Ecozone [Surface (S), F–max (F), Intermediate and Bottom (I / B)].

Factor	**F**	**df**	***p***
Focus Site (FS)	1.433	3	0.282
Ecozone (E)	2.004	2	0.177
FS * E	0.390	6	0.872

Assumptions of Normality (Z = 0.947, p = 0.331) and Heterogeneity (F = 0.000, p = 1.000) were both satisfied.

Similarly to the lack of significant differences of the P / B ratios between focus sites, there was no significant difference between ecozones (Tbl. 3.2.2).

3.3: Winter Cruise – Synoptic sampling sites

Results for the second cruise undertaken during the winter months of 2010, during the synoptic sampling of the KZN–B, are shown below. The data presented below are in the same format as for the summer cruise. Transect lines are at the same locations as for the summer cruise above.

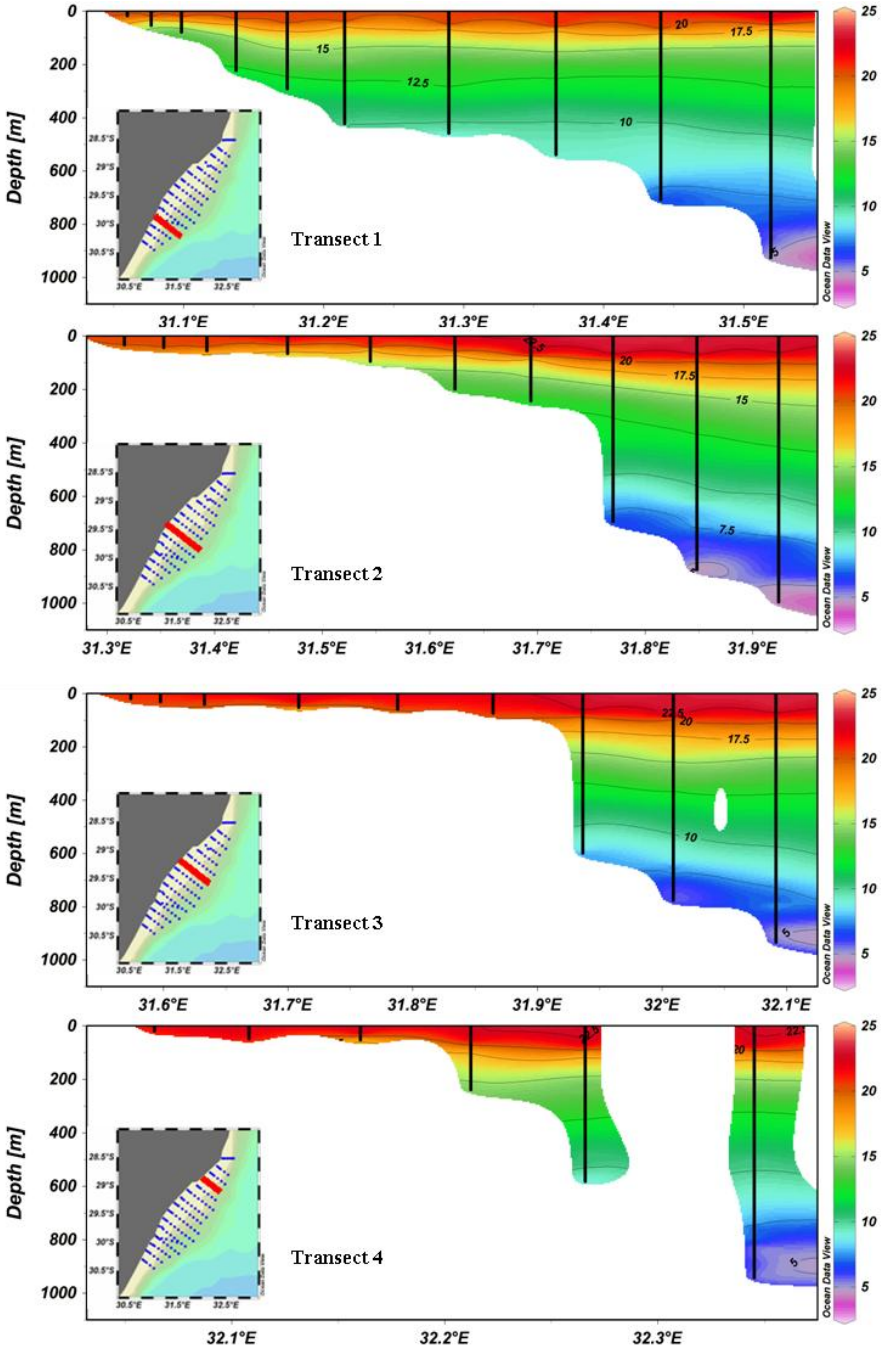

Figure 3.3.1: Temperature (°C) profile at selected lines through the KZN–B for the winter synoptic cruise using full CTD hydrographic data. Black vertical lines represent individual stations while contour lines represent isotherms. The inset within each image shows the location of the transect line in red. All subsequent profiles are the same format.

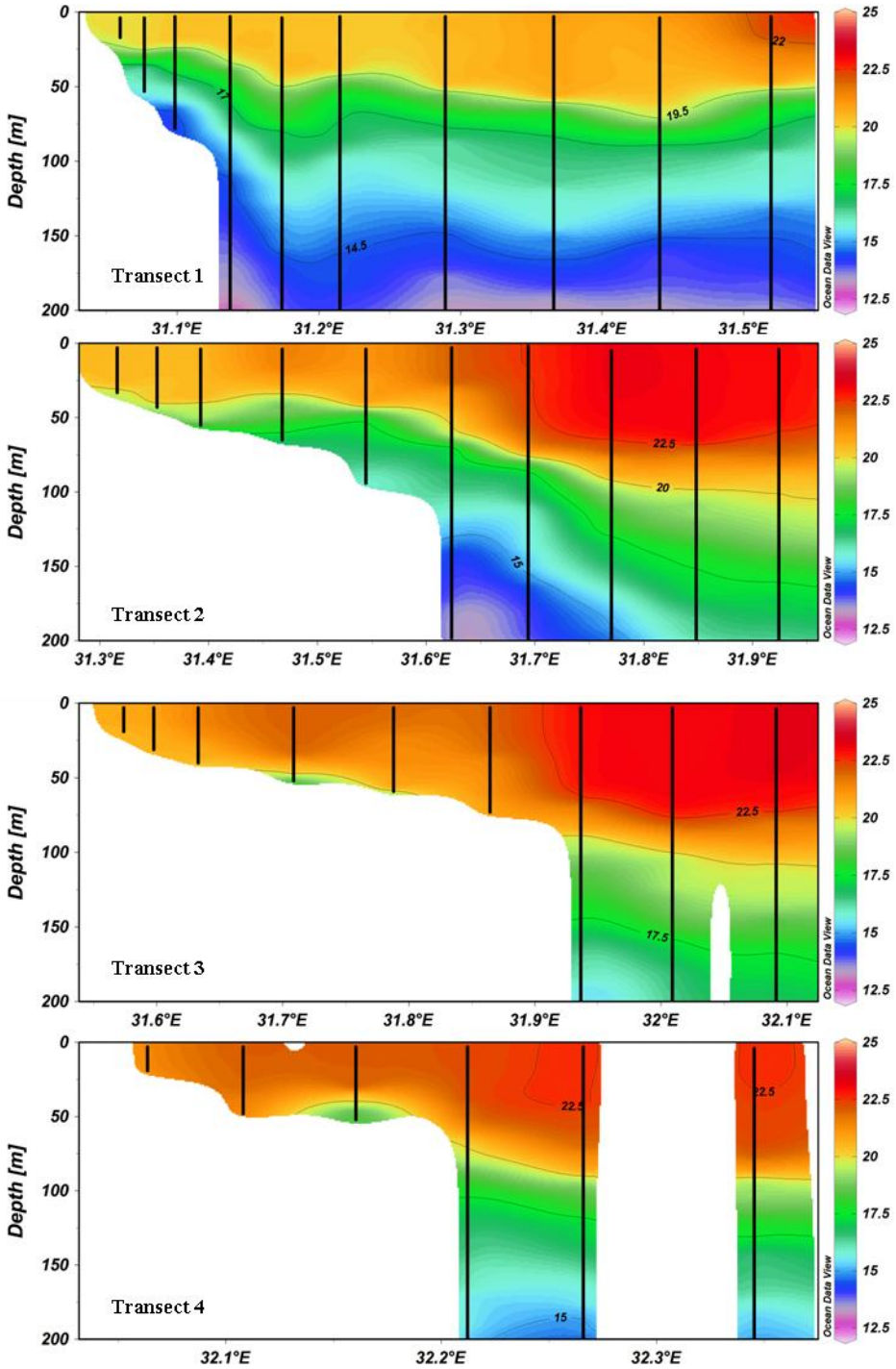

Figure 3.3.2: Temperature (°C) profile for the first 200 m at selected lines through the KZN–B for the winter synoptic cruise using full CTD hydrographic data.

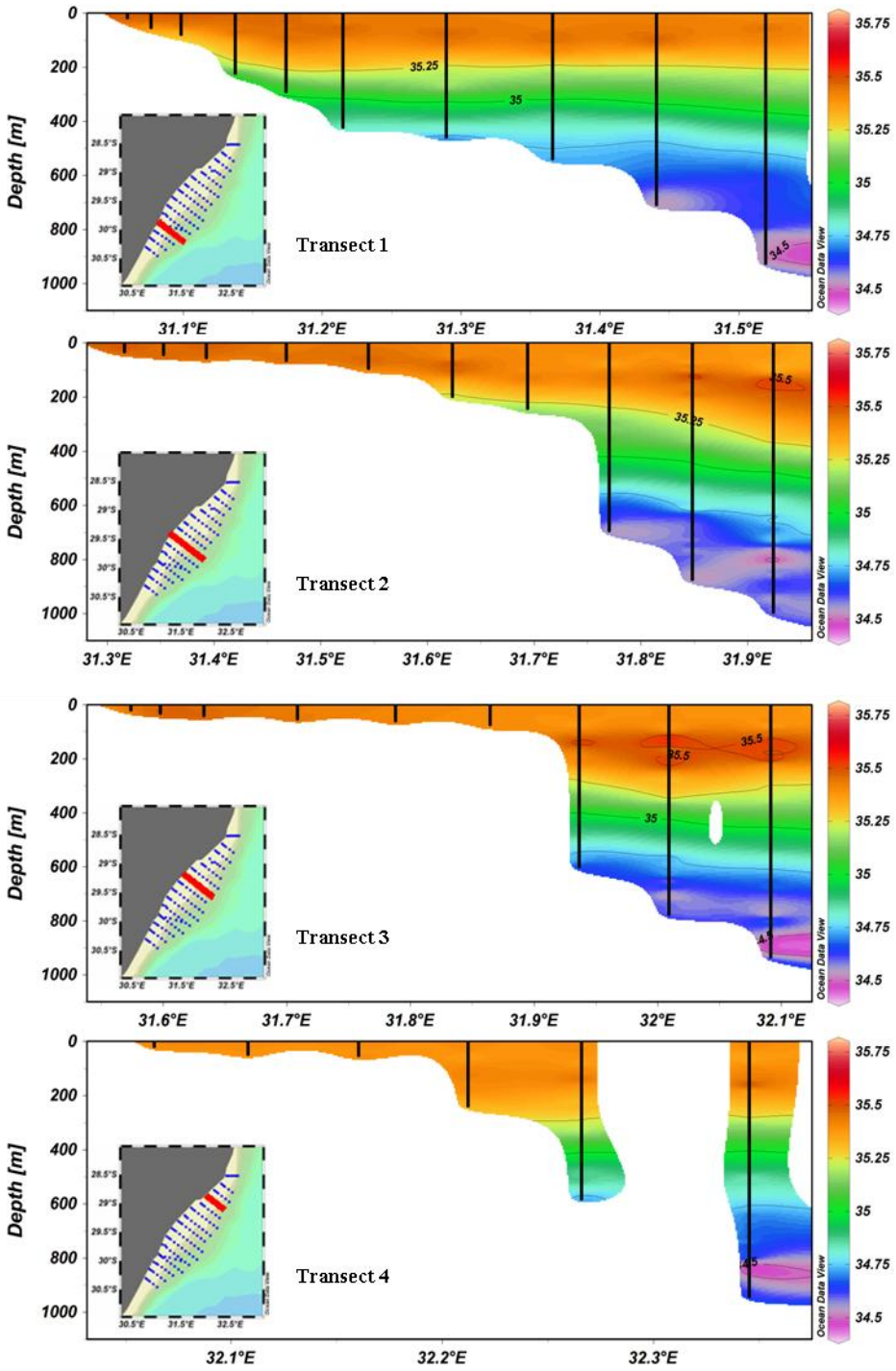

Figure 3.3.3: Salinity profile at selected lines through the KZN–B for the winter synoptic cruise using full CTD hydrographic data.

Surface waters across the KZN–B were very well mixed during the winter cruise showing temperatures between 20 and 22.5°C within the upper 50 to 75 m (Figs. 3.3.1 and 3.3.2) with the northern KZN–B being the warmest ($F = 5.238$, $df = 2$, $p = 0.006$, post–hoc $p < 0.001$, Tbl. 3.5.7, pg 87), while across the whole KZN–B, temperatures ranged from 4.3 to 23.2°C. Salinity levels were also very well mixed within the surface waters but extended much deeper, down to about 200 to 300 m, with 35.25 to 35.5 (Fig. 3.3.3), ranging from 34.4 to 35.5. This is supported by post–hoc tests performed within the ANOVA showing that the SE and FE had higher salinity levels compared to the IE and BE ($F = 6.137$, $df = 3$, $p < 0.001$, post–hoc $p < 0.05$, Tbl. 3.5.7, pg 87). The presence of a very weak thermocline (17.5 to 20°C) varied with depth across the KZN–B but stayed within the upper 200 m. The halocline (35 to 35.25) appeared to follow the 12.5°C isotherm throughout the KZN–B. Below the thermocline and halocline, water temperature as well as salinity appeared to be well stratified. Waters colder than 10°C and showing salinity levels between 34.7 and 34.9 were only found below about 400 m for T1, with a significant difference found for both temperature and salinity between ecozones ($F = 66.027$, $df = 3$, $p < 0.001$ and $F = 6.137$, $df = 3$, $p < 0.001$, respectively, with post–hoc $p < 0.05$ for both, Tbl 3.5.7, pg 87). During this winter cruise, this water mass did not substantially encroach onto the shelf as it did within the summer cruise. This cold, and less saline water mass, was found deeper than 500 m below the shelf from T2 to T4. The “protuberance” as previously described during the summer cruise did not appear to be present at the same location (between 31.7°E and 31.8°E) or anywhere else along T2.

Figs. 3.3.4 to 3.3.7 below present data for nutrients that was accessible to all members of the ACEP II team as common data. These include silicate, phosphate, nitrate and nitrite. Minimum and maximum values recorded from the whole KZN–B sampling area, for the winter cruise, for each nutrient are as follows; silicate: below the detection limit (0.01) to 54.43 μmol $Si \cdot L^{-1}$; phosphate: below the detection limit (0.01) to 3.02 μmol $P \cdot L^{-1}$; nitrate: below the detection limit (0.01) to 33.53 μmol $N \cdot L^{-1}$ and nitrite: below the detection limit (0.01) to 0.94 μmol $N \cdot L^{-1}$, respectively.

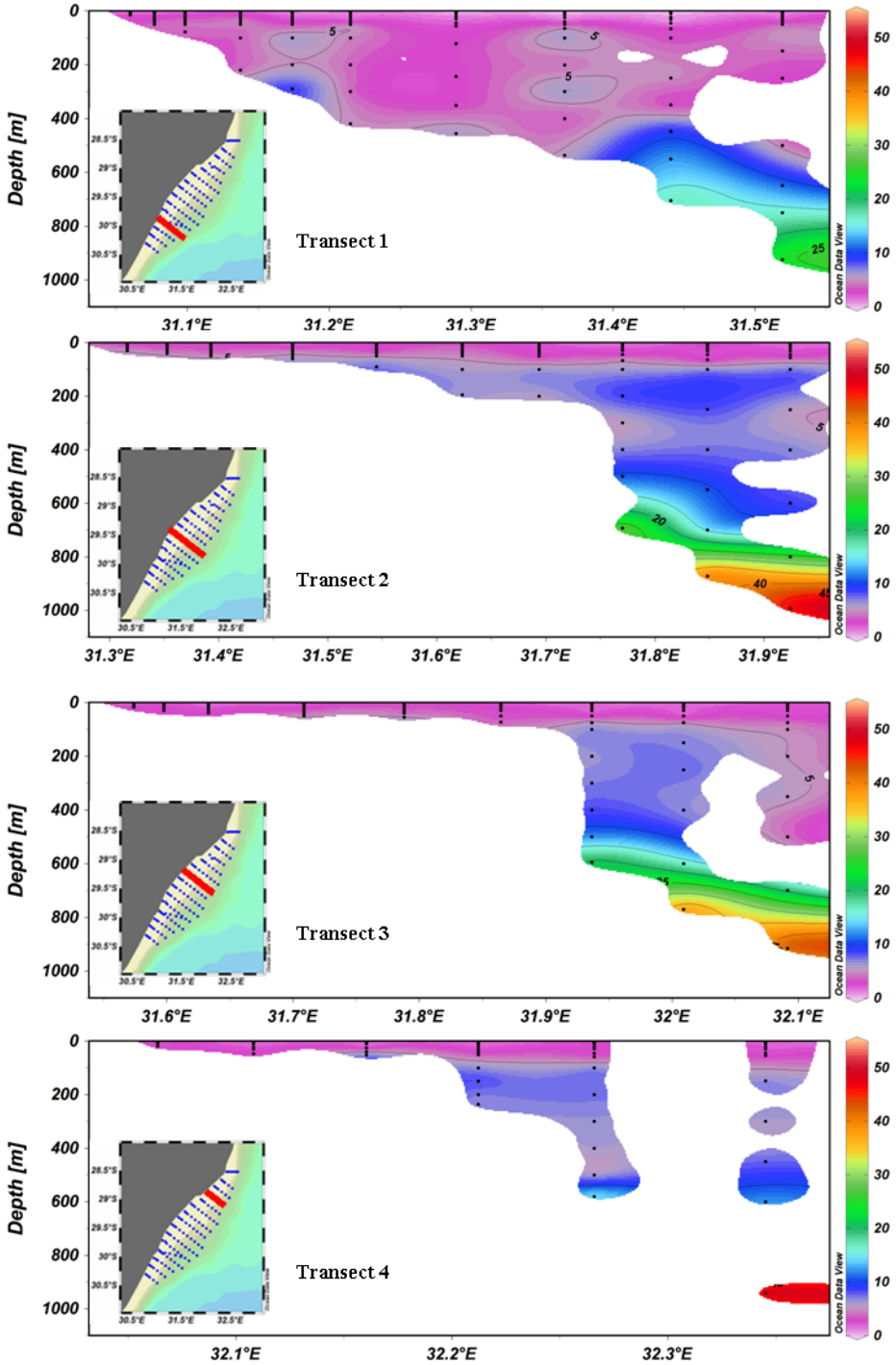

Figure 3.3.4: Silicate (µmol $Si \cdot L^{-1}$) profile at selected survey lines through the KZN–B for the winter synoptic cruise using full bottle collection data.

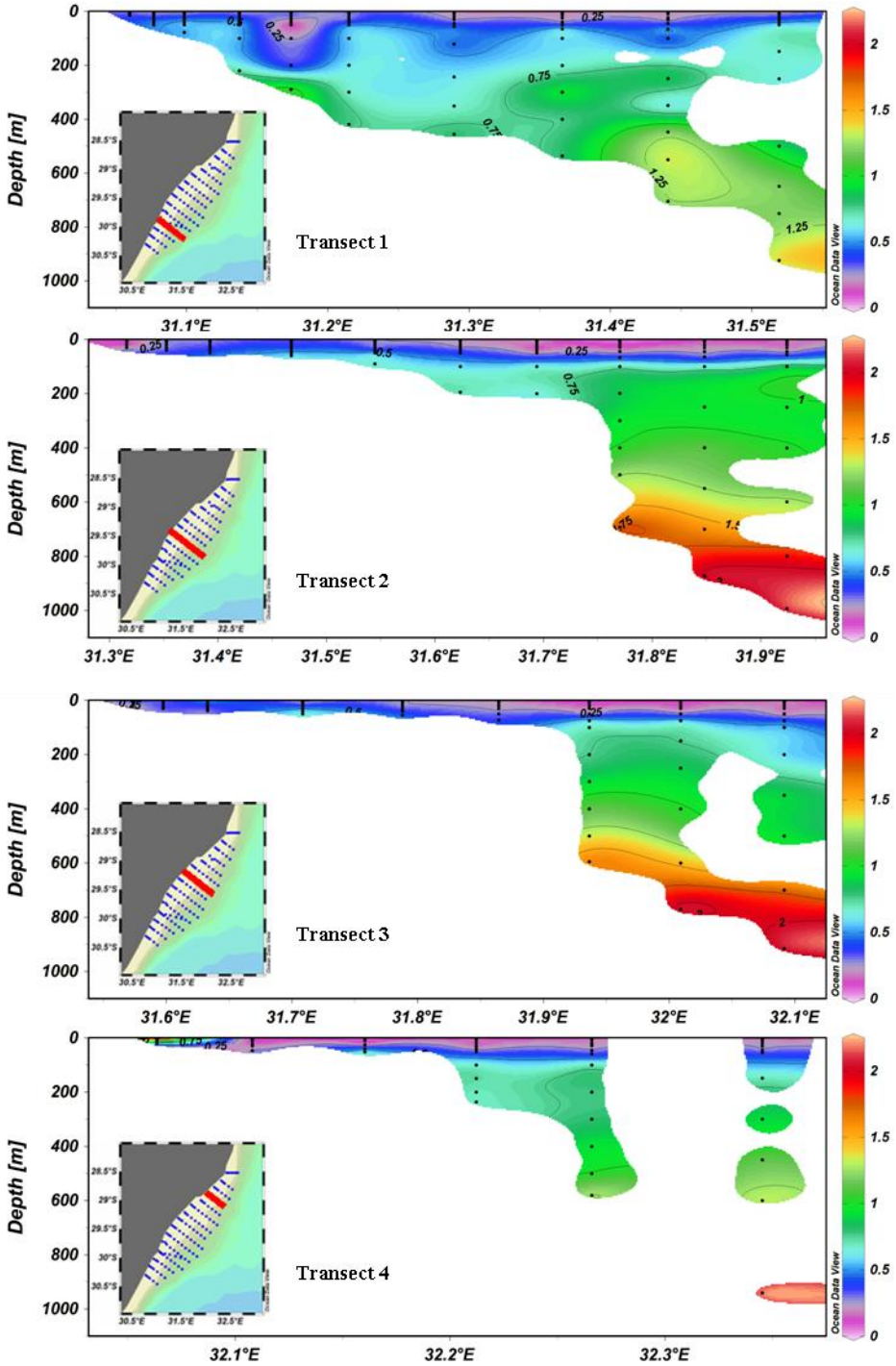

Figure 3.3.5: Phosphate (µmol P·L^{-1}) profile at selected survey lines through the KZN–B for the winter synoptic cruise using full bottle collection data.

Silicate concentrations were the lowest in the surface waters (SE) of the KZN–B ($F = 29.943$, $df = 3$, $p < 0.001$, post–hoc $p < 0.001$, Tbl 3.5.7, pg 87) ranging from below the detection limit (0.01) to 2 μmol $Si{\cdot}L^{-1}$ (Fig. 3.3.4), while for the whole KZN–B ranged from below the detection limit (0.01) to 54.43 μmol $Si{\cdot}L^{-1}$. Along T1, down to about 400 m, silicate levels were low (up to 5 μmol $Si{\cdot}L^{-1}$) when compared to the same depth along the other three transect lines (up to 10 μmol $Si{\cdot}L^{-1}$). There was a statistical difference between sections ($F = 22.018$, $df = 2$, $p < 0.001$, Tbl. 3.5.7, pg 87) with the southern section showing the lowest concentration (post–hoc $p < 0.001$, Tbl. 3.5.7, pg 87). Between 600 and 800 m, at least for T2 and T3, silicate concentrations drastically increased from water column concentrations of around 5 μmol $Si{\cdot}L^{-1}$ to around 20 μmol $Si{\cdot}L^{-1}$. This is reflected by the statistical difference between ecozones ($F = 29.943$, $df = 3$, $p < 0.001$, Tbl. 3.5.7, pg 87) where the BE showed highest concentrations followed by the IE (post–hoc $p < 0.001$ Tbl. 3.5.7, pg 87). At the same depth along T1, silicate concentrations were between 15 and 20 μmol $Si{\cdot}L^{-1}$. Below 800 m for T2 and T3, silicate concentrations reached a maximum of about 40 to 45 μmol $Si{\cdot}L^{-1}$. Overall, silicate concentrations appeared to increase with depth as well as with distance from the coast line.

Surface phosphate concentrations appeared variable with distance from the coast as well as with depth within the water column (Fig. 3.3.5), with a statistical difference between ecozones ($F = 42.599$, $df = 3$, $p < 0.001$, Tbl. 3.5.7, pg 87), and ranged from below the detection limit (0.01) to 3.02 μmol $P{\cdot}L^{-1}$ for the whole KZN–B. Phosphate concentrations along T1 within the upper 400 m were low, 0.5 to 0.75 μmol $P{\cdot}L^{-1}$ compared to the other transects at the same depth, 1 μmol $P{\cdot}L^{-1}$, however, there was no statistical difference found between sections ($F = 0.104$, $df = 2$, $p = 0.901$, Tbl 3.5.7, pg 87). Phosphate concentrations along T2 and T3 appeared to be the highest of all transects, reaching levels between 2.1 and 2.2 μmol $P{\cdot}L^{-1}$ below 800 m. At the same depths along T1, phosphate concentrations reached 1.25 μmol $P{\cdot}L^{-1}$. Water column phosphate concentrations along T4 appeared to be very similar to those along T1. Phosphate levels as for silicate concentrations (Fig. 3.3.4) appeared to increase with distance from the coast as well as with depth.

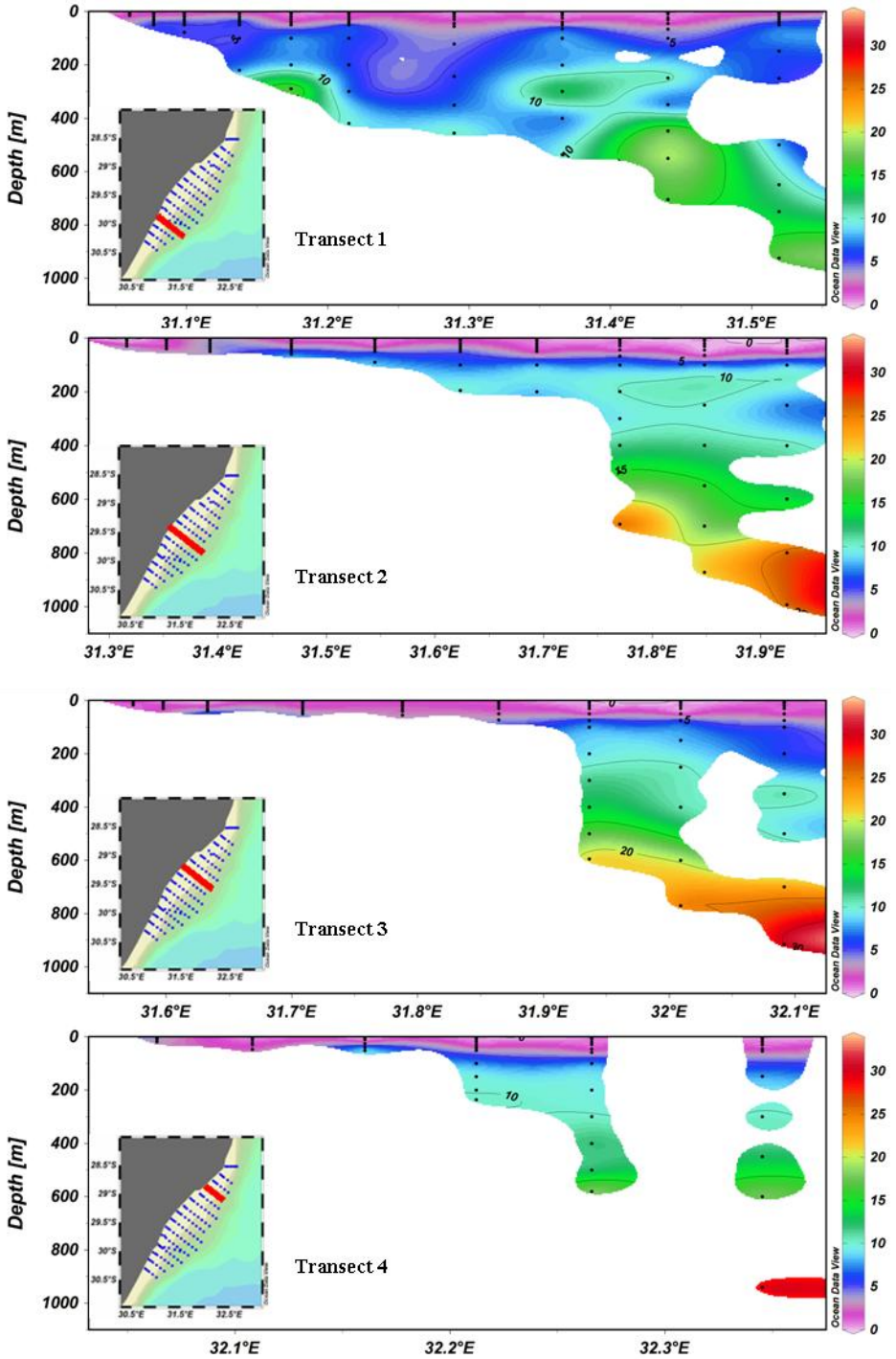

Figure 3.3.6: Nitrate (µmol $N \cdot L^{-1}$) profile at selected survey lines through the KZN–B for the winter synoptic cruise using full bottle collection data.

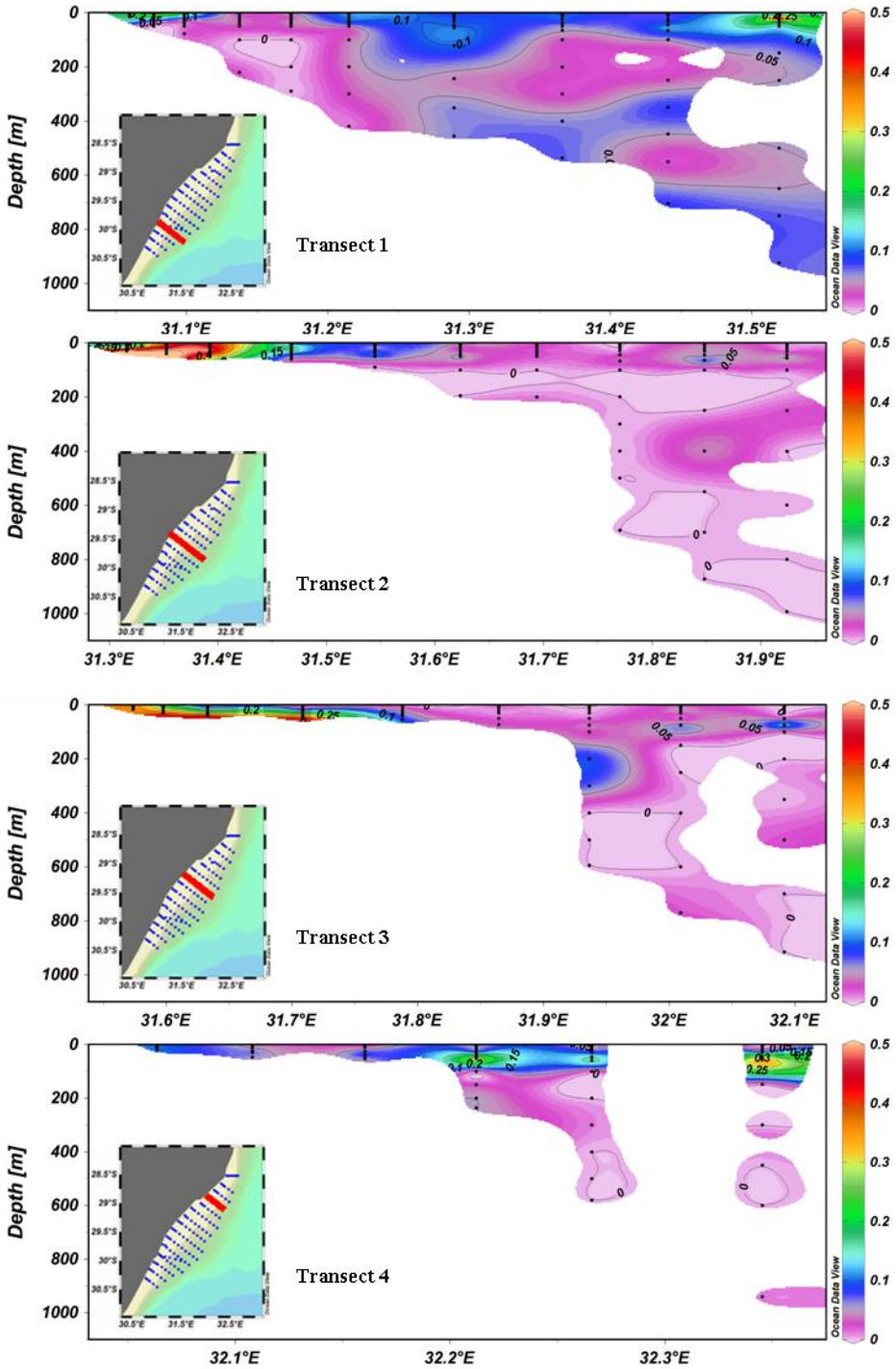

Figure 3.3.7: Nitrite (µmol N·L^{-1}) profile at selected survey lines through the KZN–B for the winter synoptic cruise using full bottle collection data.

Nitrate concentrations (Fig. 3.3.6) appear to follow the same patterns as silicate and phosphate (Figs. 3.3.4 and 3.3.5 respectively) with nitrate concentrations ranging from below the detection limit (0.01) to 33.53 μmol $N{\cdot}L^{-1}$ for the whole KZN–B. Surface nitrate concentrations were low throughout the KZN–B when compared to other ecozone ($F = 65.396$, df = 3, $p < 0.001$, post–hoc $p < 0.001$, Tbl. 3.5.7, pg 87). Water column nitrate concentrations up to 400 m along T1 were lower (5 to 10 μmol $N{\cdot}L^{-1}$) when compared to T2 and T3 (5 to 12.5 μmol $N{\cdot}L^{-1}$) at the same depth, but showed no statistical difference between sections ($F = 0.080$, df = 2, $p = 0.923$, Tbl. 3.5.7, pg 87). T2 and T3 showed the highest concentration of nitrate below 800 m, between 28 and 32 μmol $N{\cdot}L^{-1}$. T4 showed similar water column characteristics for nitrate as for T1. Nitrate concentrations appeared to increase with distance from the coast, and increased with depth, with significant differences found between ecozones ($F = 65.396$, df = 3, $p < 0.001$, Tbl. 3.5.7, pg 87), with the IE and BE showing the highest concentrations (post–hoc $p < 0.001$, Tbl. 3.5.7, pg 87).

Nitrite concentrations within the KZN–B did not follow all of the same patterns as presented for silicate, phosphate and nitrate above (Figs. 3.3.4, 3.3.5 and 3.3.6 respectively) and ranged from below the detection limit (0.01) to 0.94 μmol $N{\cdot}L^{-1}$ (Fig. 3.3.7), with the highest concentrations present within the FE ($F = 5.140$, df = 3, $p = 0.002$, post–hoc $p < 0.05$, Tbl. 3.5.7, pg 87). Nitrite concentrations decreased with depth along T2 to T4 reaching levels below the detection limit at the bottom with higher concentrations present within the surface waters of the KZN–B (Fig. 3.3.7). Highest concentrations of nitrite were found along T2 and T3 close to the coast with 0.5 μmol $N{\cdot}L^{-1}$. Nitrite concentrations along T1 within the water column were much more variable compared to levels found between T2 to T4, but no statistical difference was found between sections ($p = 0.106$, Tbl. 3.5.7, pg 87). At the end of the sample line, over deeper waters, T1 and T4 showed higher nitrite concentrations within surface waters compared to nearer the coast. Overall, nitrite concentrations along T1 and T4 appeared to increase with distance from the coast, while nitrite concentrations along T2 and T3 appeared to decrease with distance from the coast. For all transects, nitrite levels decreased with depth.

Figs. 3.3.8 to 3.3.10 below present corrected fluorescence and Chl–*a* data that were accessible to all members of the ACEP II team as common data. Minimum and maximum values recorded from the whole KZN–B sampling area, for the winter cruise, for corrected fluorescence were 0 and 2.152 $mg{\cdot}m^{-3}$, while for Chl–*a* was 0.014 and 3.649 $mg{\cdot}m^{-3}$, respectively.

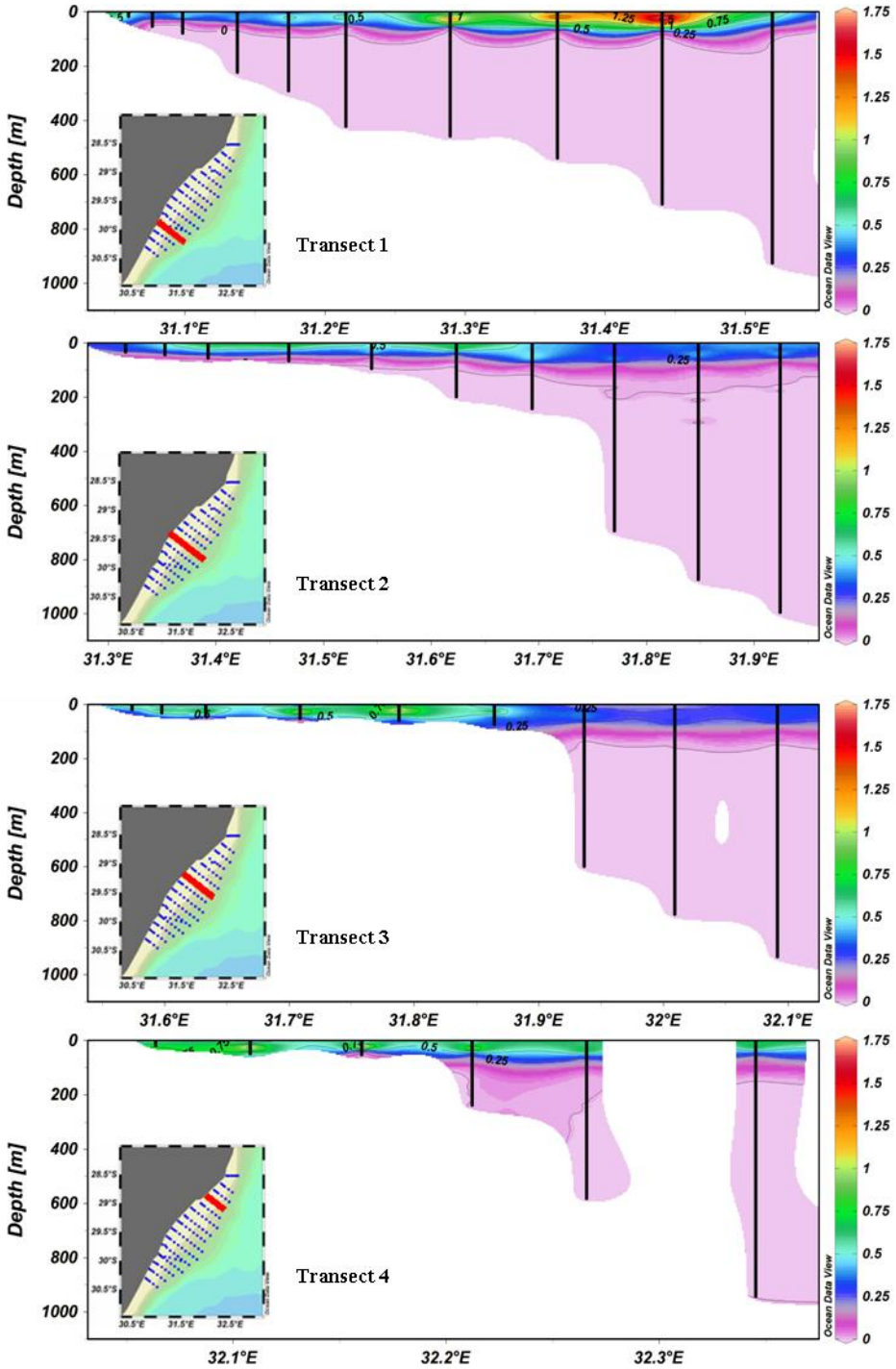

Figure 3.3.8: Corrected fluorescence ($mg \cdot m^{-3}$) profile at selected lines through the KZN–B for the winter synoptic cruise using full CTD hydrographic data.

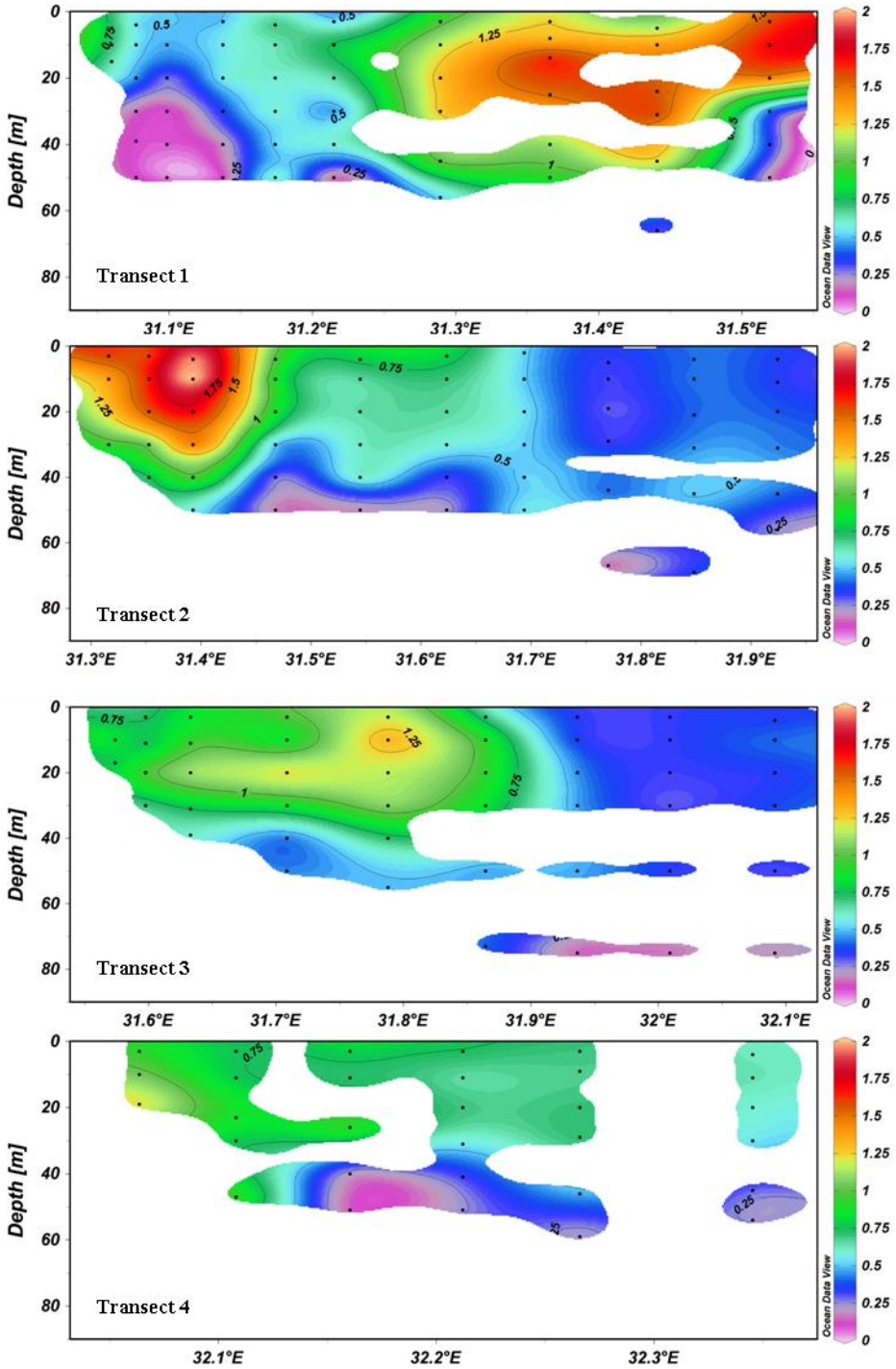

Figure 3.3.9: Chlorophyll–*a* (mg·m^{-3}) profiles at selected lines through the KZN–B for the winter synoptic cruise using full CTD hydrographic data.

Corrected fluorescence values for the KZN–B during the winter cruise (Fig. 3.3.8) indicate that all of the detected Chl–*a* was located within the upper 75 m of the water column and ranged from 0 to 2.152 mg·m^{-3}. Corrected fluorescence detection also appeared to start much closer to the surface during the winter cruise. Below 100 m, corrected fluorescence values were below the detection limit for all transects throughout the water column. Sample waters for Chl–*a* as collected by bottle data (Fig. 3.3.9) indicated that the majority of the Chl–*a* was present within the upper 50 to 60 m of the water column and ranged from 0.014 and 3.649 mg·m^{-3} with the FE showing the highest Chl–*a* concentrations of all the ecozones ($F = 43.269$, df = 3, $p < 0.001$, post–hoc $p < 0.001$, Tbl. 3.5.7, pg 87). Higher Chl–*a* concentrations were found along T1 and T2. T1 showed highest Chl–*a* concentrations over deeper waters within the first 20 m of the surface, with a maximum around 1.75 mg·m^{-3}. T2 on the other hand showed highest Chl–*a* concentrations closer to the coast line, also within the first 20 m of the water column, up to 2 mg·m^{-3}. T4 showed the lowest Chl–*a* concentrations of the four transects with 1.25 mg·m^{-3}. There was no statistical difference for Chl–*a* betweens sections ($F = 1.109$, df = 2, $p = 0.332$, Tbl. 3.5.7, pg 87). Overall Chl–*a* concentrations throughout the KZN–B were variable and patchy (Fig. 3.3.10). Chl–*a* data integrated over depth are presented further (Tbl. 3.3.1).

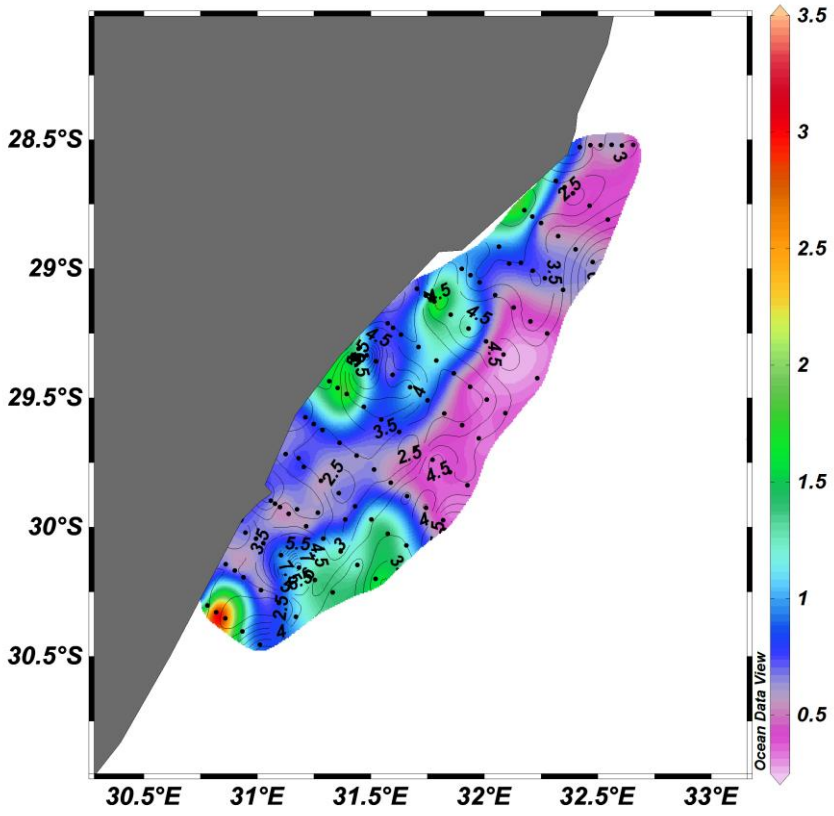

Figure 3.3.10: Chlorophyll–*a* (mg·m^{-3}) isosurface plot for the winter cruise, surface ecozone, using all available data. Contour lines show approximate depth (m) of sampling. Sampling stations in the background are shown as black dots. All subsequent profiles are the same format.

Figs. 3.3.11 and 3.3.12 below present ecozone bacterial numbers and biomass that were the focal point of this study. Minimum and maximum values recorded from the whole KZN–B sampling area, for the winter cruise, for bacterial numbers were 7.26×10^{3} and 2.21×10^{5} cells·ml^{-1}, and for bacterial biomass was 3.61×10^{-10} and 2.56×10^{-8} gC·ml^{-1}, respectively.

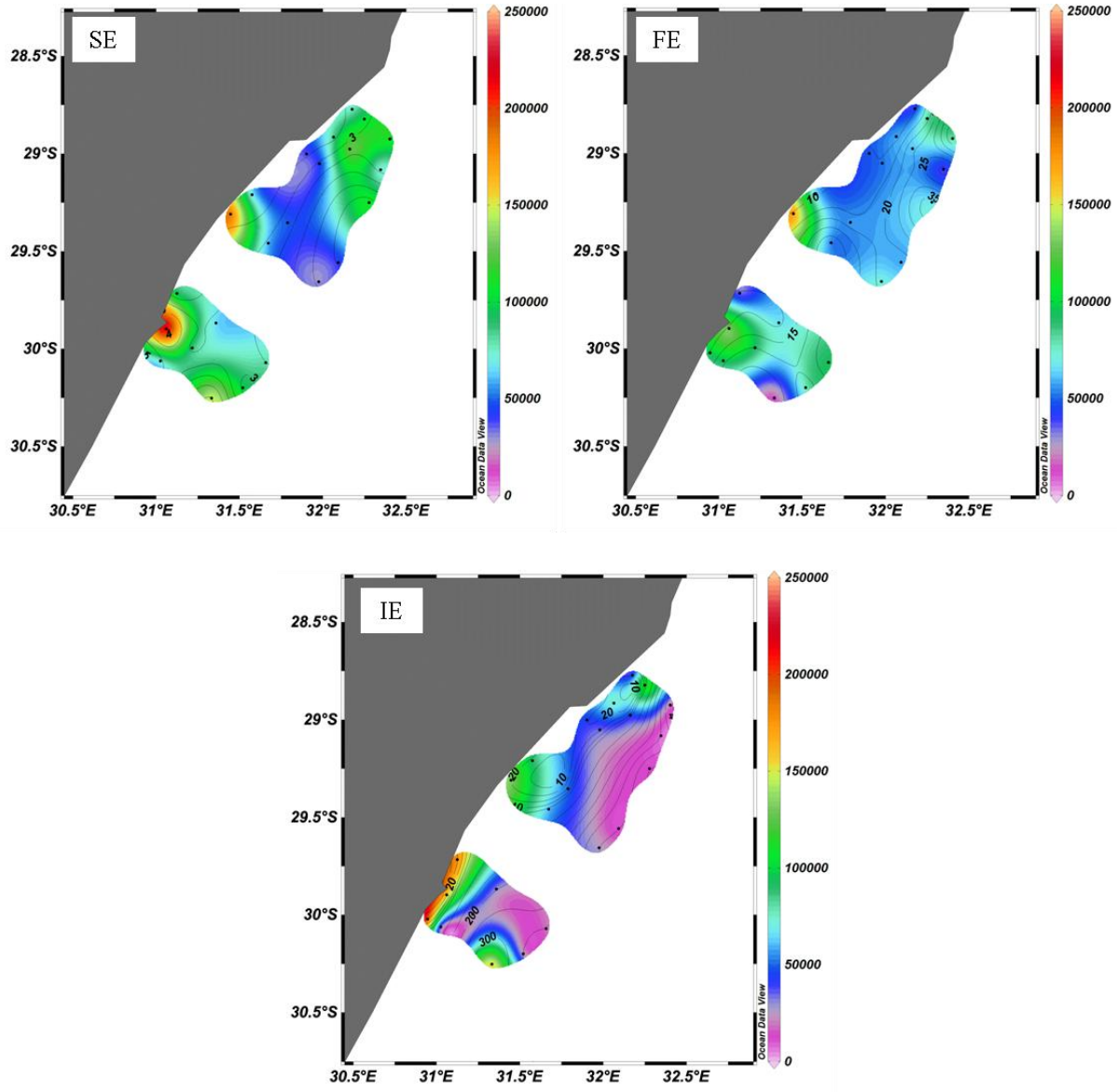

Figure 3.3.11: Bacterial numbers (cells·ml^{-1}) isosurface plots for the winter cruise, sample depths. The ecozones that are plotted are: SE (Surface Ecozone), FE (F–max Ecozone) and IE (Intermediate Ecozone).

Bacterial numbers within the surface waters of the KZN–B (SE and FE), were higher than the IE and BE (F = 16.748, df = 3, $p < 0.001$, post–hoc $p < 0.001$, Tbl. 3.5.3, pg 85), and appeared to be higher near Durban and within the vicinity of the Thukela River (Fig. 3.3.11). Bacterial numbers ranged from 7.26×10^{3} to 2.21×10^{5} cells·ml^{-1} for the whole KZN–B. Bacterial numbers were also higher within the northern sampling area of Richards Bay, but only within the SE when compared to the FE. There was however, no statistical difference between sections (F = 1.372, df = 2, $p = 0.255$, Tbl. 3.5.3, pg 85). Bacterial numbers within the IE were higher near Durban, while the highest concentration of bacterial cells for this winter cruise was found within the SE near Durban, with around 2×10^{5} cells·ml^{-1}.

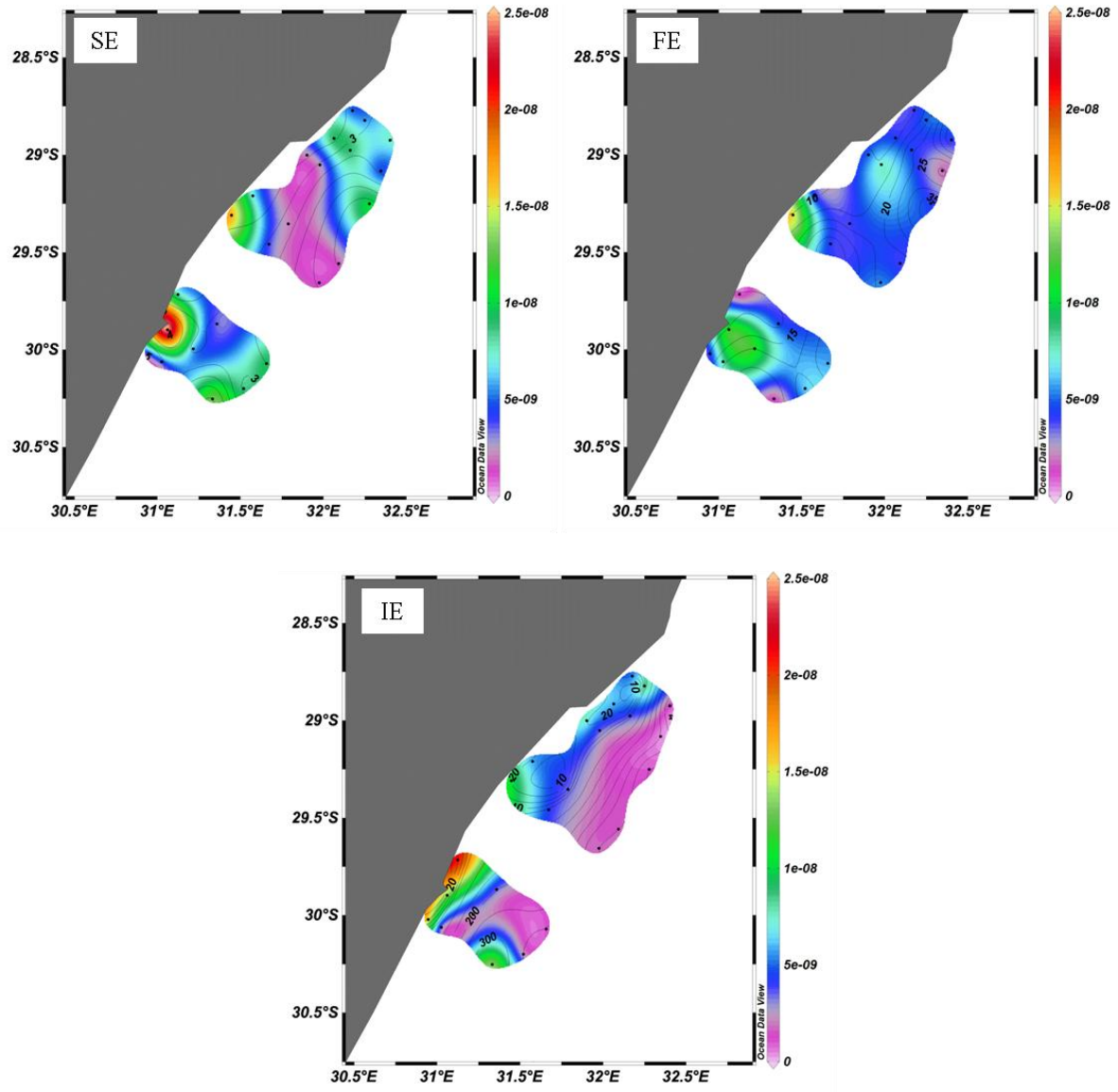

Figure 3.3.12: Bacterial biomass (gC·ml^{-1}) isosurface plots for the winter cruise, sample depths. The ecozones that are plotted are: SE (Surface Ecozone), FE (F–max Ecozone) and IE (Intermediate Ecozone).

Bacterial biomass (Fig. 3.3.12) appears to follow the same patterns as bacterial numbers above (Fig. 3.3.11) and ranged from 3.61×10^{-10} and 2.56×10^{-8} gC·ml^{-1}. Bacterial biomass within the surface waters of the KZN–B (SE and FE) were higher than the other ecozones ($F = 6.931$, df = 3, $p < 0.001$, post–hoc $p < 0.05$, Tbl 3.5.4, pg 85), and although patchy, appeared to be limited to around Durban and the Thukela River with no statistical difference found between sections ($F = 1.593$. df = 2, $p = 0.205$, Tbl 3.5.4, pg 85). Higher bacterial biomass within the IE also appears to be limited around the Durban inshore sample station. Highest bacterial biomass for this winter cruise was found near Durban, with around 2.4×10^{-8} gC·ml^{-1}.

Table 3.3.1: Chlorophyll–*a* (Chl–*a*) and bacterial numbers and biomass data integrated by maximum (max) depth for the winter cruise. Lines 4, 10 and 13 correspond to transect 1, 3 and 4 respectively. The three stations within each line correspond to a coastal station (1st station), shelf station (2nd station) and an ocean station (3rd station). Note that bacterial biomass here is presented as mgC·m^{-2} to match the units of Chl–*a*.

			Integrated Depth (·m^{-2} sea surface)		
Line	**Station**	**Max depth (m)**	**Chl–*a* (mg)**	**Numbers (cells)**	**Biomass (mgC)**
4	1	16.49	11.71	3.06×10^{6}	3.20×10^{-4}
	4	196.78	8.52	1.09×10^{7}	9.81×10^{-4}
	8	247.59	45.02	1.23×10^{7}	1.16×10^{-3}
10	1	17.86	14.37	1.30×10^{6}	9.32×10^{-5}
	5	30.62	38.26	1.77×10^{6}	1.15×10^{-4}
	9	349.89	8.72	7.51×10^{6}	1.09×10^{-3}
13	1	18.27	19.65	1.29×10^{6}	1.13×10^{-4}
	3	39.25	33.08	3.32×10^{6}	2.48×10^{-4}
	6	300.42	17.59	5.27×10^{6}	2.65×10^{-4}

When integrated over depth, overall data (Tbl. 3.3.1) indicate no patterns between line or station sampled ($F = 0.503$, $F = 2.500$, $F = 2.077$, respectively for the dependent variables, with df = 2 and $p > 0.05$ for all, Tbl. 3.3.2). Chl–*a* increases with distance from the coast along line 4 to a maximum of 45.02 mg·m^{-2}, while along lines 10 and 13, the maximum is found over the shelf station. Bacterial numbers increased with distance from the coast line reaching cell abundances into the millions per m^2 of sea surface and into the tens of millions per m^2 of sea surface along line 4. Patterns for bacterial biomass vary by line and station. Bacterial biomass decreases with distance from the coast along line 13 while increases along 10. Along line 4, bacterial biomass decreases from station 1 to 4, then increases an order of magnitude at station 8, nearly equalling the bacterial biomass found within line 10, station 9.

Table 3.3.2: Results from a parametric multi–way ANOVA performed on depth integrated data (Tbl. 3.3.1) for the winter synoptic cruise. The main factor is Position (Coastal, Shelf and Oceanic).

Factor	Dependent Variable	F	df	*p*
Position	Chl a	0.503	2	0.628
	Bacterial Numbers	2.500	2	0.162
	Bacterial Biomass	2.077	2	0.206

Assumptions of Normality [(Z = 0.323, p = 1.000), (Z = 0.726, p = 0.668), (Z = 0.381, p = 0.999), respectively] and Heterogeneity (F = 0.000, p = 1.000) were both satisfied.

There was no significant difference of depth–integrated Chl–a, bacteria numbers and biomass between the coastal, shelf and oceanic position (Tbl. 3.3.2).

3.4: Winter Cruise – Focus sampling sites

Results for the second cruise undertaken during the winter months of 2010 for the four focus sampling sites within the KZN–B are shown below. Temperature, salinity and corrected fluorescence were chosen to represent vertical profiles to show the structure of the water column during the time of sampling. Bacterial data are presented as bar graphs due to the distance between sample sites.

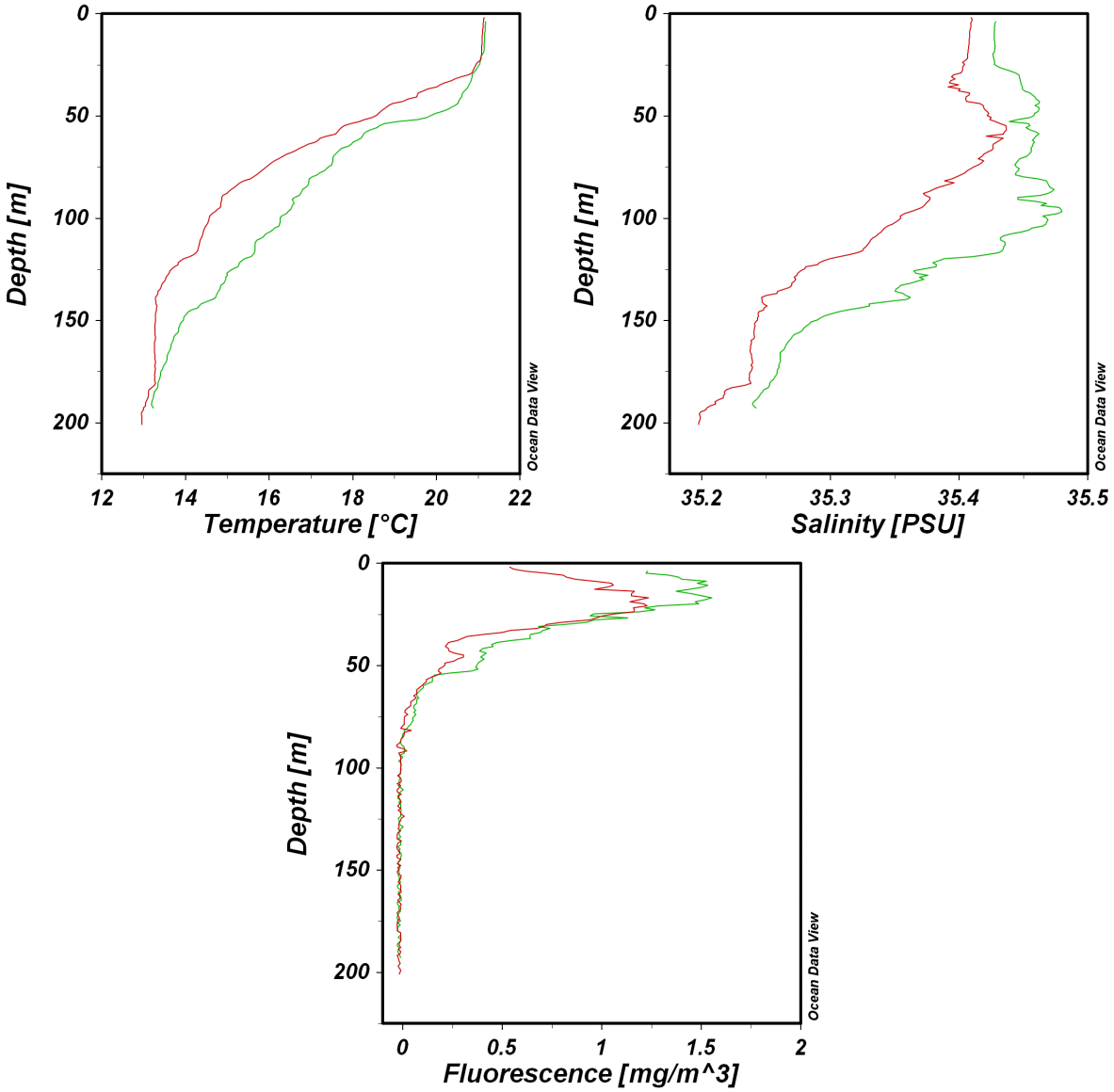

Figure 3.4.1: Vertical profiles through the water column at the Durban Eddy focus site during the winter cruise showing temperature, salinity and corrected fluorescence with depth. The red line indicates the first day of sampling while the green line the second.

The water structure for the Durban Eddy for the two sample days was very similar (Fig. 3.4.1). The temperature profile clearly shows a surface water temperature around 21°C with a distinct thermocline between 20 to 30 m, below this, the water column was very strongly stratified. Water temperature gradually dropped to about 13°C near 200 m. Salinity levels for both days within the upper 25 m were very similar, about 35.44. Below the halocline, also found between 20 to 30 m, salinity levels also decreased gradually with depth to around 35.2 to 35.25 near 200 m. Maximum corrected fluorescence was found within the upper 50 m. The presence and depth of the thermocline and halocline were measured on both sampling days at the focus site.

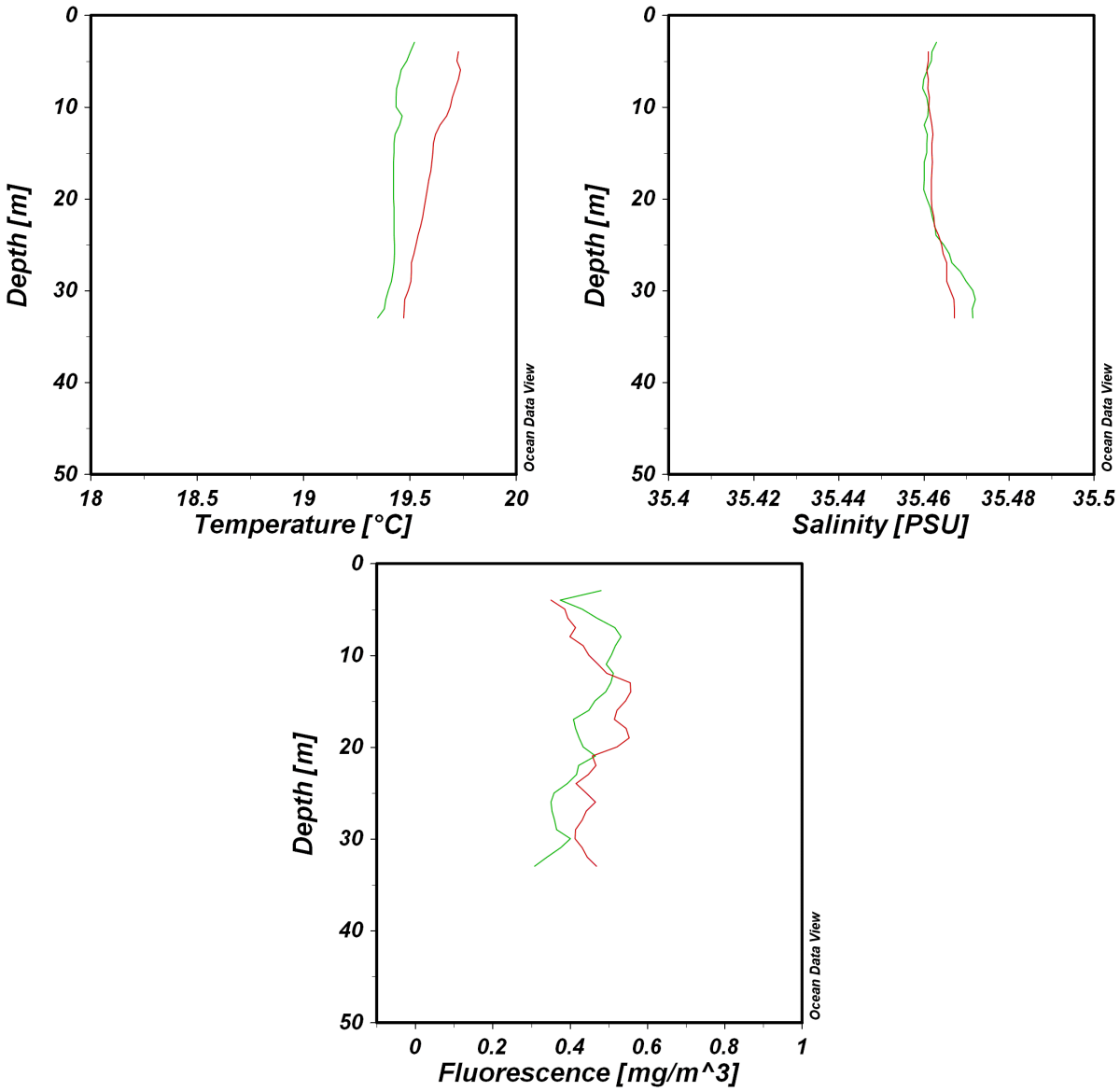

Figure 3.4.2: Vertical profiles through the water column at the Thukela Mouth focus site during the winter cruise showing temperature, salinity and corrected fluorescence with depth. The red line indicates the first day of sampling while the green line the second.

The Thukela Mouth water profile shows that the entire water column for both sampled days was completely mixed (Fig. 3.4.2). There was no thermocline or halocline and corrected fluorescence values showed no true F–max.

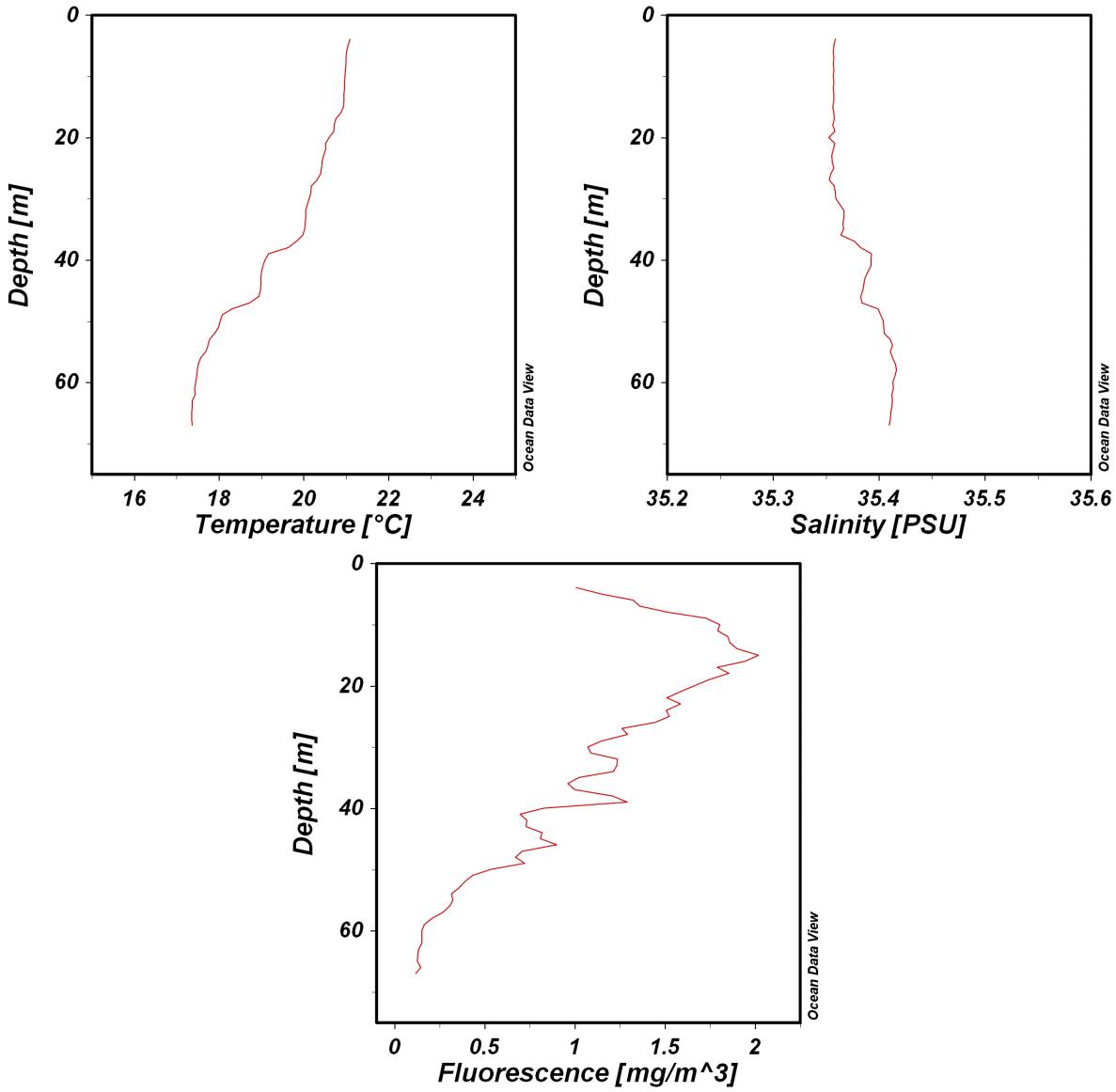

Figure 3.4.3: Vertical profiles through the water column at the Richards Bay South focus site during the winter cruise showing temperature, salinity and corrected fluorescence with depth. Only one day of sampling was possible (day two) due to extreme weather conditions.

Water profiles through the Richards Bay South focus site indicate that this water column during the time of sampling was well mixed (Fig. 3.4.3). Temperatures gradually dropped from a surface maximum of about 21°C down to about 17.5°C near 68 m while salinity differences with depth were slight. Corrected fluorescence values were high for this focus site reaching about 2 $mg \cdot m^{-3}$.

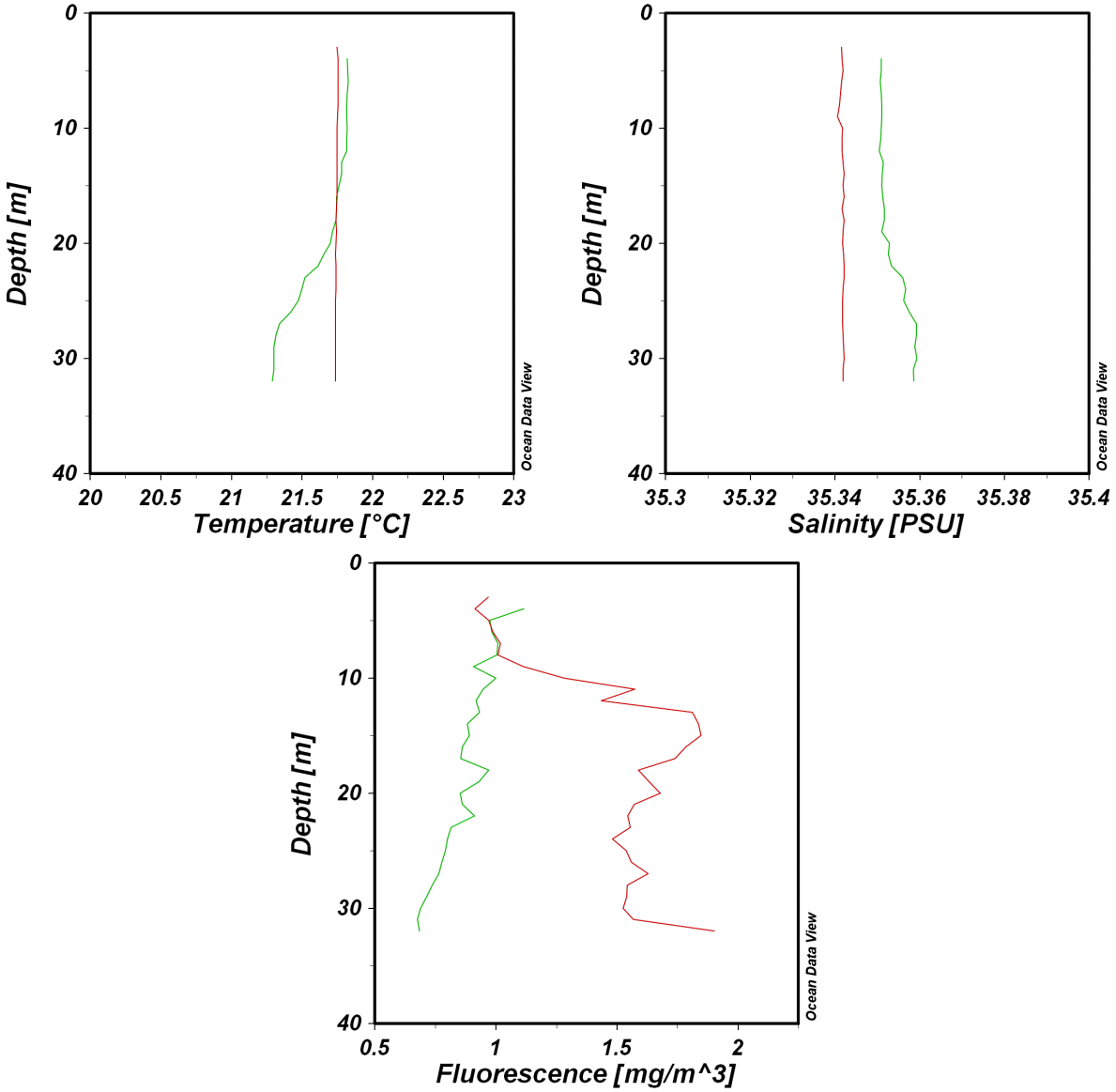

Figure 3.4.4: Vertical profiles through the water column at the Richards Bay North focus site during the winter cruise showing temperature, salinity and corrected fluorescence with depth. The red line indicates the first day of sampling while the green line the second.

As for the Thukela Mouth focus site (Fig. 3.4.2), the water column at the Richards Bay North focus site (Fig. 3.4.4) was completely mixed. Temperature (21.55°C) and salinity (35.34) within the water column during day one did not alter at all from the surface down to about 32 m. During day two down to 20 m, there was no change in temperature or salinity, while below 20 m, the temperature dropped by about 1°C. There was no thermocline or halocline and corrected fluorescence values showed no true F–max.

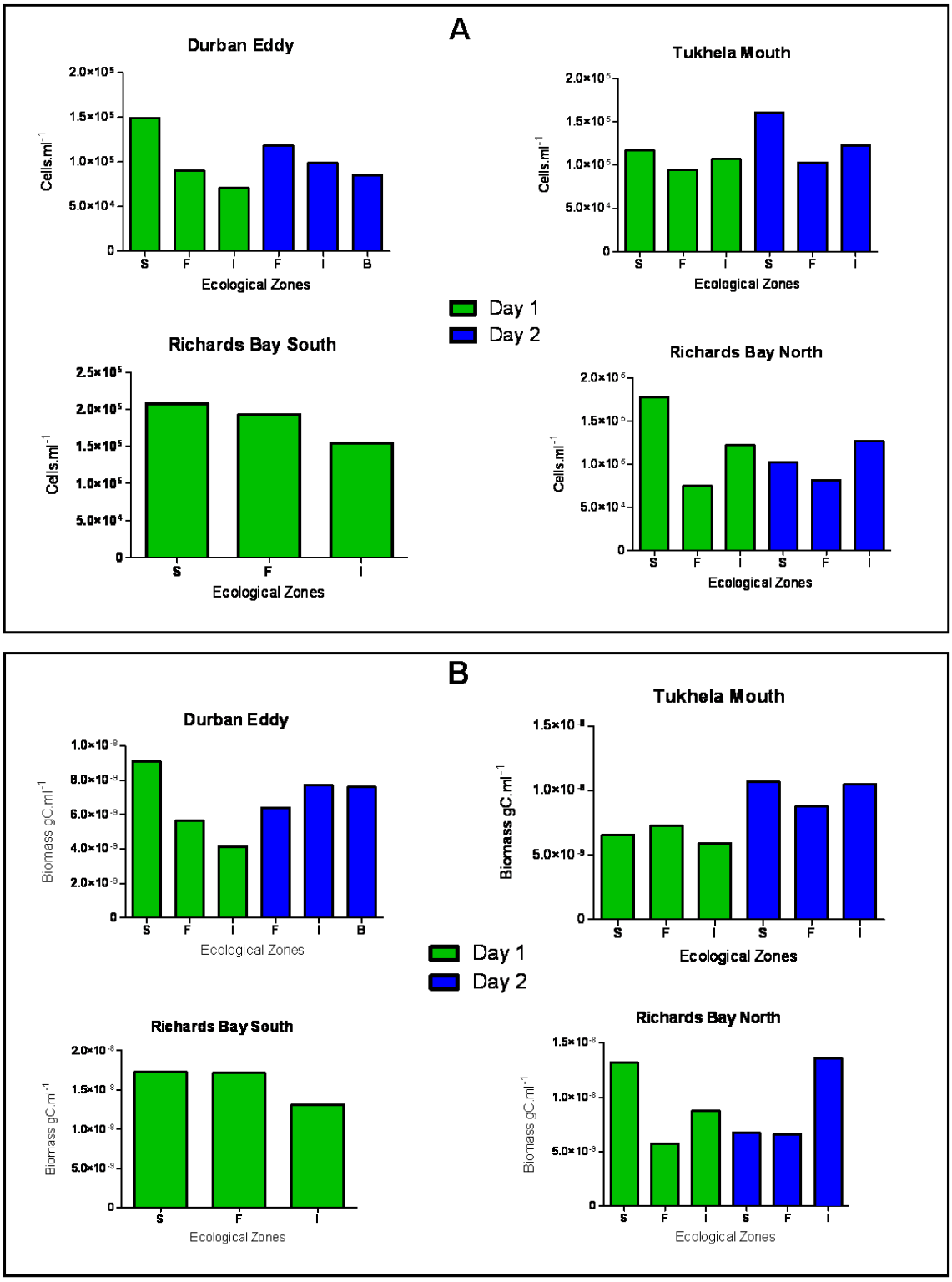

Figure 3.4.5: Bacterial numbers (cells·ml^{-1}) [A] and bacterial biomass (gC·ml^{-1}) [B] for the four focus sites during the winter cruise. The ecological zones (ecozones) that are plotted here are: S (Surface Ecozone); F (F–max Ecozone) and I (Intermediate Ecozone). For the Durban Eddy day 2, there is no S, there is a B (Bottom Ecozone).

For the winter focus cruise, bacterial productivity ranged from 4.12×10^{2} to 4.52×10^{3} cells·ml^{-1}·hr^{-1} and 9.49×10^{-12} to 1.04×10^{-10} gC·ml^{-1}·hr^{-1}. Bacterial numbers and biomass (Fig. 3.4.5) did not vary considerably between sample days and ecozone. Highest bacterial numbers were found within the Richards Bay South focus area within the SE, about 2×10^{5} cells·ml^{-1}. Bacterial numbers (Fig. 3.4.5 A) were higher in all the SE for all the focus sites, while bacterial biomass (Fig. 3.4.5 B) was also generally higher within the SE with an exception in Richards Bay North.

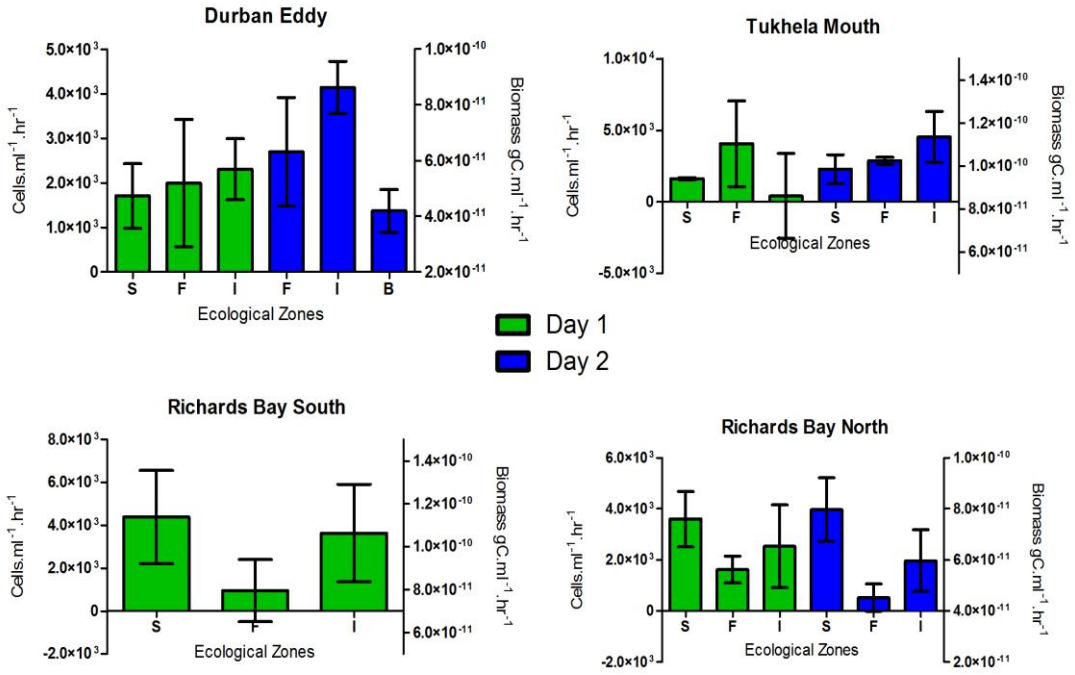

Figure 3.4.6: Bacterial productivity as determined by numbers (cells·ml^{-1}·hr^{-1}) and biomass (gC·ml^{-1}·hr^{-1}) for the four focus sites during the winter cruise. The ecological zones (ecozones) that are plotted here are: S (Surface Ecozone); F (F–max Ecozone) and I (Intermediate Ecozone). For the Durban Eddy day 2, there is no S, there is a B (Bottom Ecozone).

Bacterial productivity during the winter cruise was extremely variable over all the focus sites (Fig. 3.4.6). Bacterial productivity showed no pattern with regard to sample day or ecozone. Bacterial productivity at the Durban Eddy focus site on day one increased with increasing ecozone depth, while during day two, the BE was the lowest. The Thukela Mouth focus site showed higher bacterial productivity at the FE on day one compared to the other ecozones, while on day two, bacterial productivity increased with increasing ecozone depth. The lowest bacterial productivity at the Richards Bay South focus site was found within the FE, while the SE and the IE were similar. Bacterial productivity at the Richards Bay North focus site showed high bacterial productivity at the SE, which then decreased within the FE, then increased again within the IE. There was no statistical

difference between ecozones for bacterial productivity regarding numbers or biomass of the Durban Eddy, Thukela Mouth and Richards Bay North focus sites (F = 0.034, df = 2, p = 0.966 and F = 0.188, df = 2, p = 0.830, respectively Tbls. 3.5.5 and 3.5.6, pg 86). There was however, a significant difference between these three focus sites for bacterial productivity regarding numbers and biomass (F = 12.084, df = 2, p = 0.001 and F = 5.029, df = 2, p = 0.019, respectively, Tbls. 3.5.5 and 3.5.6, pg 86), with the Durban Eddy showing the lowest productivity in numbers and biomass (post–hoc $p < 0.05$ for all, Tbls. 3.5.5 and 3.5.6 pg 86).

Table 3.4.1: Daily productivity biomass (P / B) ratios for the winter cruise focus sites, for two days of sampling, at the Surface Ecozone (SE), F–max Ecozone (FE) and the IE (Intermediate Ecozone) or the BE (Bottom Ecozone).

		Focus Sample Site			
Day	**Ecozone**	**Durban Eddy**	**Thukela Mouth**	**Richards Bay South**	**Richards Bay North**
1	SE	0.0044	0.0057	**	0.0063
	FE	0.0083	0.0129	**	0.0065
	IE / BE	0.013	0.0016	**	0.0067
2	SE	*	0.0049	0.0058	0.0135
	FE	0.008	0.0075	0.0013	0.0018
	IE / BE	0.0125	0.0099	0.0064	0.0033

* Surface sample was missed for this focus area during day 2
** No samples taken due to severe weather conditions

P / B ratios for all the focus sample sites for the winter cruise were low (Tbl. 3.4.1). The highest P / B ratio was 0.0135 within the Richards Bay North focus site within the SE. There was no discernable pattern or difference among the sample days, ecozones or between focus sites ($p > 0.05$ for all factors, Tbl. 3.4.2).

Table 3.4.2: Results from a parametric two–way ANOVA performed on P / B data for the winter focus cruise (Tbl 3.4.1). The main factors are Focus Site [Durban Eddy (DE), Thukela Mouth (TM), Richards Bay South (RS) and Richards Bay North (RN)] and Ecozone [Surface (S), F–max (F), Intermediate and Bottom (I / B)].

Factor	**F**	**df**	***p***
Focus Site (FS)	0.854	3	0.503
Ecozone (E)	0.344	2	0.719
FS * E	1.882	6	0.200

Assumptions of Normality (Z = 0.494, p = 0.968) and Heterogeneity (F = 0.000, p = 1.000) were both satisfied.

A two-way ANOVA on the P / B ratio data (Tbl. 3.4.2) showed no statistical difference for Focus Site or Ecozone.

3.5: Cruise Comparison – Summer vs. Winter

Relevant data from the two cruises undertaken are presented below. Data are tabulated to compare seasons by standardizing line, station as well as depth sampled between Chl–*a* and bacterial numbers and bacterial biomass. Results are also presented after statistical evaluation of all bacterial data in determining if any significant differences were present between seasons.

Table 3.5.1: Chlorophyll–*a* (Chl–*a*) and bacterial numbers (Numbers) and biomass (Biomass) for both the summer and winter cruise, integrated by depth to the deepest common depth (DCD). Lines 4, 8, 10 and 13 correspond to transect 1, 2, 3 and 4 respectively. The three stations within each line correspond to a coastal station (1st station), shelf station (2nd station) and an ocean station (3rd station). Bacterial biomass here is presented as $mgC \cdot m^{-2}$ to match the units of Chl–*a*.

			Depth Integration ($\cdot m^{-2}$ sea surface)					
			Chl–*a* (mg)		**Numbers (cells)**		**Biomass (mgC)**	
Line	**Station**	**DCD (m)**	**Summer**	**Winter**	**Summer**	**Winter**	**Summer**	**Winter**
	1	16	7.39	11.36	2.11×10^{6}	2.97×10^{6}	2.40×10^{-4}	3.10×10^{-4}
4	4	30	1.46	1.30	9.52×10^{5}	1.67×10^{6}	3.50×10^{-4}	1.50×10^{-4}
	8	247	13.71	44.91	6.45×10^{6}	1.23×10^{7}	1.27×10^{-3}	1.16×10^{-3}
	1	16	10.71	*	6.07×10^{6}	*	1.02×10^{-3}	*
8	5	30	8.25	*	4.37×10^{6}	*	9.44×10^{-4}	*
	9	247	7.76	*	9.21×10^{6}	*	2.14×10^{-3}	*
	1	16	10.57	12.87	3.83×10^{6}	1.17×10^{6}	7.67×10^{-4}	8.35×10^{-5}
10	5	30	10.18	37.49	8.24×10^{6}	1.74×10^{6}	2.00×10^{-3}	1.13×10^{-4}
	9	247	10.95	6.16	1.57×10^{7}	5.30×10^{6}	4.79×10^{-3}	7.72×10^{-4}
	1	16	8.19	17.21	4.44×10^{6}	1.13×10^{6}	1.46×10^{-3}	9.88×10^{-5}
13	3	30	7.65	25.29	4.64×10^{6}	2.54×10^{6}	1.53×10^{-3}	1.89×10^{-4}
	6	247	12.97	14.46	9.60×10^{6}	4.33×10^{6}	2.40×10^{-3}	2.18×10^{-4}

* Data not available

Chl–*a* and bacterial numbers and bacterial biomass for the selected sample lines were compared over both cruises by integrating the data to the deepest common depth (Tbl. 3.5.1). Chl–*a* concentrations were mainly higher during the winter season compared to the summer season, however the difference was not significant ($F = 0.542$, $df = 1$, $p = 0.512$, Tbl. 3.5.2). However, Chl–*a* data integrated down to the DCD of 247 m should be taken with some caveats, as Chl–*a* data presented here (Figs. 3.1.9 and 3.3.9) within the KZN–B indicate that the presence of Chl–*a* below 100 m is highly unlikely. Bacterial numbers along line 4 were higher in the winter than the summer season, while along lines 10 and 13 were higher in the summer for all stations. Bacterial numbers over the deepest DCD were often an order of magnitude higher compared to the opposite season with a

statistical difference found between seasons (F = 16.180, df = 1, p = 0.001, Tbl. 3.5.2). Bacterial biomass along line 4 for both seasons showed no distinct pattern between station or season, while along lines 10 and 13, bacterial biomass was higher in the summer season, often by an order of magnitude when compared to the winter season also showing a statistical difference between seasons (F = 13.892, df = 1, p = 0.002, Tbl. 3.5.2). For both seasons, bacterial numbers were highest over the deeper DCD (oceanic) for the lines presented (F = 5.743, df = 2, p = 0.012, post–hoc $p < 0.05$, Tbl. 3.5.2). Bacterial biomass however, unlike bacterial numbers, was not highest over the deeper DCD except along line 4. Chl–*a* and bacterial numbers showed a significant difference between position (F = 5.177, F = 5.743, $p < 0.05$ for all, Tbl. 3.5.2), with the oceanic positions showing the highest values (post–hoc $p < 0.05$ for all, Tbl. 3.5.2).

Table 3.5.2: Results from a parametric multi–way ANOVA performed on depth integrated data (Tbl. 3.5.1) comparing seasonal data. The main factors are Cruise (Summer, Winter) and Position (Coastal, Shelf and Oceanic).

Factor	Dependent Variable	F	df	*p*
Season (S)	Chl a	0.452	1	0.512
	Bacterial Numbers	16.18	1	0.001
	Bacterial Biomass	13.892	1	0.002
Position (P)	Chl a	4.874	2	0.023
	Bacterial Numbers	10.742	2	0.001
	Bacterial Biomass	5.208	2	0.019
S * P	Chl a	2.318	2	0.133
	Bacterial Numbers	5.119	2	0.020
	Bacterial Biomass	3.854	2	0.045

Assumptions of Normality [(Z = 0.533, p = 0.939), (Z = 0.785, p = 0.568), (Z = 1.192, p = 0.117), respectively] and Heterogeneity (F = 0.000, p = 1.000) were both satisfied.
Post–Hoc Test (Tukey) showed the following differences:
1) Position
1.1) Chl a: (Coastal, Shelf) < (Shelf, Oceanic) with $p < 0.05$
1.2) Numbers: (Coastal, Shelf) < Oceanic with $p < 0.05$
1.3) Biomass: (Coastal, Shelf) < (Shelf, Oceanic) with $p < 0.05$

A significant interaction effect between season and position was determined for depth integrated bacterial numbers and biomass data (Tbl. 3.5.2).

Table 3.5.3: Results from a parametric three–way ANOVA performed on bacterial numbers for the synoptic cruise. The main factors are Season (Summer and Winter), Ecozone [Surface (S), F–max (F), Intermediate (I) and Bottom (B)] and Section [Southern (composed of lines 1 to 5), Central (composed of lines 6 to 12) and Northern (composed of lines 13 to 16)].

Factor	F	df	*p*
Season (S)	1.597	1	0.207
Ecozone (E)	16.748	3	< 0.001
Section (SEC)	1.372	2	0.255
S * E	3.762	3	0.011
S * SEC	11.672	2	< 0.001
E * SEC	0.433	6	0.857
S * E * SEC	0.313	6	0.930

Assumptions of Normality (Z = 1.068, $p = 0.204$) and Heterogeneity (F = 0.000, $p < 0.001$) were both satisfied.
Post–Hoc Test (Tukey) showed the following differences:
1) Ecozone: (I, B) < (F, S) with $p < 0.001$

Bacterial numbers for the synoptic section (Tbl. 3.5.3) showed no significant difference between season (F = 1.597, df = 1, $p = 0.207$) or section (F = 1.372, df = 2, $p = 0.255$), but a significant difference between ecozones (F = 16.748, df = 3, $p < 0.001$) with surface waters (F and S) showing highest numbers (post–hoc $p < 0.001$). Bacterial biomass for the synoptic section (Tbl. 3.5.4) showed a significant difference between season (F = 36.082, df = 1, $p < 0.001$) as well as ecozone (F = 6.931, df = 3, $p < 0.001$) with surface waters (F and S) showing highest biomass (post–hoc $p < 0.05$).

Table 3.5.4: Results from a non–parametric three–way ANOVA performed on bacterial biomass for the synoptic cruise. The main factors are Season (Summer and Winter), Ecozone [Surface (S), F–max (F), Intermediate (I) and Bottom (B)] and Section [Southern (composed of lines 1 to 5), Central (composed of lines 6 to 12) and Northern (composed of lines 13 to 16)].

Factor	F	df	*p*
Season (S)	36.082	1	< 0.001
Ecozone (E)	6.931	3	< 0.001
Section (SEC)	1.593	2	0.205
S * E	3.735	3	0.012
S * SEC	13.697	2	< 0.001
E * SEC	0.344	6	0.913
S * E * SEC	0.265	6	0.953

Post–Hoc Test (Tukey) showed the following differences:
1) Ecozone: I < (B, F) < (F, S) with $p < 0.05$

Table 3.5.5 Results from a parametric three–way ANOVA performed on bacterial productivity for numbers during the focus cruise. The main factors are Season (Summer and Winter), Ecozone [Surface (S), F–max (F), Intermediate (I) and Bottom (B)] and Focus Site [Durban Eddy (DE), Thukela Mouth (TM) and Richards Bay North (RN)]. The Mid shelf and Richards Bay South focus sites were deleted from the data set as each of these were season dependent sites.

Factor	F	df	*p*
Season (S)	90.868	1	< 0.001
Ecozone (E)	0.034	2	0.966
Focus Site (FS)	12.084	2	0.001
S * E	0.539	2	0.593
S * FS	16.542	2	< 0.001
E * FS	0.933	4	0.468
S * E * FS	2.550	4	0.077

Assumptions of Normality (Z = 0.929, $p = 0.353$) and Heterogeneity (F = 0.000, $p = 1.000$) were both satisfied.
Post–Hoc Test (Tukey) showed the following differences:
1) Focus Site: DE < (RBN, TM) with $p < 0.05$

Statistical analysis on the productivity of bacterial cells, as assessed by ^{3}H–Thymidine and converted into bacterial abundance productivity (Tbl. 3.5.5) by using equation 12 (page 27), showed a significant difference between season (F = 90.868, df = 1, $p < 0.001$), as well as focus site (F = 12.084, df = 2, $p = 0.001$) with a significant interaction effect between season and focus site (F = 16.542, df = 2, $p < 0.001$). The Tukey post–hoc test showed that the Durban Eddy had the lowest numbers in terms of productivity ($p < 0.05$).

Table 3.5.6: Results from a non–parametric three–way ANOVA performed on bacterial biomass productivity data for the focus cruise. The main factors are Season (Summer and Winter), Ecozone [Surface (S), F–max (F), Intermediate (I) and Bottom (B)] and Focus Site [Durban Eddy (DE), Thukela Mouth (TM) and Richards Bay North (RN)]. The Mid shelf and Richards Bay South focus sites were deleted from the data set as each of these were season dependent sites.

Factor	F	df	*p*
Season (S)	83.588	1	< 0.001
Ecozone (E)	0.188	2	0.830
Focus Site (FS)	5.029	2	0.019
S * E	0.714	2	0.504
S * FS	6.130	2	0.010
E * FS	1.285	4	0.315
S * E * FS	3.029	4	0.047

Post–Hoc Test (Tukey) showed the following differences:
1) Focus Site: (DE, RN) < (RN, TM) with $p < 0.05$

Statistical analysis on the productivity of bacterial cells during the focus cruise, as assessed by ^{3}H–Thymidine and converted into bacterial carbon productivity (Tbl. 3.5.6) by using equation 13 (page 27), also showed a significant difference between season ($F = 83.588$, $df = 1$, $p < 0.001$), and focus site ($F = 5.029$, $df = 2$, $p = 0.019$) with a significant interaction effect between season and focus site ($F = 6.130$, $df = 2$, $p = 0.010$) and season, ecozone and focus site ($F = 3.029$, $df = 4$, $p = 0.047$). Again, the Tukey post–hoc test showed that the Durban Eddy had the lowest biomass in terms of productivity ($p < 0.05$).

Table 3.5.7: Results from a non–parametric multi–way ANOVA performed on nutrient and Chl–*a* data for the synoptic sections. The main factors are; Season (Summer and Winter), Section [Southern (composed of lines 1 to 5), Central (composed of lines 6 to 12) and Northern (composed of lines 13 to 16)], and Ecozone [Surface (S), F–max (F), Intermediate (I) and Bottom (B).

Factor	Dependent Variable	F	df	*p*
Season	Temperature	5.855	1	0.016
	Salinity	39.595	1	< 0.001
	Chl a	88.498	1	< 0.001
	Silicate	5.971	1	0.015
	Phosphate	4.217	1	0.041
	Nitrate	0.400	1	0.528
	Nitrite	15.303	1	< 0.001
Section	Temperature	5.238	2	0.006
	Salinity	7.315	2	0.001
	Chl a	1.109	2	0.332
	Silicate	22.018	2	< 0.001
	Phosphate	0.104	2	0.901
	Nitrate	0.080	2	0.923
	Nitrite	2.266	2	0.106
Ecozone	Temperature	66.027	3	< 0.001
	Salinity	6.137	3	< 0.001
	Chl a	43.269	3	< 0.001
	Silicate	29.943	3	< 0.001
	Phosphate	42.599	3	< 0.001
	Nitrate	65.396	3	< 0.001
	Nitrite	5.140	3	0.002
Season * Section	Temperature	1.520	2	0.221
	Salinity	0.070	2	0.932
	Chl a	0.159	2	0.853
	Silicate	1.189	2	0.306
	Phosphate	0.138	2	0.871
	Nitrate	1.183	2	0.308
	Nitrite	0.589	2	0.556

	Temperature	16.642	3	< 0.001
	Salinity	3.856	3	0.010
Season	Chl a	7.796	3	< 0.001
*	Silicate	4.033	3	0.008
Ecozone	Phosphate	3.745	3	0.012
	Nitrate	8.958	3	< 0.001
	Nitrite	0.965	3	0.410
	Temperature	0.463	6	0.836
	Salinity	0.195	6	0.978
Section	Chl a	1.260	6	0.276
*	Silicate	0.179	6	0.982
Ecozone	Phosphate	0.244	6	0.961
	Nitrate	0.700	6	0.650
	Nitrite	0.652	6	0.689
	Temperature	0.243	6	0.962
Season	Salinity	0.299	6	0.937
*	Chl a	0.635	6	0.702
Section	Silicate	0.200	6	0.067
*	Phosphate	0.534	6	0.783
Ecozone	Nitrate	1.532	6	0.168
	Nitrite	0.596	6	0.733

Post–Hoc Test (Tukey) showed the following differences:

1) Section:
   1.1) Temperature: (Southern, Central) < Northern with $p < 0.001$
   1.2) Salinity: Northern < (Central, Southern) with $p < 0.05$
   1.3) Silicate: Southern < (Northern, Central) with $p < 0.001$
2) Ecozone:
   2.1) Temperature: (B, I) < F < S with $p < 0.001$
   2.2) Salinity: (B, I) < (S, F) with $p < 0.05$
   2.3) Chl a: (I, B) < S < F with $p < 0.001$
   2.4) Silicate: S < F < I < B with $p < 0.001$
   2.5) Phosphate: S < F < (I, B) with $p < 0.001$
   2.6) Nitrate: S < F < (I, B) with $p < 0.001$
   2.7) Nitrite: (I, S, B) < F with $p < 0.05$

Statistical evaluation of the physico–chemical data for the synoptic sections (Tbl. 3.5.7) shows a significant difference between ecozones for all tested variables ($p < 0.05$). As expected for a summer and winter cruise, there was a significant difference for temperature ($F = 5.855$, $df = 1$, $p = 0.016$) and Chl–*a* ($F = 88.498$, $df = 1$, $p < 0.001$) between seasons sampled with temperature showing a statistical difference between sections ($F = 5.238$, $df = 2$, $p = 0.006$). Besides temperature and Chl–a, other variables showing a statistical difference between season were salinity ($F = 39.595$, $df = 1$, $p < 0.001$)

and silicate (F = 5.971, df = 1, p = 0.015), phosphate (F = 4.217, df = 1, p = 0.041) and nitrite (F = 15.303, df = 1, p < 0.001).

Table 3.5.8: Results from a multi–way ANOVA performed on nutrient and Chl–*a* data for the focus sections. The main factors are Season (Summer and Winter), Section [Southern (composed of lines 1 to 5), Central (composed of lines 6 to 12) and Northern (composed of lines 13 to 16)], and Ecozone [Surface (S), F–max (F), Intermediate (I) and Bottom (B).

Factor	Dependent Variable	F	df	*p*
Season	Temperature	29.824	1	< 0.001
	Salinity	28.487	1	< 0.001
	Chl a	37.521	1	< 0.001
	Silicate	0.651	1	0.429
	Phosphate	10.094	1	0.005
	Nitrate	0.764	1	0.392
	Nitrite	0.390	1	0.540
Focus Site	Temperature	23.101	2	< 0.001
	Salinity	9.451	2	0.001
	Chl a	12.133	2	< 0.001
	Silicate	2.720	2	0.090
	Phosphate	2.281	2	0.128
	Nitrate	1.010	2	0.382
	Nitrite	18.805	2	< 0.001
Ecozone	Temperature	37.378	2	< 0.001
	Salinity	5.393	2	0.013
	Chl a	1.307	2	0.293
	Silicate	11.292	2	0.001
	Phosphate	4.121	2	0.032
	Nitrate	20.120	2	< 0.001
	Nitrite	4.340	2	0.027
Season * Site	Temperature	5.349	2	0.014
	Salinity	13.597	2	< 0.001
	Chl a	10.134	2	0.001
	Silicate	0.561	2	0.579
	Phosphate	10.359	2	0.001
	Nitrate	0.852	2	0.442
	Nitrite	5.931	2	0.009
Season * Ecozone	Temperature	33.279	2	< 0.001
	Salinity	5.299	2	0.014
	Chl a	2.228	2	0.134
	Silicate	3.193	2	0.063
	Phosphate	9.645	2	0.001
	Nitrate	7.052	2	0.005
	Nitrite	3.107	2	0.067

	Temperature	1.331	4	0.293
	Salinity	1.155	4	0.360
Focus Site	Chl a	2.952	4	0.046
*	Silicate	1.305	4	0.302
Ecozone	Phosphate	1.526	4	0.233
	Nitrate	3.375	4	0.029
	Nitrite	0.232	4	0.917
	Temperature	1.306	4	0.302
Season	Salinity	1.216	4	0.335
*	Chl a	1.037	4	0.413
Focus Site	Silicate	0.286	4	0.883
*	Phosphate	0.274	4	0.891
Ecozone	Nitrate	0.152	4	0.960
	Nitrite	0.145	4	0.963

Assumptions of Normality [(Z = 1.046, p = 0.224), (Z = 0.864, p = 0.444), (Z = 1.315, p = 0.063), (Z = 0.542, p = 0.931), (Z = 0.792, p = 0.557)] and Heterogeneity (F = 0.000, p = 1.000) were both satisfied for the parametric variables; Temperature, Salinity, Chl a, Silicate and Nitrate, respectively.
Post Hoc Test (Tukey) showed the following differences:

1) Focus Site
   1.1) Temperature: (TM, DE) < RN with $p < 0.05$
   1.2) Salinity: RN < (DE, TM) with $p < 0.05$
   1.3) Chl a: TM < (RN, DE) with $p < 0.05$
   1.4) Nitrite: (RN, DE) < TM with $p < 0.05$
2) Ecozone
   2.1) Temperature: I < F < S with $p < 0.05$
   2.2) Salinity: (S, F) < (F, I) with $p < 0.05$
   2.3) Silicate: (S, F) < I with $p < 0.05$
   2.4) Phosphate: (S, F) < (F, I) with $p < 0.05$
   2.5) Nitrate: (S, F) < I with $p < 0.001$
   2.6) Nitrite: (S, F) < (F, I) with $p < 0.05$

Statistical evaluation of the physico–chemical data for the focus sections (Tbl. 3.5.8) shows a significant difference between ecozones for all tested variables ($p < 0.05$) except Chl–a (F = 1.307, df = 2, p = 0.293). As for the synoptic cruise, there was a significant difference between seasons sampled during the focus cruise for temperature (F = 29.824, df = 1, $p < 0.001$) and Chl–*a* (F = 37.521, df = 1, $p < 0.001$) with temperature and Chl–a showing a statistical difference between focus sites (F = 23.101, df = 2, $p < 0.001$ and F = 12.133, df = 2, $p < 0.001$). Besides temperature and Chl–a, other variables showing a statistical difference between season were salinity (F = 28.487, df = 1, $p < 0.001$) and phosphate (F = 10.094, df = 1, p = 0.005).

CHAPTER 4: DISCUSSION

4.1: Structure of the KZN–B

The KZN–B is an indented region of the coastline situated along the eastern coast of South Africa (Meyer et al., 2002). The continental shelf along which the KZN–B lies is for the most part very narrow, being only about 15 km wide to the north and south of the KZN–B (Lutjeharms, 2006). Within the KZN–B itself, the shelf widens considerably to an average of 50 km from the coast line towards the 200 m isobath (Lutjeharms, 2006). This widening begins near Cape St. Lucia and levels out from Richards Bay towards the Thukela River, and then decreases down towards Durban.

The east Madagascar Current's southern limb extension, as described by Lutjeharms and Machu (2000), creates an inshore upwelling region characterised by cold surface water and high Chl–*a* concentrations [see Fig.1 in Lutjeharms and Machu (2000)] where the bathymetry moves from a narrow shelf and steep slope, to one of a wider shelf and more obtuse slope. This, also seen along the eastern Agulhas Bank where Lutjeharms et al. (2000a) describes the Agulhas Current as following along the shelf edge, but that the current itself displays an increasing propensity to meander, which is accompanied by edge shear upwelling and cyclonic eddies. It is known that the change in bathymetry from a narrow continental shelf to a wider continental shelf induces kinematically induced upwelling (Lutjeharms et al., 2000a; Lutjeharms and Machu, 2000; Lutjeharms et al., 2000b; Meyer et al., 2002), but it is the change in the steepness of the continental slope towards a more obtuse slope (Lutjeharms et al., 2000a; Lutjeharms and Machu, 2000) that appears to induce these extensions and meanderings of bottom flowing currents. Such shelf and slope attributes as described above are found within the KZN–B.

The shelf of the KZN–B, for the most part from T4 down until T2 (Fig. 3.1.1, the curve of the white shaded area to the left of the plotted data indicates the steepness) appears rather steep (as seen within all the horizontal depth profiles here). Along T1, the shelf slope is much more gentle than the shelf along the other transect lines. Due to this steepness, the deep Agulhas Current is most likely unable to uplift to a greater degree along the shelf edge, possibly causing a meandering effect and therefore edge shear effects between T3 and T2 (Lutjeharms et al., 2000a; Lutjeharms and Machu, 2000). This possible shelf edge induced meandering of Agulhas water onto the KZN–B shelf, according to Lutjeharms et al. (2000b) can also be explained by bottom Ekman veering. This is supported by previous thermal infra–red satellite imagery data from Lutjeharms et al. (2000a), where

the authors suggest that the 17°C isotherm is a good reference point for the presence of upwelled water at the sea surface.

4.2: Possible origins of nutrients

van Ballegooyen et al. (2007) reported that nutrient input into the KZN–B region from groundwater sources for nitrogen was < 0.14 $\mu mol \cdot L^{-1}$, while DWAF (1995) in Source–to–Sea (2004) reported average estimated nitrogen concentrations of 3.57 $\mu mol \cdot L^{-1}$ and average estimated phosphorus concentrations of 0.61 $\mu mol \cdot L^{-1}$ near the Thukela River. Nutrient supply from groundwater and river sources should theoretically be more regular, uninfluenced by wind, current speed or topography, but influenced by seasonal precipitation. Such a nutrient source could presumably be a reason as to why Chl–*a* concentrations, and bacterial numbers and biomass were generally higher near and around the coast, especially near and around river mouths. N and P concentrations emanating from the Thukela River exceeded surface N and P concentrations within the surrounding area. This allochthonous input of inorganic nutrients would undoubtedly have influenced phytoplankton primary production of DOM within the euphotic waters surrounding the nutrient source within the KZN–B. Fuhrman and Azam (1980) have previously concluded that substantial bacterial growth can occur in the absence of large particles. Sherr et al. (2002) have reported that the detrital volume off Cape Hatteras was generally higher around the inner shelf region (coastal) and lower towards the ocean, and that heterotrophic bacterial activity was suggested to be closely related to the presence of organic matter, while Painting et al. (1989), have shown that an increase in particulate carbon does affect bacterial numbers and biomass. Bacterial numbers (Figs. 3.1.11 and 3.3.11) and bacterial biomass (Figs. 3.1.12 and 3.3.12) were visibly higher near the coast within the KZN–B for both cruises. This suggests that nutrient availability (DOM or POM) and concentration around coastal areas was higher compared to the more open water within the KZN–B.

Lutjeharms et al. (2000b) suggest that the movement of deeper offshore water towards the coastline is where the isotherms conform to the directional slope of the shelf topography. Lutjeharms et al. (2000b) describe four water movements within the KZN–B including the St. Lucia upwelling cell, bottom water movement, the Durban Eddy and water exchange along the shelf edge. Here, at least for the water exchange along the shelf edge, offshore deeper water clearly extends onto the KZN–B shelf along T1 and T2 during the summer period and along T1 during the winter period. Such an extension is strikingly visible along T1 (Fig. 3.1.1) as seen by water colder than 10°C encroaching onto the slope. Due to the gentleness of the slope, Agulhas Current derived water is able to kinematically uplift (meander) and penetrate well up to 300 m within the KZN–B (Figs 3.1.1 and

3.3.1) carrying with it colder, less saline, and more nutrient rich water (Lutjeharms et al., 2000a), but there is no evidence of surface upwelling.

The encroachment of this water mass was also observed by Lutjeharms et al. (2000a) within their study area (the eastern Agulhas Bank) along the shelf slope. Here, Lutjeharms et al. (2000a) describe the water mass upwelling up to 100 m, with a temperature of 12°C and salinity of 35.00. This same water mass is also present within the KZN–B along T1 with temperatures ca. 12°C and salinities ca. 35. The presence of deeper, colder water near the shelf bank and on the shelf was therefore consistent in both cruises, while the presence of surface upwelling was absent (Lutjeharms et al., 2000a; Lutjeharms et al., 2000b).

Nutrient supply into KZN–B euphotic waters from the St. Lucia upwelling cell during both cruises was unlikely as shown by temperature (Figs. 3.1.1 and 3.3.1), salinity (Figs. 3.1.3 and 3.3.3) and poor surface Chl–*a* concentrations (Figs. 3.1.10 and 3.3.10) to the north of Richards Bay. The more likely scenario is that the upwelling within the area of Cape St. Lucia was the source of the water flowing along the shelf and the bank of the KZN–B, as upwelling in this area has been described to be present for much of the year (Lutjeharms et al., 2000a; Lutjeharms and Machu, 2000; Lutjeharms, 2006). Data here however, cannot substantiate whether the St. Lucia upwelling cell was present or not due to the positioning of the transect lines. Nutrient input from the Durban Eddy during the time of study was unlikely as evidence for the upliftment of bottom water into the surface was absent along T1 for the summer and winter cruise.

As discussed above, the evidence that surface upwelling was absent during both cruises for this study possibly indicates that the euphotic waters of the KZN–B were more dependent on nutrients (DOM and POM) supplied by the Thukela River (and possibly other river sources) and the distribution of these nutrients by water movement within the KZN–B.

4.3: Possible impacts of nutrients

Across the whole sampling area, nutrient concentrations within surface waters, or close to the surface, were often at the detection limit (Tbls. 3.5.7 and 3.5.8), with the exception of nitrite (Figs. 3.1.7 and 3.3.7), with Chl–*a* concentrations across the whole KZN–B being extremely variable (Figs. 3.1.10 and 3.3.10).

Nutrients, especially N and P, influence phytoplankton biomass with new production being nitrate limited within euphotic waters, therefore affecting Chl–*a* concentrations (Probyn et al., 1995; Pérez et al., 2005; Zohary et al., 2005). A microcosm experiment performed by Zohary et al. (2005)

within the P–limited waters of the eastern Mediterranean showed that the addition of N to surface seawater previously exposed to P resulted in a tenfold increase in Chl–*a* (as well as other pigments) within a four day period, with no significant change in bacterial abundance, but a substantial change in bacterial activity measured by ^{14}C–Leucine incorporation, as well an increase in ciliate abundance (Zohary et al., 2005). Zohary et al. (2005) discuss that this bacterial pattern was due to an increase in grazing pressure on the bacterial standing stock by bacterivores such as ciliates and heterotrophic nanoflagellates.

It is well known that heterotrophic bacteria utilise exudates from phytoplankton [usually those from viral lysis, sloppy feeding, cellular exudates and cellular death (Fuhrman and Azam, 1980; Rheinheimer, 1985; Rivkin et al., 1996; Fuhrman, 1999; Gasol and Duarte, 2000; Lovejoy et al., 2000; Wommack and Colwell, 2000; Menge and Weitz, 2009)] being mainly in the form of DOM, for their organic nutrient needs, resulting in an increase in bacterial numbers, biomass and productivity (Fuhrman and Azam, 1980; Azam et al., 1983; Painting et al., 1989; Goosen et al., 1997; Church et al., 2000; Sherr et al., 2002; Li et al., 2004; Fenchel, 2008). The resulting increase in bacterial numbers, biomass and productivity from the introduction of dissolved material into a usable form eventually becomes available to higher trophic levels as available bacterial biomass (Fuhrman and Azam, 1980).

4.4: Comparison of summer / winter water mass structure

During the summer period, above the thermocline and halocline, the surface waters were very well stratified (Figs. 3.1.2, 3.2.1 to 3.2.4) indicating a lack of surface wind mixing and storm action within the sampling period with higher temperatures in the surface ecozone (Tbl. 3.5.7), while during the winter period, the water column was very well mixed down to about 100 m (Figs. 3.3.2 and 3.4.1 to 3.4.4). The presence of a well defined thermocline and halocline for both cruises, forming a pycnocline, probably reinforced the inability of either kinematically, edge shear or eddy induced complete surface upwelling to occur, resulting in the warm, highly saline and nutrient poor status of KZN–B surface waters during the time of study.

During both sampling periods, bottom water was possibly present within the photic zone along T1 (31.1ºE to 31.2ºE) and T2 (31.5ºE to 31.8ºE), while only along T3 during summer sampling (31.6ºE to 31.9ºE) as seen more clearly within Figs. 3.1.2 and 3.3.2. The 17°C isotherm, as seen within Figs. 3.1.1, 3.1.2, 3.3.1 and 3.3.2 along T1 and T2, was found to reach into the upper 100 m of the water column possibly supplying bottom water derived nutrients into the photic zone. Nutrient concentrations within surface waters, or close to the surface, were often at the detection limit, while below the surface waters and the pycnocline, nutrient concentrations were much higher and often

increased with depth (Tbls. 3.5.7 and 3.5.8). This nutrient pattern was also described by Goosen et al. (1997) within Kenyan coastal waters, with similar nutrient concentrations within surface waters, also increasing with depth.

For the summer (Figs. 3.2.1 to 3.2.4) and winter focus sites (Figs. 3.4.1 to 3.4.4) there appeared to be no substantial difference between water structure for the two sampling days for any location except for Richards Bay North during summer. For all focus sites, both temperature and salinity data showed no break in the thermocline or halocline.

4.5: Comparison of summer / winter nutrient structure

Nutrient concentrations within the surface waters for both cruises appeared to be similarly low compared to the deeper waters (Tbls. 3.5.7 and 3.5.8), with the exception of nitrite concentrations being much higher within surface waters and near the coast. As for the remainder of the water column, overall nutrient concentrations appeared to be within the same range with differences existing in the spatial distribution of the nutrients only. Nitrite concentrations along T2 and T3 for both cruises were higher near the coast, probably due to the vicinity of the Thukela Mouth. Nutrient concentrations presented for both ACEP II cruises during the summer and winter sampling period of 2010 were very similar to those presented by Meyer et al. (2002) in the KZN–B in 1989 as well as by Goosen et al. (1997) within Kenyan coastal waters in 1992.

4.6: Comparison of summer / winter Chl–*a* structure

Chl–*a* concentrations during the winter sampling period (Fig. 3.3.9) were highest much closer to the surface and were more evenly distributed within the water column due to decreased intensity of irradiance and the mixing of the water column during this period. Chl–*a* concentrations during the summer sampling period (Fig. 3.1.9) appeared to follow the pattern of the thermocline (Figs. 3.1.1 and 3.1.2) and halocline (Fig. 3.1.3) forming a distinct pycnocline, possibly caused by the stratification of the water column during this sampling period. Such a pycnocline would slow phytoplankton sinking rates between the surface and intermediate depths causing accumulation (Probyn et al., 1995) which most likely resulted in the banding of the Chl–*a* layers (Fig. 3.1.9) seen during the summer cruise. The patterns described above for Chl–*a* concentrations for each season were similar to those found for each of the focus sites for both cruises (Figs. 3.2.1 to 3.2.4 and 3.4.1 to 3.4.4 respectively). During both cruises, isosurface Chl–*a* data (Figs. 3.1.10 and 3.3.10) indicated that surface concentrations were

patchy, but when integrated over depth, data (Tbl. 3.5.1) indicate that overall Chl–*a* concentration was higher during the winter cruise compared to the summer cruise, although there was no statistical difference between season (Tbl. 3.5.2).

Within the KZN–B, areas of higher phosphate and nitrate concentrations were associated with higher corrected fluorescence values (Figs. 3.1.8 and 3.3.8) and Chl–*a* concentrations (Figs. 3.1.9, 3.1.10, 3.3.9 and 3.3.10) within these areas based on geographic matches. Previous studies by Probyn et al. (1995) in the eastern Agulhas Bank, Pérez et al. (2005) in the Equatorial Atlantic and Zohary et al. (2005) in the eastern Mediterranean reported similar results with phosphate, nitrate and Chl–*a* supporting these observations made within the KZN–B. Contrary to this, in areas of low phosphate and nitrate concentrations, especially away from the coast line and over deeper waters, Chl–*a* concentrations were extremely low. Pérez et al. (2005) reported similar results where the nutrient depleted surface waters of the Equatorial Atlantic showed low Chl–*a* concentrations. Other areas of high Chl–*a* concentrations within the KZN–B were therefore also most likely influenced by the addition of fresh input of N and P, especially within the vicinity of the Thukela River, where over both cruises, Chl–*a* concentrations remained above 1 $mg \cdot m^{-3}$.

4.7: Comparison of summer / winter bacterial numbers, biomass and productivity

Highest bacterial numbers (Fig. 3.1.11 and 3.3.11) and bacterial biomass (Fig. 3.1.12 and 3.3.12) were found closest to the coast during both cruises with 6.20×10^{5} $cells \cdot ml^{-1}$ and 1.83×10^{-7} $gC \cdot ml^{-1}$ along line 16, station 1 at 35 m. This was most likely due to the input of nutrients from terrestrial origin, the effects of which can potentially be seen as bacterial hot spots along the coast, mainly in the vicinity of the Thukela River. Bacterial numbers and biomass during summer sampling along the coast line to the south of Durban were very low when compared to the northern coast line, while during winter sampling the opposite occurred, with highest bacterial numbers and biomass appearing in the south. Bacterial numbers and biomass showed no statistical difference between sections (Tbls. 3.5.3 and 3.5.4).

The spatial extent of the coast line within the KZN–B, compared to the KZN–B as a whole, is small. With KZN–B coastal waters potentially being influenced by terrestrial nutrient input, these areas would have a higher nutrient concentration compared to open waters, therefore, the open waters of the KZN–B must / should be considered separately from the coast line.

As such, during the summer cruise, bacterial numbers above 2.0×10^{5} $cells \cdot ml^{-1}$ and bacterial biomass above 5.0×10^{-8} $gC \cdot ml^{-1}$ (Figs. 3.1.11 and 3.1.12 respectively) appear to have been limited to

the central KZN–B. The central KZN–B is described here as being the area between Durban and Richards Bay (lines 6 to 12). Both bacterial numbers and biomass during the summer cruise were much reduced within the southern (south of Durban, lines 1 to 5) and northern (north of Richards Bay, lines 13 to 16) KZN–B compared to the central KZN–B (Figs. 3.1.11, 3.1.12 and Tbl. 3.5.1). Here, bacterial numbers within the central KZN–B remained relatively constant, with bacterial biomass being very patchy within the same area. The bacterial numbers and biomass pattern seen during summer sampling was most likely due to the concentration of Chl–*a* within these areas and the associated biological implications, especially on bacterial biomass.

During the winter cruise, bacterial numbers above 1.0×10^{5} cells·ml^{-1} and bacterial biomass above 1.0×10^{-8} gC·ml^{-1} (Figs. 3.3.11 and 3.3.12 respectively) appear to have been limited to the more southern KZN–B and around the Thukela Mouth, areas where Chl–*a* concentrations were higher. During the winter cruise, bacterial numbers and biomass showed very similar patterns regarding geographic positioning of hot spots, a pattern that was not present during summer sampling. These bacterial patterns appear to remain constant with increasing depth. For both cruises, bacterial numbers and biomass appear to drop below ca. 150 m, while below 250 m, bacterial numbers and biomass drop substantially further. Significant differences for bacterial numbers and biomass were found between ecozones (Tbls. 3.5.3 and 3.5.4). This pattern is similar to that found by Goosen et al. (1997) in the oligotrophic coastal waters off Kenya. Both bacterial numbers and biomass were generally higher during the summer sampling when integrated over depth (Tbl. 3.5.1).

During sampling at the focus sites, bacterial numbers at the Durban Eddy for both cruises (Figs. 3.2.5 A and 3.4.5 A) over both days decreased with increasing ecozone depth. This was most likely due to the very well layered water column during both days of sampling (Figs. 3.2.1 and 3.4.1) with the appearance of a distinct pycnocline possibly slowing sinking rates between the surface and intermediate depths causing accumulation (Probyn et al., 1995). Such accumulation was possibly seen during the first day of sampling at Durban Eddy during the summer cruise (Fig. 3.2.6), where bacterial productivity was highest at the FE. During the winter cruise, bacterial productivity at the Durban Eddy focus site increased with increasing ecozone depth, until the IE, for both days sampled with similar patterns at the Thukela Mouth focus site on the second day of sampling (Fig. 3.4.6). Such a pattern is possibly due to the very well mixed water column at the Thukela Mouth focus site during winter. Corrected fluorescence values for both cruises for the Thukela Mouth focus site (Figs. 3.2.2 and 3.4.2) were low, yet bacterial numbers, biomass and productivity here for both sampling times (Figs. 3.2.5, 3.2.6 and 3.4.5, 3.4.6 respectively) were relatively high. Corrected fluorescence, a proxy for Chl–*a*, was low, possibly indicating that organic matter contribution by phytoplankton within the Thukela Mouth focus site for both cruises was low, while bacterial numbers, bacterial biomass and bacterial

productivity were relatively high. This possibly indicates the influence the Thukela River has on the waters of the KZN–B in providing organic material for the heterotrophic bacteria to assimilate [see Bizsel et al. (2011) as an example of POM contribution from a river source]. Bacterial productivity during the summer cruise at the Thukela Mouth focus site (Fig. 3.2.6) was very consistent over both days of sampling, staying above 2.0×10^{4} cells·ml^{-1}·hr^{-1} and 1.0×10^{-9} gC·ml^{-1}·hr^{-1} at all ecozones, while during winter, bacterial productivity was much reduced when compared to summer. For bacterial productivity regarding both numbers and biomass, a statistical difference was found between season (Tbls. 3.5.5 and 3.5.6). This was possibly due to the decreased availability of organic matter and reduced precipitation during the winter period. Bacterial productivity similarly assessed by Goosen et al. (1997) within Keyan coastal waters showed the highest Thymidine incorporation near the Galana River during their A1 cruise, with 15.8 pmol TdR·L^{-1}·h^{-1}. All other incorporation rates were much lower than this, averaging 3.1 ± SD 1.4 and 6.6 ± SD 2.4 pmol TdR·L^{-1}·h^{-1} during cruise A1 and A2 respectively (Goosen et al., 1997). This suggests the importance of rivers in such systems.

The Richards Bay North focus site during summer sampling (Fig. 3.2.4) showed a very shallow pycnocline, around 10 m, with a weak F–max near 22 m with a corrected fluorescence value of 1.5 mg·m^{-3} on day one of sampling. The abrupt change in water density during day two negatively impacted bacterial numbers and biomass, while positively influencing bacterial productivity by at least an order of magnitude for all sampled ecozones within the water column. This was possibly due to the pycnocline being reinforced by the increase in water density strengthening accumulation (Probyn et al., 1995). Such accumulation of phytoplankton and bacterial cells would potentially attract predators and thereby reduce bacterial numbers and bacterial biomass. The organic exudates from live phytoplankton cells, as well as from sloppy feeding, faecal matter etc, would then be assimilated by the active heterotrophic bacterial population resulting in an increase in bacterial productivity. This pattern was different during the winter sampling period, where no change was present within the water column during sampling, with no substantial change in bacterial numbers, biomass or productivity.

The Mid shelf focus site was sampled during the summer cruise due to the appearance of what appeared to be an ephemeral phytoplankton bloom in the area resulting in a corrected fluorescence value of over 1.5 mg·m^{-3} on day one, which increased to over 2.5 mg·m^{-3} on day two (Fig. 3.2.3). Bacterial numbers, biomass and productivity (Figs. 3.2.5 and 3.2.6) within this focus site were much higher at the SE during day one of sampling. During day two at the SE, bacterial numbers, biomass and productivity decreased substantially while for all the remaining ecozones bacterial numbers and biomass remained constant while bacterial productivity increased at the FE and IE. This instance during day two was possibly top–down controlled, however a more simple explanation was that the patch of Chl–*a* simply dissipated with currents. Only one day of sampling was possible for Richards

Bay South during the winter cruise and as such comparative analysis over a time series is not possible. During the summer cruise, Richards Bay South was not sampled.

Bacterial productivity over both seasonal cruises was very different. Bacterial productivity during the winter sampling cruise for all focus sites did not exceed 5000 cells·ml^{-1}·hr^{-1} (Fig. 3.4.6). These values are similar to those found at the Durban Eddy during the summer cruise, with the highest productivity here being just over 6000 cells·ml^{-1}·hr^{-1} (Fig. 3.2.6). During summer sampling, bacterial productivity was highest at the Mid Shelf station probably due to the ephemeral phytoplankton bloom, resulting in maximal bacterial productivity exceeding 8.0×10^{4} cells·ml^{-1}·hr^{-1} and 3.5×10^{-9} gC·ml^{-1}·hr^{-1} at the SE on day one. For the remaining ecozones at the Mid Shelf site over both days, maximal bacterial productivity exceeded 4.0×10^{4} cells·ml^{-1}·hr^{-1} and 2.0×10^{-9} gC·ml^{-1}·hr^{-1}. Maximum bacterial productivity for the Thukela Mouth and Richards Bay North focus sites during summer exceeded 4.0×10^{4} cells·ml^{-1}·hr^{-1} and 1.5×10^{-9} gC·ml^{-1}·hr^{-1}. Bacterial productivity during winter sampling showed the Durban Eddy focus site (Fig. 3.4.6) to be relatively consistent over both sampling days over all ecozones compared to the Thukela Mouth and Richards Bay North focus sites. Overall, bacterial numbers, biomass and productivity were very inconsistent over both days of sampling but are comparable to other studies (Tbl. 4.8.1, pg. 109). Kirchman et al. (1993), within the oceanic subarctic Pacific have shown that daily differences in bacterial dynamics were mainly due to grazing pressure rather than environmental factors. Both DuFour and Torréton (1996) and Tanaka and Rassoulzadegan (2002) provided evidence that bacterial biomass is mainly top–down controlled. It can therefore be suggested within the KZN–B, that daily differences in bacterial numbers, biomass and productivity within the photic zone were probably influenced by top–down control via grazing pressure, while over a seasonal scale, bacterial numbers, biomass and productivity were probably influenced by summer induced high primary productivity, resulting in increased bacterial productivity, and winter induced low primary productivity resulting in low bacterial productivity.

4.8: Relationship of bacterial dynamics to KZN–B dynamics as a whole

For the summer and winter cruise, relationships between Chl–*a* and bacterial numbers and bacterial biomass were evident: Chl–*a* concentration and bacterial numbers and bacterial biomass were generally higher nearer and around the coast; Chl–*a* concentration and bacterial biomass generally decreased with distance from the coast towards the open ocean whilst bacterial numbers generally did not; bacterial numbers and bacterial biomass decreased with depth.

As discussed previously, Sherr et al. (2002) showed that detrital volume decreases with distance from the coast, so it is not surprising that these authors also determined that there was a higher

percentage of metabolically active bacterial cells in inshore waters when compared to offshore waters. It is quite clear when looking at the results here, within the SE and the FE, that Chl–*a* concentration (Fig. 3.1.10 and 3.3.10) and bacterial biomass (Figs. 3.1.12 and 3.3.12) generally decreased with distance from the coast towards the open ocean, whilst bacterial numbers (Figs. 3.1.11 and 3.3.11) generally did not. The bacterial numbers pattern within the KZN–B is similar to that found by Goosen et al. (1997) within Kenyan coastal waters in 1992, who also found little change in bacterial abundance with distance from the Kenyan coast (except for their Gazi transect). Thymidine incorporation experiments also performed by Goosen et al. (1997) within Kenyan coastal surface waters showed a decrease in incorporation rates with increasing distance from the coast. Although bacterial productivity experiments within the KZN–B were only performed at preselected locations near the coast, the bacterial numbers pattern present between the KZN–B and Kenyan coastal waters presented by Goosen et al. (1997) potentially indicate very similar patterns between these two systems for all bacterial dynamics, including bacterial productivity. This may suggest that bacterial productivity within the KZN–B may follow a similar pattern to that found by Goosen et al. (1997) within Kenyan coastal waters. DuFour and Torréton (1996) through a number of biological parameters suggested a bottom–up control mechanism for bacterial biomass that increases with distance from the coast line towards the open ocean. Although the effects of bottom–up control have yet to be substantiated here, bacterial biomass patterns within the KZN–B for both cruises (Figs. 3.1.12 and 3.3.12) show to some extent, similar bacterial biomass patterns to those described by DuFour and Torréton (1996). DuFour and Torréton (1996) also by means of biological parameters suggested that bacterial biomass is also under a moderate but increasing bottom–up control mechanism, which is due to decreasing resources from the coast towards the open ocean, as well as from the surface down to the deep sea. Such bottom–up control may therefore be influencing bacterial dynamics within the KZN–B.

Bacterial numbers and biomass within the KZN–B for both cruises also decreased with increasing ecozone depth (Figs. 3.1.11, 3.3.11, 3.1.12 and 3.3.12 respectively) with significant differences found between ecozones (Tbls. 3.5.3 and 3.5.4). Sherr et al. (2002) determined a similar pattern in the waters off Cape Hatteras with total bacterial abundance decreasing with depth, while Goosen et al. (1997) determined that below 500 m or more, bacterial abundance decreased with depth and that below 250 m, bacterial abundance was frequently a factor of ten lower than abundances in the surface waters. Tanaka and Rassoulzadegan (2002) reported similar results within the oligotrophic NW Mediterranean Sea. Studies of the effects of temperature on bacterial dynamics have been performed (Rivkin et al., 1996; Kirchman et al., 2005) with Rivkin et al. (1996) determining that bacterial growth during summer was regulated by substrate supply, grazers and viral lysis while during winter, bacterial growth was temperature controlled. Others such as Lovejoy et al. (2000) determined

that actively respiring cells showed a significant negative relationship with temperature below the euphotic zone.

Bacterial dynamics within the KZN–B above the pycnocline were probably influenced by grazers, viral lysis and substrate supply, while below the pycnocline, bacterial dynamics were probably influenced more by substrate supply and temperature with the depth of the pycnocline altered by either summer stratification or winter mixing. Irrespective of season, with grazers, viral lysis, temperature or substrate supply, all of these relate to the control of bacterial dynamics in a bottom–up control mechanism that appears to increase with increasing depth

Bacterial numbers (Figs. 3.1.11 and 3.3.11) and bacterial biomass (Figs. 3.1.12 and 3.3.12) for both sampling periods within the SE of the KZN–B do generally coincide geographically with higher Chl–*a* concentrations (Figs. 3.1.10 and 3.3.10). During summer sampling, there were three coinciding areas within the KZN–B regarding bacterial dynamics and Chl–*a* concentrations: firstly within an isolated spot within the central KZN–B; secondly around the Thukela River mouth and thirdly near Richards Bay. During the limited winter sampling period, the only geographic match appears to be around the Thukela Mouth. Such geographic matches were not evident within the southern KZN–B during summer sampling. In the northern KZN–B (north of Richards Bay) during both cruises, and in the central KZN–B during the winter cruise, low Chl–*a* concentrations as well as low bacterial numbers and bacterial biomass were present. Within these areas, the absence of sufficient nitrate and phosphate within the SE possibly resulted in low Chl–*a* concentrations, however, the influence of grazing pressure cannot be eliminated. This possibly indicates a lack of external nutrient input to fuel phytoplankton growth and productivity as shown previously by Probyn et al. (1995), Pérez et al. (2005) and Zohary et al. (2005). This could therefore have resulted in a lack of sufficient organically derived organic matter to sufficiently increase bacterial numbers and biomass within the northern KZN–B.

For either high or low values of biological, geographically coinciding areas within the KZN–B, heterotrophic bacteria were potentially influenced by the presence or absence of DOM release by phytoplankton (Fuhrman and Azam, 1980; Azam et al., 1983; Goosen et al., 1997; Church et al., 2000; Sherr et al., 2002; Li et al., 2004; Fenchel, 2008). It has been shown numerous times that there is a general relationship between increasing primary productivity and bacterial dynamics (Azam et al., 1983; Kirchman et al., 1995; Goosen et al., 1997; Gasol and Duarte, 2000; Lovejoy et al., 2000; Sherr et al., 2002; Li et al., 2004; Fenchel, 2008), but also that the statistically derived relationship between them is not absolute (Kirchman et al., 1995; Lovejoy et al., 2000; Li et al., 2004). Then why in the

southern KZN–B during both cruises were there areas of high Chl–*a*, but bacterial numbers and bacterial biomass within this area were relatively low?* This pattern is the opposite to the more central section of the KZN–B during summer and along the southern coast line during winter, with low levels of Chl–*a*, but higher counts of bacterial numbers as well as bacterial biomass. So the question arises, why is the general relationship between phytoplankton and bacteria not followed within the central and southern KZN–B during these cruises?

It has been suggested by Li et al. (2004), that 1 mg of chlorophyll has the carrying capacity (maximum population size that a parameter can sustain) to support approximately 7 trillion bacteria (1×10^{12}) based on empirical observations, which does not come close to the highest cell count within this study of 6.20×10^{5} cells.ml^{-1} during the summer synoptic cruise. This upper limit in the ocean as discussed by Li et al. (2004) is controlled by phytoplankton, and will never be reached in productive waters due to grazing and viral lysis. Within the southern KZN–B it is apparent that nutrient levels, especially phosphate (Figs. 3.1.5 and 3.3.5) and nitrate (Figs. 3.1.6 and 3.3.6) along T1 were much higher in photic waters (probably affecting Chl–*a* concentrations, see Figs. 3.1.10 and 3.3.10). Potentially, this would translate to more inorganic nutrients within the photic zone for phytoplankton to utilise possibly resulting in an increase in Chl–*a* concentration within this area and therefore an increase in DOM release. Therefore, bottom–up control should not have been an issue suppressing bacterial populations within the southern KZN–B. The diminished Chl–*a* concentrations and bacterial numbers and biomass within the southern KZN–B could be caused by a high degree of herbivory on phytoplankton, and even higher bacterivory on heterotrophic bacteria. In fact, Li et al. (2004) using a bivariate regression analysis between chlorophyll and bacteria, showed that the observed positive bacterial regression slope at low chlorophyll levels changes to a negative regression slope at higher chlorophyll levels, usually around the 1 mg.m^{-3} mark, and that this alteration can indicate a change from bottom–up to top–down control. A study performed by Ducklow et al. (2000) in the Ross Sea, from January to February 1997, showed a similar pattern regarding bacterial activity in relation to Chl–*a* concentration.

Bottom–up control, usually nutrient influenced, may have been the driver for the bacterial patterns seen within the euphotic zone of the central KZN–B during the summer cruise and along the

---

* It must be noted here that although Chl–*a* concentrations were determined for both cruises within the KZN–B, measurements of primary productivity were not. Experiments performed by Schleyer (1981) on a reef near Durban, South Africa, determined that although the mean Chl–*a* concentration was 2.13 mg·m^{-3}, mean annual primary productivity was low with 12.82 mgC·m^{-3}·h^{-1}. Results from Schleyer (1981) also showed a total bacterial count of 2.02×10^{6} cells·ml^{-1}.

southern coast line during the winter cruise. The lack of inorganic nutrients probably resulted in low levels of Chl–*a*, but bacterial numbers and bacterial biomass were still relatively high. A regression analysis run by DuFour and Torréton (1996), as part of their study on the control mechanisms of bacterioplankton, determined a slope of 0.48, while Li et al. (2004) during their comparative analysis on the global relationship between bacteria and chlorophyll within biogeochemical provinces determined a slope of 0.46. Regression analyses performed by Andrade et al. (2003) between bacterial productivity and Chl–*a* concentration resulted in a slope of 0.83, while between Chl–*a* and bacterial abundance the slope was 0.97. All this suggests that resource availability moderately controls bacterial biomass as well as bacterial numbers with all the slopes above having a positive value suggesting bottom–up control mechanisms (Wright and Coffin, 1984; DuFour and Torréton, 1996; Andrade et al., 2003; Li et al., 2004).

Comparing the euphotic zones of the three trophic status sites within the study conducted by DuFour and Torréton (1996) in the tropical north eastern Atlantic Ocean, the oligotrophic site had a higher percentage of active cells (abundance) and a lower overall cell volume (biomass) when compared to the mesotrophic and eutrophic sites within their study. This is what is seen within the euphotic zone (SE and FE) of the central KZN–B during the summer cruise and along the southern coast line during the winter cruise, low Chl–*a* concentrations, higher bacterial numbers but lower, patchy and variable bacterial biomass, all clearly indicative of bottom–up control. During their study in 2001, Tanaka et al. (2007) reported a wider range for bacterial biomass, compared to their study in 2002, with bacterial productivity being much smaller suggesting that bacterial biomass was bottom–up controlled during their time of study within the euphotic zone. Church et al. (2000) had similar results indicating that the availability of DOM was a primary factor hindering bacterial growth. As discussed also by Tanaka and Rassoulzadegan (2002) their mean regression slopes for the seasonal variation for bacterial numbers and biomass was –0.557 ± SD 0.125, they determined that the decrease in bacterial numbers and biomass with depth was resource controlled. It can therefore be suggested that during bottom–up control, heterotrophic bacteria within the KZN–B partition more resources towards replication, resulting in higher bacterial abundance, rather than towards increasing their biomass and hence size. This is in complete opposition to the results obtained by Petit et al. (1999), studying bacterial production in French lakes, where the authors determined that when under unfavourable conditions bacteria partitioned more resources towards increasing their biomass rather than replication.

It has been shown by both Bernard et al. (2000) and Sherr et al. (2002) that predators / grazers selectively feed on the larger, more productive bacterial cells within a system, leaving the smaller, less productive proportion to constitute the bacterial standing stock of the water column Top–down control, usually predation / lysis / grazing mediated (DuFour and Torréton, 1996), was potentially the

driver for the bacterial patterns seen within the SE in the southern KZN–B for both cruises and can possibly be attributed to changes in trophic level feeding via cascade effects (Landry and Kirchman, 2002). In the southern KZN–B, inorganic nutrient levels were high within the surface waters positively affecting Chl–*a* concentrations within the surrounding waters, while bacterial numbers and biomass remained relatively low. It is known that the major bacterivores in the nutrient limited open ocean are nanoflagellates (1 to 5 µm) as well as flagellates (3 to 10 µm) and microzooplankton (10 to 80 µm), which are capable of limiting bacterial populations in these waters, seen when total bacterial counts are low (also possibly bacterial biomass) suggesting high loss rates, while microzooplankton such as ciliates, control the nanoflagellate populations (Azam et al., 1983; Wright and Coffin, 1984; Alonso et al., 2000; Lovejoy et al., 2000; Landry and Kirchman, 2002; Chen et al., 2009).

A study performed by Chen et al. (2009) in the South China Sea, where the authors separated predators and prey by size fractionation, was used to determine the microbial food web within the system. Reporting here on only the high DNA bacteria after Chen et al. (2009) removed the B–IV group [described by Jochem (2001) as being rods, curved bacteria and large cocci, and by Chen et al. (2009) as having increased size (side scatter) and increased DNA content (green fluorescence)[*]] from their data, they found that the 10 to 60 µm grazers mainly fed off the 5 to 10 µm heterotrophic nanoflagellates, while the 60 to 200 µm grazers fed mainly off the 10 to 60 µm grazers. Interpreting these data from Chen et al. (2009) to the biological pattern within the southern KZN–B, bacterial numbers and biomass were low, possibly because the pressure on nanoflagellates was reduced because the ciliates were being consumed at a higher rate by their grazers, thus releasing the pressure on the nanoflagellates. The nanoflagellates, grazing pressure now partly released, would then consume the bacterial population at an increased rate.

Such patterns are also seen within the high nutrient – low chlorophyll–*a* region of the Equatorial Pacific. Here Kirchman et al. (1995) reported bacterial abundance to range from 0.020 to 0.500×10^{6} cells·ml^{-1} during March 1992. The upper range presented by Kirchman et al. (1995) is close to the upper range within the KZN–B of 0.620×10^{6} cells·ml^{-1}, during January to February 2010. Kirchman et al. (1995) continue to report that the lack of high bacterial biomass within their sampling region could possibly be caused by microzooplankton grazing. This was likely the case within the southern KZN–B for both cruises. This was also seen by Zohary et al. (2005), who reported an increase in bacterial activity which did not coincide with bacterial abundance, suggesting that the standing stock was being controlled by bacterivores.

[*] See Jochem (2001) for better illustrations.

During their study in 2002, Tanaka et al. (2007) reported a narrower range for bacterial biomass compared to 2001 with bacterial productivity being much larger, suggesting that bacterial biomass was top–down controlled during their time of study within the euphotic zone. This was also seen by Goosen et al. (1997) in Kenyan coastal waters with lower bacterial numbers but higher abundance of heterotrophic nanoflagellates and increased bacterial production, most notably around their coastal stations. As put forward by DuFour and Torréton (1996), Andrade et al. (2003) and Li et al. (2004), a positive regression slope indicates a degree of bottom–up control by bacteria–phytoplankton trophic coupling, while Li et al. (2004) also suggests that a negative slope indicates top–down control.

The upper abundance range of bacterial numbers during the first cruise during the summer months (0.620×10^6 cells·ml^{-1}) are comparable to other upper abundance data sources within other oligotrophic sites during the same season. Available data sources for bacterial numbers, biomass and productivity are presented in Tbl. 4.8.1 below (pg. 109). As part of their study, Andrade et al. (2003) assessed bacterioplankton within the oligotrophic southwest Atlantic Ocean during April 2000 by use of flow cytometry, and determined bacterial numbers to range from 0.037 to 0.550×10^6 cells·ml^{-1}. Chen et al. (2009) in their study of the microbial food web within the oligotrophic South China Sea, during summer, determined bacterial numbers to range from 0.280 to 0.810×10^6 cells·ml^{-1}, while overall bacterial numbers within the study by Goosen et al. (1997) were low during the monsoon and inter–monsoon seasons, never exceeding 6×10^5 cells·ml^{-1}, with their second cruise (November – December 1992) showing the lowest abundance because of high grazing rates by heterotrophic nanoflagellates. The high nutrient – low chlorophyll–*a* region of the tropical Pacific described within Landry and Kirchman (2002) showed bacterial abundances ranging within 0.600 to 0.900×10^6 cells·ml^{-1}, while within the oligotrophic HOT (Hawaii Ocean Time–series) study, bacterial abundance was 0.300 to 0.600×10^6 cells·ml^{-1}. The elevated bacterial abundances within the high nutrient – low chlorophyll–*a* region was explained by Landry and Kirchman (2002) as being due to the presence of more DOC within the water column possibly due to the persistent input of inorganic nutrients.

Other areas such as the Cyprus Eddy in the Levantine Basin within the eastern Mediterranean, reported by Tanaka et al. (2007) as well as in the NW Mediterranean Sea reported by Tanaka and Rassoulzadegan (2002), describe both of these systems as extremely oligotrophic as well as P starved. Bacterial numbers reported by Tanaka et al. (2007) ranged between 0.046 to 0.410×10^6 cells·ml^{-1} while Tanaka and Rassoulzadegan (2002) reported bacterial numbers from 0.030 to 0.710×10^6 cells·ml^{-1}. Within the Levantine Basin, because of the extreme P deficiency of the water column, Tanaka et al. (2007) described a close coupling nutrient recycling within the euphotic zone that was present between the predators and prey, suggesting a close link between predator and prey within such nutrient limiting systems. Bacterial biomass within the extremely oligotrophic Cyprus Eddy, still

within Tanaka et al. (2007), ranged from 1.04×10^{-9} to 4.36×10^{-9} gC·ml^{-1}, closer to the lower range of bacterial biomass determined within the KZN–B. The lower range of bacterial numbers within the KZN–B during this cruise was extremely low, 0.003×10^{6} cells·ml^{-1}, with no other system presented within Tbl. 4.8.1 (pg. 109) coming close.

Reports by authors from other systems similar to the KZN–B such as Goosen et al. (1997) within Kenyan coastal waters conclude that bacterial growth rates are similar to growth rates found within open ocean regions. Systems to the west of the KZN–B such as the southern Benguela, a known upwelling region have shown bacterial biomass to range from 4.40×10^{-9} to 1.75×10^{-7} gC·ml^{-1} with the highest biomass recorded as 1.9×10^{-7} gC·ml^{-1} (Painting et al., 1993). This is well within range of the bacterial biomass recorded within the KZN–B, with the highest bacterial biomass measured as 1.83×10^{-7} gC·ml^{-1} at line 16 station 1 at 35m with a corresponding highest bacterial numbers with 6.20×10^{5} cells·ml^{-1}.

The original hypotheses set out for this work were 1. Bacterial populations vary seasonally; 2. Bacterial populations vary by depth; 3. Bacterial populations are distributed in close relation to their organic nutrient sources: and 4. Phytoplankton are distributed in close relation to their inorganic nutrient sources. It can be said with some certainty that there is a seasonal difference between bacterial numbers and bacterial biomass shown by the significant difference between seasons for bacterial numbers ($p < 0.001$) and bacterial biomass ($p < 0.001$). Differences between bacterial productivity between the two cruises undertaken within this study potentially appear to relate more to daily grazing rates rather than seasonal patterns.

The differences within and between seasons for hypothesis 2, 3 and 4, appear to relate to the degree of inorganic nutrient supply to the phytoplankton, resulting in the formation of DOM for use by the heterotrophic bacteria, and the resulting availability of said DOM via a bottom–up control mechanism that increases with distance from the coast as well as with depth. These differences however, also appear to relate to the level of Chl–*a* within the euphotic zone inducing either top–down or bottom–up control mechanisms on the heterotrophic bacteria directly affecting their numbers, biomass and productivity.

Studies conducted within the KZN–B in the future should aim to incorporate bacterial community structure, regarding size and composition of bacterial cells (by use of epifluorescent microscopy or flow cytometry), as it has been shown that there is a change in the bacterial community structure with changing compositions of phytoplankton dynamics (Painting et al., 1989). Painting et al. (1989) describe a microcosm experiment with the starting bacterial population dominated by small rods and large cocci with a slow turnover rate, moving to a population dominated by small cocci and

large rods. This change was influenced by the presence of detrital carbon (Painting et al., 1989). It has been shown elsewhere that bacteria in the environment convert to a coccoid shape and become smaller when under low nutrient conditions (Novitsky and Morita, 1976; Chowdhury et al., 1995). Fergusen and Rublee (1976) have shown that rod shaped cells are more dominant on particulate material (75%) and contribute over 60% of bacterial carbon as compared to cocci. Fergusen and Rublee (1976) continue to discuss that while only 15% of rods were found on particulate material, out of the total bacterial standing stock, they accounted for 45% of the total bacterial carbon contribution. It can therefore be said, that in coastal areas, where the input of particulate matter is high, as well as areas of high nutrient input, that such pleomorphic changes within the bacterial community are possible, which can lead to high bacterial numbers and biomass within the system.

4.9: Critical Assessment

The initial limitation for this study was the filtration technique which does not allow for a homogeneous distribution of bacterial cells on the filter. To this effect, the viewing of stained bacterial cells under epifluorescent microscopy could either lead to one field of view containing 10 cells and the next containing 100 cells on the same filter. Added to this were the differential degrees of Z stacking required to get one image of a field of view in focus in order for the counting and sizing of bacterial cells to be accurate. In some cases up to 25 images of one field of view required to be stacked along the Z axis in order for the whole field of view to be in focus. Although 10 fields of view for each filter were assessed for this study, which is sufficient to give a statistical mean, the filtration techniques need to be improved to provide this homogeneous distribution as well as improved degrees of Z stacking. However, given the small size of bacterial cells and the distance between the filter and liquid substrate interface providing a large Z axis, the improvement of the filtration techniques becomes redundant if bacterial cells cannot be viewed in focus.

The development of the macro's within this thesis were undertaken as a side project to assist in the counting and sizing of bacterial cells. As such, time was limited and the macros were developed in 3 weeks, but after sufficient use and additional research, there were still some minor flaws. First of which was the inability to distinguish between a single highly pixellated area which mimicked a bacterial cell and an actual bacterial cell based simply on the density of colour and the lack of an edge, something which a trained eye performing this task manually would have been able to distinguish. The use of an "if" function based on a pre–selected range of bacterial cells within the macro to distinguish between these events would have been useful. Adding to this were the instances where two or more bacterial cells would overlap each other, something that with some precise measuring, a trained eye

would also able to separate manually, but something which the developed macro was not able to differentiate between. After some additional research, the addition of a watershed algorithm to the lines of code for the separation of such instances would have been useful. However, due to the time constraints for this project and the fact that the current developed macro was performing as required, the addition of this algorithm was excluded as much of the data had already been analysed. In addition, from personal experience with the saving and use of images, captured images should not be stored for extended periods of time before being analysed. There were many occasions where after I stored images for more than a few months, the images became corrupted and could either not be retrieved, or other data was written over the image leaving streaks or ghost images. For these sets of images, I needed to redo the samples and well as additional controls. It is therefore suggested that images captured should be analysed weekly in order to avoid this from occurring.

Apart from all this, the project was completed, adding useful information about bacterial numbers, biomass and productivity within the KZN–B. Since this study presents an initial overview of the bacterial dynamics within the KZN–B as well as some surrounding waters, future studies within the waters of the KZN–B on bacterial dynamics should aim to perform a more expansive study on the temporal dynamics. Also, the differences in depth between the F–max, intermediate, intermediate and bottom depths was large, and as such, future studies should aim take more samples between these depths to provide a complete depth profile. In addition to this, since there was no upwelling event during the time of this study, another study should address the impacts of an upwelling event on the bacterial numbers, biomass and productivity.

In addition to the methods presented here, the use of flow cytometry to enumerate bacterial populations should be considered due to its speed and the ability to enumerate all cells that pass through the system.

Table 4.8.1: Bacterial numbers, biomass and carbon productivity from available data sources, including those from the current study within the KZN–B.

Source	Area	Date / Season	Numbers ($\times 10^6$ cells $\cdot ml^{-1}$)	Biomass ($gC \cdot ml^{-1}$)	Productivity ($gC \cdot ml^{-1} \cdot h^{-1}$)
Andrade et al. (2003)**	SW Atlantic Ocean	April (2000)	0.037 – 0.550	*	4.60×10^{-12} – 1.26×10^{-10}
Azam and Smith (2001)	Arabian Sea	July (2001)	0.013 – 1.290	*	1.22×10^{-13} – 7.84×10^{-10}
Bianchi (1992)	Atlantic	May – June (1992)	0.142 – 3.478	*	5.79×10^{-9} – 7.83×10^{-7}
Chen et al. (2009)	South China Sea	Summer (2006)	0.280 – 0.810	*	*
Ducklow (1998)	Ross Sea	April (1998)	0.051 – 0.178	*	6.80×10^{-13} – 1.29×10^{-11}
Ducklow (2002)***	Arabian Sea	Feb (2002)	0.026 – 2.93	*	6.80×10^{-14} – 6.85×10^{-9}
Ducklow et al. (2000)	Ross Sea	Oct – Nov (1996) + Jan – Feb (1997)	0.100 – 2.900	8.53×10^{-9} – 1.86×10^{-8}	1.23×10^{-8} – 6.69×10^{-8}
Ducklow et al. (2003)	North Atlantic	April – May (1989)	0.010 – 3.130	*	1.36×10^{-12} – 8.50×10^{-10}
DuFour and Torréton (1996)	NE Atlantic Ocean	May – June (1992)	0.012 – 3.900	1.20×10^{-10} – 4.7×10^{-8}	2.00×10^{-14} – 9.60×10^{-10}
Goosen et al. (1997)**	W Indian Ocean	June – July (1992)	0.170 – 0.590	*	*
		Nov – Dec (1992)	0.080 – 0.380		
Heywood et al. (2006)**	Atlantic Ocean – Oligotrophic Gyre	May (1998)	0.400 – 1.600	*	*
		May (2003)	0.400 – 1.200	*	*
		Sept (2003)	0.200 – 1.200	*	*
		April (2004)	0.200 – 1.200	*	*
Kirchman (2001)***	Equatorial Pacific	April (1998)	0.086 – 1.523	*	5.44×10^{-13} – 1.75×10^{-10}
Kirchman et al. (1995)**	Equatorial Pacific	March (1992)	0.020 – 0.500	*	*

Source	Area	Date / Season	Numbers ($\times 10^6$ cells $\cdot ml^{-1}$)	Biomass ($gC \cdot ml^{-1}$)	Productivity ($gC \cdot ml^{-1} \cdot h^{-1}$)
KZN–B – ACEP II	KZN–B	Jan – Feb (2010)	0.003 – 0.620	1.45×10^{-10} – 1.83×10^{-7}	5.85×10^{-11} – 1.84×10^{-8}
		July – Aug (2010)	0.007 – 0.221	3.61×10^{-10} – 2.56×10^{-8}	4.46×10^{-11} – 2.93×10^{-9}
Landry and Kirchman (2002)	Tropical Pacific	2002	0.600 – 0.900	0.0141 ± SD 0.0028	*
Lovejoy et al. (2000)**	Gulf of St Lawrence	Spring (1994)	0.213 – 0.391	*	*
		Summer (1994)	0.344 – 0.959	*	*
	Coast of Nova Scotia	Summer (1994)	0.194 – 0.781	*	*
Marie et al. (1997)**	Equatorial Pacific	Nov (1994)	0.027 – 0.872	*	*
Painting et al. (1993)**	S Benguela	Summer (1983)	*	2.00×10^{-8} – 1.90×10^{-7}	*
Schut et al. (1993)**	Resurrection Bay	April (1989)	0.710	1.04×10^{-5}	*
		Dec (1989)	0.830	1.39×10^{-5}	
		Mar (1990)	0.200	3.60×10^{-6}	*
		Aug (1990)	1.070	2.77×10^{-5}	*
	North Sea	Feb (1991)	0.110	2.40×10^{-6}	*
Sherr et al. (2006)**	NE Pacific Ocean	March – Sept (2001 – 2002)	0.500 – 6.500	*	*
Tanaka and Rassoulzadegan (2002)	NW Mediterranean	May 1999 – March 2000	0.030 – 0.710	*	*
Tanaka et al. (2007)	E Mediterranean	May (2001 – 2002)	0.046 – 0.410	1.04×10^{-9} – 4.36×10^{-9}	1.44×10^{-11} – 1.33×10^{-11}

* Data not available

** Data from the mixed / upper layer

***Data from the euphotic zone
All other data are from full profiles

REFERENCES

Alonso, M. C., Rodriguez, V., Rodriguez, J. and Borrego, J. J. 2000. Role of ciliates, flagellates and bacteriophages on the mortality of marine bacteria and on dissolved–DNA concentration in laboratory experimental systems. Experimental Marine Biology and Ecology, 244. 239–252.

Andrade, L., Gonzalez, A. M., Araujo, F. V. and Paanhos, R. 2003. Flow cytometry assessment of bacterioplankton in tropical marine environments. Microbiological Methods, 55. 841–850.

Azam, F., Fenchel, T., Field, J. G., Gray, J. S., Meyer–Reil, L. A. and Thingstad, T. F. 1983. The Ecological Role of Water–Column Microbes in the Sea. Marine Ecology Progress Series, 10. 257–263.

Azam, F. and Smith, D. "Bacteria abundance and thymidine / leucine incorporation." United States JGOFS Data Server. Woods Hole Oceanographic Institution, USA: U.S. JGOFS Data Management Office, iPub: July 9, 2001. Accessed 22 July 2011. http://usjgofs.whoi.edu/jg/serv/jgofs/arabian/ttn-043/bacteria.html0%7Bdir=usjgofs.whoi.edu/jg/dir/jgofs/arabian/ttn-043/,info=usjgofs.whoi.edu/jg/info/jgofs/arabian/ttn-043/bacteria%7D

Berman, T., Hoppe, H. G. and Gocke, K. 1994. Response of aquatic bacterial populations to substrate enrichment. Marine Ecology Progress Series, 104. 173–184.

Bernard, L., Courties, C., Servais, P., Troussellier, M., Petit, M. and Lebaron, P. 2000. Relationships among bacterial cell size, productivity, and genetic diversity in aquatic environments using cell sorting and flow cytometry. Microbial Ecology, 40. 148–158.

Bianchi, M. "Bacteria." FRANCE_JGOFS EUMELI. EUMELI 4: L'Atalante. Accessed 22 July 2011. http://www.obs-vlfr.fr/cd_rom_dmtt/eu_main.htm

Bizsel, K. C., Suzal, A., Demirdağ, A., İnanan, B. E. and Esen, E. 2011. Particulate organic matter controbution of Gediz River to the Aegean Sea. Fisheries and Aquatic Sciences, 11. 547–559.

Bratbak, G. 1985. Bacterial biovolume and biomass estimations. Applied and Environmental Microbiology, 49. 1488–1493.

Chen, B. C., Liu, H. and Wang, Z. 2009. Trophic interactions within the microbial food web in the South China Sea revealed by size–fractionation method. Experimental Marine Biology and Ecology, 368. 59–66.

Chowdhury, M. A. R., Xu, B., Montilla, R., Hasan, J. A. K., Huq, A. and Colwell, R. R. 1995. A simplified immunofluorescence technique for detection of viable cells of *Vibrio cholerae* O1 and O139. Microbiological Methods, 24. 165–170.

Church, M. J., Hutchins, D. A. and Ducklow, H. W. 2000. Limitation of bacterial growth by dissolved organic matter and iron in the Southern Ocean. Applied and Environmental Microbiology, 66. 455–466.

Daley, R. J. and Hobbie, J. E. 1975. Direct counts of aquatic bacteria by a modified epifluorescence technique. Limnology and Oceanography, 20. 875–882.

Ducklow, H. "Bacterial abundance, cell volume, thymidine and leucine incorporation." United States JGOFS Data Server. Woods Hole Oceanographic Institution, USA: U.S. JGOFS Data Management Office, iPub: February 27, 2002. Accessed 22 July 2011. http://usjgofs.whoi.edu/jg/serv/jgofs/southern/nbp96_4A/bacteria.html0%7Bdir=usjgofs.whoi.edu/jg/dir/jgofs/southern/nbp96_4A/,info=usjgofs.whoi.edu/jg/info/jgofs/southern/nbp96_4A/bacteria%7D

Ducklow, H. "Bacterial abundance, cell volume, thymidine and leucine incorporation." United States JGOFS Data Server. Woods Hole Oceanographic Institution, USA: U.S. JGOFS Data Management Office, iPub: February 27, 2002. Accessed 22 July 2011. http://usjgofs.whoi.edu/jg/serv/jgofs/arabian/ttn-045/bacteria.html0%7Bdir=usjgofs.whoi.edu/jg/dir/jgofs/arabian/ttn-045/,info=usjgofs.whoi.edu/jg/info/jgofs/arabian/ttn-045/bacteria%7D

Ducklow, H., Sieracki, M., Stoecker, D. and Verity, P. "Merged biological measurements from above investigators." United States JGOFS Data Server. Woods Hole Oceanographic Institution, USA: U.S. JGOFS Data Management Office, iPub: January 14, 2003. Accessed 22 July 2011. http://usjgofs.whoi.edu/jg/serv/jgofs/nabe/atlantisII/biology.html0%7Bdir=usjgofs.whoi.edu/jg/dir/jgofs/nabe/atlantisII/,info=usjgofs.whoi.edu/jg/info/jgofs/nabe/atlantisII/biology%7D

Ducklow, H. W., Dickson, M. L., Kirchman, D. L., Steward, G., Orchardo, J., Marra, J. and Azam, F. 2000. Constraining bacterial production, conversion efficiency and respiration in the Ross Sea, Antartica, January–February, 1997. Deep Sea Research II, 47. 3227–3247.

DuFour, P. H. and Torréton, J. P. 1996. Bottom–up and top–down control of bacterioplankton from eutrophic to oligotrophic sites in the tropical northeastern Atlantic Ocean. Deep Sea Research I, 43. 1305–1320.

Fenchel, T. 1987. *Ecology of Protozoa. The biology of free–living phagotrophic protists* (1st edition). Springer–Verlag. Berlin.

Fenchel, T. 2008. The microbial loop – 25 years later. Experimental Marine Biology and Ecology, 366. 99–103.

Fergusen, R. L. and Rublee, P. 1976. Contribution of bacteria to standing crop of coastal plankton. Limnology and Oceanography, 21. 141–145.

Francisco, D. E., Mah, R. A. and Rabin, A. C. 1973. Acridine orange–epifluorescence technique for counting bacteria in natural waters. Transactions of the American Microscopical Society, 92. 416–421.

Fuhrman, J. A. 1999. Marine viruses and their biogeochemical and ecological effects. Nature, 399. 541–548.

Fuhrman, J. A. and Azam, F. 1980. Bacterioplankton secondary production estimates for coastal waters of British Columbia, Antarctica, and California. Applied and Environmental Microbiology, 39. 1085–1095.

Gasol, J. M., del Giorgio, P. A., Massana, R. and Duarte, C. M. 1995. Active versus inactive bacteria: size–dependence in a coastal marine plankton community. Marine Ecology Progress Series, 128. 91–97.

Gasol, J. M. and Duarte, C. M. 2000. Comparitive analysis in aquatic microbial ecology: how far do they go? Microbiology Ecology, 31. 99–106.

Goosen, N. K., van Rijswijk, P., De Bie, M., Peene, J. and Kromkamp, J. 1997. Bacterioplankton abundance and production and nanozooplankton abundance in Kenyan coastal waters (Western Indian Ocean). Deep Sea Research II, 44. 1235–1250.

Haas, L. W. and Webb, K. L. 1979. Nutritional mode of several non–pigmented microflagellates from the York River estuary, Virginia. Experimental Marine Biology and Ecology, 39. 125–134.

Heywood, J. L., Zubkov, M. V., Tarran, G. A., Fuchs, B. M. and Holligan, P. M. 2006. Prokaryoplankton standing stocks in oligotrophic gyre and equatorial provinces of the Atlantic Ocean: Evaluation of inter–annual variability. Deep Sea Research II, 53. 1530–1547.

Hobbie, J. E., Daley, R. J. and Jasper, S. 1977. Use of nucleopore filters for counting bacteria by fluorescence microscopy. Applied and Environmental Microbiology, 33. 1225–1228.

Hymel, S. N. and Plante, C. J. 1998. Improved method of bacterial enumeration in sandy and deposit–feeder gut sediments using the fluorescent stain 4, 6–diamidino–2–phenylindole (DAPI). Marine Ecology Progress Series, 173. 299–304.

Jochem, F. J. 2001. Morphology and DNA content of bacterioplankton in the northern Gulf of Mexico: analysis by epifluorescence microscopy and flow cytometry. Aquatic Microbial Ecology, 25. 179–194.

Karydis, M. 2009. Eutrophication assessment of coastal waters based on indicators: A literature review. Global NEST, 11. 373–390.

Kirchman, D. "Bacterial abundance, thymidine and leucine incorporation." United States JGOFS Data Server. Woods Hole Oceanographic Institution, USA: U.S. JGOFS Data Management Office, iPub: August 27, 2001 Accessed 22 July 2011. http://usjgofs.whoi.edu/jg/serv/jgofs/eqpac/tt007/bacteria.html0%7Bdir=usjgofs.whoi.edu/jg/dir/jgofs/eqpac/tt007/,info=usjgofs.whoi.edu/jg/info/jgofs/eqpac/tt007/bacteria%7D

Kirchman, D. L., Keil, R. G., Simon, M. and Welschmeyer, N. A. 1993. Biomass and production of heterotrophic bacterioplankton in the oceanic subarctic Pacific. Deep Sea Research I, 40. 967–988.

Kirchman, D. L., Malmstrom, R. R. and Cottrell, M. T. 2005. Control of bacterial growth by temperature and organic matter in the Western Arctic. Deep Sea Research II, 52. 3386–3395.

Kirchman, D. L., Rich, J. H. and Barber, R. T. 1995. Biomass and biomass production of heterotrophic bacteria along 140^{o}W in the equatorial Pacific: Effect of temperature on the microbial loop. Deep Sea Research II, 42. 603–619.

Landry, M. R. and Kirchman, D. L. 2002. Microbial community structure and variability in the tropical Pacific. Deep Sea Research II, 49. 2669–2693.

Li, W. K. W., Head, E. J. H. and Harrison, G. W. 2004. Macroecological limits of heterotrophic bacterial abundance in the ocean. Deep Sea Research I, 51. 1529–1540.

Lønborg, C., Álvarez–Salgado, X. A., Davidson, K. and Miller, A. E. J. 2009a. Production of bioavailable and refractory dissolved organic matter by coastal heterotrophic microbial populations. Estuarine, Coastal and Shelf Science, 82. 682–688.

Lønborg, C., Davidson, K., Álvarez–Salgado, X. A. and Miller, A. E. J. 2009b. Bioavailability and bacterial degradation rates of dissolved organic matter in a temperate coastal area during an annual cycle. Marine Chemistry, 113. 219–226.

Lovejoy, C., Legendre, L., Therriault, J. C., Tremblay, J. E., Klein, B. and Ingram, R. G. 2000. Growth and distribution of marine bacteria in relation to nanoplankton community structure. Deep Sea Research II, 47. 461–487.

Luna, G. M., Manini, E. and Danovaro, R. 2002. Large fraction of dead and inactive bacteria in coastal marine sediments: Comparison of protocols for determination and ecological significance. Applied and Environmental Microbiology, 68. 3509–3513.

Lutjeharms, J. R. E. 2006. The northern Agulhas Current. *In: The Agulhas Current* (Lutjeharms, J. R. E.), 1st edition. 121–150. Springer. Sturtz AG, Wurzburg, Germany.

Lutjeharms, J. R. E., Cooper, J. and Robers, M. 2000a. Upwelling at the inshore edge of the Agulhas Current. Continental Shelf Research, 20. 737–761.

Lutjeharms, J. R. E. and Machu, E. 2000. An upwelling cell inshore of the East Madagascar Current. Deep Sea Research I, 47. 2405–2411.

Lutjeharms, J. R. E., Valebtine, H. R. and van Ballegooyen, R. C. 2000b. The hydrography and water mases of the Natal Bight, South Africa. Continental Shelf Research, 20. 1907–1939.

Marie, D., Partensky, F., Jacquet, S. and Vaulot, D. 1997. Enumeration and cell cycle analysis of natural populations of marine picoplankton by flow cytometry using the nucleic acid stain SYBR green I. Applied and Environmental Microbiology, 63. 186–193.

Menge, D. N. L. and Weitz, J. S. 2009. Dangerous nutrients: Evolution of phytoplankton resource uptake subject to virus attack. Theoretical Biology, 257. 104–115.

Meyer, A. A., Lutjeharms, J. R. E. and de Villiers, S. 2002. The nutrient characteristics of the Natal Bight, South Africa. Marine Systems, 35. 11–37.

Munn, C. B. 2004. *Marine Microbiology: Ecology & Applications* (1st edition). Garland Science / BIOS Scientific. London and New York.

Novitsky, J. A. and Morita, R. Y. 1976. Morphological chracterization of small cells resulting from nutrient starvation of a pyschrophilic marine vibrio. Applied and Environmental Microbiology, 32. 617–622.

Painting, S. J., Lucas, M. J. and Muir, D. G. 1989. Fluctuations in heterotropic bacterial community structure, activity and production in response to development and decay of phytoplankton in a microcosm. Marine Ecology Progress Series, 53. 129–141.

Painting, S. J., Lucas, M. J., Peterson, W. T., Brown, P. C., Hutchings, L. and Mitchell–Innes, B. A. 1993. Dynamics of bacterioplankton, phytoplankton and mesozooplankton communities during the development of an upwelling plume in the southern Benguela. Marine Ecology Progress Series, 100. 35–53.

Pérez, V., Fernández, E., Marañón, E., Serret, P., Varela, R., Bode, A., Varela, M., Varela, M. M., Anxelu, X., Morán, G., Malcolm, E., Woodward, S., Kitidis, V. and Garcia-Soto, C. 2005. Latitudinal distribution of microbial plankton abunance, production, and respiration in the Equatorial Atlantic in autumn 2000. Deep Sea Research I, 52. 861–880.

Petit, M., Servais, P. and Lavandier, P. 1999. Bacterial production measured by leucine and thymidine incorporation rates in French lakes. Freshwater Biology, 42. 513–524.

Porter, K. G. and Feig, Y. S. 1980. The use of DAPI for identifying and counting aquatic microflora. Limnology and Oceanography, 25. 943–948.

Probyn, T. A., Mitchell–Innes, B. A. and Searson, S. 1995. Primary productivity and nitrogen uptake in the subsurface chlorophyll maximum on the Eastern Agulhas Bank. Continental Shelf Research, 15. 1903–1920.

Rheinheimer, G. 1985. *Aquatic Microbiology* (3rd edition). John Wiley & Sons, Ltd. German Democratic Republic.

Ribbink, A. J. and Roberts, M. 2006. African Coelacanth Ecosystem Programme: An overview of the conference contributions. South African Journal of Science, 102. 409–415.

Richardson, T. L. and Jackson, G. A. 2007. Small phytoplankton and carbon export from the surface ocean. Science, 315. 838–840.

Rivkin, R. B., Anderson, R. M. and Lajzerowicz, C. 1996. Microbial processes in cold oceans. I. Relationship between temperature and bacterial growth rate. Aquatic Microbial Ecology, 10. 243–254.

Roszak, D. B. and Colwell, R. R. 1987. Metabolic activity of bacterial cells enumerated by direct viable count. Applied and Environmental Microbiology, 53. 2889–2983.

Schleyer, M. H. 1980. A preliminary evaluation of heterotrophic utilisation of a labelled algal extract in a subtidal reef environment. Marine Ecology Progress Series, 3. 223–229.

Schleyer, M. H. 1981. Microorganisms and detritus in the water column of a subtidal reef of Natal. Marine Ecology Progress Series, 4. 307–320.

Schlitzer, R. 2010. Ocean Data View. http://odv/awi.de,2010. Last accessed 5 March 2010.

Schönholzer, F., Hahn, D., Zarda, B. and Zeyer, J. 2002. Automated image analysis and in situ hybridization as tools to study bacterial populations in food resources, gut and cast of *Lumbricus terrestris* L. Microbiological Methods, 48. 53–68.

Schut, F., De Vries, E. J., Gottschal, J. C., Robertson, B. R., Harder, W., Prins, R. A. and Button, D. K. 1993. Isolation of typical marine bacteria by dilution culture: Growth, maintenance, and characteriatics of isolates under laboratory conditions. Applied and Environmental Microbiology, 59. 2150–2160.

Sherr, E. B., Sherr, B. F. and Longnecker, K. 2006. Distribution of bacterial abundance and cell–specific nucleic acid content in the Northeast Pacific Ocean. Deep Sea Research I, 53. 713–725.

Sherr, E. B., Sherr, B. F. and Verity, P. G. 2002. Distribution and relation of total bacteria, active bacteria, bactivory, and volume or organic detritus in Atlantic continental shelf waters off Cape Hatteras NC, USA. Deep Sea Research II, 49. 4571–4585.

Smetacek, V., Scharek, R. and Nöthing, E. M. 1990. Seasonal and regional variation in the pelagial and its relationship to the life history cycle of krill. *In: Antarctic ecosystems, ecological change and conservation* (Kerry, K. R. and Hempel, G.), 1st edition. 103–114. Springer. Berlin.

Smith, D. C. and Azam, F. 1992. A simple, economical method for measuring bacterial protein synthesis rates in seawater using ^{3}H–leucune. Marine Microbial Food Webs, 6. 107–114.

Source–to–Sea. 2004. Thukela water project decision support phase – Reserve determination model – Appendices to Thukela Estuarine flow requirements. DWAF, IWR. PBV000–00–10308.

Stevenson, L. L. 1978. A case for bacterial dormancy in aquatic systems. Microbial Ecology, 4. 127–133.

Suzuki, M. T., Sherr, E. B. and Sherr, B. F. 1993. DAPI direct counting underestimates bacterial abundances and average cell size compared to AO direct counting. Limnology and Oceanography, 38. 1566–1570.

Tanaka, T. and Rassoulzadegan, F. 2002. Full-depth profile (0–2000m) of bacteria, heterotrophic nanoflagellates and ciliates in the NW Mediterranean Sea: Vertical partitioning of microbial trophic structures. Deep Sea Research II, 49. 2093–2107.

Tanaka, T., Zohary, T., Krom, M. D., Law, C. S., Pitta, P., Psarra, S., Rassoulzadegan, F., Thingstad, T. F., Tselepides, A., Malolm, E., Woodward, E. M. S., Flaten, G. A. F., Skjoldal, E. F. and Zodiatis, G. 2007. Microbial community structure and function in the Levantine Basin of the eastern Mediterranean. Deep Sea Research I, 54. 1721–1743.

Tranvik, L. J., Sherr, E. B. and Sherr, B. F. 1993. Uptake and utilization of 'colloidal DOM' by heterotrophic flagellates in seawater. Marine Ecology Progress Series, 92. 301–309.

Umorin, P. P. 1992. Competition between bacterivorous flagellates and bacterivorous ciliates for food resources. Oikos, 63. 175–179.

van Ballegooyen, R. C., Taljaard, S., van Niekerk, L., Lamberth, S. J., Theron, A. K. and Weerts, S. P. 2007. Freshwater flow dependency in South African marine ecosystems: A proposed assessment framework and initial assessment of South African marine ecosystems. CSIR, WRC. WRC Report No. KV 191/07.

Watson, S. W., Novitsky, T. J., Quinby, H. L. and Valois, F. W. 1977. Determination of bacterial number and biomass in the marine environment. Applied and Environmental Microbiology, 33. 940–946.

Wiebinga, C. J., Veldhuis, M. J. W. and De Baar, H. J. W. 1997. Abundance and productivity of bacterioplankton in relation to seasonal upwelling in the northwest Indian Ocean. Deep Sea Research I, 44. 451–476.

Wommack, E. K. and Colwell, R. R. 2000. Virioplankton: Viruses in aquatic ecosystems. Microbiology and Molecular Biology Reviews, 64. 69–114.

Wood, F. E. J. 1965. *Marine Microbial Ecology* (1st edition). Chapman and Hall Ltd. London.

Wright, R. T. and Coffin, R. B. 1984. Measuring microzooplankton grazing on planktonic marine bacteria by its impact on bacterial production. Microbial Ecology, 10. 137–149.

www1. 2010. http://www.angelfire.com/biz7/julian_s/julian/julians_macros.htm. Last accessed 02 November 2010.

www2. 2010. http://www.ozgrid.com/VBA/VBACode.htm. Last accessed 02 November 2010.

www3. 2010. http://www.mvps.org/dmcritchie/excel/delempty.htm. Last accessed 02 November 2010.

www4. 2010. http://www.cpearson.com/excel/deleting.htm. Last accessed 02 November 2010.

www6. 2012. http://www.saiab.ac.za/index.php?pid=253. Last accessed 24 May 2012.

Zohary, T., Herut, B., Krom, M. D., Mantoura, R. F. C., Pitta, P., Psarra, S., Rassoulzadegan, F., Stambler, N., Tanaka, T., Thingstad, T. F. and Woodward, E. M. S. 2005. P–limited bacteria but N and P co–limited phytoplankton in the Eastern Mediterranean – a microcosm experiment. Deep Sea Research II, 52. 3011–3023.

APPENDIX

This appendix contains all the macro script / coding used to automate and simplify the counting, sizing and analysis of data obtained from the epifluorescent microscope images of fluorescently stained / labelled bacteria from the ACEP II project. I must bring your attention to the fact that all the macros below were written specifically by me and for me, and therefore certain lines of code relate to me personally, by means of name. Warning should be given for other users of the macro script / coding below, in that if any changes are to be made to any lines of the code, then all subsequent lines of code must also be changed. I must say here that the development of these macros was not part of the ACEP II programme and was taken upon by myself as a side project.

Stacking Macro

This first macro was designed to stack multiple unfocused images, taken from an epifluorescent microscope, into one focused image. This macro was written for a maximum of 10 captured fields of view, with each field captured consisting of a maximum of 25 images. This allowed all unfocused areas of the field of view to be captured and later stacked. As it stands, this macro has the capacity to stack and rename a single TIFF image, or up to a maximum of 25 TIFF images, by using IPP's Extended Depth of Field (EDF) option. For more than 25 images, one needs only to expand the macro, and incorporate all sub lines of code relevant to that image. For reasons of space, only the first section of the code is shown here. This involves the stacking of images named '1.1.tif' until '1.25.tif', and saving the stacked image as '1.tif'. This section of code can be copied numerous times, and the 1.1.tif, 1.2.tif, 1.3.tif, etc., can be renamed to 2.1.tif, 2.2.tif, 2.3.tif etc. Also to note, is that the final quality of the stacked image depends on the quality of the initial images being fed into the macro. Attributes such as background intensity and the differences between un–stacked images within the group has a great impact on the quality of the final stacked image. Images for this macro do not have to be opened manually within IPP, the relevant images to be stacked need only be placed into a master file that will be used for all subsequent operations until the macro has been completed. The original files can then be removed manually from the master file, and new images replaced.

Sections of code that are categorized and highlighted below for this current macro are where changes could be made for individual uses. The following is a description of each highlighted section of code.

1. Sub Travis_Stacking() – "Travis_Stacking()" is the macro's name. "Sub" is required to indicate the starting point of the macro.

2. '<c><s>1 – This means "control+shift+1", and is the shortcut key to initialise the macro.
3. This is an identification label and is not required to run the macro.
4. This determines where the un–stacked file, labelled "1.1.tif" can be found, i.e., the file directory where the master file is kept.
5. This determines where the new stacked image will be saved, along with the new image name.
6. "End Sub" – This indicates the end of the current macro.

```
Sub Travis_Stacking() ──────► 1

'<c><s>1 ──────► 2
' For Automatic Stacking of Pre-Taken Images up to 25 ──────► 3
        ret = IpWsLoad("U:\Automatic Stacking\Unstacked\1.1.tif","tif") ──────► 4
        ret = IpWsLoad("U:\Automatic Stacking\Unstacked\1.2.tif","tif")
        ret = IpWsLoad("U:\Automatic Stacking\Unstacked\1.3.tif","tif")
        ret = IpWsLoad("U:\Automatic Stacking\Unstacked\1.4.tif","tif")
        ret = IpWsLoad("U:\Automatic Stacking\Unstacked\1.5.tif","tif")
        ret = IpWsLoad("U:\Automatic Stacking\Unstacked\1.6.tif","tif")
        ret = IpWsLoad("U:\Automatic Stacking\Unstacked\1.7.tif","tif")
        ret = IpWsLoad("U:\Automatic Stacking\Unstacked\1.8.tif","tif")
        ret = IpWsLoad("U:\Automatic Stacking\Unstacked\1.9.tif","tif")
        ret = IpWsLoad("U:\Automatic Stacking\Unstacked\1.10.tif","tif")
        ret = IpWsLoad("U:\Automatic Stacking\Unstacked\1.11.tif","tif")
        ret = IpWsLoad("U:\Automatic Stacking\Unstacked\1.12.tif","tif")
        ret = IpWsLoad("U:\Automatic Stacking\Unstacked\1.13.tif","tif")
        ret = IpWsLoad("U:\Automatic Stacking\Unstacked\1.14.tif","tif")
        ret = IpWsLoad("U:\Automatic Stacking\Unstacked\1.15.tif","tif")
        ret = IpWsLoad("U:\Automatic Stacking\Unstacked\1.16.tif","tif")
        ret = IpWsLoad("U:\Automatic Stacking\Unstacked\1.17.tif","tif")
        ret = IpWsLoad("U:\Automatic Stacking\Unstacked\1.18.tif","tif")
        ret = IpWsLoad("U:\Automatic Stacking\Unstacked\1.19.tif","tif")
        ret = IpWsLoad("U:\Automatic Stacking\Unstacked\1.20.tif","tif")
        ret = IpWsLoad("U:\Automatic Stacking\Unstacked\1.21.tif","tif")
        ret = IpWsLoad("U:\Automatic Stacking\Unstacked\1.22.tif","tif")
        ret = IpWsLoad("U:\Automatic Stacking\Unstacked\1.23.tif","tif")
        ret = IpWsLoad("U:\Automatic Stacking\Unstacked\1.24.tif","tif")
        ret = IpWsLoad("U:\Automatic Stacking\Unstacked\1.25.tif","tif")
        ret = IpEDFShow(1)
        ret = IpEDFAdd(0)
        ret = IpEDFAdd(1)
        ret = IpEDFAdd(2)
        ret = IpEDFAdd(3)
        ret = IpEDFAdd(4)
        ret = IpEDFAdd(5)
        ret = IpEDFAdd(6)
        ret = IpEDFAdd(7)
        ret = IpEDFAdd(8)
        ret = IpEDFAdd(9)
        ret = IpEDFAdd(10)
        ret = IpEDFAdd(11)
        ret = IpEDFAdd(12)
        ret = IpEDFAdd(13)
```

```
ret = IpEDFAdd(14)
ret = IpEDFAdd(15)
ret = IpEDFAdd(16)
ret = IpEDFAdd(17)
ret = IpEDFAdd(18)
ret = IpEDFAdd(19)
ret = IpEDFAdd(20)
ret = IpEDFAdd(21)
ret = IpEDFAdd(22)
ret = IpEDFAdd(23)
ret = IpEDFAdd(24)
ret = IpEDFSet(EDF_NORMALIZE, 0, 0)
ret = IpEDFSet(EDF_CRITERIA, EDF_MAX_LOCALCONTRAST, 0)
ret = IpEDFSet(EDF_ORDER, EDF_TOPDOWN, 0)
ret = IpEDFCreate(EDF_COMPOSITE)
ret = IpWsSaveAs("U:\Automatic Stacking\Stacked\1.tif", "tif") ──────► 5
ret = IpEDFShow(0)
ret = IpDocClose()
ret = IpAppSelectDoc(24)
ret = IpDocClose()
ret = IpAppSelectDoc(23)
ret = IpDocClose()
ret = IpAppSelectDoc(22)
ret = IpDocClose()
ret = IpAppSelectDoc(21)
ret = IpDocClose()
ret = IpAppSelectDoc(20)
ret = IpDocClose()
ret = IpAppSelectDoc(19)
ret = IpDocClose()
ret = IpAppSelectDoc(18)
ret = IpDocClose()
ret = IpAppSelectDoc(17)
ret = IpDocClose()
ret = IpAppSelectDoc(16)
ret = IpDocClose()
ret = IpAppSelectDoc(15)
ret = IpDocClose()
ret = IpAppSelectDoc(14)
ret = IpDocClose()
ret = IpAppSelectDoc(13)
ret = IpDocClose()
ret = IpAppSelectDoc(12)
ret = IpDocClose()
ret = IpAppSelectDoc(11)
ret = IpDocClose()
ret = IpAppSelectDoc(10)
ret = IpDocClose()
ret = IpAppSelectDoc(9)
ret = IpDocClose()
ret = IpAppSelectDoc(8)
ret = IpDocClose()
ret = IpAppSelectDoc(7)
ret = IpDocClose()
ret = IpAppSelectDoc(6)
ret = IpDocClose()
ret = IpAppSelectDoc(5)
ret = IpDocClose()
```

```
ret = IpAppSelectDoc(4)
ret = IpDocClose()
ret = IpAppSelectDoc(3)
ret = IpDocClose()
ret = IpAppSelectDoc(2)
ret = IpDocClose()
ret = IpAppSelectDoc(1)
ret = IpDocClose()
ret = IpAppSelectDoc(0)
ret = IpDocClose()
ret = IpIOvrShow(0)
ret = IpAnShow(0)
ret = IpEDFShow(0)

End Sub ⟶ 6
```

Counting Macro (fully automated)

This macro was designed to automatically count and size all objects within the captured field of view, using IPP, and to export the data acquired to an MS Excel file. This macro will work best in conjunction with the images stacked from "Stacking Macro" above. For this macro, the user must manually open the relevant stacked images into IPP and then proceed with macro initialization. The macro's name "Sub Travis_Auto_Counting_67_255()", the 67_255 indicates the segmentation range that this macro was written for. This is a fully automated macro, and will only count and size the objects within the range of 67 to 255, running though all images opened (1–10, maximum) nonstop, unless halted manually.

Please note, that if a scale bar is present within the image, it will most likely also be sized and counted, something to consider when going through the final data. It is recommended that when digitally capturing images, that only the fist image of that set should have a scale bar for comparison against system calibration. Before counting that image, the scale bar can simply be removed by erasing that section in a program such as Paint. Also, in many environmental samples, such things as detritus and artefacts can clutter up and "blind the image" with high intensity auto–fluorescence. For this reason, it is also suggested that for those images, the areas of nuisance be manually removed, also using a program such as Paint.

Sections of code that are categorized and highlighted for this current macro are where changes could be made for individual uses. The following is a description of each highlighted section of code.

1) "Travis_Auto_Counting_67_255()" – This is the macro's name.
2) '<c><s>2 – This means "control+shift+2", and is the shortcut key to initialise the macro.
3) The identification label.

4) This is the system calibrated pixel measurement for IPP that the user must define prior to running the macro. This system setting is made from the scale bar present, during digital image capture, and is a required setting.
5) "67,255" – This is the lower (67) and upper (255) range of segmentation.
6) These are the parameters that IPP was instructed to measure. More can be included, and some can be removed if unwanted.
7) Location where the Excel file is to be written to. Please note that data written into this Excel file range from column A to column F, if individual user data differ, lines of code will have to be changed in Appendix 6.3.

```
Sub Travis_Auto_Counting_67_255() ----------> 1

'<c><s>2 ----------> 2
' For EPI Microscopy ----------> 3
        ret = IpDocMinimize()
        ret = IpAppSelectDoc(8)
        ret = IpDocMinimize()
        ret = IpAppSelectDoc(7)
        ret = IpDocMinimize()
        ret = IpAppSelectDoc(6)
        ret = IpDocMinimize()
        ret = IpAppSelectDoc(5)
        ret = IpDocMinimize()
        ret = IpAppSelectDoc(4)
        ret = IpDocMinimize()
        ret = IpAppSelectDoc(3)
        ret = IpDocMinimize()
        ret = IpAppSelectDoc(2)
        ret = IpDocMinimize()
        ret = IpAppSelectDoc(1)
        ret = IpDocMinimize()
        ret = IpAppSelectDoc(0)
        ret = IpDocMinimize()
        ret = IpAppSelectDoc(9)
        ret = IpAppSelectDoc(0)
        ret = IpDocMaximize()
        ret = IpDocMove(-4, -30)
        ret = IpDocRestore()
        ret = IpDocMove(0, 0)
        ret = IpDocMaximize()
        ret = IpSCalSetLong(SCAL_SYSTEM_CAL, SCAL_APPLY, 0)
        ret = IpSCalSelect("Travis") ----------> 4
        ret = IpSCalShowEx(SCAL_DLG_SELECT, SCAL_HIDE)
        ret = IpWsConvertImage(IMC_GRAY, CONV_SCALE, 0, 0, 0, 0)
        ret = IpBlbShow(1)
        ret = IpSegSetRange(0, 0, 255) ----------> 5
        ret = IpSegPreview(CURRENT_C_T)
        ret = IpSegSetRange(0, 67, 255) ----------> 5
        ret = IpSegPreview(CURRENT_C_T)
        ret = IpBlbSetRange(67, 255) ----------> 5
```

```
ret = IpSegShow(0)
ret = IpBlbEnableMeas(BLBM_MAXCALIP, 1)
ret = IpBlbEnableMeas(BLBM_MINCALIP, 1)
ret = IpBlbEnableMeas(BLBM_LENGTH, 1)
ret = IpBlbEnableMeas(BLBM_WIDTH, 1)
ret = IpBlbCount()
ret = IpBlbUpdate(0)
ret = IpBlbSaveData("U:\EDF'd\Data.xls",  S_DATA+S_HEADER+S_Y_AXIS)
ret = IpDocClose()
ret = IpAppSelectDoc(0)
ret = IpDocClose()
ret = IpAppSelectDoc(9)
ret = IpAppSelectDoc(1)
ret = IpDocMaximize()
ret = IpDocRestore()
ret = IpDocMove(0, 0)
ret = IpDocMaximize()
ret = IpSCalSelect("Travis")
ret = IpSCalShowEx(SCAL_DLG_SELECT, SCAL_HIDE)
ret = IpWsConvertImage(IMC_GRAY, CONV_SCALE, 0, 0, 0, 0)
ret = IpSegSetRange(0, 0, 255)
ret = IpSegPreview(CURRENT_C_T)
ret = IpSegSetRange(0, 67, 255)
ret = IpSegPreview(CURRENT_C_T)
ret = IpBlbSetRange(67, 255)
ret = IpSegShow(0)
ret = IpBlbCount()
ret = IpBlbUpdate(0)
ret = IpBlbSaveData("U:\EDF'd\Data.xls",  S_APPEND+S_HEADER+S_Y_AXIS)
ret = IpDocClose()
ret = IpAppSelectDoc(1)
ret = IpDocClose()
ret = IpAppSelectDoc(9)
ret = IpAppSelectDoc(2)
ret = IpDocMaximize()
ret = IpDocRestore()
ret = IpDocMove(0, 0)
ret = IpDocMaximize()
ret = IpSCalSelect("Travis")
ret = IpSCalShowEx(SCAL_DLG_SELECT, SCAL_HIDE)
ret = IpWsConvertImage(IMC_GRAY, CONV_SCALE, 0, 0, 0, 0)
ret = IpSegSetRange(0, 0, 255)
ret = IpSegPreview(CURRENT_C_T)
ret = IpSegSetRange(0, 67, 255)
ret = IpSegPreview(CURRENT_C_T)
ret = IpBlbSetRange(67, 255)
ret = IpSegShow(0)
ret = IpBlbCount()
ret = IpBlbUpdate(0)
ret = IpBlbSaveData("U:\EDF'd\Data.xls",  S_APPEND+S_HEADER+S_Y_AXIS)
ret = IpDocClose()
ret = IpAppSelectDoc(2)
ret = IpDocClose()
ret = IpAppSelectDoc(9)
ret = IpAppSelectDoc(3)
ret = IpDocMaximize()
ret = IpDocRestore()
ret = IpDocMove(0, 0)
```

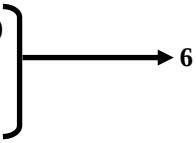

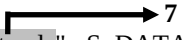

```
ret = IpDocMaximize()
ret = IpSCalSelect("Travis")
ret = IpSCalShowEx(SCAL_DLG_SELECT, SCAL_HIDE)
ret = IpWsConvertImage(IMC_GRAY, CONV_SCALE, 0, 0, 0, 0)
ret = IpSegSetRange(0, 0, 255)
ret = IpSegPreview(CURRENT_C_T)
ret = IpSegSetRange(0, 67, 255)
ret = IpSegPreview(CURRENT_C_T)
ret = IpBlbSetRange(67, 255)
ret = IpSegShow(0)
ret = IpBlbCount()
ret = IpBlbUpdate(0)
ret = IpBlbSaveData("U:\EDF'd\Data.xls",  S_APPEND+S_HEADER+S_Y_AXIS)
ret = IpDocClose()
ret = IpAppSelectDoc(3)
ret = IpDocClose()
ret = IpAppSelectDoc(9)
ret = IpAppSelectDoc(4)
ret = IpDocMaximize()
ret = IpDocRestore()
ret = IpDocMove(0, 0)
ret = IpDocMaximize()
ret = IpSCalSelect("Travis")
ret = IpSCalShowEx(SCAL_DLG_SELECT, SCAL_HIDE)
ret = IpWsConvertImage(IMC_GRAY, CONV_SCALE, 0, 0, 0, 0)
ret = IpSegSetRange(0, 0, 255)
ret = IpSegPreview(CURRENT_C_T)
ret = IpSegSetRange(0, 67, 255)
ret = IpSegPreview(CURRENT_C_T)
ret = IpBlbSetRange(67, 255)
ret = IpSegShow(0)
ret = IpBlbCount()
ret = IpBlbUpdate(0)
ret = IpBlbSaveData("U:\EDF'd\Data.xls",  S_APPEND+S_HEADER+S_Y_AXIS)
ret = IpDocClose()
ret = IpAppSelectDoc(4)
ret = IpDocClose()
ret = IpAppSelectDoc(9)
ret = IpAppSelectDoc(5)
ret = IpDocMaximize()
ret = IpDocRestore()
ret = IpDocMove(0, 0)
ret = IpDocMaximize()
ret = IpSCalSelect("Travis")
ret = IpSCalShowEx(SCAL_DLG_SELECT, SCAL_HIDE)
ret = IpWsConvertImage(IMC_GRAY, CONV_SCALE, 0, 0, 0, 0)
ret = IpSegSetRange(0, 0, 255)
ret = IpSegPreview(CURRENT_C_T)
ret = IpSegSetRange(0, 67, 255)
ret = IpSegPreview(CURRENT_C_T)
ret = IpBlbSetRange(67, 255)
ret = IpSegShow(0)
ret = IpBlbCount()
ret = IpBlbUpdate(0)
ret = IpBlbSaveData("U:\EDF'd\Data.xls",  S_APPEND+S_HEADER+S_Y_AXIS)
ret = IpDocClose()
ret = IpAppSelectDoc(5)
ret = IpDocClose()
```

```
ret = IpAppSelectDoc(9)
ret = IpAppSelectDoc(6)
ret = IpDocMaximize()
ret = IpDocRestore()
ret = IpDocMove(0, 0)
ret = IpDocMaximize()
ret = IpSCalSelect("Travis")
ret = IpSCalShowEx(SCAL_DLG_SELECT, SCAL_HIDE)
ret = IpWsConvertImage(IMC_GRAY, CONV_SCALE, 0, 0, 0, 0)
ret = IpSegSetRange(0, 0, 255)
ret = IpSegPreview(CURRENT_C_T)
ret = IpSegSetRange(0, 67, 255)
ret = IpSegPreview(CURRENT_C_T)
ret = IpBlbSetRange(67, 255)
ret = IpSegShow(0)
ret = IpBlbCount()
ret = IpBlbUpdate(0)
ret = IpBlbSaveData("U:\EDF'd\Data.xls",  S_APPEND+S_HEADER+S_Y_AXIS)
ret = IpDocClose()
ret = IpAppSelectDoc(6)
ret = IpDocClose()
ret = IpAppSelectDoc(9)
ret = IpAppSelectDoc(7)
ret = IpDocMaximize()
ret = IpDocRestore()
ret = IpDocMove(0, 0)
ret = IpDocMaximize()
ret = IpSCalSelect("Travis")
ret = IpSCalShowEx(SCAL_DLG_SELECT, SCAL_HIDE)
ret = IpWsConvertImage(IMC_GRAY, CONV_SCALE, 0, 0, 0, 0)
ret = IpSegSetRange(0, 0, 255)
ret = IpSegPreview(CURRENT_C_T)
ret = IpSegSetRange(0, 67, 255)
ret = IpSegPreview(CURRENT_C_T)
ret = IpBlbSetRange(67, 255)
ret = IpSegShow(0)
ret = IpBlbCount()
ret = IpBlbUpdate(0)
ret = IpBlbSaveData("U:\EDF'd\Data.xls",  S_APPEND+S_HEADER+S_Y_AXIS)
ret = IpDocClose()
ret = IpAppSelectDoc(7)
ret = IpDocClose()
ret = IpAppSelectDoc(9)
ret = IpAppSelectDoc(8)
ret = IpDocMaximize()
ret = IpDocRestore()
ret = IpDocMove(0, 0)
ret = IpDocMaximize()
ret = IpSCalSelect("1")
ret = IpSCalSelect("Travis")
ret = IpSCalShowEx(SCAL_DLG_SELECT, SCAL_HIDE)
ret = IpWsConvertImage(IMC_GRAY, CONV_SCALE, 0, 0, 0, 0)
ret = IpSegSetRange(0, 0, 255)
ret = IpSegPreview(CURRENT_C_T)
ret = IpSegSetRange(0, 67, 255)
ret = IpSegPreview(CURRENT_C_T)
ret = IpBlbSetRange(67, 255)
ret = IpSegShow(0)
```

```
    ret = IpBlbCount()
    ret = IpBlbUpdate(0)
    ret = IpBlbSaveData("U:\EDF'd\Data.xls",  S_APPEND+S_HEADER+S_Y_AXIS)
    ret = IpDocClose()
    ret = IpAppSelectDoc(8)
    ret = IpDocClose()
    ret = IpAppSelectDoc(9)
    ret = IpDocMaximize()
    ret = IpDocRestore()
    ret = IpDocMove(0, 0)
    ret = IpDocMaximize()
    ret = IpSCalSelect("Travis")
    ret = IpSCalShowEx(SCAL_DLG_SELECT, SCAL_HIDE)
    ret = IpWsConvertImage(IMC_GRAY, CONV_SCALE, 0, 0, 0, 0)
    ret = IpSegSetRange(0, 0, 255)
    ret = IpSegPreview(CURRENT_C_T)
    ret = IpSegSetRange(0, 67, 255)
    ret = IpSegPreview(CURRENT_C_T)
    ret = IpBlbSetRange(67, 255)
    ret = IpSegShow(0)
    ret = IpBlbCount()
    ret = IpBlbUpdate(0)
    ret = IpBlbSaveData("U:\EDF'd\Data.xls",  S_APPEND+S_HEADER+S_Y_AXIS)
    ret = IpDocClose()
    ret = IpAppSelectDoc(9)
    ret = IpDocClose()
    ret = IpIOvrShow(0)
    ret = IpAnShow(0)
    ret = IpBlbShow(0)

End Sub
```

Counting Macro (semi automated)

I wrote these next sets of macros that require user input for each image where the background intensity was either too bright or to dark for fully automated analysis (which was the case for many images). This macro requires manually setting the segmentation range before each image is counted. I found that if the image was to dark, and the cells very dimly lit, that the lower range of segmentation should be adjusted to the left, i.e. from 67_255, to 47_255 or 27_255 (user discretion required). For images that were very bright, the opposite would occur. This also depends on the microscopes NDF setting. A higher NDF will require a lower segmentation range, while no NDF will need a much higher segmentation range.

This first macro named “Black and White” is used to convert the RGB (red, green, blue) images, obtained from stacked or un–stacked images, into greyscale for optimal segmentation. It also sets the system required pixel calibration for size, and sets the parameters to be measured. Images to be grey scaled must be opened manually within IPP.

Sections of code that are categorized and highlighted for this current macro are where changes could be made for individual uses. The following is a description of each highlighted section of code.

1) This is the macro's name.
2) This is the system calibrated pixel measurement for IPP that the user must define prior to running the macro. This system setting is made from the scale bar present, during digital image capture, and is a required setting.
3) These are the parameters that IPP was instructed to measure. More can be included, and some can be removed if unwanted.

```
Sub Black_and_White() ──────► 1

    ret = IpWsConvertImage(IMC_GRAY, CONV_SCALE, 0, 0, 0, 0)
    ret = IpSCalSelect("Travis") ──────► 2
    ret = IpSCalShowEx(SCAL_DLG_SELECT, SCAL_HIDE)
    ret = IpDocMinimize()
    ret = IpAppSelectDoc(9)
    ret = IpDocClose()
    ret = IpAppSelectDoc(8)
    ret = IpWsConvertImage(IMC_GRAY, CONV_SCALE, 0, 0, 0, 0)
    ret = IpSCalSelect("Travis")
    ret = IpSCalShowEx(SCAL_DLG_SELECT, SCAL_HIDE)
    ret = IpDocMinimize()
    ret = IpAppSelectDoc(8)
    ret = IpDocClose()
    ret = IpAppSelectDoc(7)
    ret = IpWsConvertImage(IMC_GRAY, CONV_SCALE, 0, 0, 0, 0)
    ret = IpSCalSelect("Travis")
    ret = IpSCalShowEx(SCAL_DLG_SELECT, SCAL_HIDE)
    ret = IpDocMinimize()
    ret = IpAppSelectDoc(7)
    ret = IpDocClose()
    ret = IpAppSelectDoc(6)
    ret = IpWsConvertImage(IMC_GRAY, CONV_SCALE, 0, 0, 0, 0)
    ret = IpSCalSelect("Travis")
    ret = IpSCalShowEx(SCAL_DLG_SELECT, SCAL_HIDE)
    ret = IpDocMinimize()
    ret = IpAppSelectDoc(6)
    ret = IpDocClose()
    ret = IpAppSelectDoc(5)
    ret = IpWsConvertImage(IMC_GRAY, CONV_SCALE, 0, 0, 0, 0)
    ret = IpSCalSelect("Travis")
    ret = IpSCalShowEx(SCAL_DLG_SELECT, SCAL_HIDE)
    ret = IpDocMinimize()
    ret = IpAppSelectDoc(5)
    ret = IpDocClose()
    ret = IpAppSelectDoc(4)
    ret = IpWsConvertImage(IMC_GRAY, CONV_SCALE, 0, 0, 0, 0)
    ret = IpSCalSelect("Travis")
    ret = IpSCalShowEx(SCAL_DLG_SELECT, SCAL_HIDE)
    ret = IpDocMinimize()
```

```
ret = IpAppSelectDoc(4)
ret = IpDocClose()
ret = IpAppSelectDoc(3)
ret = IpWsConvertImage(IMC_GRAY, CONV_SCALE, 0, 0, 0, 0)
ret = IpSCalSelect("Travis")
ret = IpSCalShowEx(SCAL_DLG_SELECT, SCAL_HIDE)
ret = IpDocMinimize()
ret = IpAppSelectDoc(3)
ret = IpDocClose()
ret = IpAppSelectDoc(2)
ret = IpWsConvertImage(IMC_GRAY, CONV_SCALE, 0, 0, 0, 0)
ret = IpSCalSelect("Travis")
ret = IpSCalShowEx(SCAL_DLG_SELECT, SCAL_HIDE)
ret = IpDocMinimize()
ret = IpAppSelectDoc(2)
ret = IpDocClose()
ret = IpAppSelectDoc(1)
ret = IpWsConvertImage(IMC_GRAY, CONV_SCALE, 0, 0, 0, 0)
ret = IpSCalSelect("Travis")
ret = IpSCalShowEx(SCAL_DLG_SELECT, SCAL_HIDE)
ret = IpDocMinimize()
ret = IpAppSelectDoc(1)
ret = IpDocClose()
ret = IpAppSelectDoc(0)
ret = IpWsConvertImage(IMC_GRAY, CONV_SCALE, 0, 0, 0, 0)
ret = IpSCalSelect("Travis")
ret = IpSCalShowEx(SCAL_DLG_SELECT, SCAL_HIDE)
ret = IpDocMinimize()
ret = IpAppSelectDoc(0)
ret = IpDocClose()
ret = IpAppSelectDoc(10)
ret = IpBlbShow(1)
ret = IpBlbEnableMeas(BLBM_MAXCALIP, 1)
ret = IpBlbEnableMeas(BLBM_MINCALIP, 1)
ret = IpBlbEnableMeas(BLBM_LENGTH, 1)
ret = IpBlbEnableMeas(BLBM_WIDTH, 1)
```

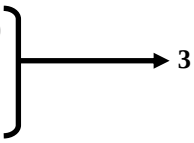


```
End Sub
```

After the above macro has been run, the user must manually choose the segmentation range, within the open segmentation window, and hit the “Count” button in the open window for each grey scaled image. This next sub macro was written to write the initial data into an MS Excel worksheet.

Sections of code that are categorized and highlighted for the following macro are where changes could be made for individual uses. The following is a description of each highlighted section of code.

1) This determines where the file will be saved, along with the file name.

```
Sub First_Entry()

        ret = IpBlbSaveData("U:\EDF'd\Data.xls",  S_DATA+S_HEADER+S_Y_AXIS)
        ret = IpDocClose()                                              1
        ret = IpAppSelectDoc(10)

End Sub
```

The next sub macro is intended to be used after the one above has been run at least once. When writing data to an unopened Excel file, there is the possibility that the next set of data will overwrite the data before it. The macro below should be used to append the next set of data after the previous set of data in the Excel file. It was found that using this macro alone (Sub Next_Entry) without the above was sufficient.

Sections of code that are categorized and highlighted for the following macro are where changes could be made for individual uses. The following is a description of each highlighted section of code.

1) This determines where the file with appended data will be saved, along with the file name.

```
Sub Next_Entry()
'<c><s>9
        ret = IpBlbSaveData("U:\EDF'd\Data.xls",  S_APPEND+S_HEADER+S_Y_AXIS)
        ret = IpDocClose()                                              1
        ret = IpAppSelectDoc(10)

End Sub
```

Main MS Excel Macro

This macro was written for MS Excel, using VBA, to automatically analyse and calculate required data for this thesis and for the overall ACEP II project. This macro is the main MS macro where all subsequent MS macros are directed and run. To run this macro, the lines of code should be copied into MS Excel VBA; using different VBA's for each sub macro routine ("Run"), and the worksheets named in conjunction to the macro code. If the user choices to rename any component, they should also change any and all subsequent lines of code to match the change made. This macro is initiated by pressing "control + O" (phonetic), within the file where it was coded, and is good for up to 5000 rows of data.

What will happen when this macro is initiated is that the user is requested to select a file where data from the above macros has been saved. This will be an Excel file containing data from 10 fields of view. The macro will then select columns A to F within the original data source Excel file and copy them into the master Excel macro file into the worksheet “Macro Input”. From here the macro will run as instructed.

Sections of code that are categorized and highlighted for this current macro are where changes could be made for individual uses. The following is a description of each highlighted section of code.

1) File name / directory where the macro is run from.
2) The name of the first worksheet where raw data is imported / copied.
3) The lower limit set for length. Any data point found within this column that is <0.2, the entire row will be deleted.
4) The upper limit set for length. Any data point found within this column that is >2.4, the entire row will be deleted.
5) The lower limit set for width. This bit of code was written specifically for cocci shaped cells in mind. Any data point found within this column that is < 0.2, the entire row will be deleted.
6) The name of the next worksheet where data from the previous worksheet will be assessed.
7) The name of the next worksheet where data from the previous worksheet will be assessed. Here, biovolume will be calculated.
8) The name of the next worksheet where data from the previous worksheet will be assessed.
9) The name of the next worksheet where data from the previous worksheet will be assessed. Here, biomass will be calculated.
10) The name of the next worksheet where data from the previous worksheet will be assessed. In between point 9 and 10, the values from the control runs were deleted from the data set (see Appendix 6.8).
11) The name of the next worksheet where data from the previous worksheet will be assessed.

```
Sub OpenFileLocation()

Run "Reset"  ──────────►  Start running “Secondary MS Excel Macro”

NewFN = Application.GetOpenFilename(Title:="Please select a file")
If NewFN = False Then
' They pressed Cancel
MsgBox "Stopping because you did not select a file"
Exit Sub
Else
Workbooks.Open Filename:=NewFN
End If
```

```
Columns("A:F").Select
Selection.Copy
Windows("Working Macro File - O - R - Excellent.xls").Activate
Sheets("Macro Input").Select
Range("A1").Select
ActiveSheet.Paste

Sheets("Macro Input").Select
Range("A1:G5000").Select
Rng = Selection.Rows.Count
ActiveCell.Offset(0, 0).Select
Application.ScreenUpdating = False
For i = 1 To Rng
If ActiveCell.Value = "#Total Count:" Then
Selection.EntireRow.Delete
Else
ActiveCell.Offset(1, 0).Select
End If
Next i
Application.ScreenUpdating = True

Range("A1:G5000").Select
Rng = Selection.Rows.Count
ActiveCell.Offset(0, 0).Select
Application.ScreenUpdating = False
For i = 1 To Rng
If ActiveCell.Value = " Obj#" Then
Selection.EntireRow.Delete
Else
ActiveCell.Offset(1, 0).Select
End If
Next i
Application.ScreenUpdating = True

Range("A1:G5000").Select
Rng = Selection.Rows.Count
ActiveCell.Offset(0, 0).Select
Application.ScreenUpdating = False
For i = 1 To Rng
If ActiveCell.Value = "" Then
Selection.EntireRow.Delete
Else
ActiveCell.Offset(1, 0).Select
End If
Next i
Application.ScreenUpdating = True

Columns("G:G").Select
Application.CutCopyMode = False
Selection.Delete Shift:=xlToLeft

Columns("A:A").Select
Application.CutCopyMode = False
Selection.Delete Shift:=xlToLeft

Range("F1").Select
ActiveCell.FormulaR1C1 = "=OR(RC[-1]<0.2)"
Range("F1").Select
```

1

2

3

```
Selection.AutoFill Destination:=Range("F1:F5000"), Type:=xlFillDefault
Range("F1:F5000").Select

Range("F1:F5000").Select
Rng = Selection.Rows.Count
ActiveCell.Offset(0, 0).Select
Application.ScreenUpdating = False
For i = 1 To Rng
If ActiveCell.Value = "True" Then
Selection.EntireRow.Delete
Else
ActiveCell.Offset(1, 0).Select
End If
Next i
Application.ScreenUpdating = True

Columns("F").Select
Selection.ClearContents

Range("F1").Select
ActiveCell.FormulaR1C1 = "=OR(RC[-1]>2.4)"
Range("F1").Select
Selection.AutoFill Destination:=Range("F1:F5000"), Type:=xlFillDefault
Range("F1:F5000").Select

Range("F1:F5000").Select
Rng = Selection.Rows.Count
ActiveCell.Offset(0, 0).Select
Application.ScreenUpdating = False
For i = 1 To Rng
If ActiveCell.Value = "True" Then
Selection.EntireRow.Delete
Else
ActiveCell.Offset(1, 0).Select
End If
Next i
Application.ScreenUpdating = True

Columns("F").Select
Selection.ClearContents

Range("F1").Select
ActiveCell.FormulaR1C1 = "=OR(RC[-2]<0.2)"
Range("F1").Select
Selection.AutoFill Destination:=Range("F1:F5000"), Type:=xlFillDefault
Range("F1:F5000").Select

Range("F1:F5000").Select
Rng = Selection.Rows.Count
ActiveCell.Offset(0, 0).Select
Application.ScreenUpdating = False
For i = 1 To Rng
If ActiveCell.Value = "True" Then
Selection.EntireRow.Delete
Else
ActiveCell.Offset(1, 0).Select
End If
Next i
```

4

5

```
Application.ScreenUpdating = True

Columns("F").Select
Selection.ClearContents

Sheets("Macro Input").Select
Range("A1:E5000").Select
Selection.Copy
```

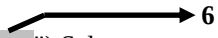


```
Sheets("Macro Output").Select
Range("A1").Select
ActiveSheet.Paste
```

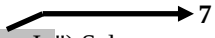


```
Sheets("Biovolume In").Select
Range("A2:C5001").Select
Selection.Copy
```

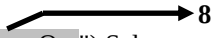


```
Sheets("Biovolume Out").Select
Range("A2").Select
Selection.PasteSpecial Paste:=xlPasteValues, Operation:=xlNone, SkipBlanks _
:=False, Transpose:=False
```

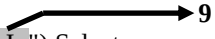


```
Sheets("Biomass In").Select
Range("C2").Select
ActiveCell.FormulaR1C1 = "=OR(RC[-1],0)"
Range("C2").Select
Selection.AutoFill Destination:=Range("C2:C5001"), Type:=xlFillDefault
Range("C2:C5001").Select

Range("C2:C5001").Select
Rng = Selection.Rows.Count
ActiveCell.Offset(0, 0).Select
Application.ScreenUpdating = False
For i = 1 To Rng
If ActiveCell.Value = "False" Then
Selection.EntireRow.Delete
Else
ActiveCell.Offset(1, 0).Select
End If
Next i
Application.ScreenUpdating = True

Range("C2:C5001").Select
Selection.ClearContents

Sheets("Biomass In").Select
Range("A2:B5001").Select
ActiveWorkbook.Worksheets("Biomass In").Sort.SortFields.Clear
ActiveWorkbook.Worksheets("Biomass In").Sort.SortFields.Add Key:=Range("A2"), _
   SortOn:=xlSortOnValues, Order:=xlAscending, DataOption:=xlSortNormal
With ActiveWorkbook.Worksheets("Biomass In").Sort
   .SetRange Range("A2:B5001")
   .Header = xlNo
   .MatchCase = False
   .Orientation = xlTopToBottom
   .SortMethod = xlPinYin
   .Apply
End With
```

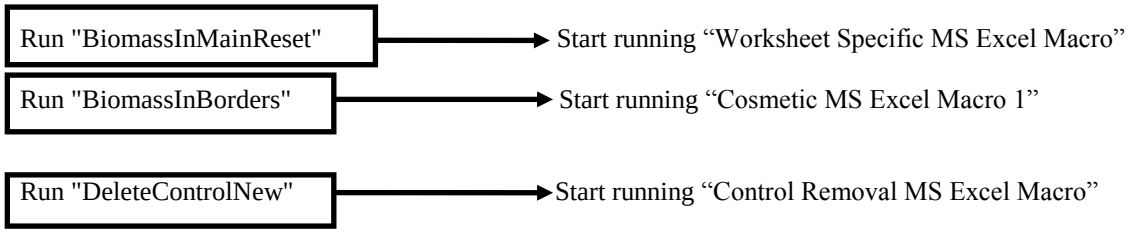


```
Sheets("Biomass In").Select
Range("A1:G5000").Select
Selection.Copy

Sheets("Biomass Out").Select
Range("A1").Select
Selection.PasteSpecial Paste:=xlPasteValues, Operation:=xlNone, SkipBlanks _
:=False, Transpose:=False

Columns("A:A").Select
Application.CutCopyMode = False
Selection.Delete Shift:=xlToLeft

Columns("B:B").Select
   Selection.Insert Shift:=xlToRight, CopyOrigin:=xlFormatFromLeftOrAbove
   Range("B1").Select
   ActiveCell.FormulaR1C1 = "Limits"
   Range("B2").Select

Columns("A:A").Select
   Selection.NumberFormat = "0.00E+00"
   Columns("E:E").Select
   Selection.NumberFormat = "0.00E+00"
   Columns("G:G").Select
   Selection.NumberFormat = "0.00E+00"

Columns("A:G").Select
   With Selection
      .HorizontalAlignment = xlCenter
      .VerticalAlignment = xlBottom
      .WrapText = False
      .Orientation = 0
      .AddIndent = False
      .IndentLevel = 0
      .ShrinkToFit = False
      .ReadingOrder = xlContext
      .MergeCells = False
   End With

Columns("B:C").Select
Application.CutCopyMode = False
Selection.Delete Shift:=xlToLeft

Sheets("Biomass Out").Select
Range("A1:F5000").Select
Selection.Copy

Sheets("Biomass Final").Select
Range("A1").Select
Selection.PasteSpecial Paste:=xlPasteValues, Operation:=xlNone, SkipBlanks _
```

10

11

```
:=False, Transpose:=False

Columns("A:E").Select
   Selection.ColumnWidth = 15

Columns("A:A").Select
   Selection.NumberFormat = "0.00E+00"
   Range("C2").Select
   Selection.NumberFormat = "0"
   Range("C3:C17").Select
   Selection.NumberFormat = "0.00E+00"
   Range("E2").Select
   Selection.NumberFormat = "0"
   Range("E3:E17").Select
   Selection.NumberFormat = "0.00E+00"

Columns("A:E").Select
   With Selection
      .HorizontalAlignment = xlCenter
      .VerticalAlignment = xlBottom
      .WrapText = False
      .Orientation = 0
      .AddIndent = False
      .IndentLevel = 0
      .ShrinkToFit = False
      .ReadingOrder = xlContext
      .MergeCells = False
   End With

Run "BiomassFinalBorders"
```

→ Start running “Cosmetic MS Excel Macro 2”

```
Columns("A:E").Select
Selection.Copy

End Sub
```

Secondary MS Excel Macro

This macro was written to reset all equations, parameters, constants, etc. within the MS Excel macro file. When running the combined macros, there are lines of code that instruct certain values to be removed by deleting the entire row. Sometimes, that row within the Excel worksheet contains an equation, parameter, constant, etc. This macro therefore returns the backbone of the overall MS Excel macro to its original form, including deleting all data input from the previous run. This macro is the first sub macro to be run and is run before data are imported.

Sections of code that are categorized and highlighted for this current macro are where changes could be made for individual uses. Please refer to the previous MS Excel macro “Main MS Excel Macro” for worksheet names where relevant.

```
Sub Reset()

Sheets("Biomass Final").Select
Range("A1:F5000").Select
Selection.ClearContents
Range("A1").Select

Sheets("Biomass Out").Select
Range("A1:I5000").Select
Selection.ClearContents
Range("A1").Select

Sheets("Biomass In").Select
Range("A2").Select
ActiveCell.FormulaR1C1 = "='Biovolume Out'!RC[1]*(5.6*10^-13)"
Range("A2").Select
Selection.AutoFill Destination:=Range("A2:A5001"), Type:=xlFillDefault
Range("A1").Select

Sheets("Biomass In").Select
Range("B2").Select
ActiveCell.FormulaR1C1 = "='Biovolume Out'!RC[1]*(5.6*10^-13)"
Range("B2").Select
Selection.AutoFill Destination:=Range("B2:B5001"), Type:=xlFillDefault
Range("A1").Select
```

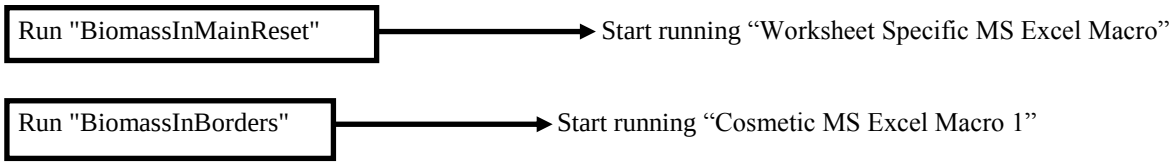


```
Range("A1").Select

Sheets("Biovolume Out").Select
Range("A2:C5001").Select
Application.CutCopyMode = False
Selection.ClearContents
Range("A1").Select

Sheets("Biovolume In").Select
Application.CutCopyMode = False
Range("B2").Select
ActiveCell.FormulaR1C1 = _
"=(3.14159265358979/4)*'Macro Output'!R[-1]C[1]^2*('Macro Output'!R[-1]C-'Macro Output'!R[-1]C[1]/3)"
Range("B2").Select
Selection.AutoFill Destination:=Range("B2:B5001"), Type:=xlFillDefault
Range("B2:B5001").Select

Sheets("Biovolume In").Select
Range("C2").Select
ActiveCell.FormulaR1C1 = _
"=(3.14159265358979/4)*'Macro Output'!R[-1]C[1]^2*('Macro Output'!R[-1]C[2]-'Macro Output'!R[-1]C[1]/3)"
Range("C2").Select
Selection.AutoFill Destination:=Range("C2:C5001"), Type:=xlFillDefault
Range("A1").Select
```

```
Sheets("Biovolume In").Select
Range("A2:A5001").Select
Selection.ClearContents
Range("A1").Select

Sheets("Macro Output").Select
Range("A1:G5000").Select
Application.CutCopyMode = False
Selection.ClearContents
Range("A1").Select

Sheets("Macro Input").Select
Range("A1:G5000").Select
Application.CutCopyMode = False
Selection.ClearContents
Range("A1").Select

Sheets("Macro Input").Select
Range("A1:G5000").Select
Application.CutCopyMode = False
Selection.ClearContents
Range("A1").Select

End Sub
```

Worksheet Specific MS Excel Macro

This macro was written to reset the equations, constants, etc. within a specific worksheet while not deleting or removing any data values within. This worksheet is where the main calculations for biomass are performed. This macro is separate from the overall "Reset" macro found in "Main MS Excel Macro".

Sections of code that are categorized and highlighted for this current macro are where changes could be made for individual uses. The following is a description of each highlighted section of code. For code that is highlighted without accompanying numbers, please refer to previous MS Excel macros for worksheet names where relevant.

1) This is the total area for all combined captured fields of view. Each individual captured field was 15115.11111 μm^2, so 10 fields would be thus indicated as in the macro.
2) Calculates bacterial numbers before the control values are removed ($cells.ml^{-1}$). Calculates numbers per volume filtered, from 1 to 5 ml.
3) Calculates bacterial biomass before the control values are removed ($gC.ml^{-1}$). Calculates biomass per volume filtered, from 1 to 5 ml.

4) Calculates the sum, average, minimum and maximum biomass values before the control values are removed.
5) Calculates bacterial numbers after the control values are removed (cells.ml^{-1}). Calculates numbers per volume filtered, from 1 to 5 ml.
6) Calculates bacterial biomass after the control values are removed (gC.ml^{-1}). Calculates biomass per volume filtered, from 1 to 5 ml.
7) Calculates the sum, average, minimum and maximum biomass values after the control values are removed.

```
Sub BiomassInMainReset()

Sheets("Biomass In").Select
Range("E2").Select
ActiveCell.FormulaR1C1 = "=COUNTIF(R[0]C[-3]:R[4999]C[-3],"">0"")"
Range("E2").Select

Sheets("Biomass In").Select
Range("E8").Select
ActiveCell.FormulaR1C1 = "=SUM(R[-6]C[-3]:R[4993]C[-3])"
Range("E8").Select

Sheets("Biomass In").Select
Range("I1").Select
   ActiveCell.FormulaR1C1 = "151151.1111"  ⟶ 1

Sheets("Biomass In").Select
   Range("D2").Select
   ActiveCell.FormulaR1C1 = "Before Count"
   Range("D3").Select
   ActiveCell.FormulaR1C1 = "N 1ml"
   Range("D4").Select
   ActiveCell.FormulaR1C1 = "N 2ml"
   Range("D5").Select
   ActiveCell.FormulaR1C1 = "N 3ml"
   Range("D6").Select
   ActiveCell.FormulaR1C1 = "N 4ml"
   Range("D7").Select
   ActiveCell.FormulaR1C1 = "N 5ml"
   Range("D2:D7").Select
   With Selection
      .HorizontalAlignment = xlCenter
      .VerticalAlignment = xlBottom
      .WrapText = False
      .Orientation = 0
      .AddIndent = False
      .IndentLevel = 0
      .ShrinkToFit = False
      .ReadingOrder = xlContext
      .MergeCells = False
   End With
   Range("E3:E7").Select
```

```
    Selection.NumberFormat = "0.00E+00"

Sheets("Biomass In").Select
Range("E3").Select
    ActiveCell.FormulaR1C1 = "=((R[-1]C)*(1.77*10^8))/((R[-2]C[4])*(1))"
Range("E4").Select
    ActiveCell.FormulaR1C1 = "=((R[-2]C)*(1.77*10^8))/((R[-3]C[4])*(2))"
Range("E5").Select
    ActiveCell.FormulaR1C1 = "=((R[-3]C)*(1.77*10^8))/((R[-4]C[4])*(3))"
Range("E6").Select
    ActiveCell.FormulaR1C1 = "=((R[-4]C)*(1.77*10^8))/((R[-5]C[4])*(4))"
Range("E7").Select
    ActiveCell.FormulaR1C1 = "=((R[-5]C)*(1.77*10^8))/((R[-6]C[4])*(5))"
```

2

```
Sheets("Biomass In").Select
    Range("D8").Select
    ActiveCell.FormulaR1C1 = "Before Biomass"
    Range("D9").Select
    ActiveCell.FormulaR1C1 = "B 1ml"
    Range("D10").Select
    ActiveCell.FormulaR1C1 = "B 2ml"
    Range("D11").Select
    ActiveCell.FormulaR1C1 = "B 3ml"
    Range("D12").Select
    ActiveCell.FormulaR1C1 = "B 4ml"
    Range("D13").Select
    ActiveCell.FormulaR1C1 = "B 5ml"
    Range("D8:D13").Select
    With Selection
        .HorizontalAlignment = xlCenter
        .VerticalAlignment = xlBottom
        .WrapText = False
        .Orientation = 0
        .AddIndent = False
        .IndentLevel = 0
        .ShrinkToFit = False
        .ReadingOrder = xlContext
        .MergeCells = False
    End With
    Range("E8:E13").Select
    Selection.NumberFormat = "0.00E+00"

Sheets("Biomass In").Select
Range("E9").Select
    ActiveCell.FormulaR1C1 = "=((R[-1]C)*(1.77*10^8))/((R[-8]C[4])*(1))"
Range("E10").Select
    ActiveCell.FormulaR1C1 = "=((R[-2]C)*(1.77*10^8))/((R[-9]C[4])*(2))"
Range("E11").Select
    ActiveCell.FormulaR1C1 = "=((R[-3]C)*(1.77*10^8))/((R[-10]C[4])*(3))"
Range("E12").Select
    ActiveCell.FormulaR1C1 = "=((R[-4]C)*(1.77*10^8))/((R[-11]C[4])*(4))"
Range("E13").Select
    ActiveCell.FormulaR1C1 = "=((R[-5]C)*(1.77*10^8))/((R[-12]C[4])*(5))"
```

3

```
Sheets("Biomass In").Select
    Range("D14").Select
    ActiveCell.FormulaR1C1 = "Sum"
    Range("D15").Select
```

```
    ActiveCell.FormulaR1C1 = "Average"
    Range("D16").Select
    ActiveCell.FormulaR1C1 = "Min"
    Range("D17").Select
    ActiveCell.FormulaR1C1 = "Max"
    Range("E14").Select
    ActiveCell.FormulaR1C1 = "=SUM(R[-12]C[-3]:R[4987]C[-3])"
    Range("E15").Select
    ActiveCell.FormulaR1C1 = "=AVERAGE(R[-13]C[-3]:R[4986]C[-3])"
    Range("E16").Select
    ActiveCell.FormulaR1C1 = "=MIN(R[-14]C[-3]:R[4985]C[-3])"
    Range("E17").Select
    ActiveCell.FormulaR1C1 = "=MAX(R[-15]C[-3]:R[4984]C[-3])"
```

4

```
Sheets("Biomass In").Select
    Range("F2").Select
    ActiveCell.FormulaR1C1 = "After Count"
    Range("F3").Select
    ActiveCell.FormulaR1C1 = "N 1ml"
    Range("F4").Select
    ActiveCell.FormulaR1C1 = "N 2ml"
    Range("F5").Select
    ActiveCell.FormulaR1C1 = "N 3ml"
    Range("F6").Select
    ActiveCell.FormulaR1C1 = "N 4ml"
    Range("F7").Select
    ActiveCell.FormulaR1C1 = "N 5ml"
    Range("F2:F7").Select
    With Selection
        .HorizontalAlignment = xlCenter
        .VerticalAlignment = xlBottom
        .WrapText = False
        .Orientation = 0
        .AddIndent = False
        .IndentLevel = 0
        .ShrinkToFit = False
        .ReadingOrder = xlContext
        .MergeCells = False
    End With
    Range("G3:G7").Select
    Selection.NumberFormat = "0.00E+00"

Sheets("Biomass In").Select
Range("G3").Select
    ActiveCell.FormulaR1C1 = "=((R[-1]C)*(1.77*10^8))/((R[-2]C[2])*(1))"
Range("G4").Select
    ActiveCell.FormulaR1C1 = "=((R[-2]C)*(1.77*10^8))/((R[-3]C[2])*(2))"
Range("G5").Select
    ActiveCell.FormulaR1C1 = "=((R[-3]C)*(1.77*10^8))/((R[-4]C[2])*(3))"
Range("G6").Select
    ActiveCell.FormulaR1C1 = "=((R[-4]C)*(1.77*10^8))/((R[-5]C[2])*(4))"
Range("G7").Select
    ActiveCell.FormulaR1C1 = "=((R[-5]C)*(1.77*10^8))/((R[-6]C[2])*(5))"
```

5

```
Sheets("Biomass In").Select
    Range("F8").Select
    ActiveCell.FormulaR1C1 = "After Biomass"
    Range("F9").Select
```

```
    ActiveCell.FormulaR1C1 = "B 1ml"
    Range("F10").Select
    ActiveCell.FormulaR1C1 = "B 2ml"
    Range("F11").Select
    ActiveCell.FormulaR1C1 = "B 3ml"
    Range("F12").Select
    ActiveCell.FormulaR1C1 = "B 4ml"
    Range("F13").Select
    ActiveCell.FormulaR1C1 = "B 5ml"
    Range("F8:F13").Select
    With Selection
        .HorizontalAlignment = xlCenter
        .VerticalAlignment = xlBottom
        .WrapText = False
        .Orientation = 0
        .AddIndent = False
        .IndentLevel = 0
        .ShrinkToFit = False
        .ReadingOrder = xlContext
        .MergeCells = False
    End With
    Range("G9:G13").Select
    Selection.NumberFormat = "0.00E+00"

Sheets("Biomass In").Select
Range("G9").Select
    ActiveCell.FormulaR1C1 = "=((R[-1]C)*(1.77*10^8))/((R[-8]C[2])*(1))"
Range("G10").Select
    ActiveCell.FormulaR1C1 = "=((R[-2]C)*(1.77*10^8))/((R[-9]C[2])*(2))"
Range("G11").Select
    ActiveCell.FormulaR1C1 = "=((R[-3]C)*(1.77*10^8))/((R[-10]C[2])*(3))"
Range("G12").Select
    ActiveCell.FormulaR1C1 = "=((R[-4]C)*(1.77*10^8))/((R[-11]C[2])*(4))"
Range("G13").Select
    ActiveCell.FormulaR1C1 = "=((R[-5]C)*(1.77*10^8))/((R[-12]C[2])*(5))"

Sheets("Biomass In").Select
    Range("F14").Select
    ActiveCell.FormulaR1C1 = "Sum"
    Range("F15").Select
    ActiveCell.FormulaR1C1 = "Average"
    Range("F16").Select
    ActiveCell.FormulaR1C1 = "Min"
    Range("F17").Select
    ActiveCell.FormulaR1C1 = "Max"
    Range("G14").Select
    ActiveCell.FormulaR1C1 = "=SUM(R[-12]C[-5]:R[4987]C[-5])"
    Range("G15").Select
    ActiveCell.FormulaR1C1 = "=AVERAGE(R[-13]C[-5]:R[4986]C[-5])"
    Range("G16").Select
    ActiveCell.FormulaR1C1 = "=MIN(R[-14]C[-5]:R[4985]C[-5])"
    Range("G17").Select
    ActiveCell.FormulaR1C1 = "=MAX(R[-15]C[-5]:R[4984]C[-5])"
Range("A1").Select

End Sub
```

Cosmetic MS Excel Macro 1

This macro is purely cosmetic. It places borders, specific fonts, line weights and colour to delineate and separate certain sections where data can be found. It is not required for data calculation.

```
Sub BiomassInBorders()

Sheets("Biomass In").Select
   Range("D2:G17").Select
   Selection.Borders(xlDiagonalDown).LineStyle = xlNone
   Selection.Borders(xlDiagonalUp).LineStyle = xlNone
   With Selection.Borders(xlEdgeLeft)
      .LineStyle = xlContinuous
      .ColorIndex = 0
      .TintAndShade = 0
      .Weight = xlMedium
   End With
   With Selection.Borders(xlEdgeTop)
      .LineStyle = xlContinuous
      .ColorIndex = 0
      .TintAndShade = 0
      .Weight = xlMedium
   End With
   With Selection.Borders(xlEdgeBottom)
      .LineStyle = xlContinuous
      .ColorIndex = 0
      .TintAndShade = 0
      .Weight = xlMedium
   End With
   With Selection.Borders(xlEdgeRight)
      .LineStyle = xlContinuous
      .ColorIndex = 0
      .TintAndShade = 0
      .Weight = xlMedium
   End With
   Range("D2:G7,D8:G13").Select
   Range("D8").Activate
   Selection.Borders(xlDiagonalDown).LineStyle = xlNone
   Selection.Borders(xlDiagonalUp).LineStyle = xlNone
   With Selection.Borders(xlEdgeLeft)
      .LineStyle = xlContinuous
      .ColorIndex = 0
      .TintAndShade = 0
      .Weight = xlMedium
   End With
   With Selection.Borders(xlEdgeTop)
      .LineStyle = xlContinuous
      .ColorIndex = 0
      .TintAndShade = 0
      .Weight = xlMedium
   End With
   With Selection.Borders(xlEdgeBottom)
      .LineStyle = xlContinuous
```

```
    .ColorIndex = 0
    .TintAndShade = 0
    .Weight = xlMedium
  End With
  With Selection.Borders(xlEdgeRight)
    .LineStyle = xlContinuous
    .ColorIndex = 0
    .TintAndShade = 0
    .Weight = xlMedium
  End With
  Selection.Borders(xlInsideHorizontal).LineStyle = xlNone
  Range("D2:E17").Select
  Selection.Borders(xlDiagonalDown).LineStyle = xlNone
  Selection.Borders(xlDiagonalUp).LineStyle = xlNone
  With Selection.Borders(xlEdgeLeft)
    .LineStyle = xlContinuous
    .ColorIndex = 0
    .TintAndShade = 0
    .Weight = xlMedium
  End With
  With Selection.Borders(xlEdgeTop)
    .LineStyle = xlContinuous
    .ColorIndex = 0
    .TintAndShade = 0
    .Weight = xlMedium
  End With
  With Selection.Borders(xlEdgeBottom)
    .LineStyle = xlContinuous
    .ColorIndex = 0
    .TintAndShade = 0
    .Weight = xlMedium
  End With
  With Selection.Borders(xlEdgeRight)
    .LineStyle = xlContinuous
    .ColorIndex = 0
    .TintAndShade = 0
    .Weight = xlMedium
  End With
  Selection.Borders(xlInsideVertical).LineStyle = xlNone
  Range("A1").Select

End Sub
```

Control Removal MS Excel Macro

This macro was written to subtract allotted control calculated bacterial numbers and biomass from the overall data, after main bacterial numbers and biomass have been calculated. Control values are calculated with the main macro “Main MS Excel Macro", but then must be manually copied into the relevant cells in the worksheet “Control”, from the “Biomass Final” worksheet.

```
Sub DeleteControlNew()
```

```
Sheets("Biomass In").Select
Range("G2").Select
   ActiveCell.FormulaR1C1 = "=R[0]C[-2]-Control!R[-1]C[-5]"
   Range("F18").Select
Range("G3").Select
   ActiveCell.FormulaR1C1 = "=R[0]C[-2]-Control!R[-1]C[-5]"
   Range("F18").Select
Range("G4").Select
   ActiveCell.FormulaR1C1 = "=R[0]C[-2]-Control!R[-1]C[-5]"
   Range("F18").Select
Range("G5").Select
   ActiveCell.FormulaR1C1 = "=R[0]C[-2]-Control!R[-1]C[-5]"
   Range("F18").Select
Range("G6").Select
   ActiveCell.FormulaR1C1 = "=R[0]C[-2]-Control!R[-1]C[-5]"
   Range("F18").Select
Range("G7").Select
   ActiveCell.FormulaR1C1 = "=R[0]C[-2]-Control!R[-1]C[-5]"
   Range("F18").Select
Range("G8").Select
   ActiveCell.FormulaR1C1 = "=R[0]C[-2]-Control!R[-1]C[-5]"
   Range("F18").Select
Range("G9").Select
   ActiveCell.FormulaR1C1 = "=R[0]C[-2]-Control!R[-1]C[-5]"
   Range("F18").Select
Range("G10").Select
   ActiveCell.FormulaR1C1 = "=R[0]C[-2]-Control!R[-1]C[-5]"
   Range("F18").Select
Range("G11").Select
   ActiveCell.FormulaR1C1 = "=R[0]C[-2]-Control!R[-1]C[-5]"
   Range("F18").Select
Range("G12").Select
   ActiveCell.FormulaR1C1 = "=R[0]C[-2]-Control!R[-1]C[-5]"
   Range("F18").Select
Range("G13").Select
   ActiveCell.FormulaR1C1 = "=R[0]C[-2]-Control!R[-1]C[-5]"
   Range("F18").Select

End Sub
```

Cosmetic MS Excel Macro 2

This macro is also purely cosmetic. It places borders, specific fonts, line weights and colour to delineate and separate certain sections where data can be found within the final output sheet “Biomass Final”.

```
Sub BiomassFinalBorders()

   Sheets("Biomass Final").Select
   Range("B2:E17").Select
   Selection.Borders(xlDiagonalDown).LineStyle = xlNone
   Selection.Borders(xlDiagonalUp).LineStyle = xlNone
   With Selection.Borders(xlEdgeLeft)
```

```
    .LineStyle = xlContinuous
    .ColorIndex = 0
    .TintAndShade = 0
    .Weight = xlMedium
End With
With Selection.Borders(xlEdgeTop)
    .LineStyle = xlContinuous
    .ColorIndex = 0
    .TintAndShade = 0
    .Weight = xlMedium
End With
With Selection.Borders(xlEdgeBottom)
    .LineStyle = xlContinuous
    .ColorIndex = 0
    .TintAndShade = 0
    .Weight = xlMedium
End With
With Selection.Borders(xlEdgeRight)
    .LineStyle = xlContinuous
    .ColorIndex = 0
    .TintAndShade = 0
    .Weight = xlMedium
End With
Range("B2:E7,B8:E13").Select
Range("B8").Activate
Selection.Borders(xlDiagonalDown).LineStyle = xlNone
Selection.Borders(xlDiagonalUp).LineStyle = xlNone
With Selection.Borders(xlEdgeLeft)
    .LineStyle = xlContinuous
    .ColorIndex = 0
    .TintAndShade = 0
    .Weight = xlMedium
End With
With Selection.Borders(xlEdgeTop)
    .LineStyle = xlContinuous
    .ColorIndex = 0
    .TintAndShade = 0
    .Weight = xlMedium
End With
With Selection.Borders(xlEdgeBottom)
    .LineStyle = xlContinuous
    .ColorIndex = 0
    .TintAndShade = 0
    .Weight = xlMedium
End With
With Selection.Borders(xlEdgeRight)
    .LineStyle = xlContinuous
    .ColorIndex = 0
    .TintAndShade = 0
    .Weight = xlMedium
End With
Selection.Borders(xlInsideHorizontal).LineStyle = xlNone
Range("B2:C17").Select
Selection.Borders(xlDiagonalDown).LineStyle = xlNone
Selection.Borders(xlDiagonalUp).LineStyle = xlNone
With Selection.Borders(xlEdgeLeft)
    .LineStyle = xlContinuous
    .ColorIndex = 0
```

```
    .TintAndShade = 0
    .Weight = xlMedium
  End With
  With Selection.Borders(xlEdgeTop)
    .LineStyle = xlContinuous
    .ColorIndex = 0
    .TintAndShade = 0
    .Weight = xlMedium
  End With
  With Selection.Borders(xlEdgeBottom)
    .LineStyle = xlContinuous
    .ColorIndex = 0
    .TintAndShade = 0
    .Weight = xlMedium
  End With
  With Selection.Borders(xlEdgeRight)
    .LineStyle = xlContinuous
    .ColorIndex = 0
    .TintAndShade = 0
    .Weight = xlMedium
  End With
  Selection.Borders(xlInsideVertical).LineStyle = xlNone
  Range("A1").Select

End Sub
```